Acta morphologica et anthropologica (12)

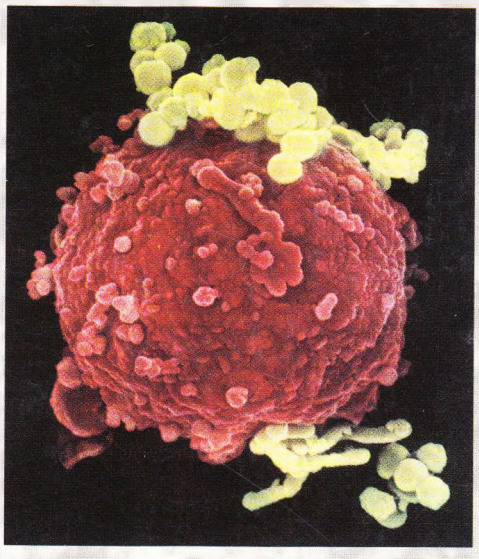

Professor Marin Drinov
Academic
Publishing House

Acta morphologica et anthropologica

is the continuation of
Acta cytobiologica et morphologica

Издаването на настоящия брой на списанието през 2007 г. е с финансовата подкрепа на Фонд „Научни изследвания“ при Министерството на образованието и науката.

Professor Marin Drinov Academic Publishing House
Bulgaria, 1113 Sofia, Acad. G. Bonchev Str., Bl. 6

Редактор *М. Зоева* Техн. редактор *Пр. Глогинска* Коректор *Б. Кременски*
Предпечатна подготовка *В. Петкова*

Формат 70×100/16 Печ. коли 14

Печатница на Академично издателство „Проф. Марин Дринов“
София 1113, ул. „Акад. Г. Бончев“, бл. 5

ISSN 0861–0509

Acta morphologica et anthropologica (12)

12 • Sofia • 2007
Institute of Experimental Morphology and Anthropology with Museum
Bulgarian Anatomical Society

Contents

Morphology

Anthropology

Review Articles

In Memoriam

Institute of Experimental Morphology and Anthropology with Museum
Bulgarian Anatomical Society

Acta morphologica et anthropologica, 12
Sofia • 2007

Morphology

GT1b Ganglioside Changes in Lewis Rat Serum During Myelination

V. Kolyovska, E. Zaprianova, D. Deleva, A. Filchev, E. Sultanov***

Institute of Experimental Morphology and Anthropology with Museum, Bulgarian Academy of Sciences, Sofia
**Faculty of Veterinary Medicine, University of Forestry, Sofia*
*** National Center of Radiology and Radiation Protection, Sofia*

Ganglioside GT1b was suggested to play a role in mediating the interactions between axons and oligodendrocytes, needful for myelination and maintenance the integrity of myelin sheath. In this study, the relative distribution of GT1b was determined in Lewis rats serum during the different brain myelination periods. A high level of GT1b was detected in the serum just before the onset of brain myelination and of the time of active myelination compared to the GT1b level after the completion of myelination. This finding further support the concept concerning the role of GT1b in mediating the interactions between axons and oligodendrocytes. An apparent correlation was observed between the GT1b levels in the rat brain during the different periods of its myelination (determined in our previous studies) and the GT1b levels in the serum. Therefore, serum GT1b gangliosides could be monitored as markers of myelination and remyelination in the brain.

Key words: ganglioside GT1b, serum, myelination, axon-oligodendrocytes interactions.

Introduction

Gangliosides are a family of sialic acid-containing glycosphingolipids highly enriched in the nervous system [19]. Trey are the major sialoconjugates in the brain. Gangliosides are mainly located on the surface of plasma membranes of neurons [9], glial cells [22] and in myelin of the central nervous system (CNS) [1]. The most abundant gangliosides in the adult mammalian brain are GM1, GD1a, GD1b and GT1b. They undergo characteristic changes in content and composition during development [18] and therefore could be used as markers for the different phases of brain maturation (synaptogenesis, myelination). We first reported [3, 4] significant ganglioside changes in rat and mouse medulla oblongata during the different periods of myelination. In the rat brain in the premyelination period and at the period of active myelination, the predominant ganglioside fraction was GT1b. Ganglioside GT1b was suggested to play a role in mediating the interactions between oligodendroglia and axons [15] needful for myelination and maintenance the integrity of myelin sheath.

Gangliosides occur also in non-cell-associated forms in blood, lymph, saliva and other body fluids. Changes in gangliosides in certain pathologies are reflected by their composition and blood serum levels [6, 7, 11, 14, 25, 26]. Therefore, information on blood serum gangliosides in normal and pathological states is of considerable importance [5].

There are no data concerning the serum ganglioside changes during brain myelination. In the present study the relative distribution of GT1b was determined in the sera of Lewis rats during the different period of myelination, characterized morphologically and histochemically by us in previous investigations [23].

Materials and Methods

Serum Samples

Sera were obtained from fifteen 9-day-old Lewis rats (the period of premyelination) (I group), fifteen 18-day-old Lewis rats (the period of active myelination) (II group) and from twenty-five 3-months old Lewis rats (the period after completion of myelination) (III group).

The relative distribution of four gangliosides (GM3, GM1, GD1a and GT1b) in the serum of Lewis rats of the three animal groups was recalculated on the basis of densitograms.

Isolation of serum gangliosides was performed by the method of I l i n o v et al. [8]. It includes the following stages:

a) dehydration of the sample by azeotropic distillation of the mixture of serum water/n-propanol = 1:10 (v/v);

b) total lipid triple extraction with cyclohexane; chloroform:methanol =1:1 (v/v) and chloroform:methanol = 1:2 (v/v);

c) non-polar lipids removal by preparative TLC with a mobile phase: chloroform : methanol: 0,3 % $CaCl_2$ = 30:18:4 (v/v/v);

d) elimination of the blood sugar by Sep Pak technique according to W i l l i a m s and M c C l u e r [20];

e) HPTLC of the ganglioside fractions with a mobile phase: chloroform:methanol: 0,1 M sodium lactate = 55:40: 10 (v/v/v).

The spots were visualized by spraying with orcinol reagent followed by local heating at 110°C and the gangliosides were quantified densitometrically. Bovine brain gangliosides (Calbiochem) and GM3 ganglioside (Sigma) were used as a test mixture for identification. Four independed analysis and quantification were conducted for each experimental group.

The relative distribution of five serum gangliosides (GM3, GM1, GD1a, GD1b and GT1b) in the serum of Lewis rats during the premyelination period, the period of active myelination and the period after completion of myelination was recalculated on the basis of densitograms (Fig. 1).

The Student's t-test was used to determine statistical differences between the groups using P value of less than 0,05 as the level of confidence.

Results

During the myelination of Lewis rats brain the relative proportion of GT1b in the serum increases from 14.30% at the premyelination period (I group) to 24.00% during the period of active myelination (II group). The relative content of GT1b decreases to 5.17% in the serum of Lewis rats after the completion of myelination (III group) (Fig. 2).

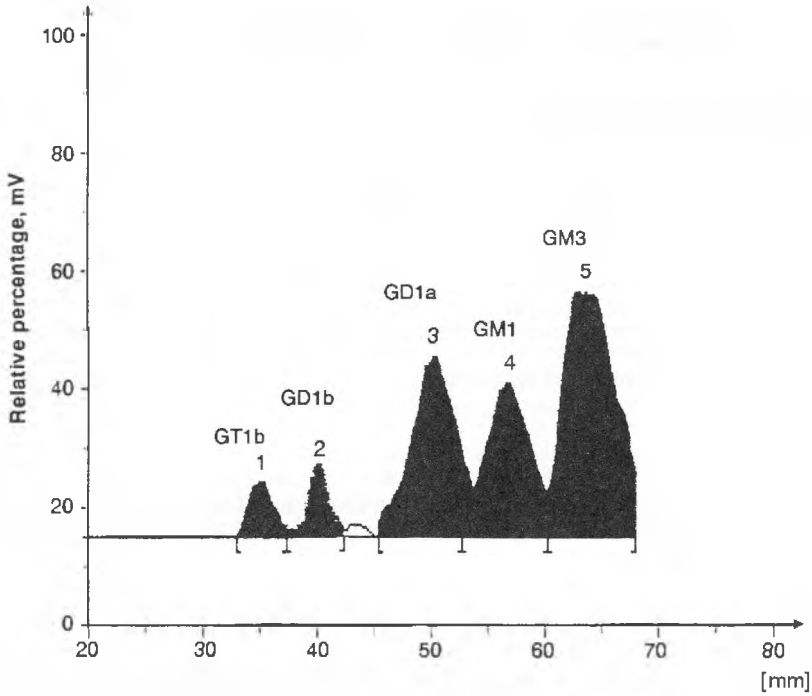

Fig. 1. Densitogram of Lewis Rats Serum Gangliosides

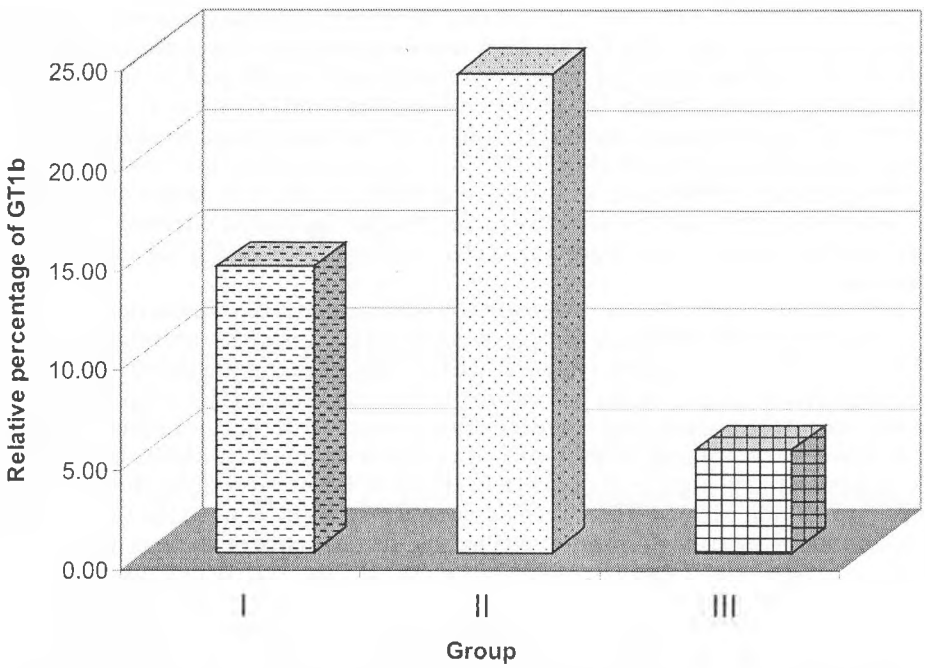

Fig. 2. Percentage Distribution of GT1b in the Serum of Lewis Rats during the Different Periods of Brain Myelination (in relative %) (I group — premyelination period; II group — period of active myelination; III group — period after completion of myelination)

The difference in relative proportion of GT1b between third group and the first and the second groups was statistically significant ($p < 0.05$) (Table 1).

Table 1. Relative Percentage of Major Gangliosides in the Serum of Lewis Rats during the Myelination in the Brain

Gangliosides	I group (n=15)	II group (n=15)	III group (n=25)
GT1b	14.30 ± 0.07	24.00 ± 0.05	5.17 ± 0.04
GD1b	42.20 ± 0.06	20.71 ± 0.04	6.94 ± 0.07
GD1a	2.90 ± 0.10	37.06 ± 0.06	19.07 ± 0.05
GM1	6.00 ± 0.08	5.14 ± 0.07	12.75 ± 0.04
GM3	34.20 ± 0.04	13.09 ± 0.08	56.07 ± 0.03

I group — premyelination period; II group — period of active myelination; III group — period after completion of myelination.

Discussion

The present study shows a high level of GT1b in the sera of Lewis rats before the onset of myelination and during the active myelination in the brain in comparison with the period of completed myelination.

The onset of myelination in rat brain is around the 10th postnatal day. For the beginning of this procees the myelinating oligodendrocyte must recognize the axon to be myelinated. The strategic location of gangliosides on the outer surface of the neural membranes, coupled with the great variability possible in the configuration of their oligosacharide chains makes them excellent candidates for selective intercellular recognition and/or adhesion molecules [10].

T i e m e y e r et al. [15] have reported that rat brain membrans contain a high-affinity structural specific protein for GT1b. They demonstrated that this receptor is found on central nervous system myelin and suggested that it may be positioned to mediate interactions between oligodendroglia and axons. On the other hand, Y a n g et al. [21] and C o l l i n s et al. [2] have proposed that GD1a and GT1b serve as complementary ligands for myelin-assosiated glycoprotein (MAG). MAG, a minor constituent of oligodendrocytes, is localized predominantly to the periaxonal glial plasmolemma [16]. Because of its periaxonal location, it is postulated that MAG may mediate axon-glial interactions [17]. The studes of S h e i k h et al. [13] on GM2/GD2 synthase knockout mice supported this hypothesis.

During the period of active myelination (17-20 postnatal days in the rat brain), when the compact myelin membrane is being formed, the interactions between oligodendrocytes and axons continue to be of great importance [24]. Since GT1b gangliosides play a role in mediating these interactions, the findings in our previuos studies [4] that GT1b fraction is predominant in the brain during premyelination period and during the active myelination, do not seem to be surprising. These results are in full concordance with the data presented here demonstating a high level of GT1b in serum of Lewis rats during the above mentioned myelination periods. There is an apparent correlation between the GT1b levels in the brain and in the serum during the myelination. The existence of such correlation is due to the fact that the blood-brain barrier in rats is not fully developed until postnatal day 24 [12]. Therefore, serum GT1b gangliosides could be used as markers of myelination, remyelination and demyelination (when the interactions between axons and oligodendroglia are disturbed). We recently first reported a significant decrease of relative portion of GT1b in the brain of Lewis rats with chronic relapsing experimental allergic encephalomyelitis, a demyelinating disease [27]. In the serum of these animals there was a significant decrease of GT1b (unpublished observations).

In conclusion, the data presented in this study clearly demonstrate for the first time that the content of GT1b in the serum of Lewis rats alter considerably during brain myelination. This finding further support the concept concerning the role of GT1b in mediating the interactions between oligodendroglia and axons, needful for myelination and maintenance the integrity of myelin sheath. Therefore, serum GT1b gangliosides could be monitored as markers of myelination and remyelination in the brain.

Acknowledgments. We thank Ginka Zaharieva for excellent technical assistance.

References

1. Cochran, F., R. Yu, R. Leeden. Myelin gangliosides in vertebrates. – J. Neurochem., **39**, 1982, 773-779.
2. Collins, B., L. Yang, G. Mukhopadhyay, M. Filbin, M. Kiso, A. Hasagawa, R. Schnaar. Sialic acid specifity of myelin-associated glycoprotein binding. – Amer. Soc. Biochem. Molec. Biol., **272**, 1997, No 2, 1248-1255.
3. Deleva, D., E. Zaprianova, P. Ilinov. Changes of major gangliosides in mouse medulla oblongata during myelination. – Compt. rend. Acad. Bulg. Sci., **45**, 1992, No 10, 123-126.
4. Deleva, D., E. Zaprianova, P. Ilinov. Ganglioside changes in rat medulla oblongata during myelination. – Compt. rend. Acad. Bulg. Sci., **46**, 1993, No 9, 113-116.
5. Dyatlovitskaya, E. Blood serum gangliosides and antibodies to gangliosides. – Biokhimiya, **57**, 1992, 1004-1010.
6. Higashi, H., Y. Hirabayashi, M. Hirota, M. Matsumoto, S. Kato. Detection of ganglioside GM2 in sera and tumor tisues of hematoma patients. – Japan J. Cancer. Res. (Gann), **78**, 1987, 1309-1313.
7. Hsiao, S., E. Hogan, A. Koonts, T. Traylor. Serum gangliosides in cerebral astrocytoma. – Ann. Neurol., **8**, 1980, 534-538.
8. Ilinov, P., D. Deleva, S. Dimov, E. Zaprianova. A variant for isolation of serum gangliosides. – J. Liquid Chrom. Rel. Technol., **20**, 1997, No 8, 1149-1157.
9. Ledeen, R. Gangliosid e structures and distribution: are they localized at the nerve ending? – J. Supramol. Struct., **8**, 1978, 1-17.
10. Ledeen, R. Gangliosides of the neuron. – Trends Neuron., **8**, 1985, 169-174.
11. Prokazova, N., L. Bergelson. Gangliosides and atherosclerosis. – Lipids, **29**, 1994, 1-5.
12. Schulze, C., J. Firth. Interendothelial junctions during blood-brain barrier development in the rat: morphological changes at the level of individual tight junctional contacts. – Brain Res. Dev., **69**, 1992, No 1, 85-95.
13. Sheikh, K., J. Sun, Y. Liu, H. Kawai, T. Crawford, R. Proia, J. Griffin, R. Schnaar. Mice lacking complex gangliosides develop Wallerian degeneration and myelination defects. – Proc. Natl. Acad. Sci. USA, **96**, 1999, 7532-7537.
14. Suzuki, K. Gangliosides and disease: a review in – Adv. Exper. Med. Biol., 174, 1985, 407-418.
15. Tiemeyer, M., P. Swank – Hill, R. Schnaar. A membrane receptor for gangliosides is associated with central nervous system myelin. – J. Biol. Chem., **265**, 1990, 11990-11999.
16. Trapp, B., S. Andrews, C. Cootauco, R. Quarles. The myelin-associated glycoprotein is enriched in multivesicular bodies and peiaxonal membranes of actively myelination oligodendrocytes. – J. Cell. Biol., **109**, 1989, 2417-2426.
17. Trapp, B. Myelin-associated glycoprotein. Location and potential functions. – Ann. N. Y. Acad. Sci., **605**, 1990, 29-43.
18. Vanier, M., M. Holm, R. Öhman, L. Svennerholm. Developmental profiles of gangliosides in human and rat brain. – J. Neurochem., **18**, 1971, 581-592.
19. Wiegandt, H. Gangliosides: a review with 677 references. – New Compr. Biochem., 10, 1985, 199.
20. Williams, A., R. McCluer. The use of Sep-Pak C18 cartridges during the isolation of gangliosides. – J. Neurochem., **35**, 1980, 266-270.
21. Yang, L., C. Zeller, N. Shaper, M. Kiso, A. Hasegawa, R. Shapiro, R. Schnaar. Gangliosides are neuronal ligands for myelin-associated glycoprotein. – Proc. Natl. Acad. Sci. USA, **93**, 1996, 814-818.
22. Yu, R., K. Iqbal. Sialosylgalactosyl ceramide as a specific marker for human myelin and oligodendroglial perikarya: gangliosides human myelin, oligodendroglia and neurons. – J. Neurochem., **32**, 1979, 293-300.

23. Z a p r i a n o v a, E. Myelination in the Central Nervous System. Sofia, Publ. House Bulg. Acad. Sci., 1980. 124 p.
24. Z a p r i a n o v a, E. Neuronal-glial cooperation in the production of myelin phospholipids. – Acta cytobiol. et morphol., **1**, 1989, 5-11.
25. Z a p r i a n o v a, E., D. D e l e v a, K. M a j t e n y i, E. S u l t a n o v, A. F i l c h e v, B. S u l t a n o v, V. K o l y o v s k a. Serum GD1a ganglioside in patterns in multiple sclerosis. – Acta morphol. et anthropol., **8**, 2003, 3-7.
26. Z a p r i a n o v a, E., D. D e l e v a, P. I l i n o v, E. S u l t a n o v, A. F i l c h e v, L. C h r i s t o v a, B. S u l t a n o v. Serum ganglioside patterns in multiple sclerosis. – Neurochem. Research, **26**, 2001, No 2, 95-100.
27. Z a p r i a n o v a, E., D. D e l e v a, A. F i l c h e v, V. K o l y o v s k a, B. S u l t a n o v. GT1b ganglioside brain changes in chronic relapsing experimental allergic encephalomyelitis induced in the Lewis rats. – Acta morphol. et anthropol., **10**, 2005, 9-12.

Institute of Experimental Morphology and Anthropology with Museum
Bulgarian Anatomical Society

Acta morphologica et anthropologica, 12
Sofia • 2007

Neuronal Degeneration at the Earliest Stages of Multiple Sclerosis

B. Sultanov

Institute of Experimental Morphology and Anthropology with Museum, Bulgarian Academy of Sciences, Sofia

In recent years, has become more evident that neuronal damage is an early pathological sign in multiple sclerosis (MS). In our study, we analysed cervical spinal cord specimens from MS patients, died accidentally during the first five years of disease duration. A severe degeneration of anterior horn neurons was detected in the specimens from two patients suffered of MS only one year. This finding reveals for the first time neuronal injury very early in MS pathogenesis. It further support the concept of multiple sclerosis as a neurodegenerative disorder. The data of the present investigation argue once again for the early neuroprotective treatment of MS patients.

Key words: multiple sclerosis, cervical spinal cord, neuron, degeneration.

Introduction

Multiple sclerosis (MS) is considered to be prototype of acquired primary demyelinating disease in the central nervous system (CNS) with extensive myelin loss and relative preservation of neurons [10]. According to this concept neuronal and axonal injury is not a dominating feature of early MS and is believed to occur as a consequence of demyelination. However, recent imaging and morphological studies has challenged this historical view of preserved neuronal and axonal integrity at the earliest clinical stages of MS [11]. Proton magnetic resonance (MR) spectroscopy by monitoring levels of N-acetylaspartate, a putative marker of axonal integrity, has been particularly illuminating by showing indirect evidence of neurodegeneration in both lesional and non-lesional brain tissues from the earliest stages of MS [3]. F i l l i p p i et al. [4] used MR imaging and spectroscopy to study abnormalities in the brain of patients with MS. They concluded that axonal and neuronal injury occurs early in the course of MS, leading to widespread damage even before the disease is diagnosed clinically. K u h l m a n n et al. [6] investigated the occurrence of acute axonal damage determined by immunocytochemistry for amyloid precursor protein (APP) which is produced in neurons and accumulates at sites of recent axon damage. Most APP-positive axons were detected within the first year after disease onset. In previous electronmicroscopic studies of ours we observed axonal degeneration which preceded demyelination in the spinal cord of Lewis rats before the onset of clinical symptoms of chronic relapsing experimental allergic encephalomyelitis (CREAE), an animal model

of MS [15]. Neuronal death also in the preclinical stage of EAE was reported by H o b o m et al. [5]. However, there are no data illustrating directly neuronal injury in early MS. Therefore, the aim of the present study was to look for neuronal changes during the early stages of MS analysing cervical spinal cord sections from clinically defined MS patients, died accidentally during the first five years of the disease.

Materials and Methods

Cervical spinal cord sections from 9 multiple sclerosis cases and from 5 control cases were used in this study from the large pathomorphological collection in the Department of Neuropathology at the Institute of Psychiatry and Neurology in Budapest, Hungary. All MS cases were patients with clinically defined MS [according to 9]. Three of them suffered of early MS (course of the disease of one year) and five of them have MS for 3-5 years. Causes of death included myocardial infarction (seven cases) and suicide (two cases). The controls were patients who died of nonneurological diseases and without pathological changes within CNS.

Sections were stained using routine neuropathological staining for neurons, glia and myelin (Nissl staining and luxol fast blue staining).

Results

Severe degeneration of motoneurons in the anterior horn, demonstrated by Nissl staining, was detected in the sections of the cervical spinal cord of two patients suffered of MS with only one year course of the disease (cause of death — suicide) (Fig. 1 and Fig. 2). Demy-

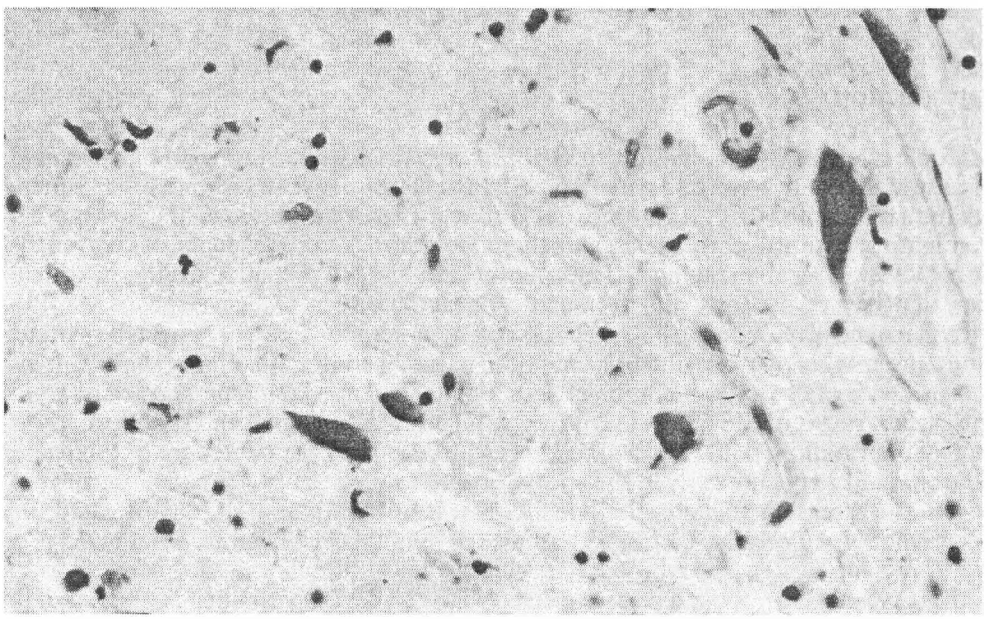

Fig.1. Degenerated motoneurons in the anterior horn of the cervical spinal cord of a patient with early MS (one year course). Nissl staining (× 250)

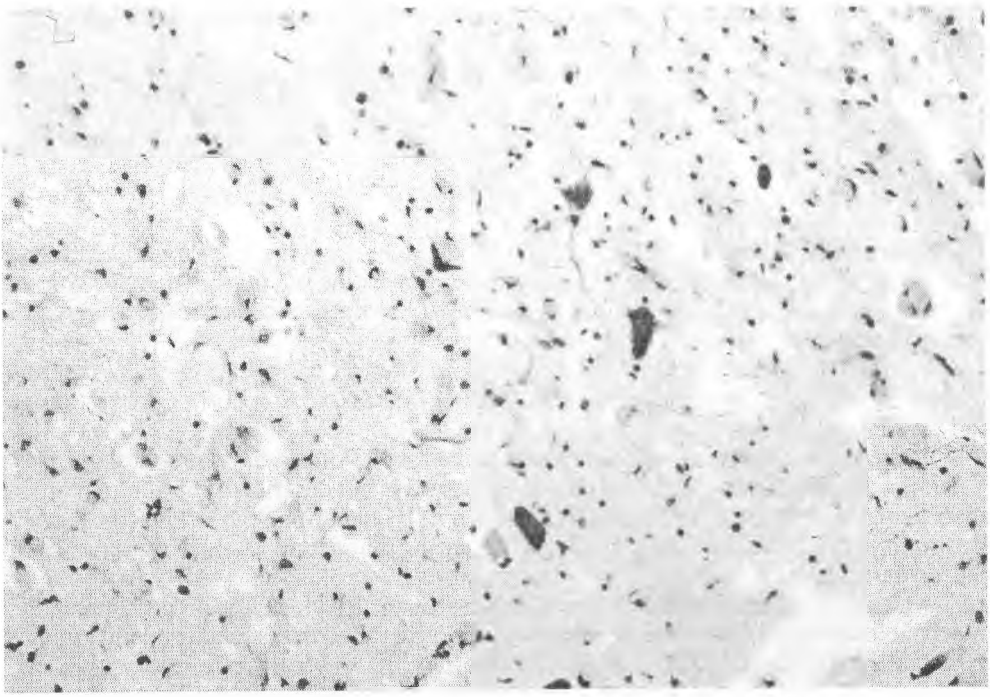

Fig. 2. Severe destruction of anterior horn neurons of the cervical spinal cord of another patient with early MS (one year course). Nissl staining (× 200)

Fig. 3. Demyelination of lateral pyramidal tract in the cervical spinal cord of a patient with early MS (one year course). Pallor of the pyramidal tract. Luxol fast blue staining (× 100)

elination of lateral pyramidal tract in cervical spinal cord was present, detected by the pallor of the tract after luxol fast blue staining (Fig. 3).

Degenerated anterior horn neurons were not found in the sections of the cervical spinal cord of others MS cases and of controls.

Discussion

The analysis of specimens from patients dying accidentally at earliest stages of MS (one year duration of the disease) revealed neuronal degeneration of anterior horn neurons in the cervical spinal cord. The cervical spinal cord has been chosen for the analysis of neuronal changes in early MS for two reasons:

a) multiple sclerosis in the spinal cord is a common presentation of the disease. Involvement of the long tracts leads to muscular weakness, sensory loss or paraesthesiae and bladder disturbances;

b) the cervical part is the most common site for MS plaques in the spinal cord [1]. Neuronal degeneration so early in MS pathogenesis was not described. Our findings are in accordance with the observations of L a s s m a n n [7] concerning the lesions in CREAE. He found in one animal in addition of demyelinating plaques an extensive anterior horn neuron destruction.

As it was mentioned above, neuronal cell death was detected to occur even before the onset of clinical symptoms of EAE [5]. The authors analysed the mechanism and kinetics of retinal ganglion cell (RGC) apoptosis by combining an electrophysiological in vivo assessment of the optic pathway with the investigation of RGC counts. They found that RGC death together with decreased visual acuity values was present before the appearance of clinical symptoms of EAE. N i c o t et al. [8] investigated the expression of genes encoding proteins that play critical roles in ions homeostasis, exocytosis, mitochondrial function and impulse conduction in the Lewis rat lumbar spinal cord during the clinical course of acute EAE. The results of their study concerning the regulation of gene expression in EAE indicate early neuronal dysfunction.

In our previous study an increase of GD1a ganglioside, one of the major human brain neuronal ganglioside fraction, was observed in the serum of patients with MS during their first attacks of the disease [14]. It was suggested that this increase is connected with the neuronal damage in early phases of MS pathogenesis.

Our findings and the data of the others authors cited above provide evidence of early neuronal injury in MS and EAE. They further support the concept of multiple sclerosis as a neuronal ganglioside ganglioside disease [12]. For the first time Z a p r i a n o v a [13] suggested that the neuronal disturbance could have some as yet undemonstrated role in MS. C h a u d h u r i and B e h a n [2] proposed that MS is not an autoimmune disease but a genetically determined disorder characterized by metabolically dependent neurodegeneration.

In conclusion, the present study reveals for the first time a severe degeneration of anterior horn neurons in cervical spinal cord of MS patients, died accidentally during the first year of the disease. The detection of neuronal injury at the earliest stages of MS argue once again for the early treatment of MS patients with agents directed towards neuronal protection.

Acknowledgements. I am grateful to Dr. Katalin Majtenyi, PhD for the priviledge of using her pathomorphological collection for my study.

References

1. A d a m s, C. W. A Colour Atlas of Multiple Sclerosis & Other Myelin Disorders. Ipswich, Suffolk, Wolfe Medical Publications Ltd, 1989. 226 p.
2. C h a u d h u r i, A., P. O. B e h a n. Multiple sclerosis is not an autoimmune disease. – Arch. Neurol., **61**, 2004, No 10, 1613-1615.
3. De S t e f a n o, N., M. L. B a r t o l o z z i, L. G u i d i, M. L. S t r o m i l l o, A. F e d e r i c o. Magnetic resonance spectroscopy as a measure of brain damage in multiple sclerosis. – J. Neurol. Sci., **15**, 2005, No 1-2, 203-208.
4. F i l i p p i, M., M. B o z z a l i, M. R o v a r i s. Evidence for widespread axonal damage at the earliest clinical stage of multiple sclerosis. – Brain, **126**, 2003, 433-437.
5. H o b o m, M., M. K. S t o r c h, R. W e i s e r, K. M a i e r, A. R a d h a k r i s h n a n, B. K r a m e r. Mechanisms and time course of neuronal degeneration in experimental autoimmune encephalomyelitis. – Brain Pathol., **14**, 2004, No 2, 148-157.
6. K u h l m a n n, T., G. L i n g f e l d, A. B i t s c h, J. S c h u c h a r d t, W. B r u c k. Acute axonal damage in multiple sclerosis in early disease stages and decreases over time. – Brain, **125**, 2002, No 10, 2202-2212.
7. L a s s m a n n, H. Comparative Neuropathology of Chronic Experimental Allergic Encephalomyelitis and Multiple Sclerosis. Berlin, Heidelberg, New York, Tokyo, Springer — Verlag, 1983. 135 p.
8. N i c o t, A., P. V. R a t n a k a r, Y. R o n, C. C. C h e n, S. M o r i c. Regulation of gene expression in experimental autoimmune encephalomyelitis indicates early neuronal dysfunction. – Brain, **126**, 2003, 398-412.
9. P o s e r, C., D. P a t y, L. S c h e i b e r g. New diagnostic criteria for multiple sclerosis: guidelines for research protocols. – Ann. Neurol., **13**, 1983, 227-231.
10. S t o r c h, M., H. L a s s m a n n. Pathology and pathogenesis of demyelination diseases. – Curr. Opin. Neurol., **45**, 1991, 37-45.
11. S u l t a n o v, B. Neuronal and axonal damage in early multiple sclerosis. – Acta morphologica et anthropologica, **9**, 2004, 208-210.
12. W a x m a n, S. Multiple sclerosis as a neuronal disease. – Arch. Neurol., **57**, 2000, 22-24.
13. Z a p r i a n o v a, E. Central nervous system myelin sheath. – In: Abstr. Regional South-East Europ. Conf. Neurol. Varna, 1984, p. 107.
14. Z a p r i a n o v a, E., D. D e l e v a, K. M a j t e n y i, E. S u l t a n o v, A. F i l c h e v, B. S u l t a n o v, V. K o l y o v s k a. Serum GD1a gandlioside in patients with multiple sclerosis. – Acta morphologica et anthropologica, **8**, 2003, 3-7.
15. Z a p r i a n o v a, E., D. D e l e v a, B. S u l t a n o v, A. F i l c h e v. Early axonal damage in chronic relapsing allergic encephalomyelitis. – In: Jubilee Scientific Collection. Sofia, 2003, 95-96.

Institute of Experimental Morphology and Anthropology with Museum
Bulgarian Anatomical Society

Acta morphologica et anthropologica, 12
Sofia • 2007

Changes of the Glycolipid Content in Rat Brain and Brain Subcellular Fractions in An Experimental Model of Cerebral Ischemia

E. Petrova, A. Dishkelov, E. Vasileva

Institute of Experimental Morphology and Anthropology with Museum, Bulgarian Academy of Sciences, Sofia

In this study, we present data from our examinations of the changes of glycolipid content in rat brain and different brain subcellular fractions in a model of cerebral ischemia. In control rats, the total glycolipid content was the highest in nuclei and the lowest in the brain homogenate. Gangliosides and cerebrosides were the major glycolipid classes and they ranged from 34% to 72% and from 28% to 66% of total glycolipids in different subcellular fractions, respectively. Cerebral ischemia led to increase of total glycolipids with the largest increase in the homogenate and microsomes — 89 and 20 times the control values, respectively. The total glycolipid content was the highest in the brain homogenate and the lowest in myelin. The accumulation of glycolipids may be interpreted as a physiological adaptive response to ischemia.

Key words: glycolipids, cerebral ischemia, subcellular fractions, rat brain.

Introduction

Glycolipids are important constituents of cells and their concentration is highest in the nervous system. Beyond structural functions, glycolipids play a variety of biological functions, including cellular recognition and adhesion as well as signalling [1, 9, 12]. These lipids can serve as tumor markers and membrane regulatory factors [3]. A number of studies have shown that gangliosides are immunogenic and they participate in multiple sclerosis pathogenesis [10].

Membrane lipid degradation plays an important role in the pathogenesis of ischemic brain damage, but there is little information on changes in total glycolipids, cerebrosides and gangliosides. The present study was undertaken to evaluate the level of glycolipids in brain homogenate and different subcellular fractions from both normal and ischemic rat brains.

Materials and Methods

Three-month-old male Wistar rats were used in the experiment. Animals were subjected to cerebral ischemia according to the model of S m i t h et al. [7] with minor modifications.

Brain subcellular fractions were isolated according to the method described by V e n k o v [11]. Lipids were extracted according to the technique described by K a t e s [13]. The content of total glycolipids was determined according to H a m i l t o n et al. [2]. Glycolipid classes were separated by thin-layer chromatography using the following eluate: chloroform:methanol:water 65:25:4 (v/v/v). The Perkin-Elmer scanning spectrophotometer was used to estimate the concentration of migrated spots.

The data were analyzed with Student's t-test.

Results

The content of total glycolipids in brain homogenate and different subcellular fractions is shown in Table 1. In control rats, total glycolipids had the highest concentration in nuclei (0.54±0.04 mg/g/ml) and the lowest in the brain homogenate (0.181±0.02 mg/g/ml). Gangliosides and cerebrosides were the two main glycolipid classes and they accounted for 34% to 72% and for 28% to 66% of total glycolipids in different subcellular fractions, respectively (Fig. 1).

Table 1. Changes of the glycolipid content in rat brain after cerebral ischemia

Brain fraction		Gangliosides	Cerebrosides	Total glycolipids
Hom	Control	0.068±0.01	0.112±0.01	0.181±0.02
	Ischemia	4.744±0.06 $p<0.001$	11.354±0.06 $p<0.001$	16.098±0.12 $p<0.001$
Nuc	Control	0.216±0.02	0.324±0.03	0.54±0.04
	Ischemia	1.363±0.05 $p<0.001$	2.006±0.05 $p<0.001$	3.368±0.04 $p<0.001$
Ms	Control	0.212±0.03	0.082±0.05	0.294±0.04
	Ischemia	2.503±0.04 $p<0.001$	3.372±0.05 $p<0.001$	5.875±0.04 $p<0.001$
Myel	Control	0.107±0.03	0.118±0.03	0.225±0.04
	Ischemia	0.093±0.004 *ns*	0.307±0.02 $p<0.001$	0.4±0.02 $p<0.001$
Syn	Control	0.227±0.04	0.23±0.4	0.457±0.08
	Ischemia	0.443±0.05 $p<0.001$	0.614±0.03 $0.1<p<0.05$	1.057±0.05 $p<0.001$
Mit	Control	0.161±0.05	0.317±0.02	0.478±0.05
	Ischemia	1.526±0.05 $p<0.001$	1.349±0.06 $p<0.001$	2.875±0.09 $p<0.001$

Hom=homogenate; Nuc=nuclei; Ms=microsomes; Myel=myelin; Syn=synaptosomes; Mit=mitochondria. Values are expressed in mg/g dry lipid residue/ml, $n=5$, *ns* – indicates no significant difference.

In the brains of rats subjected to cerebral ischemia, we found increased levels of total glycolipids, gangliosides and cerebrosides in all subcellular fractions (Table 1). The increase of total glycolipids was the highest in the homogenate and microsomes – 89 and 20 times, respectively. Gangliosides made up to 23-53% of the total glycolipids in different fractions (Fig. 1). The brain homogenate contained the highest amounts of gangliosides (4.744±0.06 mg/g/ml) and myelin the lowest (0.093±0.004 mg/g/ml). Cerebrosides accounted for 47 to 77% of total glycolipids in different fractions (Fig. 1). The highest concentration of cerebrosides was observed in the brain homogenate (11.354±0.06 mg/g/ml) and the lowest (0.307±0.02 mg/g/ml) in myelin.

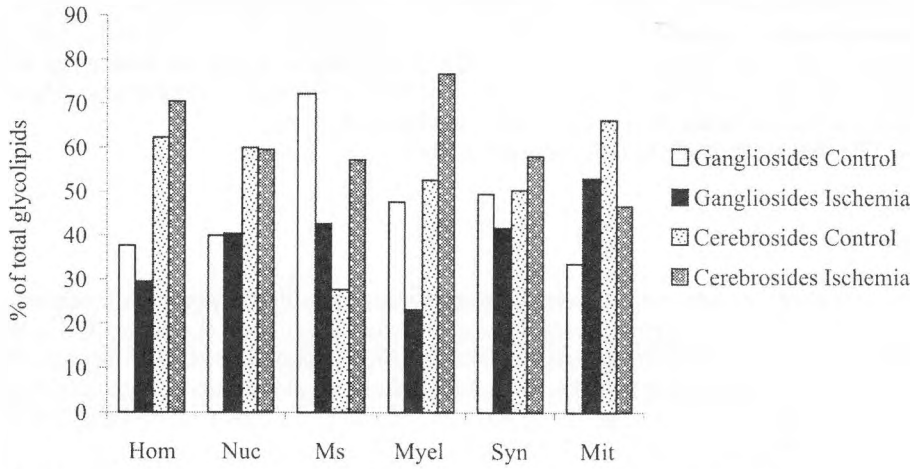

Fig. 1. Changes of gangliosides and cerebrosides in rat brain after cerebral ischemia

Discussion

In this study, we examined the changes in glycolipid content of rat brain homogenate and brain subcellular fractions in an experimental model of cerebral ischemia.

In controls, we found the highest content of total glycolipids in the nuclear fraction and it can be suggested that these lipids influence the membrane-mediated processes in the nuclei. Nuclei contained the highest amounts of cerebrosides in comparison to the homogenate and the other subcellular fractions. Gangliosides in the nuclear membrane probably play a key role in maintaining the nuclear Ca^{2+} homeostasis. Some studies suggest the presence of limited intranuclear pools of gangliosides [4].

Gangliosides are probably synthesized in the membranes of endoplasmic reticulum and this explains the observed high content of gangliosides in microsomal fraction. This proposition is supported by studies on subcellular distribution of the enzymes involved in ganglioside synthesis [9].

In myelin cerebrosides together with the polar head groups of phosphatidylserine and phosphatidylinositol provide a polyanionic surface array. Strong interactions with both the positively charged myelin basic protein at the cytosolic and hydrophobic domains of proteolipid protein at the extracytoplasmic surface might contribute to the tight compaction of the multilayer membrane system [1].

Synaptosomes contained the highest amounts of gangliosides in comparison to the homogenate and the other subcellular fractions and these results are in agreement with previous reports [14]. These data suggest the specific role of gangliosides in synaptic transmission. Gangliosides are thought to be functional in memory formation too [6, 8].

In mitochondria gangliosides probably influence the Ca^{2+} homeostasis and ionic balance and contribute to the high permeability of the mitochondrial membrane.

In the brains of rats subjected to cerebral ischemia, we found an increase in both gangliosides and cerebrosides in all subcellular fractions. As a result the total glycolipids estimated increased from 2 to 89 times in different fractions. The high concentration of glycolipids and especially gangliosides can apparently be explained by their neuroprotective effect. It is supposed that gangliosides can acutely reduce the extent of CNS injury by protection of membrane structure and function [5]. Another hypothesis sup-

ports the view that gangliosides may promote neuronal regeneration through modulation of trophic factors.

The high content of cerebrosides after ischemia probably makes the membranes steadier and it appears to be a protective and compensatory mechanism against ischemic damage. Most probably, cerebrosides contribute to a dense network of H-bonding between three hydroxy groups of cholesterol, the hydroxy group of the sphingosine, the hydroxy groups of the acyl chains and the amide bond of the sphingolipids [1].

In conclusion, the present results show that cerebral ischemia disrupts to a great extent the brain lipid metabolism and in particular the glycolipid metabolism. The accumulation of glycolipids may indicate the energy disturbances and concomitant restriction of glucose supply to the ischemic brain and may be interpreted as a physiological adaptive response to ischemia.

Acknowledgements: This study was supported by National Science Fund of Bulgaria (NSFB) under Contract MU-L-1512/05.

References

1. Bosio, A., E. Binczek, W. Stoffel. Functional breakdown of the lipid bilayers of the myelin membrane in central and peripheral nervous system by disrupted galactocerebroside synthesis. – Proc. Natl. Acad. Sci. U. S. A., **93**, 1996, 13280-13285.
2. Hamilton, P. B. A spectrometric determination of glycolipids. – Anal. Chem., **28**, 1956, 557-565.
3. Kolyovska, V. Gangliosides: chemical characterization, isolation, biological functions, role in autoimmune demyelinating diseases. – Acta morphol. et anthropol., **9**, 2004, 202-207.
4. Ledeen, R. W., G. Wu. Nuclear lipids: key signaling effectors in the nervous system and other tissues. – J. Lipid Res., **45**, 2004, 1-8.
5. Mahadik, S. P., S. K. Karpiak. Gangliosides in treatment of neural injury and disease. – Curr. Trends Rev., **15**, 2004, No 4, 337-360.
6. Rahmann, H. Brain gangliosides and memory formation. – Behav. Brain Res., **66**, 1995, No 1-2, 105-116.
7. Smith, M.-L., G. Bendek, N. Dahlgren, I. Rosén, T. Wieloch, B. K. Siesjö. Models for studying long-term recovery following forebrain ischemia in the rat. 2.A 2-vessel occlusion model. – Acta Neurol. Scand., **69**, 1984, 385-401.
8. Svennerholm, L. Gangliosides and synaptic transmission. – Adv. Exp. Med. Biol., **125**, 1980, 533-544.
9. Yu, R. K., E. Bieberich, T. Xia, G. Zeng. Regulation of ganglioside biosynthesis in the nervous system. – J. Lipid Res., **45**, 2004, 783-793.
10. Zaprianova, E., D. Deleva, P. Ilinov, E. Sultanov, A. Filchev, L. Christova, B. Sultanov. Serum ganglioside patterns in multiple sclerosis. – Neurochem. Res., **26**, 2001, No 2, 95-100.
11. Венков, Л. Получаване на обогатени фракции на елементи, изграждащи нервната тъкан. – Съвр. пробл. невроморфол., **11**, 1983, 1-60.
12. Венков, Л., А. Дишкелов. Липиди в нервната тъкан. София, БАН, 1985, с. 69.
13. Кейтс, М. Техника липидологии. Москва, Мир, 1975, с. 76.
14. Таранова, Н. Липиды центральной нервной системы при повреждающих воздействиях. Ленинград, Наука, 1988, с. 158.

Institute of Experimental Morphology and Anthropology with Museum
Bulgarian Anatomical Society

Acta morphologica et anthropologica, 12
Sofia • 2007

Structural Examination of Tryptase-, Chymase-, SP-, and VIP-Positive Mast Cells in the Human Common Bile Duct and Liver

*Maya Gulubova, Angel Vodenicharov**

Department of General and Clinical Pathology, Faculty of Medicine
**Department of Veterinary Anatomy, Histology and Embryology,*
Faculty of Veterinary Medicine, Trakia University, Stara Zagora, Bulgaria

Human mast cells are divided into two subsets: mast cells with reactivity for tryptase but not chymase (MC_T) and reactive for tryptase and chymase (MC_{TC}). We investigated the MC_T and MC_{TC} subtypes in human livers containing metastases from gastrointestinal cancers and in the common bile duct in obstruction. We have found that there were increased numbers of mast cells (MC_T and MC_{TC}) in the surrounding liver parenchyma and in liver metastases originating from gastric, colorectal and pancreatic cancers. In the common bile duct with obstruction we detected greatly increased numbers of mast cells. Among the studied mast cell types MC_{TC} ones were the most numerous.

The ultrastructural appearance of tryptase- and chymase-positive mast cells showed three different types of granules, concerning the content of the reaction product (altered granules). These types were observed in the livers with metastases and in the inflamed common bile duct. In conclusion it can be stated that mast cells in human livers with metastases and in the inflamed common bile duct increased in numbers and showed signs of activation.

Key words: mast cells, immunocytochemistry, liver, holedoch.

Introduction

Mast cell heterogeneity is a key issue in mast cell biology [5], but its nature in humans is a subject of uncertainties.

Although the immunopathological role of mast cells has been acknowledged, these cells have aroused much controversy and confusion. One explanation for the contradictory opinions on mast cell function arises from their heterogeneity, which can express itself as differences in histochemical, biochemical, and functional characteristics.

The main criterion for mast cell differentiation in rodents is formalin resistance. In humans, mast cells are distinguished by their content of the mast-cell-specific proteases, chymase and tryptase [18, 22]. Tryptase and chymase are released from mast cells following IgE-mediated activation. In contrast to the findings in rat, where both mast cell serine proteinases are of chymotryptic specifity, only one human mast cell proteinase, chymase, displays this activity whereas the other enzyme, tryptase, is of tryptic specifity [3].

Human mast cells are divided into two subsets: mast cells with reactivity for tryptase but not chymase (MC_T) and reactive for tryptase and chymase (MC_{TC}). The human mast cell chymase belongs to the group of alpha chymases [4]. It is found predominantly in connective tissue mast cells and to a lesser extent in mucosal mast cells [4, 7]. Mast cell tryptase expression is largely confined to mucosal mast cells [4]. In humans, the differentiation of mast cells into mucosal or connective tissue phenotypes is less clear cut than in rodents [17]. Mast cells with variable granule morphologies immunolabelled for tryptase and chymase have been described in human lungs, skin and small intestine [4, 7].

Mast cells are intimately involved into the "cross-communication" between the nervous and immune systems [28, 30]. Mast cells have been shown to release some neuropeptides such as vasointestinal polypeptide (VIP) [8] and substance P (SP) [29, 32]. Biogenic amines secreted by these cells act together with the released biologically active peptides from endocrine cells at mucosal sites [11] thereby contributing to neurophysiological and neuropathological processes.

The role of tryptase- and chymase-positive mast cells for the fibrogenesis, epithelial cell proliferation, metaplasia and inflammatory cells recruitment is already described in other diseases [1, 2, 6, 31].

The biological role of mast cells in liver metastases and in cancer growth still remains speculative. Mast cells contain various bioactive substances such as histamine, heparin, etc. that appear to stimulate both mitogenesis and angiogenesis [6, 24 ,25], which may be detrimental for cancer patients. On the other hand, mast cell-derived tryptase stimulates fibroblasts [26], leading to fibrosis, which can form the stroma of metastasis or may limit tumor growth. Therefore, the study of the density of mast cell subpopulations (MC_{TC} and MC_{TC}) and granule morphology in "normal" livers and in liver metastases from gastric, colorectal and pancreatic cancers elucidated mast cell heterogeneity and functions in humans.

A great amount of mast cells was already noticed in the common bile duct in secondary cholangitis [15]. It will be interesting to disclose the structural morphology and the proportions of the different subsets of these cells and also to discuss their role in physiologic and pathologic conditions. It is also interesting to study the structural morphology and the density of mast cell subpopulations (MC_T and MC_{TC}) in livers containing metastases from gastric, colorectal and pancreatic cancers.

Materials and Methods

Liver metastases. Liver tissue was collected from 30 patients with colorectal (n=15), gastric (n=8), pancreatic (n=7) cancers. The "normal" liver tissue was obtained from 5 patients operated with diagnostic purpose (explorative laparotomy). Controls had no previous history of liver diseases [13].

Extrahepatic bile duct. Surgically resected specimens from the lower part of the common bile duct (at 2 cm distance from the papilla of Vater) were collected from 50 patients (19 men and 31 women), aged between 31 and 81 years. Twenty-six patients (9 men and 17 women) had calcium-bilirubinate stones in the common bile duct, 3 had pancreatic cancers (two men and one woman) and two patients had stenosis (one male and one female). All these lesions caused acute obstruction and extrahepatic jaundice. The biopsy specimens of these patients showed secondary chronic exacerbated cholangitis. Eighteen patients (7 men and 11 women) had previous attacks of calculous obstruction and one woman had stenosis, but at the time of operation showed only secondary chronic sclerotic cholangitis. Biopsy samples were collected after resection of the common bile duct for

drainage and stone extraction. As controls, we obtained 5 specimens from patients (3 men and 2 women) who had died of myocardial infarction and had no pathology of the biliary pathways. Informed consent had been previously obtained from each patient [14].

Cryostat sections cut from one sample were prepared for light and ultrastructural immunocytochemistry. The remainder of the tissue was embedded in paraffin wax for routine histology. The methods were described earlier [13, 14, 15].

Immunochemicals. The antibodies used were mouse anti-human mast cell tryptase [clone AA1 (M7052)], mouse anti-human serotonin (N1530 from Dako, Glostrup, Denmark), mouse anti-human mast cell chymase [clone CC1 (MCA1930)], rabbit anti-human VIP (PEPA41 from Serotec, Oxford, UK), and rabbit anti-human substance P (PEPA40 from Serotec). The DAKO (Glostrup, Denmark) immunostaining detection system kit, the LSAB 2 System and HRP (K0675), was used together with either 3,3'-diaminobenzidine (DAB; from Sigma, St. Louis MO, USA) or 3-amino-9-ethylcarbazole (AEC; from Dako) as the chromogen.

Results and Discussion

Mast cells in human livers with metastases

We have found an increased numbers of mast cells (MC_T and MC_{TC}) in the liver parenchyma, situated around metastases, originating from gastric, colorectal and pancreatic cancers, as compared to controls (2.9 v.s. 0.6 cells/mm^2, p=0.003 for MC_T and 8.6 v.s. 0.7 cells/mm^2, p=0.004 for MC_{TC}). Mast cells were largely located in portal tracts surrounding metastases (13). In the sinusoids there could rarely be observed mast cells. Therefore, we can state that liver sinusoidal mast cells do not increase in parenchyma surrounding metastases from gastric, colorectal and pancreatic cancers [13]. The number of mast cells was great in the stroma of metastasis (6.9 ± 4.8 cells/mm^2 for MC_T и 22.8 ± 14.7 cells/mm^2 for MC_{TC}). Therefore, these cells actively participate in the metastatic process [13].

The current study indicates that human liver mast cells do not react with VIP and SP in "normal" liver or in the presence of metastases.

Two theories have been advocated in literature about intratumoral mast cells. The first is that mast cells may play a role in tumor growth and angiogenesis forming tumor stroma [16, 25]. The second is that mast cells exert cytotoxicity on tumor cells by immunologic mechanisms [12]. In the current work, a relatively large number of mast cells was present in the stroma of metastases and around them, suggesting that the connective tissue formation in liver malignancies may be associated at least in part with the presence of mast cells.

The ultrastructural immunocytochemical localization of tryptase and chymase revealed 3 distribution patterns of the antigen in mast cell granules: granules with darkly precipitated reaction product, electron lucent granules without reaction product and electron lucent granules with sparse reaction product (altered granules). Mast cell granules with MC_{TC}-phenotype had larger diameters (over 0.203 μm) as compared to granules positive only for tryptase (about 0.13 μm) [(7]. The mast cells, described by us in human liver had granules with larger diameters about 0.45 μm. Morphologically, they looked like mast cells with MC_{TC}-phenotype.On the basis of localization of tryptase (Fig. 1) and chymase (Fig. 2) and the mean diameters of granules, these mast cells resembled tryptase/chymase-positive (MC_{TC}) as described by G r a i g et al. [7] in human lung, intestine and skin.

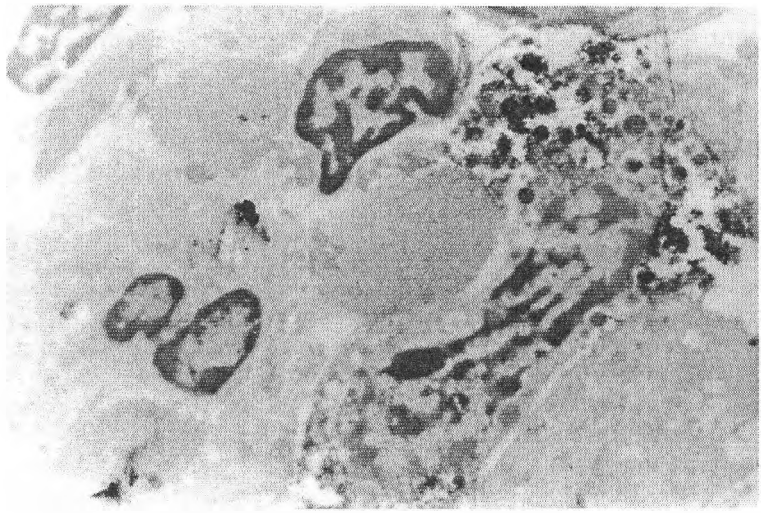

Fig. 1. Tryptase-positive mast cell with many electron dense granules in the portal tract of a liver with metastasis from gastric cancer (× 4400)

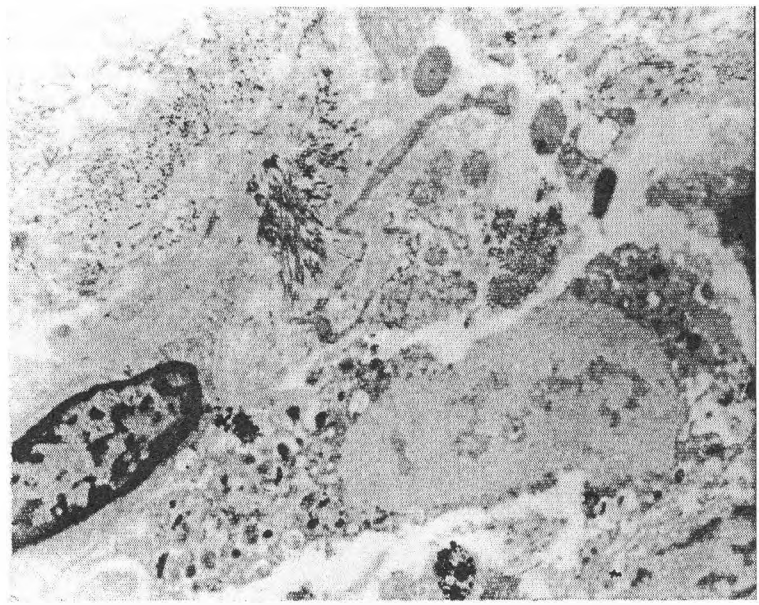

Fig. 2. Chymase-positive mast cell in the liver with metastasis from gastric cancer. Most of the granules are altered with electron-lucent matrices, having sparse amount of reaction product (× 7000)

The "altered granules" with discrete and focally located DAB reaction product observed by us, resembled to these described earlier [4, 19]. The immunoreactivity of mainly chymase and less for tryptase was largely lost in these "altered granules". This can be explained with the degranulation process of mast cells [4]. Chymase and tryptase labelling densities in our study were related to electron dense portions of granules including particulate and lattice patterns, as reported for heparin and histamine [9].

In conclusion, our immunocytochemical ultrastructural study suggested that most of chymase- and tryptase-positive mast cells showed granule diversity with many "altered" granules, considered as a state of activation.

Mast cells in the human common bile duct with obstruction

In the common bile duct with biliary obstruction we detected greatly increased numbers of mast cells [14, 15]. Among the studied mast cell types MC_{TC}-positive ones were the most numerous (mean value of 62.9 ± 14.6 cells/mm^2, $p<0.0001$, Wilcoxon Signed Rank test. VIP-positive mast cells were less in number (26.7 ± 6.6 cells/mm^2), followed by SP-positive mast cells (24.7 ± 6.3 cells/mm^2), and then by mast cells producing only tryptase MC_T (11.3 ± 7.8 cells/mm^2). In addition, some SP-, VIP-, and S-100-positive nerve fibers were observed around glands beneath surface epithelium and in muscle layer. Tryptase-positive mast cells could be found near the nerve cell bodies of multipolar neurons of the ganglionated myenteric plexus. SER-positive nerve fibers and endocrine cells were also found in hyperplastic glands.

Ultrastructural analysis: **Tryptase**-positive mast cell granules were small and large, electron-dense, particulate or with scrolls (Fig. 3). **Chymase**-positive mast cell granules were large as lattice and grating configurations and particulate structure were characteristic for them. The reaction product in both types of cells was precipitated in three different patterns: in large amount over electron-dense granules; or it was sparse over electron-dense regions of the granules (altered granules); or there were observed electron lucent granules without reaction product. We interpreted this as a sign of activation. VIP-positive mast cells contained electron-dense or particulate granules (Fig. 4). SP-positive mast cell granules were mainly of particulate/beaded pattern (Fig. 5) [14, 15].

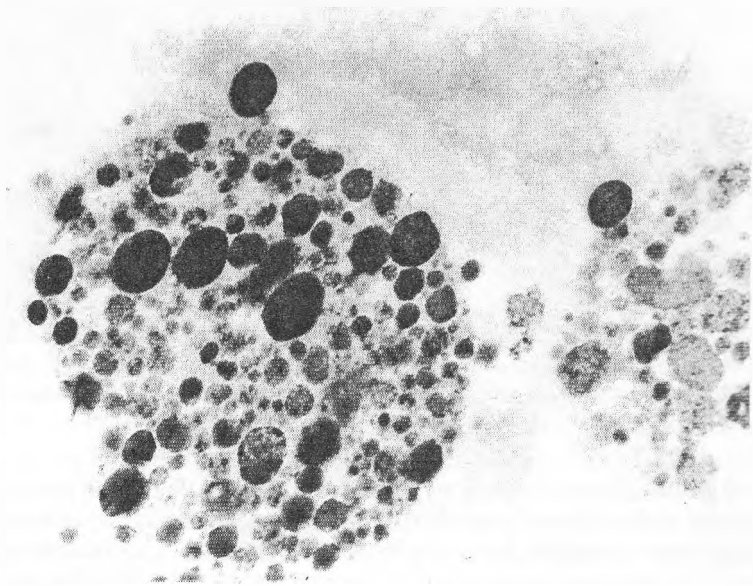

Fig. 3. Tryptase-positive mast cell in the common bile duct of a patient with chronic cholangitis (× 20 000)

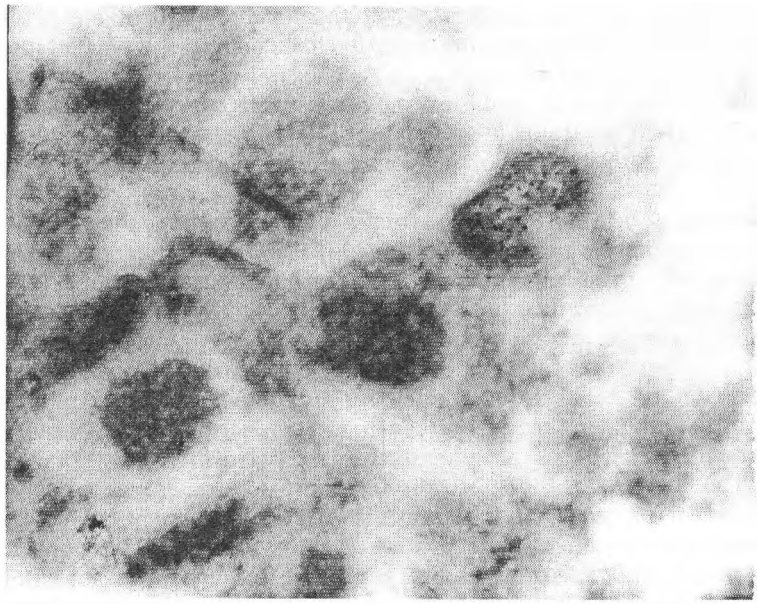

Fig. 4. VIP-positive mast cell granules in the common bile duct of a patient with chronic cholangitis (× 20 000)

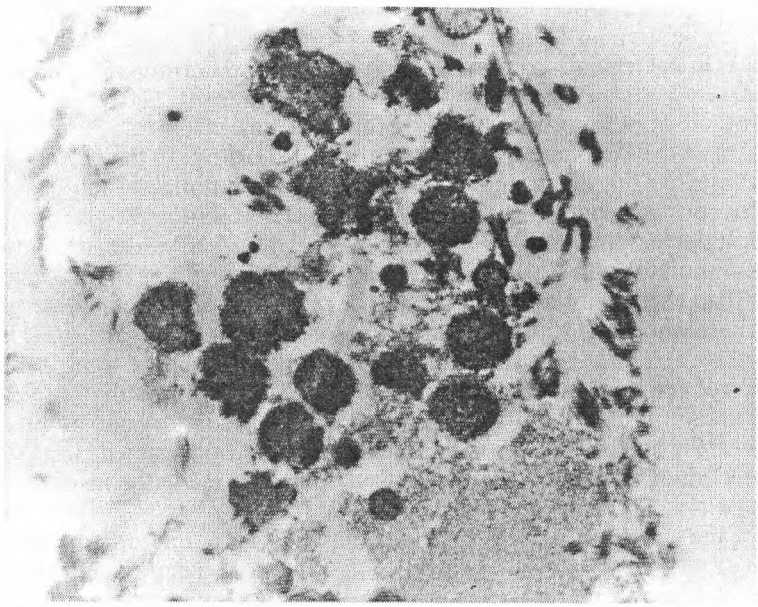

Fig. 5. SP-positive mast cell in the common bile duct of a patient with chronic cholangitis (× 20 000)

VIP-, SP- and chymase-labelled granules are commensurable (with mean values and standard deviations of 0.385±0.14; 0.357±0.8 and 0.360±0.10, respectively, $p>0.05$, t-test). Tryptase labelled granules were two types: large ones with mean value of the diameter

of 0.256±0.04 μm, and small granules with mean value of the diameter 0.109±0.04 μm. Both types tryptase-positive granules appeared to be significantly smaller than all the other studied granules ($p<0.0001$, t-test).

Similar prevalence of tryptase-positive mast cells has been reported in human liver diseases [23], at mucosal sites [4] and in lung [7]. Chymase-positive mast cells have been found predominantly in collagen rich connective tissues and to a lesser extent at mucosal surfaces [4].

It is already known that mast cells play a major role among the immune effector cells involved in neuroimmune communication [30]. Previous studies revealed an intimate association between mast cells and neurons in peripheral nervous system [28]. In our study mast cells were detected near the nerve cell bodies of multipolar neurons comprising the ganglionated myenteric plexus. Because of this proximity mast cells appear to act as bidirectional information carriers between the neurons and immune system. It has been reported that nerve endings are remodeled at the acute phase of inflammation due to the degeneration and during recovery stage due to regeneration [27]. Nerve growth factor (NGF) and SP released from peripheral sensory nerves are the cause for mast cell degranulation. The liberated by the mast cells histamine, in turn, activates peripheral sensory nerves [30]. On the other hand, SP may also trigger immune responses (in neurogenic inflammation) via binding to neuropeptide receptors located on other immune cells, such as T-cells, B-cells and macrophages, thus generating immune responses [20, 30, 32]. Therefore, our finding of mast cells near nerve fibers and nerve plexuses implies their role in neuroimmune interactions during chronic inflammation. We found ganglionated myenteric plexus and many S-100- and NSE-positive nerves in the vicinity of mucous glands in the lower part of d. choledochus situated near the sphincter of Oddi. We also observed many serotonin-positive endocrine cells from the EC type with small discoid granules in that region of choledochus. Thus, it can be supposed that lower part of the large bile duct, participates in the regulation of motility and mucous and hormonal secretion of the biliary pathway.

In two previous reports it was shown that skin mast cells in atopic dermatitis [32] and intestinal mast cells in ulcerative colitis [29] are SP-positive. In the current study, we also found SP-positive mast cells and nerve fibers in the inflammatory infiltrate in secondary cholangitis caused by bile obstruction. This suggest that prolonged chronic inflammation caused by biliary toxins stimulates mast cells to synthesize SP within their granules that in turn may stimulate sensory neurons to release more SP, resulting in prolonged inflammation. So, SP in chronic inflammation could be released from both peptidergic nerves and SP-positive mast cells. It stimulates inflammatory cells involved in chronic inflammation [20, 32], as well as mast cells themselves, which may explain the significantly increased population of activated mast cells observed in the choledochal wall.

The great number of VIP-positive mast cells in secondary cholangitis could be explained with the need of smooth muscle relaxation in the obstructed bile duct [10, 15] and of increased mucus secretion from hyperplastic glands in choledochus as a result of biliary intoxication [15, 21].

Since the large bile duct in chronic cholangitis has a thin mucous layer and a thick connective tissue layer (caused by chronic inflammation) the mast cells belong to various subsets. It is known that human mast cells at mucosal sites have more scroll granules (tryptase-positive) and connective tissue mast cells possess "lattice" or "grating-like" configuration in their granules (chymase-positive) [4].

In our study, the large bile duct tryptase-positive granules were electron-dense, particulate or with scrolls. Similar granular morphology was reported also for tryptase-positive mast cells in the human lung [4, 7]. Choledochal chymase-positive mast cell granules were mainly of the particulate and beaded pattern. The ultrastructural immunocytochem-

ical localization of tryptase and chymase revealed 3 distribution patterns of the antigen in mast cell granules: granules with darkly precipitated reaction product, electron lucent granules without reaction product and electron lucent granules with sparse reaction product (altered granules). On the basis of localization of tryptase and chymase and the diameters of granules (large and small in size), these mast cells resembled tryptase/chymase-positive as described earlier [7] in human lung, intestine and skin. The observed "altered granules" resembled those reported earlier by B e i l and P a m m e r [4]. The decrease or lack of immunoreactivity mainly for chymase and less for tryptase in the observed "altered granules" can be explained with the degranulation process of mast cells [4].

VIP- and SP-positive granules were electron-dense and particulate. Their diameters and appearance were like chymase-positive granules. Further investigations with co-localization are necessary to determine whether SP- and VIP-positive mast cells could be also chymase-positive.

Therefore the presence of such variety of mast cells, nerves, ganglionated plexus and endocrine cells in the lower part of the human large bile duct (at a 2 cm distance from the sphincter of Oddi) suggest the importance of this segment in the regulation of the process of motility, evacuation of bile in the duodenum, hormonal secretion, and some other physiological functions in human.

References

1. A l d e n b u r g, F., R. P e e k e r, M. F a l l, A. O l o f s s o n, L. E n e r b ä c k. Metaplastic transformation of urinary bladder epithelium. Effect on mast cell recruitment, distribution, and phenotype expression. – Am. J. Pathol., **153**, 1998, 149-157.
2. A r t u c, M., U. M. S t e c k e l i n g s, M. B. H e n z. Mast cell-fibroblast interactions: human mast cells as source and inducers of fibroblast and epithelial growth factors. – J. Invest. Dermatol., **118**, 2002, 391-395.
3. B a r r e t, K. E., F. L. P e a r c e. Heterogeneity of mast cells. – In: Histamine and Histamine Anatagonists, (Ed. B. Uvnäs). Berlin, Springer-Verlag, **97**, 1991, 93-116.
4. B e i l, W. J., J. P a m m e r. In situ detection of the mast cell proteases chymase and tryptase in human lung tissue using light and electron microscopy. – Histochem. Cell Biol., **116**, 2001, 483-493.
5. B e i l, W. J., M. S c h u l z, U. W e f e l m e y e r. Mast cell granule composition and tissue location — a close correlation. – Histol. Histopathol., **15**, 2000, 937-946.
6. B e n i t e z - B r i b i e s c a, L., A. W o n g, E. C a s t e l l a n o s. The role of mast cell tryptase in neoangiogenesis of premalignant and malignant lesions of the uterine cervix. – J. Histochem. Cytochem., **49**, 2001, No 8, 1061-1062.
7. C r a i g, S. S., N. M. S c h e c h t e r, L. B. S c h w a r t z. Ultrastructural analysis of human T and TC mast cells identified by immunoelectron microscopy. – Lab. Invest., **58**, 1988, 682-691.
8. C u t z, E., W. C h a n, N. S. T r a c k. Release of vasoactive intestinal polypeptide in mast cells by histamine liberators. – Nature, **275**, 1978, 661-662.
9. D v o r a k, A. M., J. J. C o s t a, E. S. M o r g a n. Diamine oxidase-gold ultrastructural localization of histamine in human skin biopsies containing mast cells stimulated to degranulate in vivo by exposure to recombinant human stem cell factor. – Blood, **90**, 1997, 2893-900.
10. F e h e r, E., G. B u r n s t o c k. Ultrastructural localization of substance P, vasoactive intestinal polypeptide, somatostatin and neuropeptide Y immunoreactivity in perivascular nerve plexuses of the gut. – Blood Vessels, **23**, 1986, 125-136.
11. F u j i m i y a, M., K. O k u m i y a, T. Y a m a n e, T. M a e d a. Distribution of serotonin-immunoreactive nerve cells and fibers in the rat gastrointestinal tract. – Histochem. Cell Biol., **107**, 1997, 105-114.
12. G h i a r a, P., D. B o r a s c h i, L. V i l l a, G. S c a p i g l i a t i, C. T a d d e i, A. T a g l i a b u e. In vitro generated mast cells express natural cytotoxicity against tumour cells. – Immunology, **55**, 1985, 317-324.
13. G u l u b o v a, M. V. Structural examination of tryptase- and chymase-positive mast cells in livers, containing metastases from gastrointestinal cancers. – Clin. Exp. Metast., **20**, 2003, 611-620.
14. G u l u b o v a, M. V., T. I. V l a y k o v a. Mast cells in human bile duct obstruction. – J. Mol. Histol., **35**, 2004, 791-801.
15. G u l u b o v a, M., A. V o d e n i c h a r o v. Structural examination of tryptase-, and VIP-positive mast cells in the common bile duct of patients with lithiasis. – Acta Histochem., **103**, 2001, 437-52.

16. Gurish, M. F., K. F. Austen. The diverse roles of mast cells. – J. Exp. Med., **194**, 2001, F1-F5.
17. Hill, P. B., R. G. Martin. A review of mast cell biology. – Vet. Dermatol., **9**, 1998, 145-166.
18. Irani, A. A., N. M. Schechter, S.S. Craig, G. DeBlois, L.B. Schwartz. Two types of human mast cells that have distinct neutral protease compositition. – Proc. Natl. Acad. Sci. USA, **83**, 1986, 4464-4468.
19. Jolly, S., C. Thomas, B. Genicot, C. E. Dessy-Doize, F. L. Coignoul, D. Desmecht. Effect of intravenous platelet-activating factor on bovine pulmonary mast cells. – J. Comp. Path., **125**, 2001, 81-89.
20. Kabashima, H., K. Nagata, K. Maeda, T. Iijima. Involvement of substance P, mast cells, TNF-a and ICAM-1 in the infiltration of inflammatory cells in human periapical granulomas. – J. Oral Pathol. Med., **31**, 2002, 175-180.
21. Kusakabe, T., H. Matsuda, Y. Gono, T. Kawakami, K. Kurihara, M. Tsukuda, T. Takenaka. Distribution of VIP receptors in the human submandibular gland: an immunohistochemical study. – Histol. Histopathol., **13**, 1998, 373-378.
22. Küther, K., L. Audigé, P. Kube, M. Welle. Bovine mast cells: distribution, density, heterogeneity and influence of fixation techniques. – Cell Tissue Res., **293**, 1998, 111-119.
23. Matsunaga, Y., T. Terada. Mast cell subpopulations in chronic Inflammatory hepatobiliary diseases. – Liver, **20**, 2000, 152-156.
24. Nielsen, H. J., U. Hansen, I. J. Christensen, C. M. Reimert, N. Brunner, F. Moesgaard. Independent prognostic value of eosinophil and mast cell infiltration in colorectal cancer tissue. – J. Pathol., **189**, 1999, 487-95.
25. Norrby, K., D. Wooly. The role of mast cells in mitogenesis and angiogenesis in normal tissue and tumor tissue. – Adv. Biosci., **89**, 1993, 71-116.
26. Rouss, S. J., T. Hartmann, G. H. Caughey. Mast cell tryptase is a mitogen for cultured fibroblasts. – J. Clin. Invest., **88**, 1991, 493-499.
27. Stead, R. H. Nerve remodelling during intestinal inflammation. In neuroimmuno-physiology of the gastrointestinal mucosa. – In: Implications for Inflammatory Diseases (Eds. R.H. Stead, M.H. Perdue, H. Cooke, D.W. Powell, K. Barett). New York, NY Acad. Sci., 1992, 443-455.
28. Stead, R. H., M. Tomioka, G. Quinonez, G. T. Simon, S. Y. Felten, K. J. Bienenstock. Intestinal mucosal mast cells in normal and nematode-infected rat intestines are in intimate contact with peptidergic nerves. – Proc. Natl. Acad. Sci. USA, **84**, 1987, 2975-2979.
29. Stoyanova, I. I., M. V. Gulubova. Mast cells and inflammatory mediators in chronic ulcerative colitis. – Acta Histochem., **104**, 2002, 185-192.
30. Theodorou, V., J. Fioramonti, L. Bueno. Integrative neuroimmunology of the digestive tract. – Vet. Res., **27**, 1996, 427-442.
31. Tomimori, Y., T. Muto, H. Fukami, K. Sato, C. Horikawa, N. Tsuruoka, M. Saito, M. Sugiura, K. Yamashiro, M. Sumida, S. Kukutani, Y. Fukuda. Chymase participates in chronic dermatitis by inducing eosinophil infiltration. – Lab. Invest., **82**, 2002, 789-794.
32. Toyoda, M., T. Makino, M. Kagaoura. Immunolocalization of substance P in human skin mast cells. – Arch. Dermatol. Res., **292**, 2000, 418-421.

Institute of Experimental Morphology and Anthropology with Museum
Bulgarian Anatomical Society

Acta morphologica et anthropologica, 12
Sofia • 2007

Localization, Density, Shape and Dimensions of Mast Cells in Feline Prostate Gland

R. Dimitrov, A. Vodenicharov, P. Yonkova,
G. Gostadinov, Hr. Hristov

Department of Veterinary Anatomy, Histology and Embryology
Faculty of Veterinary Medicine, Trakia University, 6000 Stara Zagora, Bulgaria

The localization, density, shape and dimensions of mast cells in prostate glands of 9 sexually mature clinically healthy male cats, aged 1-2 years were investigated following euthanasia. The material was fixed in Carnoy's fixative, dehydrated, embedded in parrafin and stained with toluidine blue. The localization and the shape of mast cells were observed via light microscopy whereas the density and their dimensions - by an eyepiece micrometer. The data were statistically processed (Descriptive statistics, Data Analysis, Excel). It was found out that the predilection site of mast cells was in prostatic stroma. A considerable concentration of mast cells was observed in the interstitium by the glandular epithelium unlike the peripheral subcapsular stroma. Single mast cells, located by the basal membrane of the glandular epithelium, intraepithelially and intraluminally in tubuloalveolar parenchyma were detected. The shape of mast cells observed in feline prostate gland was most commonly fusiform and more rarely, oval cells were encountered.

Key words: mast cells, prostate gland, tomcat.

Introduction

The data referring to mast cells in mammalian prostate glands are relatively scarce and they are primarily about men and rats, both in normal and pathological states.

In the urogenital tract of humans, rat and mice, mast cells are found out in the connective tissue under the epithelial layers adjacent to blood and lymph vessels and peripheral nerves [6, 8, 9].

Localization of mast cell in the genitals of male rats showed that both their number and density were high [5].

The density of mast cells in the ventral part of prostate in the rat during puberty was high and decreased considerably with age [7].

The localization and the number of mast cells in human male genitals and especially in prostate gland, vary depending on the influence of exogenous and endogenous factors such as stress, allergy, inflammations and vascular thrombosis [1, 3, 6, 12]. Their density is significantly altered in benign and malignant prostatic lesions thus determining their role in the specific prevention of tissue metaplasia. The increased concentration of mast cells and the difference between the density in the intratumoural and peritumoural prostatic regions evidenced their biological importance in these processes [2, 4, 11].

The mast cell profile in prostatic lesions is always changed and therefore, is a confident marker of initial pathology of the gland [1].

The lack of data about the localization, density, shape and dimensions of mast cells in feline prostate gland motivated the present study in order to reveal their functional role in the prostate of these animal species.

Materials and Methods

Prostate glands of 9 clinically healthy, sexually mature male European shorthair cats (at the age of 1-2 years), weighing 2.8-4 kg were studied. The cats were euthanized i.v. with 200 mg Thiopental (Biochemie, Austria).

The material was fixed in Carnoy's fixative for 4 hours, then put in 70° ethanol for 12 hours, dehydrated in an ascending ethanol series, cleared in xylene and embedded in paraffin.

The cross-sections (5-7 μm) were stained with 0.1% solution of toluidine blue in McIvane's buffer, pH 3 [10].

The localization and the shape of mast cells were determined via light microscopy and their density (in mm^2) and dimensions (in μm) were measured with an eyepiece micrometer.

The data were statistically processed (Descriptive statistics, Data Analysis, Excel).

Results and Discussion

The total area of studied histological sections was 204 mm^2, the stromal area being 132 mm^2 (64.7%) and the parenchyma – 72 mm^2 (35.3%).

From 2992 observed mast cells, 2924 (97.7%) were into the glandular stroma and the other 68 (2.3%) — into the parenchyma. The mast cells counts in stroma were 22.15 per mm^2, whereas in parenchyma – 1.06 per mm^2.

The average mast cell counts in the stroma of a histological section was 328.22 ± 26.01, standard deviation 78.04 and in parenchyma: 7.56 ± 2.54, standard deviations 7.35. The minimum and maximum values of these parameters were between 212 and 453 cells in the interstitium and between 0 and 21 in glandular parenchyma.

The length of cells in the interstitium varied from 10.2 μm to 34 μm (mean 21.08 ± 0.67 μm), whereas in parenchyma reached 34 μm (mean 11.26 ± 1.33 μm).

The width (thickness) of mast cells in stroma varied between 6.8–17 μm (mean 9.14 ± 0.26 μm) and in the parenchyma reached 17 μm (mean 6.07 ± 0.71 μm).

The light microscopic studies showed that the predilection site of mast cells was in prostatic stroma, particularly within the interstitium surrounding the glandular epithelium (Fig. 1) and sometimes they communicated with the basal membrane of parenchymal cells (Fig. 2).

In single cases, intraepithelial localization of mast cells was observed, as well as cells, penetrating into the tubuloalveolar glandular lumen (Fig. 2).

The considerable density of cells into the interstitium (Fig. 3) was relatively lesser than the density closely to the glandular parenchyma (Fig. 1) and higher than the density in the periphery under the capsule (Fig. 4).

A higher concentration of mast cells was observed especially around the venous vessels of the stroma than around the arterial ones (Fig. 4).

Often, the observed cells were near the interstitial lymphoid cell clusters (Fig. 3).

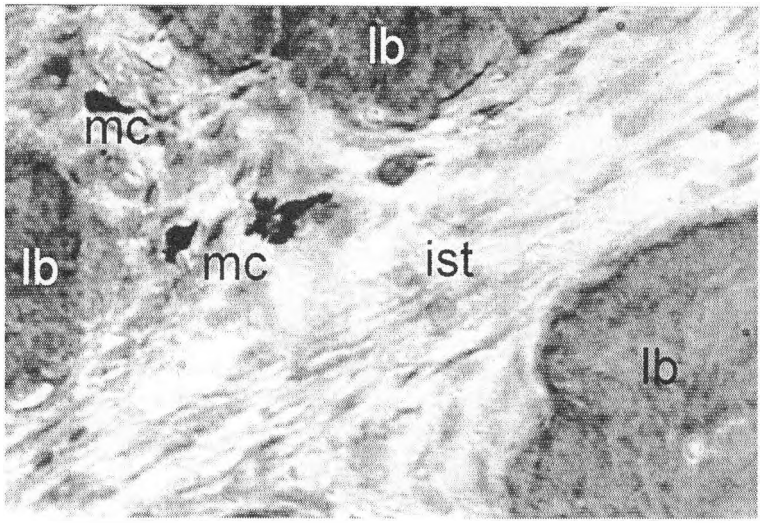

Fig. 1. Mast cells (mc) located in the trabecular interstitium (ist) between glandular lobules (lb) (× 400)

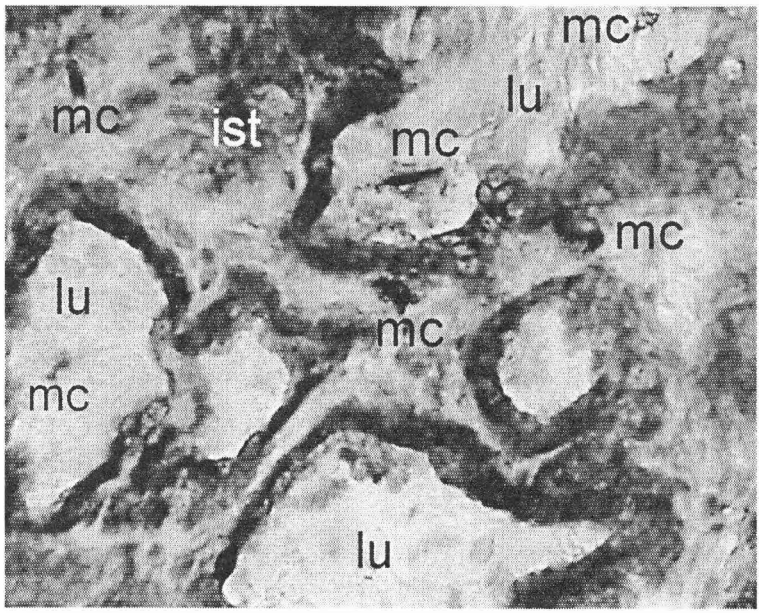

Fig. 2. Mast cells (mc) located between the basal membrane and interstitium (ist) of the glandular epithelium and penetrating the tubuloalveolar lumen (lu) (× 400)

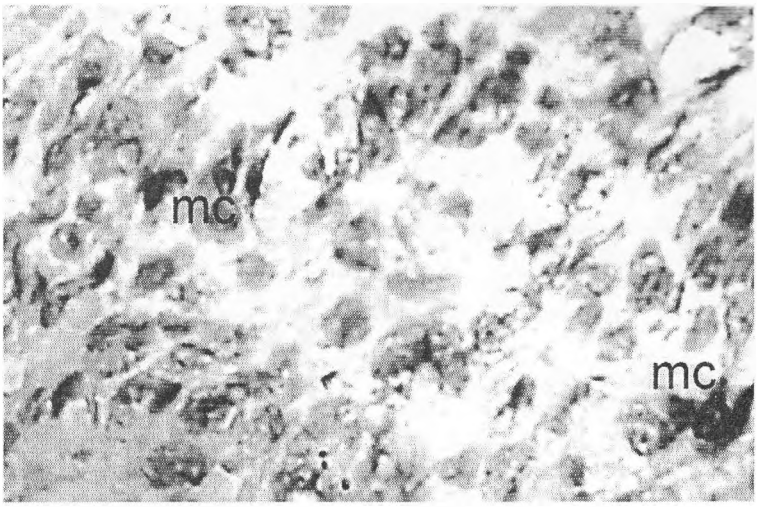

Fig. 3. Single mast cells (mc) among the connective tissue cells of the stroma (× 400)

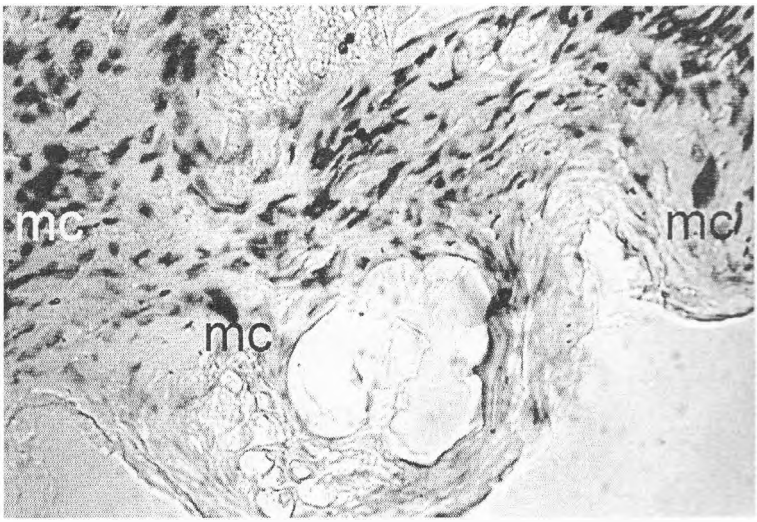

Fig. 4. Mast cells (mc) located in the prostatic myoelastic stroma immediately under the glandular capsule (× 400)

The density of studied cells was relatively reduced from the central towards the peripheral parts of glandular stroma (Fig. 4 and Fig. 1).

The most typical shape of mast cells in feline prostate in this study was fusiform and rarely oval (Fig. 1 and Fig. 3).

For the first time, intraepithelial and intraluminal localization of mast cells in the tubuloalveolar parenchyma of feline prostate gland was observed. These data add further knowledge about mast cell localization in mammalian prostates, that is known to take place only in the interstitium [5, 6, 7, 8, 9].

The predominant stromal localization of mast cells in feline prostate looked like their occurrence in rats, mice and humans [6, 7, 8, 9].

The placement of mast cells of feline prostate in the connective tissue was similar to the predominant interstitial fibromuscular prevalence of those cells in benign, malignant, inflammatory and vascular prostatic lesions, thus suggesting about the affinity of mast cells to the connective tissue component of the gland [1, 2, 3, 4, 11, 12].

Considering the opinion of G a l l i [6] it could be assumed that the mast cells in the storoma of feline prostate possibly participate in the local immune competency.

The considerably high concentration of mast cells in the glandular stroma (328.22) vs their density in the parenchyma (7.56) allowed us to imply an involvement in the motility of stromal smooth muscle cells, vascular tone regulation, microcirculation and the local organ homeostasis.

The relatively larger dimensions (length and width) of mastocytes in the interstitium vs those in the parenchyma are suggesting about their active role in the connective tissue part of the prostate in cats.

References

1. A m i r, T., R. P a i, C. R a g h u v e e r. Mast cell profile in prostatic lesions. – Indian Journal of Medical Science, **52**, 1998, No 11, 507-513.
2. A y d i n, O., D. D u s m e z, L. C i n e l, E. D o r u k, A. K a n i k. Immunohistological analysis of mast cell numbers in the intratumoral and peritumoral regions of prostate carcinoma compared to benign prostatic hyperplasia. – Pathol. Res. Pract., **198**, 2002, No 4, 267-271.
3. B a n k l, H., C. S a m o r a p o o m p i c h i t, B. P i k u l a, L. L a t i n o v i c, H. B a n k l, K. L e c h n e r, P. V a l e n t. Characterizatoin of human prostate mast cells and their increase in periprostatic vein thrombosis. – American Journal of Clinical Pathology, **116**, 2001, No 1, 97-106.
4. D e n g, W., P. L i, G. L i, Y. Z h a o. The distribution of mast cells in benign and malignant prostate lesions and its biologic significance. – Sichuan Da Xue Xue Bao Yi Xue Ban, **35**, 2004, No 5, 623-625.
5. F r i t z, F., R. P a b s t. Numbers and heterogeneity of mast cells in the male genital tract of the rat. – Int. Arch. Allergy. Appl. Immunology, **88**, 1989, No 3, 360-362.
6. G a l l i, S. J. New Concepts about the mast cell. – The New England Journal of Medicine, **328**, 1993, No 4, 257-265.
7. H a m m e l, I., P. R o i z m a n, R. M a s s a s, A. A b r a m o v i c. Ontogeny of mast cells in the ventral prostate of the rat. – Int. Arch. Allergy. Appl. Immunology, **93**, 1990, No 2-3, 212-215.
8. M a j e e d, S. K. Mast cell distribution in rat. – Arzneimittelforschung, **44**, 1994, No 3, 370-374.
9. M a j e e d, S. K. Mast cell distribution in mice. – Arzneimittelforschung, **44**, 1994, No 10, 1170-1173.
10. P e a r c e, A. — In: Histochemistry. 2th ed. London. J.& Churchill Ltd., 1960. 692 p.
11. S a r l, S., O. C a n d i r, O z t u r c and K o s a r. Mast cell variations in tumour tissue and with histopathological grading in specimens of prostatic adenocarcinoma. – BJU Internatoinal, **84**, 1998, No 7, 51-855.
12. T h e o h a r i d e s, T., N. F l a r i s, C. C r o n i n, A. U c c i, E. M e a r e s. Mast cell activation in sterile bladder and prostate inflammation. – Int. Arch. Allergy. Appl. Immunology, **92**, 1990, No 3, 281-286.

Institute of Experimental Morphology and Anthropology with Museum
Bulgarian Anatomical Society

Acta morphologica et anthropologica, 12
Sofia • 2007

Extraction Resistance of Mammalian Sperm Axonemal Microtubules

M. Markova, Ts. Marinova

Department of Biology, Medical Faculty, Medical University, Sofia

Axonemal microtubules responsible for sperm motility are more stable than cytoplasmic microtubules but the reasons are still unclear. We subjected mouse and human spermatozoa to nuclear matrix — intermediate filaments (NM—IF) extraction including sequental detergent, high salt and nuclease treatment. This protocol has been applied to other cell types and reported to dissolve all structures except nuclear matrix and intermediate filaments. In spermatozoa, however, axoneme was retained. Electron microscopic observation of extracted sperm whole mounts showed presence of microtubules in all parts of the tail. To determine whether microtubules had preserved their appearance owing to axonemal compononts other than tubulin, we performed immunofluorescent and immunoelectron microscopic localization of tubulin in extracted cells. Tubulin labeling was not diminished in treated spermatozoa compared to untreated controls. It could be concluded that in the non-physiologic conditions of this approach, sperm microtubules showed remarkable intrinsic stability comparable to that of intermediate-type filaments.

Key words: axoneme, tubulin, sperm, cytoskeleton, microscopy.

Introduction

Progressive motility and, hence, fertilizing capacity of the spermatozoon depends on the microtubular cytoskeleton of its tail — the axoneme. Axonemal microtubules are known to be considerably more stable than their cytoplasmic counterparts but few studies have addressed this issue specifically. The difference could be partly attributed to the fact that most cytoplasmic microtubules normally undergo transition between polymerization and collapse called dynamic instability [3]. However, axonemal microtubules are also likely to be intrinsically more stable because of their composition. Unlike cytoplasmic microtubules, they contain intermediate filament-like proteins called tektins [6]. The general symmetry of axoneme is preserved even after extraction of 80% of tubulin, which leaves thin tektin-rich filaments at microtubule positions [7]. A procedure known to dissolve cytoplasmic microtubules is the nuclear matrix and intermediate filaments (NM—IF) extraction including sequental Triton X-100 treatment, high salt extraction and nuclease digestion [1, 2]. We subjected mouse and human spermatozoa to NM—IF extraction and then assessed the structure and tubulin content of their microtubules by microscopic and immunocytochemical methods.

Materials and Methods

Specimens from 4 mice and 9 normozoospermic patients were used for this study. Mouse spermatozoa were obtained from vas deferens and human spermatozoa from ejaculates. Cells were subjected to NM—IF extraction as described earlier [5] with the following more important steps: permeabilization for 10 min at 4°C with 10 mM HEPES buffer pH 6.8, 100 mM NaCl, 300 mM sucrose, 3 mM $MgCl_2$, 0.5% Triton X-100, 1.2 mM phenylmethylsulfonylfluoride (PMSF); extraction for 10 min at 4°C with 10 mM HEPES pH 6.8, 250 mM $(NH_4)_2SO_4$, 300 mM sucrose, 3 mM $MgCl_2$, 0.5% Triton X-100, 1.2 mM PMSF; digestion at room temperature for 20-40 min in 10 mM HEPES pH 6.8, 50 mM NaCl, 300 mM sucrose, 3 mM $MgCl_2$, 0.5% Triton X-100, 1.2 mM PMSF, 100-200 μg/ml DNase I.

For routine whole-mount electron microscopy, cells were adhered on formvar-coated grids either before or after extraction, fixed with glutaraldehyde and OsO_4 and stained with uranyl acetate.

For immunofluorescence, extracted and unextracted spermatozoa were processed as in [9]. After fixation with methanol and acetone, they were treated for 1 h at room temperature with anti-alpha tubulin monoclonal antibody TU-01 (Prague, Inst. Mol. Genet., diluted 1:50; for detailed description of this antibody see [8]). FITC-conjugated anti-mouse polyvalent Ig (Sigma) diluted 1:100 was applied as second antibody for 30 min at room temperature.

Immunocytochemical detection of tubulin was performed also at electron microscopic level. Unextracted spermatozoa were processed for pre-embedding immunogold electron microscopy as described earlier [4] with the following more important steps: incubation with TU-01 antibody, diluted 1:50, overnight at 4°C; incubation with anti-mouse IgG-10 nm or 5 nm gold conjugate (Sigma), diluted 1:20, for 2 h at room temperature; postfixation, embedding and sectioning. Extracted spermatozoa were treated as whole mounts on grids with the same first and second antibody, fixed and observed without uranyl acetate staining. Positive and negative controls were used in all variants of the immunocytochemical reaction.

Results

Most extracted axonemes showed remarkable preservation of microtubules in all parts of the tail (middle, principal and end piece), although signs of collapse could often be seen at their ends. Virtually all mouse spermatozoa contained at least several microtubules even at end piece level. Human axonemal microtubules were slightly less stable, being present in the end piece in about 80% of tails (in the remaining cells distal fibrous sheath was "empty", devoid of microtubules). When spermatozoa were left to adhere to grids before extraction, end piece microtubules retained parallel position (Fig. 1A), while in cells extracted in suspension they generally had broom-like or more complex appearance (Fig. 1B).

Immunofluorescent staining for alpha-tubulin was observed in the entire sperm tail and its intensity was not diminished by extraction (Fig. 2). Immunoelectron microscopy showed localization of colloidal gold labelling to axonemal microtubules both in pre-embedding sections of unextracted spermatozoa and in whole-mount preparations of NM—IF extracted cells (Fig. 3).

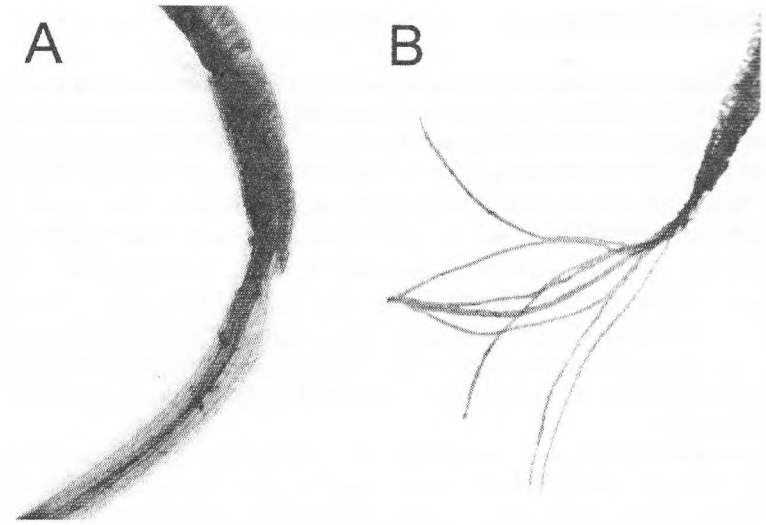

Fig. 1. End piece microtubules
A – of human spermatozoon extracted on the grid (× 22 500); B – of mouse spermatozoon extracted in suspension (× 16 000)

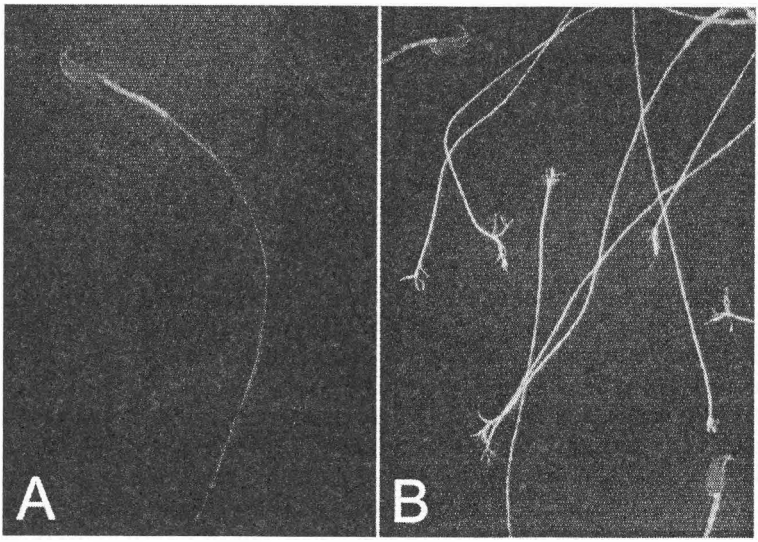

Fig. 2. Immunofluorescent detection of alpha-tubulin in mouse sperm cells
A – unextracted (× 1000); B – extracted (× 1000)

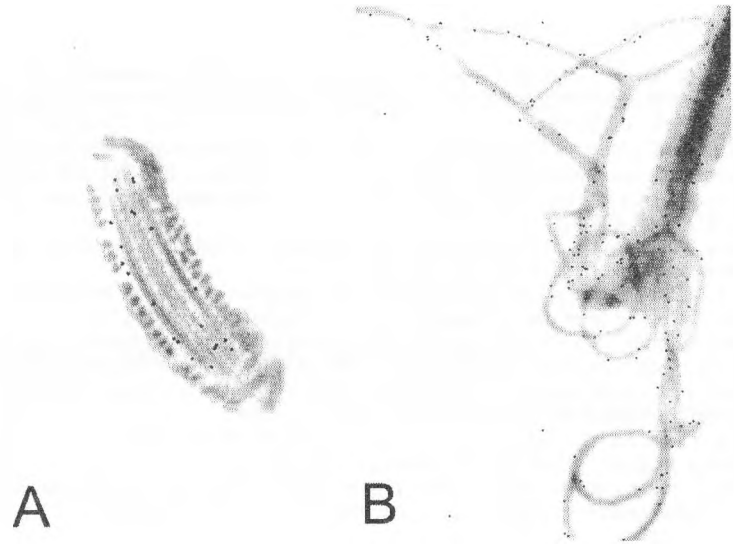

Fig. 3. Immunogold detection of alpha-tubulin in human sperm tails
A – preembedding section of unextracted cell (× 42 000); B – whole-mount of extracted cell (× 26 000)

Discussion

The NM—IF procedure had been developed to extract all cellular structures except intermediate filaments and nuclear matrix and had been shown to solubilize cytoplasmic microtubules [1, 2]. For that reason, it was surprising that in our experiments sperm axonemal microtubules were retained. Their extraction resistance was higher in mouse than in human sperm tails, consistent with the general mechanical inferiority of human spermatozoa to their rodent counterparts.

Although the microtubules appeared to be relatively well preserved, it was not clear whether they still contained most of their tubulin or had preserved their appearance owing to other extraction-resistant axonemal components such as tektins [6, 7]. To check the latter possibility, we examined the presence of tubulin in extracted cells by immunocytochemistry at light and electron microscopic level using monoclonal anti-tubulin antibody. The immunofluorescent and immunogold labelling for tubulin showed no apparent decrease in treated spermatozoa compared to untreated controls.

In conclusion, our experiment underscored the remarkable stability of sperm microtubules. Subjected to NM—IF chemical dissection, they showed resistance comparable to that of intermediate-type filaments. Because the conditions were non-physiological, this resistance could not be attributed to lack of dynamic instability but presumably was an intrinsic property of their composition and structure.

Acknowledgements. TU-01 antibody was a kind gift from Prof. Vladimir Viklický, Institute of Molecular Genetics, Prague. We thank Dr. R. Stanislavov from Seminological Laboratory, Medical University of Sofia, for providing the ejaculate samples.

References

1. F e y, E. G., K. M. W a n, S. P e n m a n. Epithelial cytoskeletal framework and nuclear matrix-intermediate filament scaffold: three-dimensional organization and protein composition. – J. Cell Biol., **98**, 1984, 1973-1984.
2. F e y, E. G., D. G. C a p c o, G. K r o c h m a l n i c, S. P e n m a n. Epithelial structure revealed by chemical dissection and unembedded electron microscopy. – J. Cell Biol., **99**, 1984, 203-208.
3. H y m a n, A. A., E. K a r s e n t i. Morphogenetic properties of microtubules and mitotic spindle assembly. – Cell, **84**, 1996, 401-410.
4. M a r i n o v a, Ts. Ts., M. D. M a r k o v a. Distribution of an N-terminal alpha-tubulin epitope in human spermatozoa. – CR Acad. Bulg. Sci., **51**, 1998, 115-118.
5. M a r k o v a, M. D. Electron microscopic observations of mouse sperm whole mounts after extraction for nuclear matrix and intermediate filaments. – Arch. Androl., **47**, 2001, 37-45.
6. P i r n e r, M. A., R. W. L i n c k. Tektins are heterodimeric polymers in flagellar microtubules with axial periodicities matching the tubulin lattice. – J. Biol. Chem., **269**, 1994, 31800-31806.
7. S t e p h e n s, R. E., S. O l e s z k o - S z u t, R. W. L i n c k. Retention of ciliary ninefold structure after removal of microtubules. – J. Cell Sci., **92**, 1989, 391-402.
8. V i k l i c k y, V., P. D r a b e r, J. H a s e k, J. B a r t e k. Production and characterization of a monoclonal antitubulin antibody. – Cell Biol. Int. Rep., **6**, 1982, 725-731.
9. Y a g i, A., J. P a r a n k o. Actin, alpha-actinin, and spectrin with specific associations with the postacrosomal and acrosomal domains of bovine spermatozoa. – Anat. Rec., **241**, 1995, 77-87.

Institute of Experimental Morphology and Anthropology with Museum
Bulgarian Anatomical Society

Acta morphologica et anthropologica, 12
Sofia • 2007

Ultrastructural and Morphometric Study of Enterochromaffin Cells from the Gastrointestinal Tract

*Nadja Penkova, Vladimir Andonov**

Department of Anatomy, Histology and Embryology, Medical University, Plovdiv, Bulgaria
**Clinic of Gastroenterology, University Hospital "St. George", Plovdiv, Bulgaria*

Serotonin (5-hydroxytryptamine, 5-HT) as a neurotransmitter and gut hormone is an important element of the not yet completely examined brain — gut axis which is part of the diffuse neural-endocrine system. Being one of the regulators of the gut motility, secretion and visceral sensitivity serotonin is the trigger of pathophysiological mechanisms of some of the symptoms of the gastro-intestinal disorders. The aim of this study is ultrastructural and morphometric characterization of the enterochromaffin (EC) cells of the gastrointestinal mucosa, one of the basic source of the serotonin in the human body. The EC cells are examined by means of electron microscope and morphometric methods in material of the biopsy specimens from stomach and duodenum of human. Character istics of the different types of serotonin receptors located in the structures – smooth muscle cells, neural fibers and neurons of the intestinal wall are also performed based on literature data.

Key words: enterochromaffin cells, serotonin, serotonin receptors, gastrointestinal tract.

Introduction

Serotonin (5-hydroxytryptamine, 5-HT) can be found in great amounts in plants and animals. It was discovered in 1930 by V. E r s p a n e r et al. [11]. They extracted a substance that can contract the smooth muscle cells of the uterus and the intestines from enterochromaffin cells of the gastrointestinal mucosa. They called it enteramin. In 1948 J. Green and J. Page extracted vasocontractive substance from blood serum. After the molecular structure of serotonin was discovered enteramin turned out to be its analog. In 1951 they synthesized serotonin chemically [7]. After that the study of its functions began. The total amount of serotonin in the human body is about 10 μg. 95% of it is located in the gastrointestinal tract. 90% of the gastrointestinal serotonin is located in the enterochromaffine (EC) cells of the covering epithelium and the glands. 10% are located in the mast cells of the wall of the gastrointestinal tract. The aim of this study is to carry out the making of ultrastructural and morphometric characteristics of the enterochromaffin (EC) cells of the gastro-intestinal mucosa.

Materials and Methods

The materials about the morphologic research of the EC cells were obtained by fibrogastroscopy on 6 female patients, 45 — 72 years old from the MBAL "St. George" Clinic of Gastroenterology in Plovdiv. The biopsy specimens were taken from the body and antrum pylori of the stomach and superior portion of the duodenum.The biopsy specimens were removed and prepared for TEM according to the routine protocol. Examination and microphotographs were done with TEM "Philips CM 12". Morphometric study: A) Determining the saturation index of the secretory granules in the endocrine cells by the method of W. C r e u t z f e l d [1]. The granules are determined as 1 — empty; 2 — half-empty (with small quantity of material); 3 — half-full, and 4 — full. The saturation index of the granules of each endocrine cell is determined by multiplying the number of granules at each level of saturation by the corresponding coefficient (1, 2, 3, 4) and dividing the obtained value by the sum of the granules in the cell. B) Determining the cytoplasmic distribution coefficient of the secretory granules by the method by C h o m e r i k i and M o r o z o v [13].The microphotographs of the different endocrine cells done with the same magnification are divided into control areas of 0,5-0,25 cm^2 each. The number of the areas with high granule concentration (2 and more granules) — A2 and the number of the areas with low granule concentration (1 or no granules) — A1 are determined. The ratio between A2 and A1 represents the coefficient of granule distribution.

Results

Enterochromaffine (EC) cells can be found in all parts of the gastrointestinal tract. But the greatest amount of EC cells is in its proximal parts — stomach, duodenum, jejunum. In the stomach they are located in the body and the antrum. EC cells are located in the whole length of the stomach glands but mostly in their basal parts. They are cone shaped with a narrow apical part turned towards the lumen of the gland and a wide basal part that lays on the basal lamina and often forms tentacles. The secretory granules of the EC cells are polymorphic with rod-like or biconcave shape and a narrow light halo. They have high electron density (Fig. 1). There are 3 types of EC cells based on the ultrascructural characteristic of the granules and the types of the secretory products — EC1, EC2 and ECn. EC1 cells are located mainly in the stomach. Their granules are polymorphic, mostly prolonged or oval. Their size is 200-300 nm. They contain serotonin and substance P (Fig. 2). EC2 cells are located in the small intestine and the colon. There are mainly oval shaped granules in the their cytoplasm sized 200-400 nm, that contain serotonin and motilin (Fig. 3). The ECn type cells are mostly located in the duodenum. They have small and middle sized granules with moderate electron density that contain serotonin. Based on their ultrastructucal characteristic and the coefficients discovered by morphometric researches we found out that EC cells show different morpho-functional stages. There are: 1. Stage of increased synthesis; 2. Stage of relative secretory rest; 3. Stage of increased secretion. In the **stage of increased synthesis** the EC1 cells have a big loose young granules that are detatched from the trans-surface of the dictiosomes. The young granules of the EC2 cells are numerous and filled a substance with low electron density. They increase their sizes and form a gritted progranule with osmiffil covering membrane. During the next ripening the core of the granules becomes homogeneous with high electron density (Fig. 4). The saturation index of the granules is 3.23 ± 0.3. During the **stage of relative secretory rest** the cytoplasm of the EC cells is filled with ripe granules that are full of secretion (Fig. 5). The saturation index of the granules is 3.45 ± 0.3. In the **stage of increased secretion** the disintegration of the granules begins. Their diameter increases, the electron density of the core

decreases, the halo of the membrane disappears. Remnants of a dispersed substance can be found later in the core of the granule. In the end there is only a membrane skeleton left (Fig. 6). The saturation index of the granules is 2.95 ± 0.2.

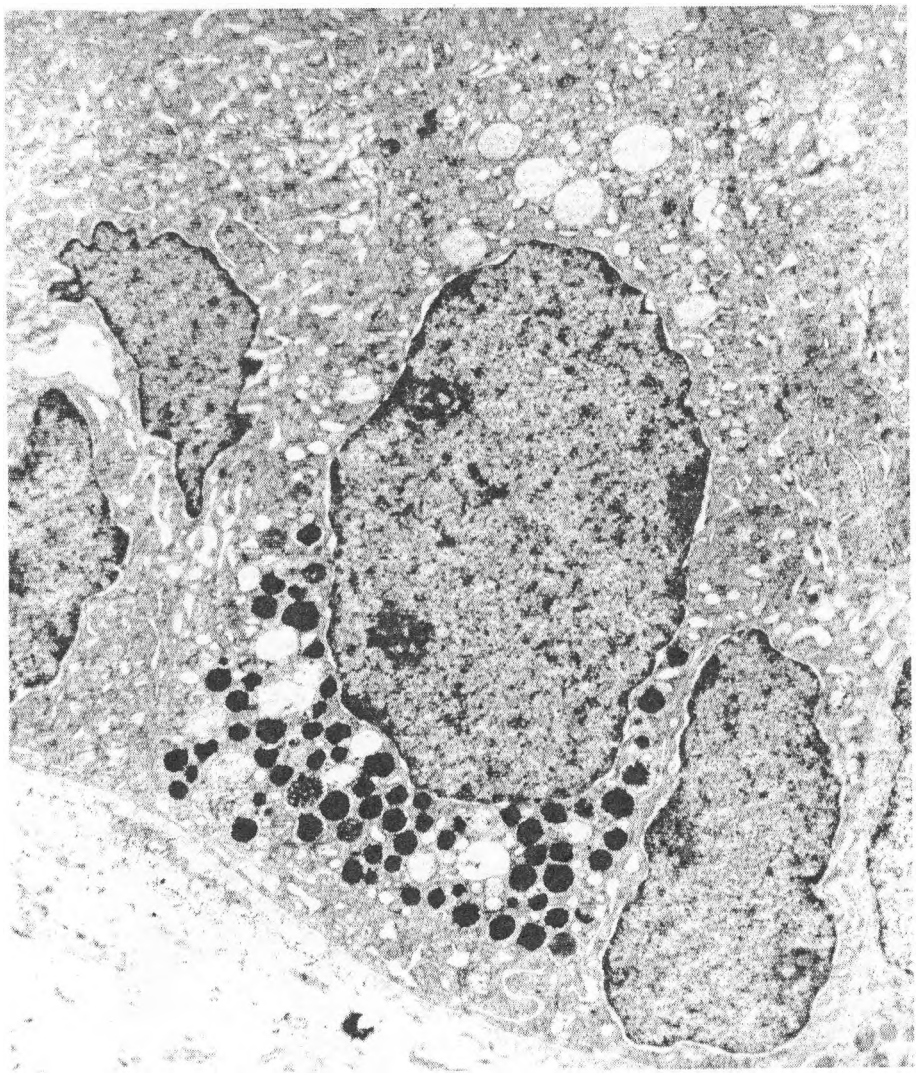

Fig. 1. Enterochromaffine cell EC2 type in duodenal gland. The basal part of the cell with polymorphic secretory granules with high electron density and narrow light halo.TEM (× 1500)

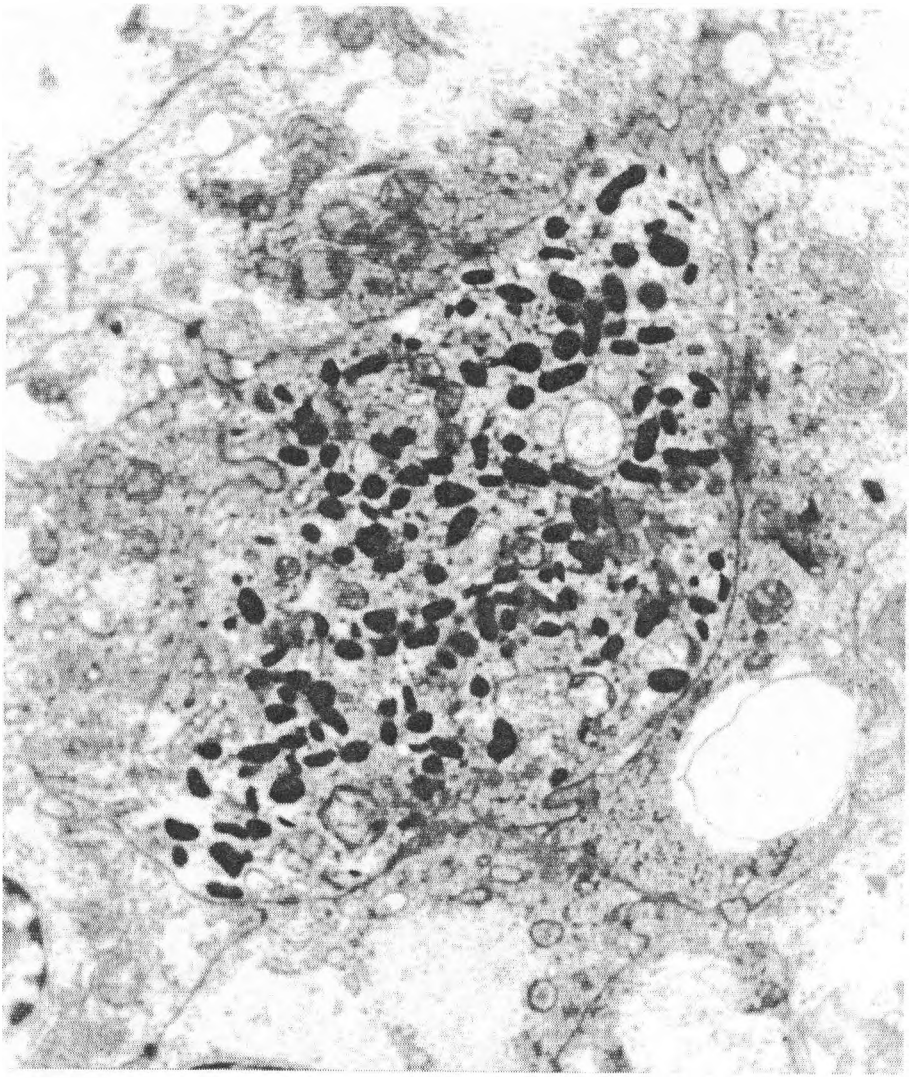

Fig. 2. Fragment from an EC1 cell in stomach gland. Polymorphic, mostly prolonged, rode-like or oval secretory granules, size 200 - 300 nm. TEM (× 2350)

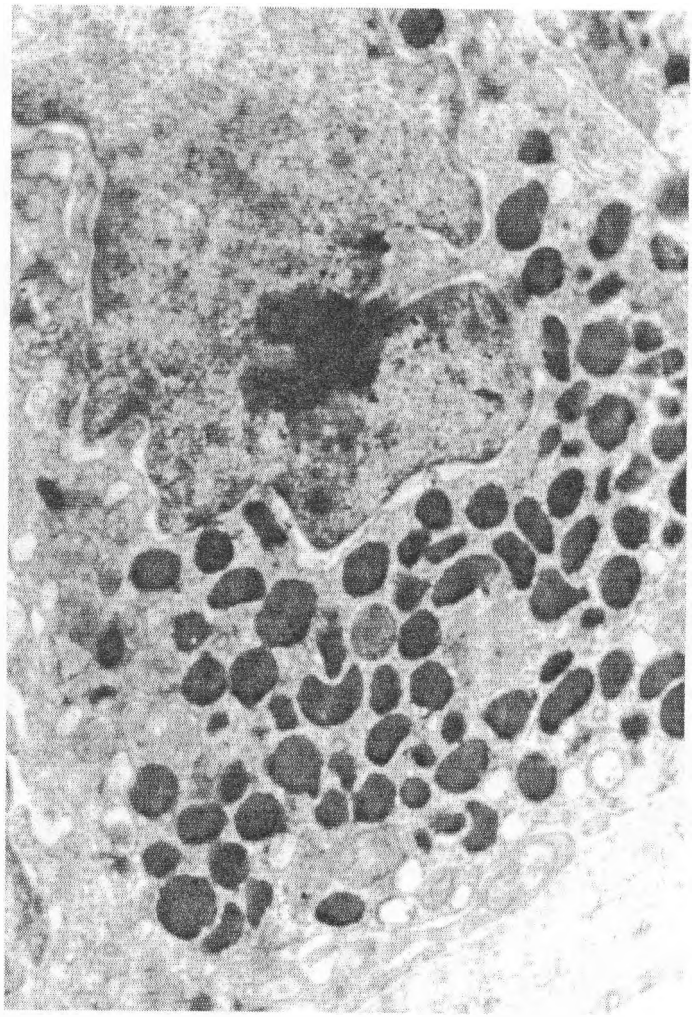

Fig. 3. Fragment from an EC2 cell in duodenal gland. Secretory granules with oval or biconcave shape, size 200 - 400 nm. TEM (× 2350)

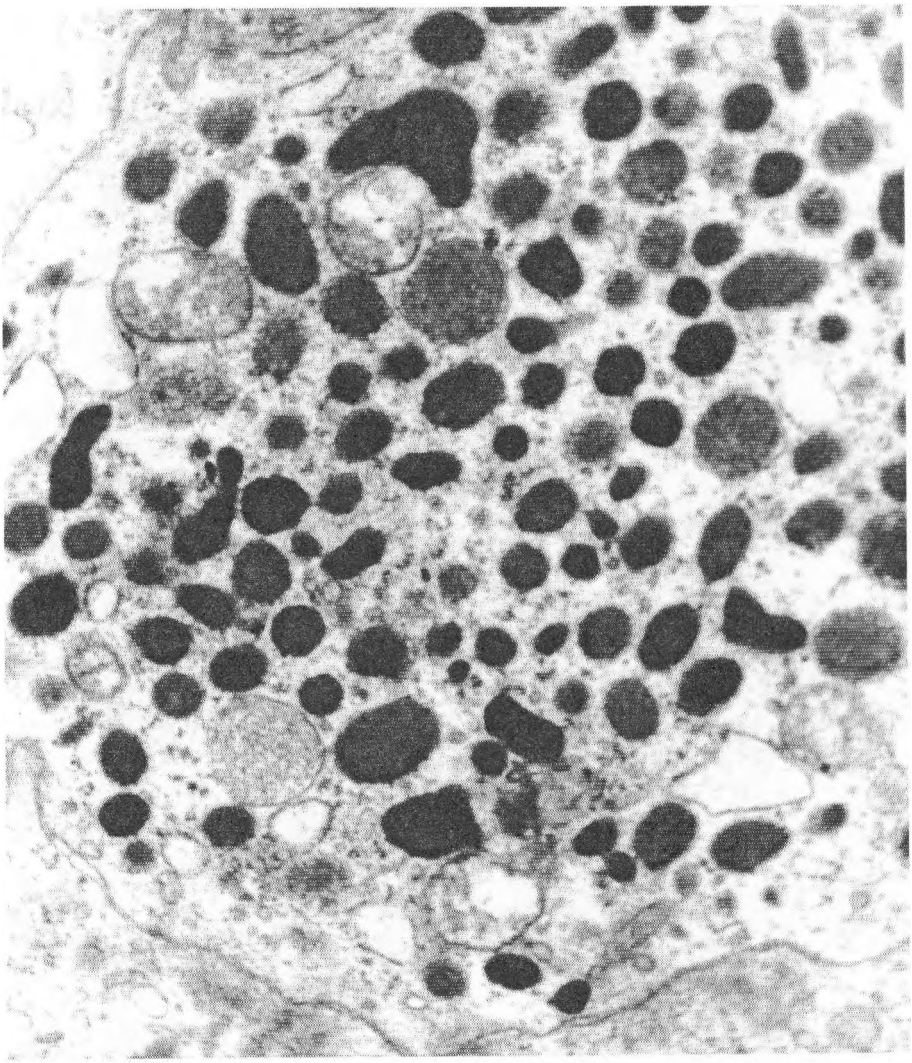

Fig. 4. Fragment from an EC2 cell in duodenal gland. Stage of increased synthesis. Young gritty progranules with low electron density. TEM (× 5000)

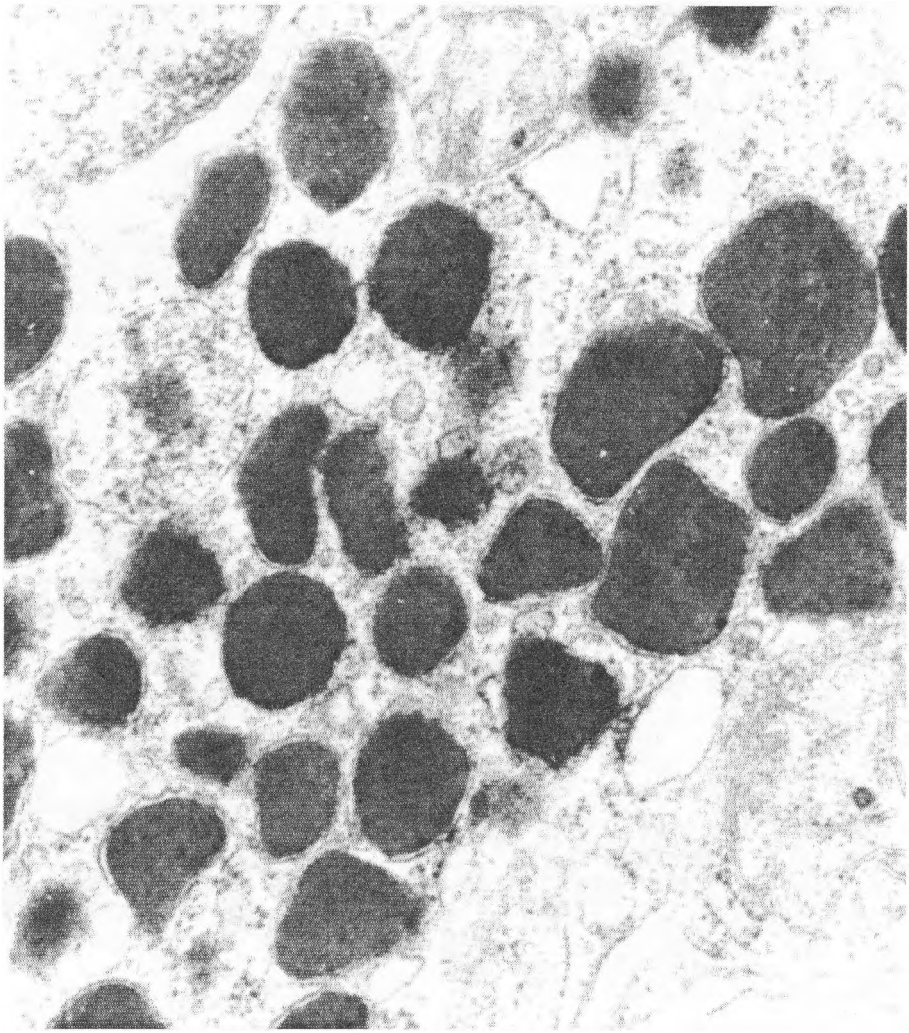

Fig. 5. Fragment from an EC2 cell in duodenal gland. Stage of relative secretory rest. Ripe secretory granules with high electron density, narrow light halo and covering membrane. TEM (× 10 500)

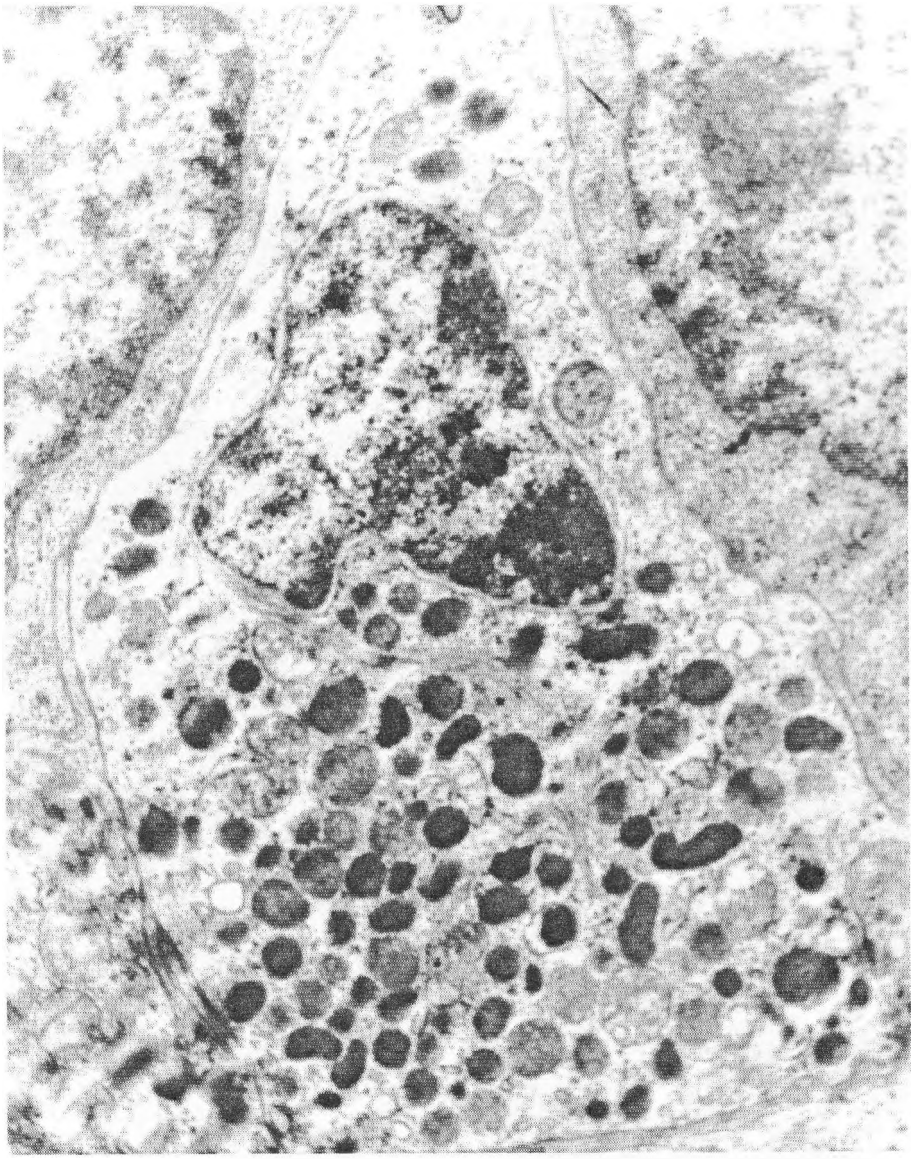

Fig. 6. Fragment from an EC2 cell in duodenal gland. Stage of increased secretion. Secretory granules with decreased electron density. Half-empty granules with remnants of a dispersed substance. TEM (× 3900)

The changes in the distribution index in the granules in the cytoplasm show an activation of the secretory processes. In the **stage of increased synthesis** the granules are uniformly dispersed in the whole cytoplasm. The number of the A1 fields with low density of the granules is lower than the number of A2 fields with high density of the granules. The distribution index of the granules is 0.70 ± 0.3. In the **stage of relative secretory rest** the granules occupy mainly the basal part of the cell. The number of the A1 fields with low density of the granules increases and the distribution index starts to decrease — 0.38 ± 0.3.

In the **stage of increased secretion** the granules are concentrated to the highest degree. There are mostly A1 fields with low electronic density. The distribution index of the granules decreases to 0.36±0.2.

Discussions

Our results of the granular contents in the 1-4 scale (empty — full) are identical with the results of other authors. According to T z a n e v a [9] the saturation index of the granules of the EC cells is 2.8-3.7±0.3. The secretion of serotonin from the EC cells is an answer to many different factors: A) lumenal — the increased amount of acid in the duodenal content or the presence of hypertonic glucose solution; B) blood and nervous factors — intestinal ishaemia, sensory and vagal stimuli; C) mechanic factors — the increase of the intralumenal pressure mechanical obstruction; D) infectious factors — viruses, bacterial toxins. The release of serotonin is thought to be calcium-dependant or voltage dependant calcium channels. Many receptors are present on the EC cells that stimulates or inhibits their activity. There are: adrenoreceptors (a2a, a2b, b1 and b2), muscarinic M3, GABA-A, nicotinic, acetylcholine, histamine-2 and serotonin (auto and paracrine) receptors. Unexpected receptors are olfactory (SCR, HGL, HFL, QIL, and EVA), vomeromasal and pheromone receptors (putative pheromone receptor) [10]. It appears that EC cells may analyse chyme, similar to other intraepithelial sensors in the airway or blood system. This data shows the important role of the EC cells and serotonin in the already discovered brain — gut axis. The function of serotonin is exerted upon its interaction with specific receptors. In 1957, Gaddum suggested that 5-HT interacted on two different receptors in isolated tissues, one on smooth muscle and one on nervous tissue. Since dibenzyline selectively

T a b l e 1. Localization and distribution of serotonin receptors in the body

Type	Subtype	Localisation	
5-HT1	1A	CNS	
	1B	only in rats	
	1C	Pl. choroideus	
	1D	CNS smooth muscle cells in blood vessels	
	1F	no data	
	1P	gastrointestinal tract — afferent somatic and vagal neurons in submucosal plexus	
5-HT2	2A	platelets	
	2B	smooth muscle cells in blood vessels	
	2C	only in rats	
5-HT3		gastrointestinal tract	smooth muscle cells
			afferent somatic and vagal neurons in myenteric plexus
5-HT4		CNS	
		heart	
		gastrointestinal tract	smooth muscle cells
			nociceptive nerve
5-HT5	5A	no data	
	5B	no data	
5-HT6		CNS, limbic system	
5-HT7		CNS, limbic system	
		gastrointestinal tract	smooth muscle cells

antagonized smooth muscle, and morphine was selective for nervous tissue, these receptors were named "D"; and "M" receptors respectively [8]. Nowadays several serotonin receptors have been cloned and are identified in seven groups. Group one (5-HT1) includes the 6 subtypes. Group two includes 3 subtypes. Group five includes 2 subtypes (Table 1).

Most of those receptors are coupled to G-proteins that affect the activities of either adenilate cyclase or phospholipase Cγ. The 5-HT3 class of receptors are ion channels. Some of serotonin receptors are presynaptic and others are postsynaptic. The cloning of new types of 5-HT receptors continues. Serotonin and its receptors play an important role in the regulation of different processes in the gastrointestinal tract — resorption of nutrients, gland secretion, motility and sensitivity. 5-HT3 and 5-HT4 receptors are discovered in the smooth muscle cells of the gastrointestinal tract [5]. 5-HT1 receptors are located in the smooth muscle cells of the circular muscle of the colon and 5-HT7 — in the longitudinal muscle [3]. 5-HT1p receptors are found in the afferent somatic nerve fibers of the submucosal plexus [4]. 5-HT3 receptors are located in the somatic and vagal neurons and nerve fibers of the myenteric plexus [12]. The detailed study of the functions of serotonin in the gastrointestinal tract that are carried out through different types of receptors as well as the creation of specific antagonists and agonists for these receptors reveals new trends in the therapy of the functional gastrointestinal disorders. Nearly 7 of 10 adults are affected by one or more functional gastrointestinal disorders, such as irritable bowel syndrome (IBS), gastroesophageal reflux disease and functional dyspepsia. Serotonin plays a key role in the pathogenesis of these disorders. Serotonin is released from the EC cells, psychosomatic mechanisms or from the mast cells during inflammatory processes. 5-HT3 receptors take part in the complicated vomit reflexes during functional gastrointestinal disorders as well as in therapy of cancer diseases. The blocking of these receptors by 5-HT3 antagonists interrupts the afferent impulses to the vestibular system, the cerebral cortex and the chemoreceptor trigger zone located in floor of the fourth ventricle that regulates the physiological emetic centre. 5-HT3 and 5-HT4 receptors take part in the gastrointestinal sensitivity. They are located in vagal and visceral nociceptive neurons that activate different pain systems. The fibers of those neurons transmit signal from the viscera to the specific lamine of the dorsal horn, nuclei of the thalamus and cerebral cortex [2]. Using distal colonic stimulation, several studies have demonstrates alterations in regional brain activation in patients with IBS compared with healthy control subjects.There is such a difference in the activity of the visceral nociceptive stimuli in the anterior midcingulate cortex, insula and dorsal pons (in the region of the periaqueductal grey) [6].

Conclusion

Being one of the regulators of the gastrointestinal motility, secretion and sensitivity serotonin plays a key role in many symptoms of gastrointestinal diseases. EC cells that secrete serotonin are filled in different degrees with secretory granules. The granules are polymorph, rod-, biconcave or oval shaped with a light halo and high electronic density. By the means of a morphometric study and ultrastructural characteristic we defined coefficients that show 3 different morphofunctional states of the EC cells: stage of increased synthesis, stage of relative secretory rest and stage of increased secretion.

References

1. Creutzfeldt, W., R. Arnold, C. Creutzfeldt, N. Jrack. Mucosal gastrin concentration, molecular forms of gastrin, number and ultrastructure of G-cells in patients with duodenal ulcer. – Gut, **17**, 1976, 745-754.
2. Crowell, M.. Role of serotonin in the pathophysiology of the irritable bowel syndrome. – British Journal of Pharmacology, **141**, 2004, 1285-1293.
3. De Ponti, F., M. Tonini. Irritable bowel syndrome: new agents targeting serotonin receptors subtypes. – Drugs, **61**, 2001, 317-332.
4. Gershon, M. Serotonin and its implication for the management of irritable bowel syndrome. – Gastroenterology, **3**, 2003, 25-34.
5. Lee, S.L., W. Wang, B. Moor, B. Faburg. Dual effect of serotonin on growth of smooth muscle cells in culture. – Cric. Res., **68**, 1991, 1362-1368.
6. Mertz, H., V. Morgan., G. Taner et al. Regional cerebral activation in irritable bowel syndrome and control subjects with painful and nonpainful rectal distinction. – Gastroenterology, 2000, No 118, 842-848.
7. National Academy of Sciences, Biographical Memoirs, www.nap.edu/books. **68**, 1995, 237-252.
8. Saxena, P., M. Ferran. From serotonin receptor classification to the antimigraine drug sumatriptan. – Cephalalgia, **12**, 1992, 187-196.
9. Tzaneva, M., Ultrastructural immunohistochemical localization of gastrinq, somatostatin and serotonin in endocrine cells of human antral gastric mucosa. – Acta Histichemica, **105**, 2003, 191-193.
10. Shafermaer, A., R. Zanner, M. Graztl, G. Sacha, Ch. Prinz. Characterization of enterochromaffin cells isolated from the rat ileum. – In: Cell Biology of the Chromaffin Cell (Eds. R. Borges, L. Gandia). E-net ISCC-12 Book, 2004, 175-185.
11. Whitaker-Azmitia, P. The discovery of serotonin and its role in neuroscience. – Neuropsychopharmacology, **21**, 2002, 2-8.
12. Wood, J., D. Alpers, P. Andrews. Fundamentals of gastroenterology. – Gut, **45**, 1999, 1-44.
13. Chomeriki, C. G., I. Morozov. Importance of quantitative estimation of distribution of secretory granules in the cytoplasm of stomach endocrine cells. – Arch. Anat. Histol. Embryol., XC, 1986, 87-91 (in Russian).

Institute of Experimental Morphology and Anthropology with Museum
Bulgarian Anatomical Society

Acta morphologica et anthropologica, 12
Sofia • 2007

Ultrastructural Characteristics of Germ Cell Apoptosis in Adult Rats after Treatment with Ethane Dimethanesulfonate (EDS)

M. Bakalska, N. Atanassova, Y. Koeva, A. Russinova, B. Nikolov, M. Davidoff***

Institute of Experimental Morphology and Anthropology with Museum, Bulgarian Academy of Sciences, Sofia
**Department of Anatomy and Histology, Medical University, Plovdiv*
***Institute of Anatomy, University of Hamburg, Germany*

EDS selectively and temporary destroys Leydig cells in the adult rat testis and thus suppresses serum and intratesticular testosterone levels. Testosterone withdrawal results in marked increase of germ cell apoptosis and disturbance of spermatogenesis. We aimed to identify more precisely the apoptosis of germ cells at ultrastructural level. The present study provides detailed description of different phases of apoptotic process. We distinguished the specific appearance of apoptotic features in different germ cell types, spermatogonia, spermatocytes and round spermatids. The specificity of apoptotic manifestation involved the manner of chromatin clump condensation and localisation as well as pattern of cellular organelles disintegration. In situ detection of DNA fragmentation and ultrastructural investigations in tandem with biochemical studies on spontaneous and induced apoptosis, open new perspectives for understanding the importance of germ cell death in normal and pathological events in the spermatogenesis.

Key words: EDS, apoptosis, spermatogenesis, electron microscopy.

Introduction

Apoptosis is an active cellular process of gene-directed self-destruction. In vivo apoptosis is detected primarily in proliferating tissues such as the epithelium of the adrenal cortex, the germinal centers of lymph nodes, and the seminiferous epithelium of the testis [11]. Germ cells at different stages of the spermatogenic cycle possess their own physiological features and respond differently to exogenous stimuli. To date, much data are available showing that germ cell apoptosis is found spontaneously [1, 4] and also it can be induced by exposure to hyperthermia [16, 7], chemotherapeutic drugs [13], radiation [5] and chemical agents such as ethane dimethanesulfonate (EDS). EDS is known to destroy selectively Leydig cells in the testis and thus suppressed serum and intratesticular testosterone to undetectable levels [7].

Adult mammalian spermatogenesis is a testosterone-dependent process. Despite decades of studies, however, the mechanism (s) by which testosterone regulates spermatoge-

nesis remains uncertain. It has been shown that cell loss by apoptosis occurs normally during spermatogenesis [6, 9]. Recent studies have shown that testosterone withdrawal from the rat testis results in increased germ cell apoptosis [12, 18, 19], suggesting that testosterone may function as a cell survival factor, in some way protecting germ cell from apoptotic death.

The molecular mechanism by which testosterone does so, however, has not yet been elucidated. The regulation of apoptosis is dependent upon specific gene production. Bcl-2 multigene family is known to includes antiapoptotic genes Bcl-2, Bcl-x (promote cell survival by inhibiting apoptosis) and pro-apoptotic genes Bax, Bad, Bak (induce cell death by blocking the ability of Bcl-2 to inhibit apoptosis. An alternative and more rapid way for programmed cell death is mediated by Fas pathway. Fas lygand is a transmembrane protein that can initiate apoptosis by binding to Fas-receptor expressing cells activating caspase enzyme cascade [21]. Ever since it was proposed as a model of cell death [8, 13], apoptosis has generally been visualized by its morphological feature. In this study, rat testes exposed to EDS treatment were examined histologically and by TUNEL method (terminal transferase-mediated digoxigenin-11-dUTP nick end labeling) as well as by electron microscopy. The examination was undertaken to identify more precisely the different stages of apoptotic process at ultrastructural level.

Materials and Methods

Adult male Wistar rats received a single intraperitoneal injection of EDS at dose of 75 mg/kg body weight. The animals were killed on days 1, 3, 7, and 21 after treatment. One testis was fixed in Bouin's solution, embedded in paraffin, and examined by light microscope. In situ assay of apoptosis: apoptotic cells were detected by using terminal deoxynucleotidyl transferase (TdT)-mediated digoxigenin-11-dUTP nick end labeling (TUNEL) method that resulted in a high degree of specificity and low background staining [14] and the quantitative assessment of apoptosis was performed according method of W o o l v e r i d g e et al. [21]. Electron microscopy: testicular fragments were fixed in 2.5% glutaraldehyde in 0.1 M cacodylate buffer, 1% osmium tetraoxide and embedded in Durcupan. Electron micrographs were made on an Opton EM 109.

Results

As we previously have shown [2] first signs of seminiferous epithelium regression were manifested three days post EDS treatment by marked increase in frequency of apoptotic germ cells identified by specific TUNEL method. The highest values of parameters for quantification of germ cell apoptosis (the number of apoptotic cells per tubule; the percentage of tubules with apoptosis and the apoptotic index) were found by 7 day after EDS which corresponded to the lowest plasma level of testosterone.

Electron microscopy confirmed the apoptotic nature of germ cell degeneration - at various phases of destruction apoptotic cells were surrounded by healthy neighbours. Ultrastructural observations revealed a unique set of degenerating germ cells, which were characterised by intense chromatine condensation, the shrinkage of cellular components and fragmentation of nuclear materials. Apoptotic cell death is characterised by nuclear and cytoplasmic condensation and usually affects single cells or small groups of cells in an asynchronous fashion. According to these features, the process of apoptosis of germ cells could be divided into three discrete stages: early, intermediate and late according to A l l a n et al. [1]. Apoptotic cells in the basal compartment of seminiferous tubules were

spermatogonia. We were also able to find the three stages of apoptosis (Fig. 1 A, B, C). In early stage of apoptosis the cheterochromatin was condensed and arranged in several sharply defined clumps which abutted against the nuclear membrane. The cytoplasm exhibited many vacuoles and dilated cisternae of the endoplasmic reticulum. The mitochondrial destruction also can be observed. Further, in the intermediate stage a massive clump of chromatin was present in the centre of nucleus and the cytoplasmic organelles were degenerated and as a result the whole cell profoundly diminished in size compared with intact spermatogonia (Fig. 1B). Finally, further disruption of the nuclear and cellular remnants was recognised and apoptotic bodies were formed (Fig. 1C).

More advanced germ cell types, spermatocytes and round spermatids also underwent apoptosis and they passed through the same stages of apoptotic process. The nucleus of apoptotic pachytene spermatocyte contained increasing amounts of chromatin. A dilatation of perinuclear space, cytoplasm vacuolisation and destruction of cellular organelles were observed (Fig. 2A). Final stages of apoptosis showed extensive shrinkage of nucleus and cytoplasm (Fig. 2B). The early apoptosis of round spermatids showed small clumps of cheterochromatin in the nucleus which were not seen in intact cells (Fig. 3A). In the later phase of apoptosis, the amount of chromatin increased and shrinkage of the cell with the complete condensation of the chromatin were appeared (Fig. 3B). In latest phases of apoptosis it is not possible to recognise the defined germ cell types and stages of differentiation.

Discussion

Testosterone withdrawal induced by EDS is a useful model for the in vivo investigation the possible role of apoptosis in the control of spermatogenesis, a phenomenon which can be considered as a result of an intriguing integration among cell proliferation, cell differentiation and cell death [20].

Although some biochemical features of apoptosis are now available, the in situ identification of DNA fragmentation by TUNEL technique and electron microscopy are the most reliable methods for detection of apoptosis.

The present study provides detailed description of different phases of apoptotic process. It was confirmed the apoptotic nature of dying cells from different stages of germ cell differentiation–spermatogonia, pachytene spermatocyte and round spermatids. We were able to visualise the common apoptotic stages described by A l l a n et al. [1], K o j i et al. [10]. Moreover, we distinguished the specific appearance of apoptotic features in different germ cell types, spermatogonia, spermatocytes and round spermatids. The specificity of apoptotic manifestation involved the manner of chromatin clump condensation and localisation as well as pattern of cellular organelles desintegration.

Several studies have indicated that spermatocytes and spermatids that died spontaneously or were killed by cytotoxic agents did not appear to be apoptotic [17]. In contrast, other authors based largely on the TUNEL methods have reported that cell death by apoptosis can be induced in spermatocytes or spermatids by hormonal changes or hyperthermia [3, 15]. The apoptosis could be triggered by many signals including the Fas and Fas ligand system and/ Bcl-2 family in the developing and adult testis [12, 18, 21]. N a n d i et al. [12] showed that EDS injection induced Fas-mediated germ cell apoptosis as a result of androgen ablation indicating an important role for testosterone in germ cell survival via suppression of Fas.

Recently S h o w et al. [17] proposed an alternative hypothesis about mechanism of spermatids death, so called anoikis involving loss of the attachment ability to the Sertoli cell (attachment-dependent cell from basal membrane) in contrast to apoptosis of less matured germ cells (spermatogonia and spermatocytes) induced by testosterone withdrawal.

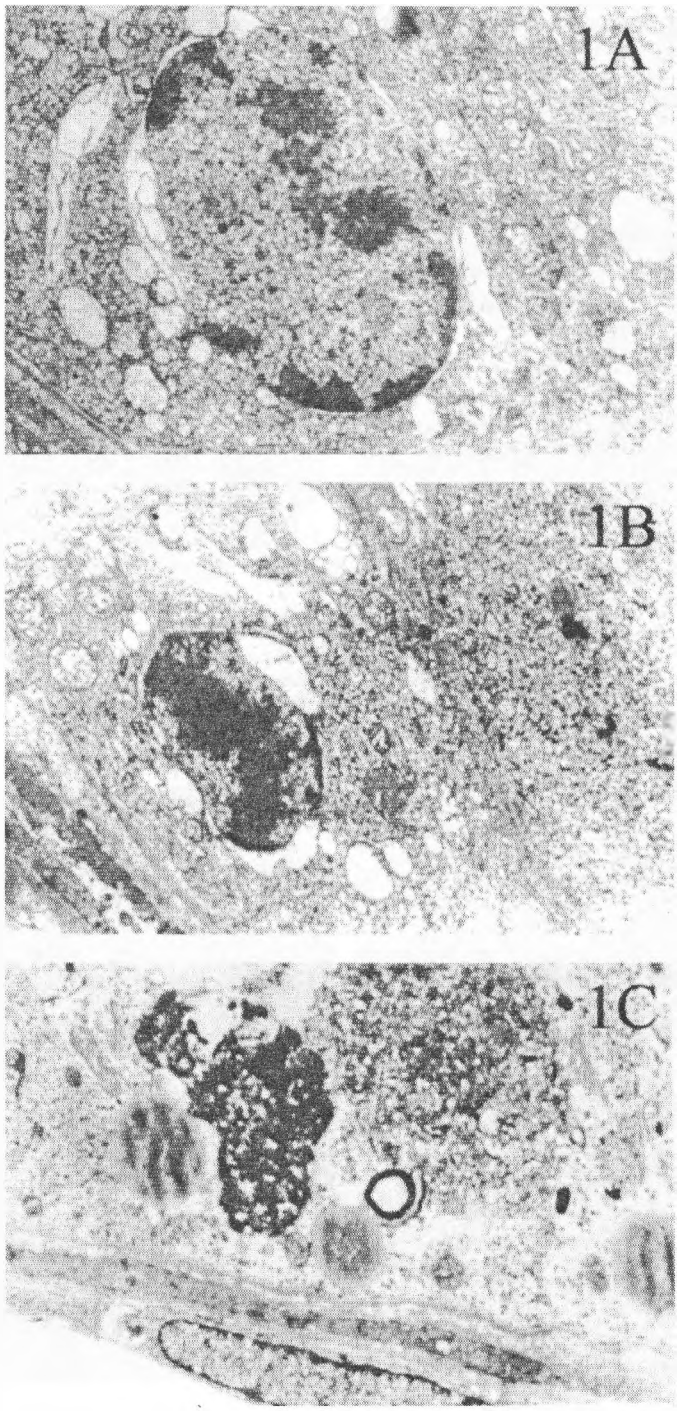

Fig. 1. Electron micrographs of spermatogonia at different stages of apoptosis (× 7000)
A — spermatogonium at early stage of apoptosis; B — an intermediate stage of apoptotic spermatogonium; C — late apoptotic stage with formation of apoptotic bodies

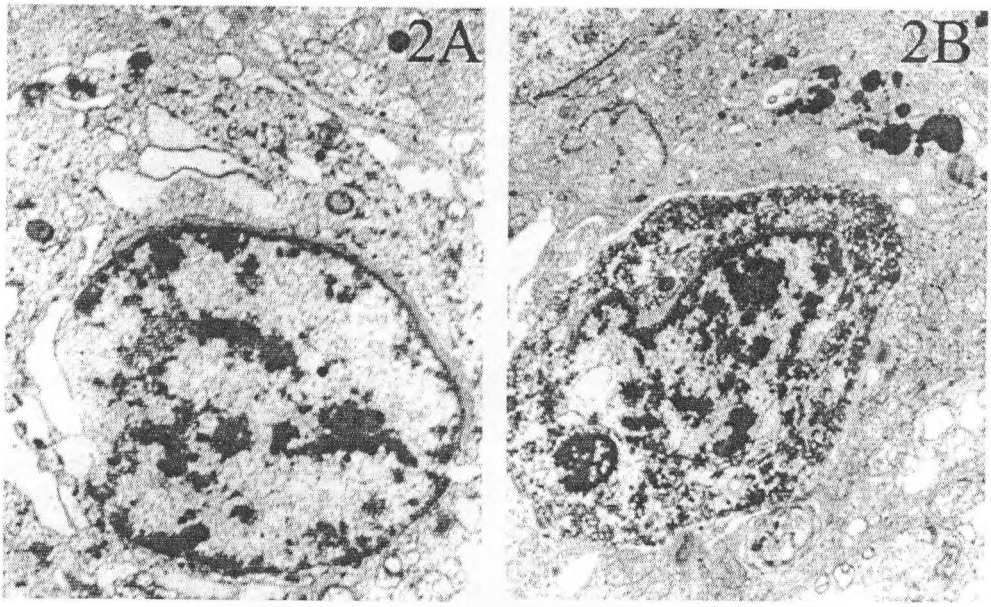

Fig. 2. Electron micrographs of spermatocytes at different stages of apoptosis (× 7000) pachytene spermatocytes in intermediate (A) and more advanced (B) state of apoptosis

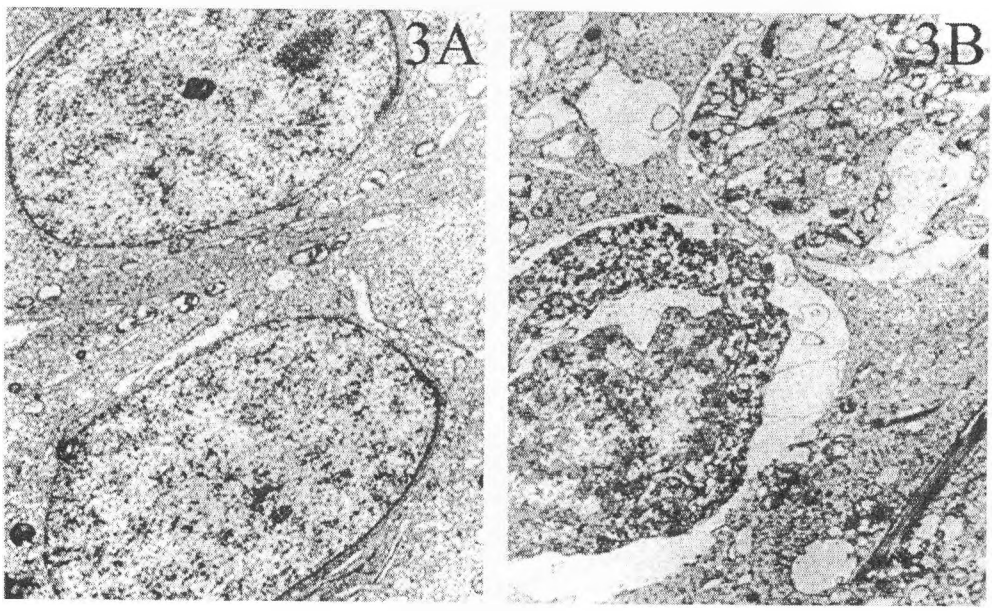

Fig. 3. Electron micrographs of round spermatids (× 4400)
A — two intact round spermatids; B — two spermatids in late stage of apoptosis

In situ detection of DNA fragmentation and ultrastructural investigations in tandem with biochemical studies on spontaneous and induced apoptosis, open new perspectives for understanding the importance of germ cell death in normal and pathological events in the spermatogenesis. Apoptosis which happens selectively to certain spermatogenic cells maintains normal spermatogenesis. However, unbalanced apoptosis could lead to spermatogenic dysfunction and infertility. Thus, a thorough understanding of the apoptosis mechanism might uncover the causes for many testicular failures and help to find efficient strategies against these defects.

References

1. Allan, D., B. Harmon, S. Roberts. Spermatogonial apoptosis has three morphologically recognizable phases and shows no circadian rhythm during normal spermatogenesis in the rat. – Cell Proliferation, **25**, 1992, 241-250.
2. Bakalska, M., N. Atanassova, Y. Koeva, B. Nikolov, M. Davidoff. Induction of male germ cell apoptosis by testosterone withdrawal after ethane dimethanesulfonate treatment in adult rats. – Endocr. Regul., **38**, 2004, 103-110.
3. Billig, H., I. Furuta, C. Rivier, J. Tapanainen, M. Parvinen, A. Hsueh. Apoptosis in testis germ cells: developmental changes in gonadotropin dependence and localization to selective tubule stages. – Endocrinology, **136**, 1995, 5—12.
4. Blanco-Rodriguez, J., C. Martinez—Garcia. Spontaneous germ cell death in the testis of the adult rat takes the form of apoptosis: re-evaluation of cell types that exhibit the ability to die during spermatogenesis. – Cell Proliferation, **29**, 1996, 13-31.
5. Hasegawa, M., G. Wilson, L. Russell, M. Meistrich. Radiation-induced cell death in the mouse testis: relationship to apoptosis. – Radiat. Res., **147**, 1997, 457-467.
6. Henriksen, K., H. Hakovirta, M. Parvinen. *In-situ* quantification of stagespecific apoptosis in the rat seminiferous epithelium: effects of shortterm experimental cryptorchidism. – Int. J. Androl., **18**, 1995, 256-262.
7. Henriksen, K., H. Hakovirta, M. Parvinen. Testosterone inhibits and induces apoptosis in rat seminiferous tubules in a stage-specific manner: in situ quantification in squash preparations after administration of ethane dimethanesulfonate. – Endocrinology **136**, 1995, 3285—3291.
8. Kerr, J., A. Wyllie, A .Currie. Apoptosis: a basic biological phenomenon with wide-ranging implications in tissue kinetics. – Br. J. Cancer., **26**, 1972, 239-257.
9. Kerr, J., B. Harmon. Definition and incidence of apoptosis: an historical perspective. – In: Current Communications in Cell and Molecular Biology: Apoptosis: The Molecular Basis of Death. (Eds L. D. Tomei and F. O. Cope FO). Vol 3. Cold Spring Harbor, NY, Cold Spring Harbor Laboratory Press, 1991, 5-29.
10. Koji, T., Y. Hishikawa. Germ cell apoptosis and its molecular trigger in mouse testes. – Arch. Histol. Cytol., **66**, 2003, No 1, 1-16.
11. Meikrantz, W., R. Schlege. Apoptosis and the cell cycle. – J. Cell Biochem., **58**, 1995, 160-174.
12. Nandi, S., P. Banerjee, B. Zirkin. Germ cell apoptosis in the testes of Sprague Dawley rats following testosterone withdrawal by ethane 1,2-dimethanesulfonate administration: Relationship to Fas? – Biol. Reprod., **61**, 1999, 70-75.
13. Searle, J., T. Lawson, P. Abbott, B. Harmon, J. Ke. An electron-microscope study of the mode of cell death induced cancer-chemotherapeutic agents in populations of proliferating normal and neoplastic cells. – J. Pathol., **116**, 1975, 129-138.
14. Sharpe, R., N. Atanassova, C. McKinnell, P. Parte, K. Turner, J. Fisher, J. Kerr, N. Groome, S. Macpherson, M. Millar, P. Sanders. Abnormalities in functional development of the Sertoli cells in rats treated neonatally with diethylstilbestrol: a possible role for estrogens in Sertoli cell development. – Biol. Reprod., **59**, 1998, 1084-1094.
15. Shetty, J., G. Marathe, R. Dighe. Specific immunoneutralization of FSH leads to apoptotic cell death of the pachytene spermatocytes and spermatogonial cells in the rat. – Endocrinology, **137**, 1996, 2179—2182.
16. Shikone, T., H. Billig, A. Hsueh. Experimentally induced cryptorchidism increases apoptosis in rat testis. – Biol. Reprod., **51**, 1994, 865-872.
17. Show, M., J. Folmer, M. Anway, B. Zirkin. Testicular expression and distribution of the rat Bcl2 modifying factor in response to reduced intratesticular testosterone. – Biol. Reprod., **70**, 2004, 1153-1161.

18. Sinha-Hikim, A., C. Wang, A. Leung, R. Swerdloff. Involvement of apoptosis in the induction of germ cell degeneration in adult rats after gonadotropin-releasing hormone antagonist treatment. – Endocrinology, **136**, 1995, 2770-2775.
19. Tapanainen, J., J. Tilly, K. Vihko, A. Hsueh. Hormonal control of apoptotic cell death in the testis: gonadotropins and androgens as testicular cell survival factors. – Mol. Endocrinol., 7, 1993, 643—650.
20. Troiano, L., M. Fustini, E. Lovato, A. Frasoldati, W. Malorni, M. Capri. Apoptosis and spermatogenesis: evidence from an in vivo model of testosterone withdrawal in the adult rat. – Biochem. Biophys. Res. Commun., **202**, 1994, 1315-1321.
21. Woolveridge, I., M. de Boer-Brouwer, K. Teerds, I. Moris. Leydig cell apoptosis after administration of ethane dimethanesulfonate to the adult male rat is a Fas-mediated process. – Endocrinology, **140**,1999, 3797-3804.

Institute of Experimental Morphology and Anthropology with Museum
Bulgarian Anatomical Society

Acta morphologica et anthropologica, 12
Sofia • 2007

Quantitative Comparative Analysis of the Influence of IFN-γ on the Erythroid (BFU-E and CFU-E) and Myeloid (CFU-GM) Progenitors *in vitro*

Y. Gluhcheva, K. Schroecksnadel, B. Wirleitner*, E. Zvetkova, G. Konwalinka*, D. Fuchs**

Institute of Experimental Morphology and Anthropology with Museum Bulgarian Academy of Sciences, Sofia
**Medical University Innsbruck, Innsbruck, Austria*

The addition of different doses of IFN-r (5000 U/ml once or 200/400 U/ml — every second day) to cultured *in vitro* purified and enriched human hematopoietic CD34+ progenitor cells stimulated significantly their proliferation and differentiation to erythroid and myeloid lineages. The cytokine enhanced the formation of primitive erythroid colonies (burst-forming unit-erythroid — BFU-E) and myeloid colony-forming units (granulocyte/macrophage — CFU-GM). IFN-γ exhibited weaker stimulatory affect on colony-forming unit — erythroid (CFU-E). Compared to the CFU-GM colony formation, BFU-E were more sensitive to the effect of IFN-r. CD34+ hematopoietic colony formation *in vitro* was quantitatively influenced not only by IFN-r but also by culture medium.

Key words: interferon-gamma (IFN-γ), human hematopoietic CD34+ progenitor cells - purified and enriched, BFU-E, CFU-E, CFU-GM.

Introduction

CD34+ hematopoietic progenitor cells are the most commonly used cell population for *in vitro* assays. Recent reports suggest that CD34 antigen is involved in the onset of hematopoietic cell proliferation and adhesion [4, 7]. The antigen expression decreases when maturing hematopoietic cells loose their capacity to form colonies *in vitro.*

Interferon-gamma (IFN-γ) is an inflammatory cytokine known to act *in vitro* (when added to bone marrow cultures) as inhibitor of erythroid cell proliferation [8, 9, 14]. The results demonstrating the inhibitory effect of IFN-γ on human hematopoietic progenitor cells suggest that it is mediated by accessory cells as T-lymphocytes and macrophages [8, 12]. On the other hand there are reports showing the synergistic effects of IFN-γ with SCF and IL-3 and thus IFN-γ stimulates hematopoiesis [10]. The cytokine switches monocyte differentiation to macrophages instead of dendritic cells [3]. Due to the bipotent activities of this inflammatory cytokine [2, 5, 9, 10, 12, 13], special attention must be paid to its affects on the hematopoietic progenitor cells — both *in vitro* and *in vivo.*

When added to *in vitro* cultures of erythroid/myeloid cells the affects of IFN-γ depend on the cytokine's doses, duration time, the other growth factors present in the culture medium as well as on the degree of cell maturity (differentiation).

The aim of the present work is to investigate the affects of different doses of IFN-γ on hematopoietic (erythroid and myeloid) colony formation *in vitro* (in semi-solid agar cultures of purified and enriched human hematopoietic CD34+ progenitor cells).

Materials and Methods

1. Cell cultures

Purified (92% purity) and enriched (5%) human hematopoietic CD34+ progenitor cells (kindly provided by the Laboratory for Immune Biology, Internal Medicine, Innsbruck, Austria), were thawed, washed with Hanks Balanced Salt Solution — HBSS (PAA Laboratories, Austria) and centrifuged for 15 min at 1050 rpm. After the first centrifugation the cells were washed, centrifuged again (10 min at 1000 rpm), resuspended in Iscove's Modified Dulbecco Medium (IMDM), counted and plated in 4-well Nunc Petri dishes at a density of 2.5×10^3/well for the purified and 1×10^4 cells/well — for the enriched cells. Each sample was performed in three parallels. The two phase *semi-solid agar cell cultures* were prepared in the same Petri dishes with 0.3% agar.

The superficial liquid layer of the cultures contained: IMDM, 10% fetal calf serum (FCS — Gibco), 2% bovine serum albumin (BSA-Sigma), 6 U/ml erythropoietin (Erypo-Janssen-Cilag Pharma), 2×10^{-4}M mercaptoethanol, 4 mM glutamine and recombinant cocktail — RC [consisting of recombinant human IL-3 — 50 U/ml and recombinant human stem cell factor (SCF) — 10 U/ml (Chemicon)].

Besides in RC, purified and enriched human CD34+ hematopoietic progenitor cells were also cultured in 20% *agar leukocyte conditioned medium* — Agar-LCM (CellSystems Biotechnologie Vertrieb GmbH), supplemented with 10% FCS, 2% BSA, 6 U/ml Epo, 2×10^{-4}M mercaptoethanol and 4 mM glutamine.

IFN-γ (Rentschler Biotechnologie GmbH & Co.KG) was added at different doses (5000 U/ml — once; 200 U/ml and/or 400 U/ml — every second day) to the liquid phase of both experimental systems at time of hematopoietic cell cultivation.

The *agar cell cultures* prepared were incubated at 37°C in humidified air of 5% CO_2 for 14 days. After incubation cell colonies were scored on inverted microscope. The agar layers were fixed in glutaraldehyde, mounted on glass slides and stained with May-Grünwald/Giemsa to confirm colony identity and their cytological characteristics [6].

2. Scoring criteria for hematopoietic colonies' identification

In order to classify the colonies as erythroid burst-forming-unit (BFU-E) and colony-forming unit-erythroid (CFU-E) as well as colony-forming unit-granulocyte/macrophage (CFU-GM), the following scoring criteria [1, 6] were used:

— CFU-E consists of less that 65 cells which are fully hemoglobinized after 14 days of incubation;

— BFU-E consists of more than 65 cells which form colonies with at least two clusters or bursts. They could or could not be fully hemoglobinized after 14 days of incubation;

— CFU-GM colonies are morphologically identified as having a dense central core of not well distinguished undifferentiated cells, surrounded by a less dense halo of more differentiated myeloid cells (granulocyte/macrophages).

3. Statistical analysis

To investigate quantitatively whether the applied doses of IFN-γ influence significantly and in different ways hematopoietic colony formation, the *Student's t-test* was used. A difference is assumed to be significantly large if $p<0.05$.

Results and Discussion

a) Influence of IFN-γ on the formation of erythroid – BFU-E and CFU-E colonies

The erythropoietic effect of the IFN-γ was better expressed when the cytokine was added *in vitro* in small portions (200 and/or 400 U/ml - every second day); weaker stimulatory effect was observed at high single dose — 5000 U/ml.

The stimulatory effect of IFN-γ was well defined quantitatively in both culturing conditions: at low doses — $p<0.005$, at high dose — $p<0.05$ for purified and $p<0.001$ for enriched cells (Table 1).

Table 1. Quantitative analysis of the influence of IFN-γ on erythroid and myeloid colony formation

Type of colonies	Cell type	Culture medium	Control samples	IFN-γ concentration		
				5000 U/ml once	400 U/ml/2 d	200 U/ml/2 d
	CD34+		Number of hematopoietic colonies / 0.5 ml			
BFU-E	— purified	Agar-LCM	27	49.25***	47.75*	47.7*
		RC	59	70.25	83.5**	79.75**
	— enriched	Agar-LCM	37.75	50.5*	62**	59.5****
		RC	95	141****	144.5****	143***
CFU-GM	— purified	Agar-LCM	44.25	52.25	43.5	41.5
		RC	23.5	27.25	36**	34.5*
	— enriched	Agar-LCM	19.7	30.5*	34*	35.75***
		RC	17.5	30.5**	27**	23

* $p<0.05$; ** $p<0.01$; *** $p<0.001$; **** $p<0.005$.

BFU-E showed higher proliferation and colony formation activities (2.2 fold increase for purified and 2.5 — for enriched cells) when the erythroid progenitors were cultured in RC compared to Agar-LCM ($p<0.005$ for purified and $p<0.001$ for enriched). When the cytokine was added to cultured in Agar-LCM purified cells a 1.8 fold increase of colony formation was registered (at dose 5000 U/ml $p<0.001$ and $p<0.05$ for the low doses respectively). When the same population was cultured in RC a 1.2 to 1.4 increase (5000 U/ml IFN-γ; 200 and 400 U/ml/2 days respectively) was observed.

The results from the quantitative analysis (presented in Fig. 1a, b) have shown that the addition of IFN-γ to the semi-solid agar cultures stimulated the formation of the immature erythroid colonies by BFU-E progenitors.

Unlike high cytokine concentrations, low doses of IFN-γ have more significant synergistic effects with SCF and IL-3 in the RC culture medium. The quantitative analysis for the enriched CD34+ hematopoietic cells has shown that when they were cultured in Agar-LCM, the addition of IFN-γ resulted in 1.3 (5000 U/ml IFN-γ) and 1.6 (200/400 U/ml/2 days) fold increase in the number of erythroid colonies. In RC culture conditions, a 1.5 increased colony formation was seen.

The results presented in Fig. 2a, b show that CFU-E colonies develop better in Agar-LCM. In case of the enriched cells a clear stimulatory affect of the cytokine is observed. For the purified cells only the high dose IFN-γ (5000 U/ml) stimulated insignificantly

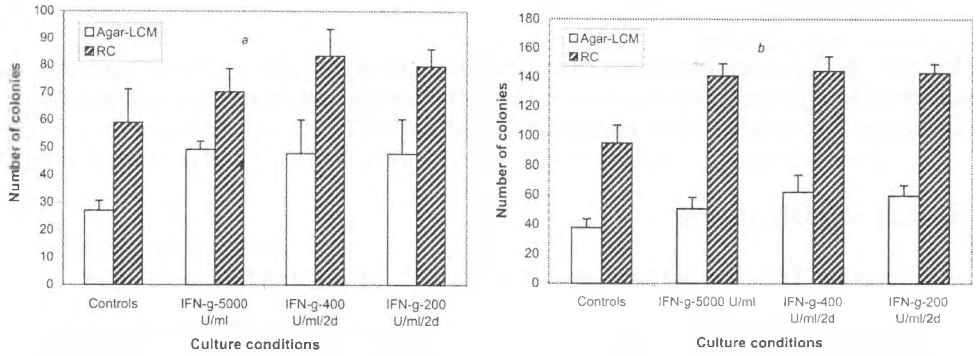

Fig. 1. BFU-E colonies formed by cultured in Agar-LCM and RC
a — purified and *b* — enriched CD34+ hematopoietic progenitor cells

colony formation in Agar-LCM. Therefore, the effect of IFN-γ is possibly inhibitory for both cell populations cultured in RC. This means that the culture conditions are important for the stimulatory or inhibitory effect of the cytokine.

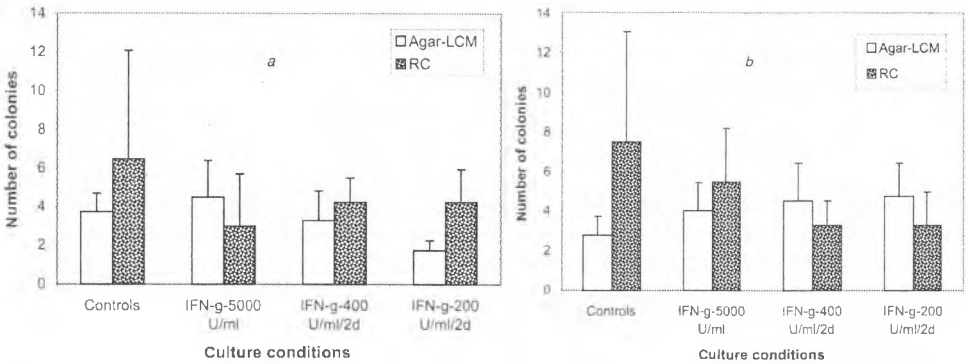

Fig. 2. CFU-E colonies formed by cultured in Agar-LCM and RC
a — purified and *b* — enriched CD34+ hematopoietic progenitor cells

The degree of cell maturity (differentiation) can be also a determining factor for the IFN-γ effect *in vitro*: more IFN-γ receptors are found on mature red blood progenitors [11].

b) Influence of IFN-γ on the formation of mixed-granulocyte/macrophage colonies (CFU-GM)

IFN-γ added *in vitro* at single high dose (5000 U/ml) stimulated significantly CFU-GM colony formation from purified CD34+ hematopoietic cells (1.2 fold increase in Agar-LCM). The same cytokine dose enhanced myeloid colony formation by enriched cells (1.5 fold, $p<0.05$) as well. The effect of IFN-γ was even stronger (1.7 to 1.8 fold increase) when the low concentrations were used (200 and/or 400 U/ml/2 days; $p<0.001$ and $p<0.05$, respectively — Table 1). In the latter case, a possible influence of the accessory mononuclear cells (in the buffy coat fraction) could be considered [9]. Surprisingly, no such stimulatory effect was observed for the purified CD34+ cells in the same culture conditions.

The addition of exogeneous IFN-γ at single dose 5000 U/ml stimulated 1.2 times myeloid colony formation by purified cells, cultured in RC. The same cytokine dose increased 1.7 times the number of CFU-GM colonies developing from enriched hematopoietic cells in the RC culture medium. In these experimental conditions, the low IFN-γ concentrations stimulated myeloid colony formation by the enriched cells: 1.3 times at dose 200 U/ml/2 days and 1.5 fold — at 400 U/ml/2 days. The same low cytokine concentrations increased 1.5 times the number of GM-colonies by purified CD34+ cells.

The quantitative analysis has shown that more CFU-GM colonies were formed when the hematopoietic cells (purified and enriched) were cultured in Agar-LCM than in RC ($p<0.05$ for purified and insignificant difference — for enriched). When the purified CD34+ cells were cultured in Agar-LCM a 1.9 fold increase in the number of myeloid colonies was observed (compared to that in RC). For the enriched cells in Agar-LCM a 1.1 fold increase was seen.

The results show (Fig. 3a, b) that the *in vitro* addition of high and low doses IFN-γ stimulated quantitatively but in a different manner mixed CFU-GM colony formation by human CD34+ hematopoietic progenitor cells.

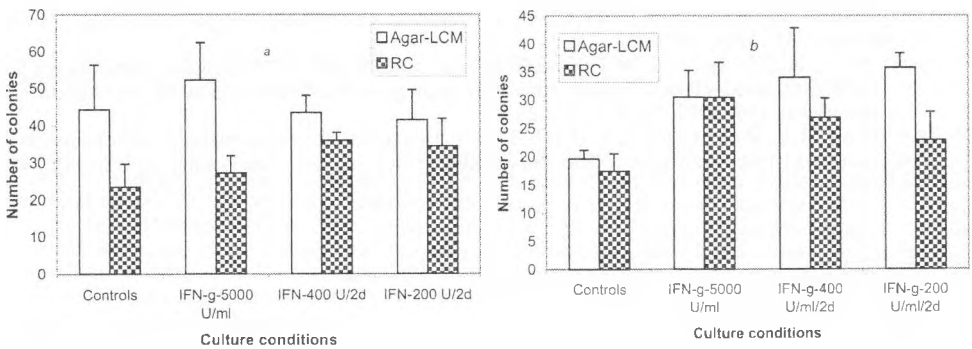

Fig. 3. CFU-GM colonies formed by cultured in Agar-LCM and RC
a — purified and *b* — enriched CD34+ hematopoietic progenitor cells

Conclusions

The effects of different doses IFN-γ exogeneously added to *in vitro* cultured (in semi-solid agar) human CD34+hematopoietic progenitor cells cannot be described as "only stimulatory or inhibitory". Our results are in agreement with the data that the influence of the cytokine on erythroid (BFU-E and CFU-E) and myeloid (CFU-GM) colony formation depends on IFN-γ doses, degree of hematopoietic cell maturity as well as on cell culture conditions.

References

1. Atlas of Human Hematopoietic Colonies. Vancouver, Canada. Stem Cell Technologies Inc., 1995.
2. Boehm, U., T. Klamp, M. Groot, C. Howard. Cellular responses to interferon-γ. – Ann. Rev. Immunol., **15**, 1997, 749-795.
3. Delneste, Y., P. Charbonnier, N. Herbault, G. Magistrelli, G. Caron, J-Y. Bonnefoy, P. Jeannin. Interferon-γ switches monocyte differentiation from dendritic cells to macrophages. – Blood, **101**, 2003, No 1, 143-150.

4. Dooley, D., B. Oppenlander, M. Xiao. Analysis of primitive CD34- and CD34+ hematopoietic cells from adults: gain and loss of CD34 antigen by undifferentiated cells are closely linked to proliferative status in culture. – Stem Cells, **22**, 2004, 556-569.
5. Flores-Guzman P., M. Gutierez-Rodriguez, H. Mayani. *In vitro* proliferation, expansion and differentiation of a CD34+ cell-enriched hematopoietic cell population from human umbilical cord blood in response to recombinant cytokines. – Arch. Med. Res., **33**, 2002, No 2, 107-114.
6. Konwalinka, G., D. Geissler, Ch. Peschel, B. Tomaschek, F. Schmalzl, H. Huber, R. Odavic, H. Braunsteiner. A micro agar culture system for cloning human erythropoietic progenitors in vitro. – Exp. Hematol., **10**, 1982, No 1, 71-77.
7. Krause, D., M. J. Fackler, C. I. Civin, W. S. May. CD34: Structure, biology and clinical utility. – Blood, **87**, 1996, No 1, 1-13.
8. Mamus, S, S. Beck – Schroeder, E. Zanjani. Suppression of normal human erythropoiesis by gamma interferon in vitro. Role of the monocytes and T lymphocytes. – J. Clin. Invest., **75**, 1985, 1496-1503.
9. Selleri, C., J. P. Maciejewski, T. Sato, N. S. Young. Interferon-γ constitutively expressed in the stromal microenvironment of human marrow cultures mediates potent hematopoietic inhibition. – Blood, **87**, 1996, 4149-4157.
10. Shiohara, M., K. Koike, T. Nakahata, A. Komiyama. Hematopoietic progenitors and synergism of interferon-γ and stem cell factor. – Leuk. Lymphoma, **14**, 1994, No 3-4, 203-211.
11. Taniguchi, S., C. H. Dai, S. B. Krantz. Specific binding of interferon-γ to high affinity receptors on human erythroid colony-forming cells. – Exp. Hematol., **25**, 1997, No 3, 193-198.
12. Tsuji, K., K. Muraoka, T. Nakahata. Interferon-γ and human megakaryopoiesis. – Leuk. Lymphoma, **31**, 1998, 107-113.
13. Tsujimura, H., T. Nagamura-Inoue, T. Tamura, K. Ozato. IFN consensus sequence binding protein/IFN regulatory factor-8 guides bone marrow progenitor cells toward the macrophage lineage. – J. Immunol., **169**, 2002, No 3, 1261-1269.
14. Zoumbos, N. C., P. Gascon, J. Y. Djeu, N. S. Young. Interferon is a mediator of hematopoietic suppression in aplastic anemia in vitro and possibly in vivo. – Proc. Natl. Acad. Sci., USA, **82**, 1985, 188-192.

Institute of Experimental Morphology and Anthropology with Museum
Bulgarian Anatomical Society

Acta morphologica et anthropologica, 12
Sofia • 2007

Effects of Fibroblast Growth Factors (FGF's) 1, 2 and 7 on the First Wave of Mouse Prospermatogonial Proliferation

Y. Martinova

Institute of Experimental Morphology and Anthropology with Museum
Bulgarian Academy of Sciences, Sofia

The onset of spermatogenesis in prepubertal males is marked by the first wave of mitosis in quiescent prospermatogonia. Since Sertoli cells at that time are nonmature and do not mediate hormonal regulation signals, it is hypothesized that this event is under the direct control of paracrine growth factors FGF 1 or FGF 2. We have used a Day 2 mouse testis organ culture assay to identify factors that may control this process. Recombinant FGF 1, FGF 2 and FGF 7 were tested. The DNA synthesis in quiescent prospermatogonia was identified immunocytochemically by using Cell Proliferation kit. In control testes the percentage of labelled germ cells was 10, while after 24 h cultivation in presence of 100 pg/ml FGF 2 the mitotic activity of prospermatogonia increased up to 57%. FGF 1 and FGF 7 stimulated mitotic activity to a lesser extend compared with FGF 2. It is concluded that growth factors from FGF's family play a key role in paracrine regulation of the first wave of prepubertal spermatogonial proliferation in mammals.

Key words: Fibroblast Growth Factors, prespermatogenesis.

Introduction

Different factors are known to stimulate DNA synthesis, proliferation and/or differentiation of germ cells in the adult testes. In the rat testis activin A increases ^{3}H-thymidine incorporation by differentiating spermatogonia [7], whereas inhibin decreases their number [8]. IL-1α, IGF – I and IGF – II stimulate DNA synthesis of differentiating spermatogonia in adult seminiferous tubules in vitro [9]. Thus several growth factors appear to regulate the proliferation of spermatogonia in adult testes but none of these data demonstrate the stimulation of DNA synthesis by the "totipotent" prospermatogonial cells on neonatal animals [5]. Using Sertoli cell secreted media isolated from rat prepubertal Sertoli cells we stimulated prospermatogonial proliferation up to 5-10 fold over the controls in organ culture [4]. We hypothesized that Sertoli cells secrete growth factors, probably FGF's family, acting as a local mitogenic factors on male germ cells.

Fibroblast growth factors make up a large family of polypeptide growth factors, found out from nematodes to humans. In vertebrates 22 members of FGF's family range in molecular mass from 17 to 34 kDa and share 13 — 71% amino acid identity. FGF's have a high affinity for heparin sulfate proteoglicans and require heparin sulfate to activate one

of four cell-surface FGF receptors [11]. FGFs are involved in many biological processes acting through kinase receptors. To date, based on recent evidences, FGF anf TGFβ family members are the only growth factors implicated in regulation of DNA synthesis in prospermatononial stem cells during the first mitotic wave in postnatal testicular development.

The aim of the present work was to study the effect of some members of FGF's family, namely recombinant FGF 1, FGF 2 and FGF 7 on mouse prospermatogonial proliferation.

Materials and Methods

Materials

Male conventional 2 days old mice were supplied by animal breeding farm of the Bulgarian Academy of Sciences (Sofia). Dulbecco's modified Eagle's medium (DMEM) and bovine serum albumin (BSA) (Sigma), OCT compound (Miles, Scientific), Procelloidin (Fluka Chemica-Biochemica), Organ culture dishes (Falkon, Becton-Dickinson), Cell proliferation kit (Amersham) were used. Recombinant Fibroblast growth factors 1, 2 and 7 were kindly provided by Prof. Anthony R. Bellve (Columbia University, New York, USA).

Tissue culture

Tissue culture were prepared as described previously [6]. Briefly, 2-day-old mouse testes were cut into 2 segments, placed on permeable celloidine membrane and placed in an organ culture dish containing DMEM supplemented with 2% BSA and 5-bromo-2-deoxyuridine (BrdU) (control). In the experimental groups the medium was additionally supplemented with FGF 1, 2 or 7 in doses of 1, 3, 10, 30, 100 and 300 pg/ml. The explants were cultured at 37°C with 5% CO_2. At 24th h the explants were immersed in OCT compound, snap-frozen in liquid nitrogen and cryosectioned at 5 μm.

Immunocytochemistry

Sections mounted on slides were fixed in Carnoy's fixative. The incorporated BrdU was detected by using Cell proliferation kit. The sections were countersatined with Harris's haematoxylin and mounted in Canada balsam.

Statistic analysis

At least 100 prospermatogonia were counted in three different testicular segments, each done in triplicate. Statistical analysis was performed by Student's t-test.

Results

On day 2 post partum (p.p.) mouse testis is composed of seminiferous cords and intersitial tissue. In the cords two cell types are well distinguished: Sertoli cells and prospermatogonia. Nonmature Sertoli cells are situated on the basal membrane. They are cylindric in shape, small in size (5-7 μm in diameter) with dark nuclei. In 2-day-old mouse testis Sertoli cells actively proliferate and intensively incorporate BrdU (Fig. 1 and Fig. 2). Prospermatogonia are located in the center of the seminiferous cords. They are big,

round cells (about 20 μm in diameter) with pale nucleus and 2-3 nucleoli (Fig. 1, Fig. 2). In control testes of all groups the percentage of labelled prospermatogonia was about 10 (Fig. 3, 4, 5). Dose-response curve of FGF1 application showed stimulation of prospermatogonial germ cell proliferation up to 27% at a dose of 100 pg/ml (Fig. 3). FGF 2 stimulated BrdU incorporation up to 57% at a dose of 100 pg/ml (Fig. 4). The effect of FGF 7 was similar to FGF 1 with maximum stimulation up to 31% at a dose of 30 pg/ml (Fig. 5). After incubation with maximally effective doses of FGF 2 many prospermatogonial cells were localized between Sertoli cells on the basal membrane of the testicular cords (Fig. 2).

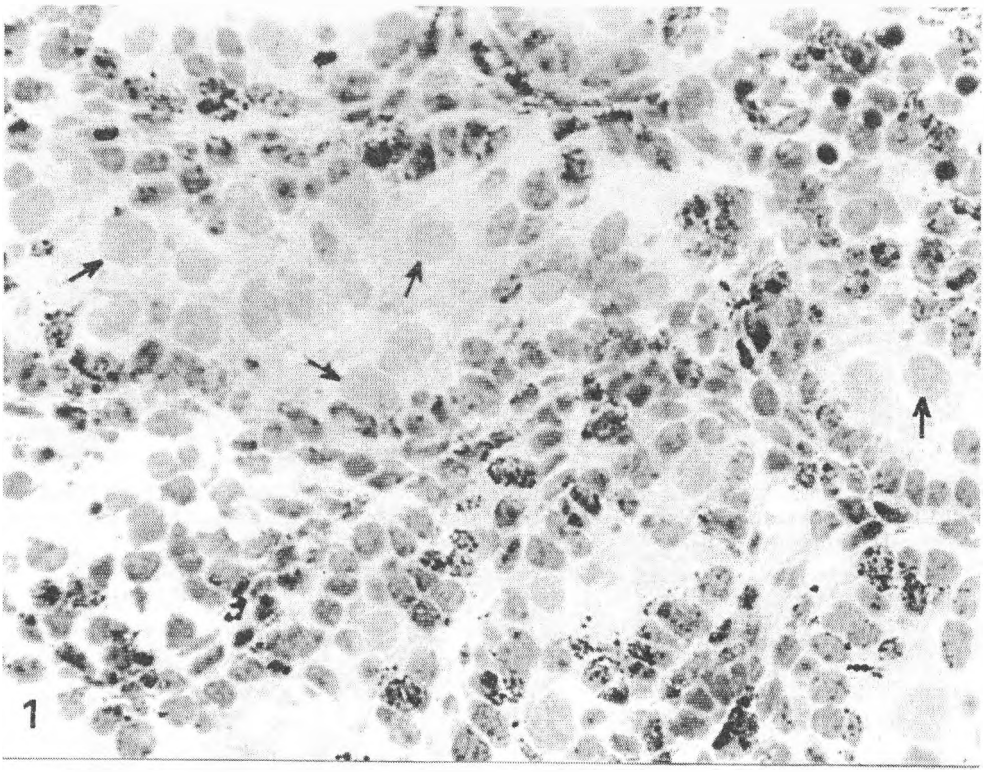

Fig. 1. Section from 2-day-old mouse testis, incubated 24 h in DMEM and BrdU only (control). Prospermatogonia are not labeled (arrows) (× 100)

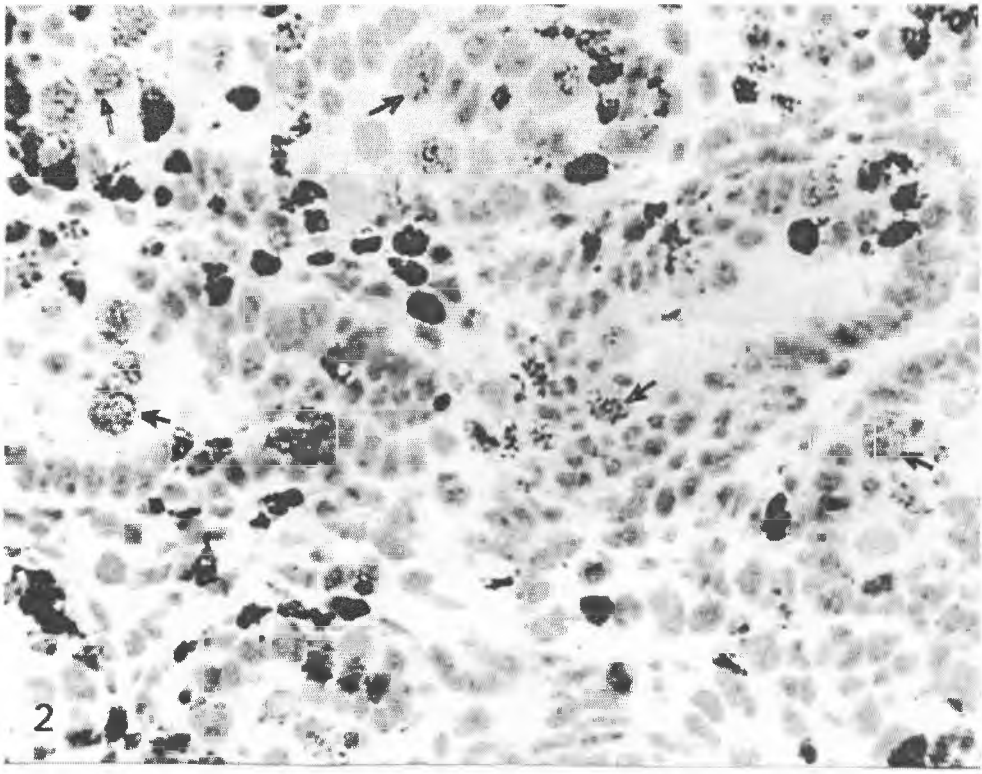

Fig. 2. Section from 2-day-old mouse testis, incubated 24 h in presence of DMEM, BrdU and 100pg/ml FGF 2. Labelled prospermatogonia in the center of the seminiferous cords and between Sertoli cells on the basal membrane (arrows) (× 100)

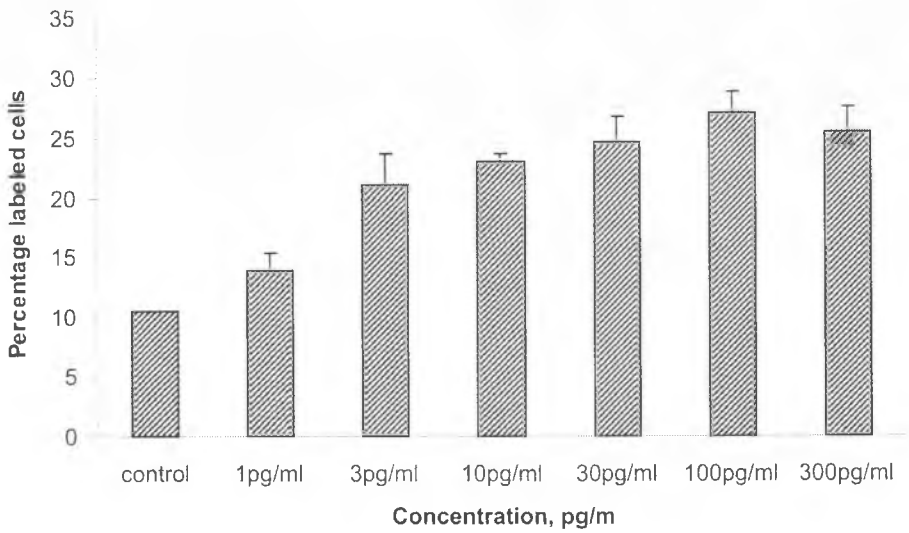

Fig. 3. Percentage (mean ± SD) of labelled prospermatogonia of 2-day-old mouse testis, 24 h after culture in presence of different doses FGF 1

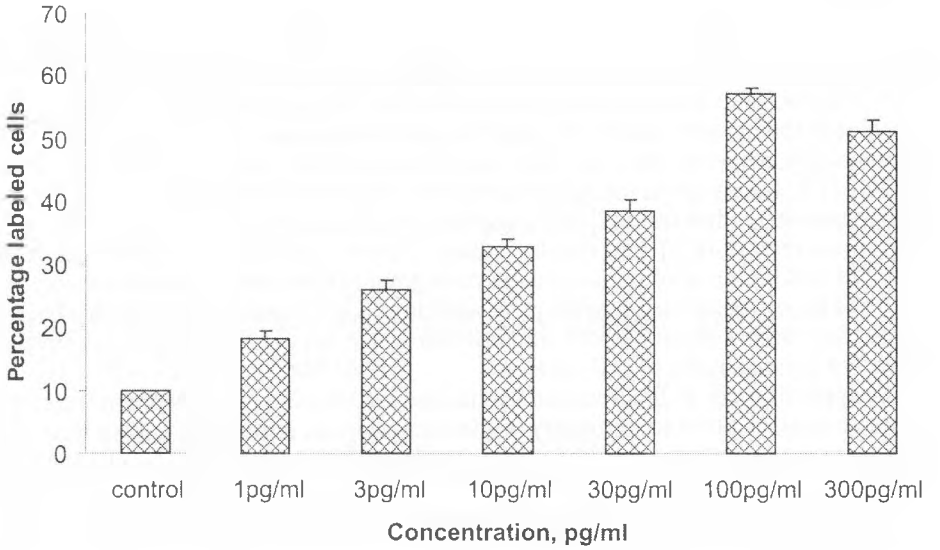

Fig. 4. Percentage (mean ± SD) of labelled prospermatogonia of 2-day-old mouse testis, incubated 24 h in presence of different doses FGF 2

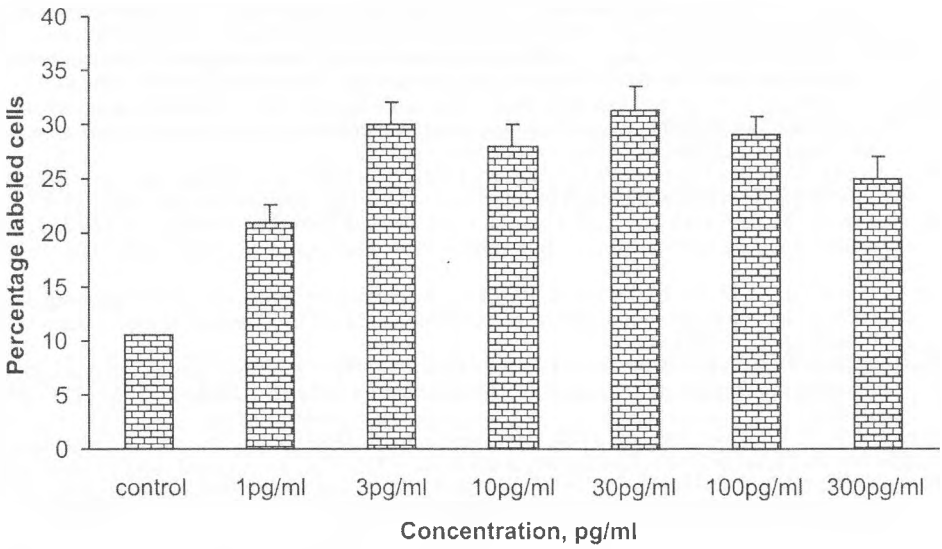

Fig. 5. Percentage (mean ± SD) of labelled prospermatogonia of 2-day-old mouse testis, 24 h after culture in presence of different doses FGF 7

Discussion

It is known that growth factors in general stimulate cell proliferation and/or differentiation by interacting with cell-surface receptors. Using RT-PCR we showed previously that FGF 1 and FGF 2 mRNA is detected in day-4 mouse testis. We suggested that at lest two FGFs are present in the mouse testis at the onset of spermatogenesis (FGF 1 and FGF 2) and prospermatogonia have at least one FGF receptor prior to the onset of spermatogenesis — FGFR — 2 [12]. Lately it was found an expression of mRNA for FGFR — 1, 2, 3 and 4 in fetal, immature and adult testis [2]. It is suggested that ligands FGFs 1 — 5 and 8 can signal through these receptors [3]. Our results indicate that not only FGF — 1 and FGF- 2 but FGF — 7 as well is able to stimulate prospermatogonial DNA synthesis and probably acts through the above mentioned receptors. In addition FGF-7 stimulates DNA synthesis in exocrine pancreatic cells in diabetic and control rats *in vitro* [10], thus being a universal mitogen for a wide variety of cell types.

The application of FGF 2 resulted in changed localization of many prospermatogonia from central location to periphery in the seminiferous cords. It is known that after increasing in gonial cell number, the ratio between germ and Sertoli cell is changed and the process of differentiation starts [1]. The first sign of germ cell diferentiation is change in their localization from the center to the periphery of the cords between Sertoli cells.

In conclusion FGF 1, FGF 2 and FGF 7 stimulate the first wave of mouse prospermatogonial proliferation. FGF 2 is the most efective growth factor acting not only on germ cell proliferation but on male germ cell differentiation as well.

References

1. Bellve, A. R. The molecular biology of mammalian spermatogenesis. – In: Oxford Reviews of Reproductive Biology (Ed. C. A. Finn). Oxford, Oxford University Press, 1979, 159-261.
2. Cancilla, B., G. P. Risbridger. Differential localization of fibroblast growth factor receptor - 1, -2, -3 and - 4 in fetal, immature and adult rat testes. – Biol. Reprod., **58**, 1998, 1138-1145.
3. Cancilla, B., A. Davies, M. Ford – Perriss, G. P. Risbridger. Discrete cell- and stage-specific localization of fibroblast growth factors and receptor expression during testis development. – J. Endocrinol., **164**, 2000, 149-159.
4. Kancheva, L., Y. Martinova, V. Georgiev. Prepubertal Sertoli cells secrete a mitogenic factor(s) that stimulates germ and somatic cell proliferation. – Mol. Cell. Endocrinol., **69**, 1990, 121-127.
5. Kubota, H., M. R. Avabrock, R. L. Brinster. Growth factors essential for self-renewal and expansion of mouse spermatogonial stem cells. – Proc. Natl. Acad. Sci. USA, **101**, 2004, 16395-16396.
6. Martinova, Y., D. Nikolova, A. Bellve. Mullerian inhibitory substance down-regulates seminiferous growth factor-stimulated rat prespermatogonial cell proliferation in vitro. – Acta Morphol. Anthropol., **6**, 2001, 45-50.
7. Mather, J. P., K. Attie, T. Woodruff, G. Rice, D. Phillips. Activin stimulates spermatogonial proliferation in germ-Sertoli cell cocultures from immature rat testis. – Endocrinology, **127**, 1990, 3206-3214.
8. Moore, A., L. Krummen, J. Mather. Inhibins, activins, their binding proteins and receptors — interactions underlying paracrine activity in the testis. – Mol. Cell. Endocrinol., **100**, 1994, 81-86.
9. Nakayama, Y., T. Yamamoto, S. Abe. IGF-I, IGF-II and insulin promote differentiation of spermatogonia to primary spermatocytes in organ culture of newt testes. – Int. J. Dev. Biol., **43**, 1999, 343-347.
10. Ogneva, V., Y. Martinova. The effect of fibroblast growth factors on cell proliferation in pancreas from normal and streptozotocin-treated rats in vitro. – Diabetes Research and Clinical Practice, **57**, 2002, 11-16.
11. Ornitz, D., N. Itoh . Fibroblast growth factors. – Genome Biol., **2**, 2001, Reviews 3005.
12. Seidensticker, M., Y. Martinova, A. Bellve. Fibroblast growth factor and the onset of spermatogenesis. – In: Proc. Northeast Reg. Confer. on Developmental Biology, 1996, Marine, USA.

Institute of Experimental Morphology and Anthropology with Museum
Bulgarian Anatomical Society

Acta morphologica et anthropologica, 12
Sofia • 2007

Changes in Blood Viscosity and Erythrocyte Indices in Chronic Heroin Abusers

Y. Savov, N. Antonova, E. Zvetkova, Y. Gluhcheva, I. Ivanov*, I. Sainova, E. Bichkidjieva, I. Ilieva*

Institute of Experimental Morphology and Anthropology with Museum, Bulgarian Academy of Sciences, Sofia
**Institute of Mechanics and Biomechanics, Bulgarian Academy of Sciences, Sofia*

Whole blood viscosity (WBV) and hematometric indices of erythrocytes as red blood cell count (RBC), mean erythrocyte volume (MCV), hemoglobin (HGB), hematocrit (HCT), mean hemoglobin content of erythrocytes (MCH), HGB/HCT values (MCHC) and red blood cell distribution width (RDW) have been studied in a group of 15 chronic opioid addicts under methadone maintenance therapy with mean age 26.53 ± 7.34 years. WBV elevation and changes in MCV, HGB, HCT, RDW were found in intravenous drug users compared to healthy individuals as well as RBC decreased leading to an increase in MCH and MCHC values. Correlation analysis suggested that the correlation among the RBC, HGB, HCT and WBV was the closest. Heroin macrocytosis (heroin macrocytic anemia) was established, related with the increased RDW in chronic heroin abusers. The results are in accordance with data revealing abnormal effects of alcohol and other drugs on whole blood rheology and hematometric/morphometric characteristics of erythrocytes.

Key words: whole blood viscosity, erythrocyte hematometric indices, chronic heroin abusers, heroin macrocytosis (heroin macrocytic anemia).

Introduction

The current circulating opiate concentrations in the blood and the hematometric indices of the erythrocytes (RBC, HGB, HCT, MCV, MCH, MCHC and RDW) are provided by blood and/or by plasma measurements. Hemorheological parameters and their relationships with the hematometric indices, influencing on blood rheology have not been studied yet despite the importance of the knowledge for better understanding the blood flow, blood cells' and blood vessels' abnormalities, observed in chronic heroin abusers [2, 8, 9]. The aim of the study is to investigate the changes, resulting under the effect of heroin on WBV and erythrocyte hematometric indices in heroin abusers under methadone maintenance therapy.

Materials and Methods

Whole blood heparinized samples from 15 chronic (HIV-seronegative) heroin addicts (3 female and 12 male; mean age 26.53 ± 7.34 years) under methadone maintenance therapy, obtained from the National Center for Addictions in Sofia have been studied. Blood samples were collected with heparinized tubes and rheological measurements were completed within 3 hours after sample preparation. Whole blood viscosity (WBV) was measured using a rotational viscometer Contraves Low Shear 30 (Switzerland) with the standard measuring system MS 1/1 at a steady flow over a shear rate range of 0.0237 s^{-1} to 128.5 s^{-1} at temperature 37°C. The results have been compared with a control group of 19 healthy subjects (9 female and 10 male; mean age 34.84 ± 4.06 years). The hematometric indices of erythrocytes (red blood cell count (RBC), mean erythrocyte volume (MCV), hemoglobin (HGB), hematocrit (HCT), mean hemoglobin content of erythrocytes (MCH), HGB/HCT ratio (MCHC) and red blood cell distribution width (RDW)) were analyzed by automated cell counter. Student's t-test for determining differences in the mean values of the examined parameters at level of significance $p<0.05$ was used. Relationships between the WBV and the erythrocyte parameters were evaluated using the simple correlation coefficient (r). Statistical analysis was done on MATLAB 6.5.

Results and Discussion

It was found that the mean whole blood viscosity values of the investigated group of heroin abusers were elevated (31.61 at mean shear rate 28.47 s^{-1}) compared to that of healthy persons (21.53) over the whole shear rate range (Table 1). These elevations were statistically significant at higher shear rates range (20.4 s^{-1}, $p = 0.1$; 94.5 s^{-1}, $p = 0.05$). At low shear rates the standard deviations were more than 50% of the mean. No significant difference was found in RBC between the control group and that of heroin abusers, although the red blood cells number of heroin addicts was lower (Fig. 1). It was determined that there are significant differences between HGB ($p<0.05$), MCV ($p<0.05$) and RDW ($p<0.005$) in erythrocytes of normal individuals and heroin addicts: increased values of MCV and RDW in heroin addicts and decreased HGB content in their erythrocytes were obtained (Figs. 2, 3 and 4). HCT was insignificantly decreased in chronic heroin users (43.37 ± 4.04) compared to the control samples (44.37 ± 3.97). The values of MCH and MCHC were increased in heroin addicts (MCH = 51.79 ± 8.57; MCHC = 355.84 ± 99.3), although statistically insignificant compared to the controls (MCH = 29 ± 1; MCHC = 330 ± 10). Linear correlation analysis shows that WBV in intravenous drug users correlates positively ($p<0.05$) only with the changes in the hematometric indices of erythrocytes — RBC, HGB and HCT. The simple correlation coefficient (r) in heroin addicts varies between $r = 0.5$ - 0.6 at different shear rates (Fig. 5). RBC of drug users was decreased leading to an increase in MCH and MCHC values (negative relationship — $p<0.05$).

The elevation of WBV at low as well as at high shear rates suggested that RBC aggregation and rigidity are probably increased, and the latter one is statistically significant. The observed decreased RBC count and blood HGB levels in heroin addicts support our previous and other data [1, 6, 8, 10] for high prevalence of anemia among chronic opioid users.

It is well known fact [4] that a low hemoglobin level is associated with an increase in RDW. We supposed that increased RDW in chronic heroin abusers is in accordance with their low hemoglobin levels. Increased RDW was also reported in cases of nicotine and alcohol abuse [7]. RDW is a coefficient of variation of mean RBC volume and is considered as a biomarker for the nutritional status of patients (vitamin B_{12}, folic acid and iron deficiency [7]). Having in mind that elevated RDW has been obtained only in pathological

Table 1. Whole blood viscosity at different shear rates in healthy individuals and drug abusers

Shear rates (s^{-1})	Whole Blood Viscosity (mPa.s)	
	Healthy subjects (n=19)	Drug abusers (n=15)
0.0237	75.11 ± 42.81	113.96 ± 75.68
0.0596	46.22 ± 21.88	72.09 ± 55.02
0.1102	37.56 ± 16.46	61.21 ± 41.77
0.512	22.78 ± 9.27	30.41 ± 14.64
1.285	16.98 ± 7.44	21.76 ± 7.84
5.96	9.73 ± 4.07	11.98 ± 3.23
11.02	7.72 ± 2.02	9.84 ± 2.43
20.04	6.48 ± 1.49	8.28 ± 1.81*
51.2	5.2 ± 0.89	6.53 ± 1.25**
94.5	4.61 ± 0.71	5.83 ± 1.1**
128.5	4.46 ± 0.77	5.83 ± 0.99

Data represent mean value ± SD; * $p<0.1$, ** $p<0.05$

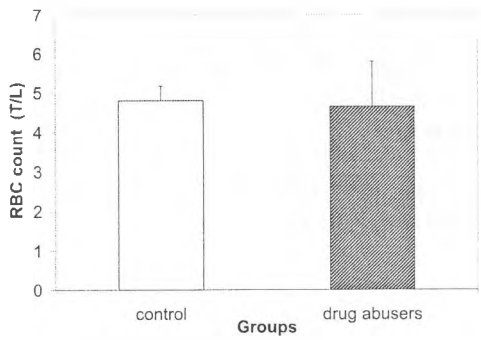

Fig 1. Red blood cell count (RBC) in healthy subjects (n=19) and in chronic heroin addicts (n=15)

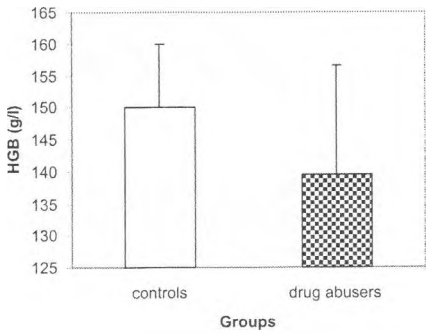

Fig 2. Hemoglobin (HGB) in healthy subjects (n=19) and in chronic heroin addicts (n=15)

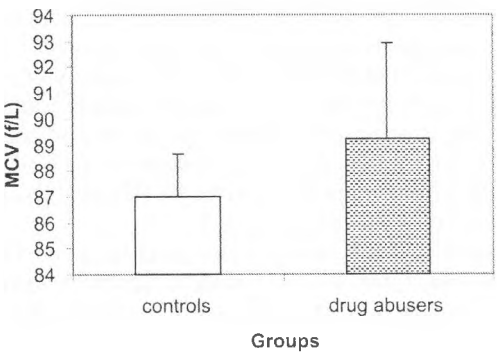

Fig 3. Mean erythrocyte volume (MCV) in healthy individuals (n=19) and in chronic heroin addicts (n=15)

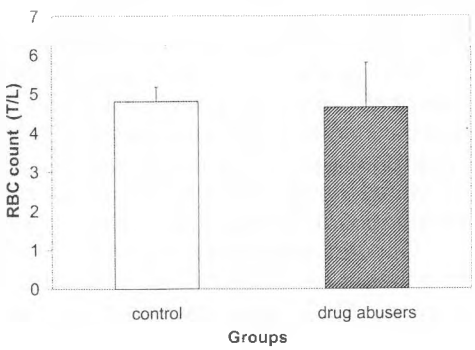

Fig 4. Red blood cell distribution width (RDW) in healthy individuals (n=19) and in chronic heroin addicts (n=15)

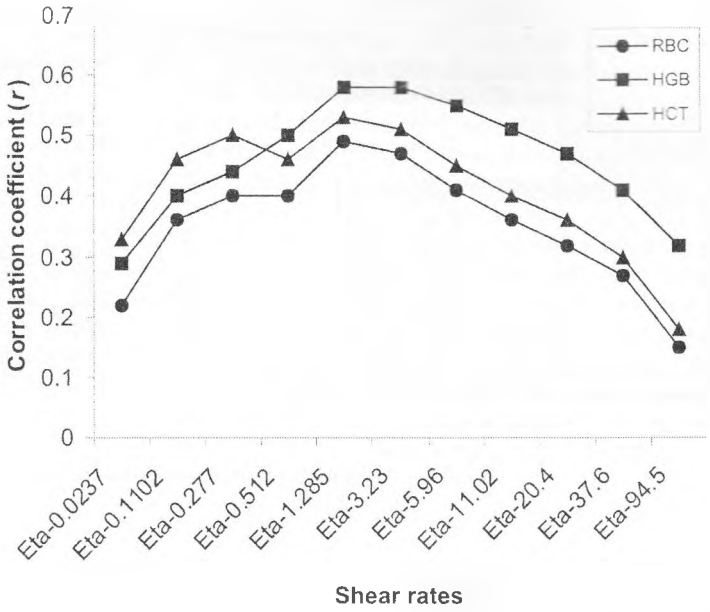

Fig 5. Correlation coefficient (r) between RBC, HGB, HCT and WBV (at different shear rates) in chronic heroin addicts (n=15)

states (e.g. in both — micro- and hypochromic anemias — [4]), we suppose that increased RDW as well as lower RBC and HGB levels, could indicate suboptimal nutritional status in heroin abusers. In addition, changes of the erythrocyte membrane properties, enzyme activities and the level of lypoperoxides were also determined among chronic opioid users [2, 9]. The low HCT values in the group of heroin addicts confirm the observed data in mice, experimentally treated with a synthetic analogous to heroin — buprenorphine [1].

We hypothesize that the changes in WBV and in the hematometric indices of erythrocytes (RBC, HGB, HCT, MCV, MCH, MCHC and RDW) of chronic heroin abusers could be associated with heroin-induced negative effects on early bone marrow hematopoiesis (erythropoiesis — [7]). Opioids, shown originally to bind to specific receptors in the brain and on red blood cells as well [8] influenced early bone marrow progenitors affecting their proliferation/differentiation and hematopoietic colony formation [5].

Our data show that elevated MCV of erythrocytes — heroin macrocytosis, is one of the principle red blood cell morphometric abnormalities in heroin addicts. Similar results (increased MCV) were observed in alcohol abusers in state of excessive ethanol consumption and were defined as "alcoholic macrocytosis" [3, 7].

We suggest that further detailed studies will evaluate whether the increased RDW and MCV as well as lower RBC, HGB and HCT levels, observed by us in chronic heroin abusers, result in heroin macrocytosis (heroin macrocytic anemia). On the other hand, RDW and MCV could be simultaneously used as sensitive quantitative indicators in medical diagnostics for establishing the possible origin of heroin macrocytic anemia (as it is pointed out by R o m e r o A r t a z a et al. [4] for early diagnostics of microcytic and hypochromic anemias). The results obtained could be also of clinical usefulness optimiz-

ing the treatment of some complications associated with chronic drug abuse, such as hypoxemia, major ischemic syndrome, circulatory disturbances, hypertension, cardiac arrhythmia, acute myocardial infarction.

References

1. Banerjee, D., N. K. Sarkar. Hematological changes in buprenorphine-treated mice. – Folia Biol. (Krakow), **45**, 1997, No 3, 157-162.
2. Galante, A., A. DeLuca, A. Pietroiusti, F. Tiratterra, E. Benincasa, B. Domenici, C. Baldelli, C. Valenzi. Effects of opiates on blood rheology. – J. Toxicol. Clin. Toxicol., **32**, 1994, No 4, 411-417.
3. Niemela, O., S. Parkkila. Alcoholic macrocytosis — is there a role for acetalaldehyde and adducts? – Addict. Biol., **9**, 2004, No 1, 3-10.
4. Romero Artaza, J., C. D. Carbia, M. F. Ceballo, N. B. Diaz. Red cell distribution width (RDW): its use in the characterization of microcytic and hypochromic anemias. – Medicina (B. Aires), **59**, 1999, No 1, 17-22.
5. Roy, S., D. Ramakrishnan, H. H. Loh, N. M. Lee. Chronic morphine treatment selectively suppresses macrophage colony formation in bone marrow. – Eur. J. Pharmacol., **195**, 1991, No 3, 359-363.
6. Savov, Y., N. Antonova, E. Zvetkova, I. Sainova, Y. Gluhcheva, I. Ivanov. Effects of heroin and methadone maintenance therapy on blood rheology in heroin abusers. – In: 13th Conference of the European Society for Clinical Hemorheology, June 26th-29th 2005, Siena — Italy, Abstract Book. p. 32-C1.5.
7. Seppa, K., P. Sillanaukee, M. Saarni. Blood count and hematologic morphology in nonanemic macrocytosis: differences between alcohol abuse and pernicious anemia. – Alcohol, **10**, 1993, 343-347.
8. Zeiger, A. R., A. A. Patkar, R. Fitzgerald, A. Lundy, S. K. Ballas, S. P. Weinstein. Changes in mu opioid receptors and rheological properties of erythrocytes among opioid abusers. – Addict. Biol., **7**, 2002, No 2, 207-217.
9. Zhou, J., P. Si, Z. Ruan, S. Ma, X. Yan, L. Sun, F. Peng, H. Yuan, D. Cai, D. Ding, S. Xu. Primary studies on heroin abuse and injury induced by oxidation and lypoperoxidation. – Chin. Med. J. (Engl.), **114**, 2001, No 3, 297-302.
10. Zvetkova, E. B., Y. Savov, N. Tomov, G. Neurauter, D. Fuchs. Urinary neopterin concentration in HIV-seronegative drug users. – Pteridines, **14**, 2003, No 2, 63-64.

Institute of Experimental Morphology and Anthropology with Museum
Bulgarian Anatomical Society

Acta morphologica et anthropologica, 12
Sofia • 2007

Investigations on Cytotoxic and Antiproliferative Effects *In Vitro* of a Newly Synthesized Mixed Ligand Copper (II) Complex

R. Alexandrova, A. Vacheva, M. Kirilova, G. Miloshev*, E.-M. Mosoarca**, R. Tudose**, O. Costisor***

Institute of Experimental Pathology and Parasitology, Bulgarian Academy of Sciences, Sofia 1113, Bulgaria
**Institute of Molecular Biology, Bulgarian Academy of Sciences, Sofia 1113, Bulgaria*
***Institute of Chemistry Timisoara of the Romanian Academy, 24 Mihai Viteazu Blvd, RO-300223, Timisoara, Romania*

The aim of the study was to evaluate cytotoxic and antiproliferative activities *in vitro* of a newly synthesized mixed ligand Cu(II) complex $Cu_2(BAMP)(dipy)Cl_4$. The permanent cell line LSCC-SF(Mc29), established from a transplantable chicken hepatoma induced by the myelocytomatosis virus Mc29, was used in the experiments. The effects of the compound on cell viability and proliferation were studied by neutral red uptake cytotoxicity test (NR), trypan blue dye exclusion technique (TB), colony-forming assay and single cell gel electrophoresis. It was found that $Cu_2(BAMP)(dipy)Cl_4$ expressed significant antitumour properties *in vitro*. Thus, applied at concentrations ≥ 10 μg/ml the compound inhibited completely colony-forming ability of chicken hepatoma cells in semisolid medium. The IC_{50} (concentrations that reduced cell viability/proliferation by 50%) established by NR and TB were found to be in the range 1 — 10 μg/ml. The ability of $Cu_2(BAMP)(dipy)Cl_4$ to induce DNA damages in the treated cells was also observed.

Key words: copper, Mannich bases, pyrazolone, cytotoxic/antiproliferative activity, tumour cells.

Introduction

The potential antineoplastic activitiy of different metals and metal compounds have been under special interest during the recent years because of the following main reasons: 1) It has been found that the disturbed balance in the essential metal metabolism of mammals results in increased susceptibility to infections and malignancies; 2) Being involved in the regulation of some definite processes of the animal organisms several metals are biological response modifiers [6, 19]. Copper is an essential element involved in many biochemical reactions supporting life. It is a part of the active site of at least 60 enzymes and takes part in many key biological processes including cellular respiration, DNA and RNA replication, maintenance of cell membrane integrity, and sequestration of free radicals. This metal is also important for the normal functioning of the immune system [3, 12, 18]. Different copper containing compounds have been reported to express antineoplastic prop-

erties *in vitro* and *in vivo* [4, 8, 11, 14, 15, 16]. It was found in our previous investigations that some Cu(I, II), Co(II), Fe(II, III) and Ni(II) complexes with Mannich type ligands - N,N′-bis(4-antipyrylmethyl)-piperazine (BAMP) and N,N′-tetra-(antipyryl-1-methyl)-1,2-diaminoethane (TAMEN), exhibited cytotoxic and antiproliferative effects on several human and animal tumour cell lines [7, 9, 10]. In order to continue the investigations in this field the aim of the study presented here was to evaluate the antitumour activity *in vitro* a newly synthesized mixed ligand copper (II) complex containing the above-mentioned Mannich base BAMP as well as 2,2-dipyridyl as a coligand.

Materials and Methods

Compounds. The copper (II) complex $Cu_2(BAMP)(dipy)Cl_4$ was obtained by direct synthesis between $CuCl_2.2H_2O$, 2,2-dipyridyl and the Mannich base N,N´-bis(4-antipyrylmethyl)-piperazine (BAMP) in ethanol. The green microcrystalline product was filtered off, washed with ethanol and dried over $CaCl_2$ in air. Yield: 48 %. Analytical data were obtained by a Perkin-Elmer Model 240C elemental analyzer. Electrical conductivities were determined on a WTW LF-340. Infrared spectra of the solid complex (KBr pellet) were recorded on an IR BIO-RAD FTS 135 spectrometer. Magnetic measurements were carried out on polycrystalline samples with a Faraday-type magnetometer.

For biological experiments, the compound was dissolved in dimethylsulfoxide (DMSO, Serva) and then diluted in culture medium. The final concentration of DMSO in the stock solution of $Cu_2(BAMP)(dipy)Cl_4$ (10 mg/ml) is 10%. The stock solutions were stored at 4°C and used no more than two weeks after their preparation.

Cell lines and cultivation. The permanent cell line LSCC-SF(Mc29), established from a transplantable chicken hepatoma induced by the myelocytomatosis virus Mc29, was used in the experiments [2]. Cells were grown as monolayer cultures in a combination of medium H-199 and Minimum Essential medium (AppliChem, Germany), supplemented with 5-10% fetal bovine serum (Cambrex, Belgium), 100 U/ml penicillin and 100 μg/ml streptomycin. The cultures were maintained at 37°C in a humidified CO_2 incubator.

Neutral red uptake cytotoxicity assay. The cells were seeded in 96-well plates (Cellstar) at a concentration of 2×10^4 cells/well. At the 24th h cells from monolayers were washed and covered with media modified with different concentrations of the compound tested (each concentration in 6 to 8 repetitions). Samples of cells grown in non-modified medium served as a control. After 24 h and 48 h incubation periods, each plate was examined under inverted microscope to identify systematic cell seeding errors and growth characteristics of control and treated cells. Alterations in monolayer morphology were registered by an adapted to an inverted microscope digital camera and a computer program EDS-1000E IS.

Neutral red uptake cytotoxicity assay was performed as described by B o r e n f r e u n d and P u e r n e r [13]. Relative cell viability, expressed as a percentage of the untreated control, was calculated for each concentration.

Trypan blue dye exclusion test. The cells were cultured and treated with the complex investigated as described for neutral red uptake cytotoxicity assay. After 24 h and 48 h incubation periods cells were tripsinized and counted after mixing (1:1/ vol:vol) with 0.2% solution of trypan blue (1:1/ vol:vol).

Single cell gel electrophoresis. The alkaline variant of Single cell gel electrophoresis ("Comet Assay"), modified by O l i v e et al. [17]. The comets in the gel were stained with 0.5 μg/ml ethidium bromide and visualized by a fluorescent microscope.

Colony-forming assay. Tumour cells (approximately 10^3 cells/well) were suspended in 0.45% purified agar (Difco) in medium containing different concentrations (ranging from 1 to 200 g/ml) of the mixed ligand copper (II) complex and layered in 24 well microplates (Cellstar). The presence/absence of colonies was registered using an inverted microscope during 20-day period.

Statistical analysis. The data are presented as mean ± standard error of the mean. Statistical differences between control and treated groups were assesses using one-way analysis of variance (ANOVA) followed by Dunnett post-hoc test.

Results

Elemental analysis of the compound. Cu2C38H42N8O2Cl4 (911.71) Found: C 51.02; H 4.71; N 12.33; Cl 15350; Cu 13.82; requires C 50.06; H 4.64; N 12.29; Cl 15.55; Cu 13.94 %. *IR spectrum* (KBr cm^{-1}):–– 1620 s (phenyl ring), 1584 s (C=C/C=N), 1520 m (dipy), 1158 w (C-O), 1130 w (C=C/C=N), 1126 s (C-N al) cm^{-1}. Far IR: 635 m (py), 609 w (M-O), 598 w (M-N al), 362 s (M-Cl), 315 s(M-Cl), cm^{-1}. *Magn. Mom.* 1.97 BM.

Spectric and magnetic properties. In the infrared spectra of the complex, bands belonging both to the pirazolonic and dipyridyl ligands can be noticed, some of them were modified as a result of coordination. Thus, the intense band at 1662 cm^{-1} assigned to the $\nu_{C=O}$ mode in the free ligand is missing in the spectrum of the complex and a weak peak in the 1158-1185 cm^{-1} region, attributable to the ν(C-O) appears. These denote the coordination of antipyrine ring through carbonylic oxygen. Additionally, the presence of ν(C=C/C=N) shows the stabilization of antipyrine. The shift of ν(C-N) toward lower frequencies proves the implication of piperazine in coordination.

The value of the magnetical moment is according to the octahedral geometry of the complex.

Neutral red uptake cytotoxicity assay. The data about the effect of $Cu_2(BAMP)(dipy)Cl_4$ on neutral red uptake in LSCC-SF(Mc29) cells are presented in Fig. 1 and Table 1. No uptake of the vital dye was detected when the complex was applied at concentrations of 100 μg/ml and 200 μg/ml for 24 h and 48 h. Administered at lower concentrations the compound was also found to reduce significantly cell viability as compared to the control. Thus, only 8.24% ± 0.69 ($p < 0.01$) and 60.03% ± 4.08 ($p < 0.01$) viable cells were found after 48 h treatment with 10 μg/ml and 1 μg/ml $Cu_2(BAMP)(dipy)Cl_4$, respectively. The IC_{50} (the concentrations producing 50% reduction of neutral red uptake) were calculated to be 3.1 μg/ml ± 0.3 (24 h) and 2.8 μg/ml ± 0.2 (48 h) (Table 1).

Table 1. Inhibitory concentrations (IC_{50}) of $Cu_2(BAMP)(dipy)Cl_4$ for LSCC-SF(Mc29) tumour cell line

Period of treatment	NR	TB	
		Total number of cells	Cell viability
24 h	3.1 ± 0.3	8.6 ± 0.6	5.8 ± 0.4
48 h	2.8 ± 0.2	5.1 ± 0.3	3.6 ± 0.2

NR – the concentrations (μg/ml) of the compound that reduced the neutral red uptake into LSCC-SF(Mc29) cells by 50% as compared to the control;
TB – the concentrations (μg/ml) of the compound established by the trypan blue dye exclusion technique that reduced the total number of cells/cell viability by 50% as compared to the control.

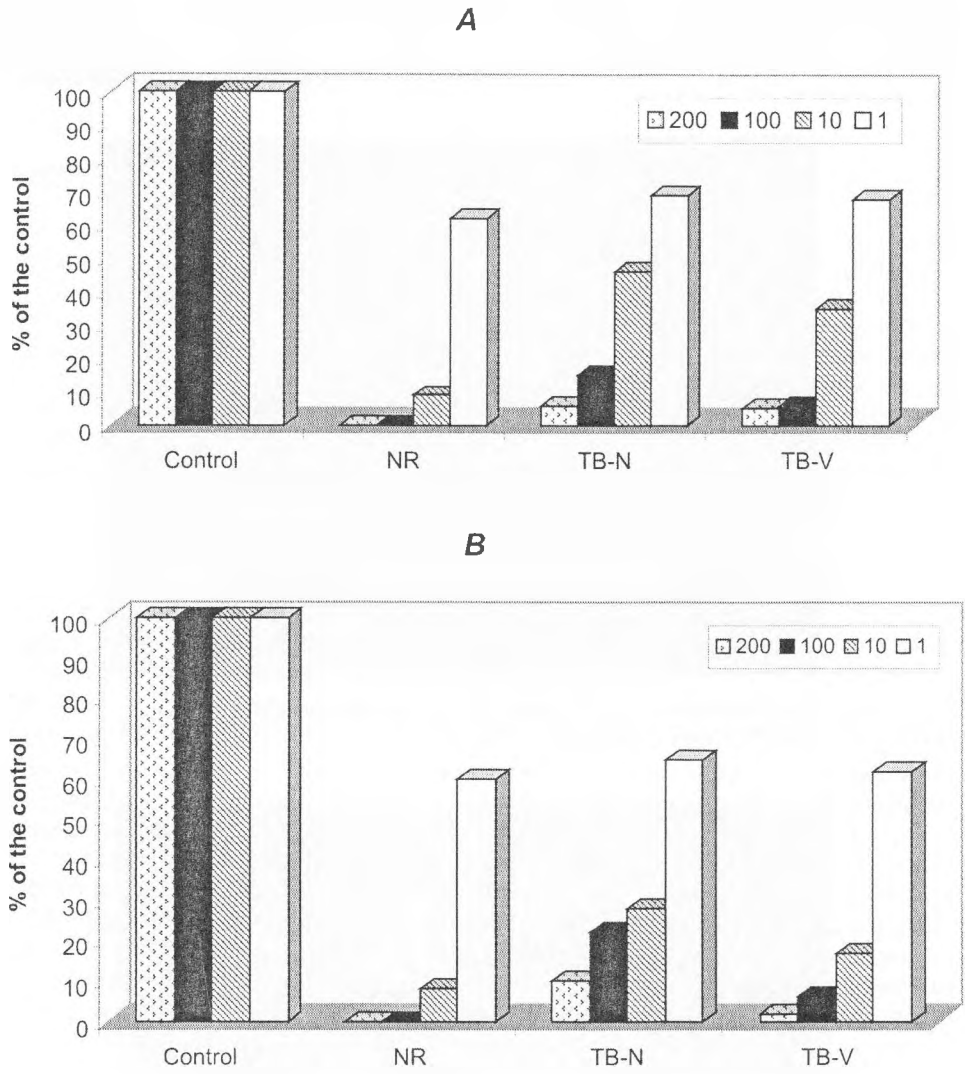

Fig 1. Changes in viability and proliferation of LSCC-SF(Mc29) chicken hepatoma cells treated for 24h (*A*) and 48h (*B*) with different concentrations (1, 10, 100, 200 μg/ml) of Cu_2(BAMP)(dipy)Cl_4: effects on neutral red uptake (**NR**) as well as influence on total cell number (**TB-N**) and cell viability (**TB-V**) established by trypan blue dye exclusion test. The figure represents data summarized from three independent experiments

Trypan blue dye exclusion test. The results obtained using trypan blue dye exclusion test are summarized in Fig. 1 and Table 1.

Cytopathological changes. An increase in number of the rounded-up cells, as well as formation of acellular zones were observed after 24 h and 48 h treatment of LSCC-SF(Mc29) cells with 1 or 10 μg/ml Cu_2(BAMP)(dipy)Cl_4 (Figs. 2, 3). Applied at higher concentrations (100, 200 μg/ml) the compound was found to induce complete cell destruction.

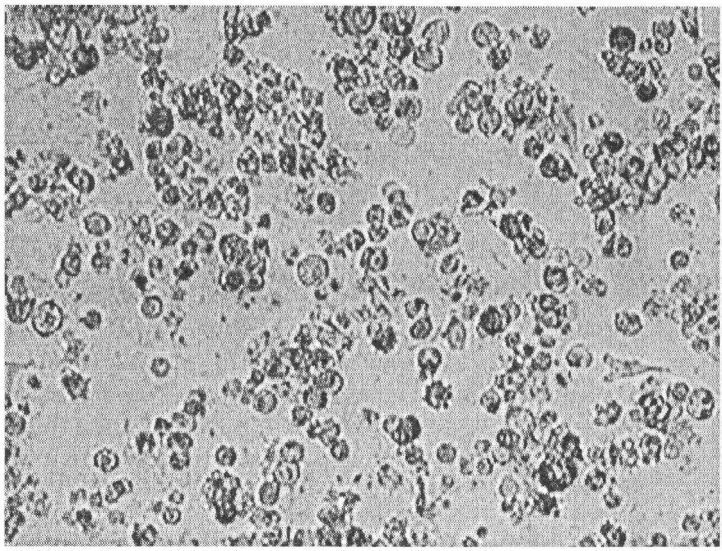

Fig. 2. Monolayer of LSCC-SF(Mc29) tumour cells treated for 24 h with 10 μg/ml Cu_2(BAMP)(dipy)Cl_4. Orig. × 6.3

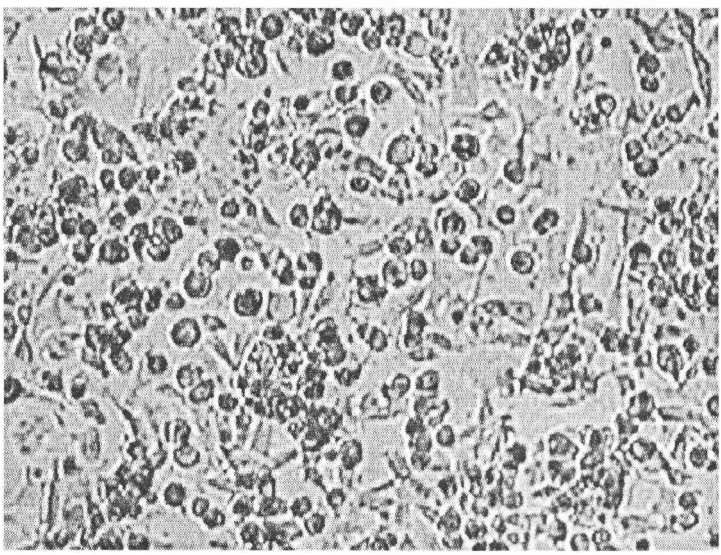

Fig. 3. Monolayer of nontreated LSCC-SF(Mc29) tumour cells. Orig × 6.3

Colony-forming assay. $Cu_2(BAMP)(dipy)Cl_4$ was shown to suppress completely the colony-forming ability of chicken hepatoma cells in semisolid medium when used at concentrations ≥ 10 μg/ml.

DNA damages. DNA damages were observed in about 65% of LSCC-SF(Mc29) tumour cells cultured for 48 h in the presence of 100 μg/ml $Cu_2(BAMP)(dipy)Cl_4$. The total number of the treated cells was found to be reduced by ≈ 84% as compared to the control.

Discussion

The need to find a safe and highly selective cure for neoplastic diseases remains a major challenge for modern science. The discovery of the antitumour efficacy of cisplatin and some related platinum complexes has stimulated the search for other metals with anticancer properties [6, 15]. In the literature there are data that different copper containing compounds possess antineoplastic activity *in vitro* and *in vivo*. Thus, some diphenylphosphinoethane-copper (I) complexes express significant cytotoxic properties against chinese hamster ovary (CHO) and human ovarian carcinoma (PA-1) cell lines as well as on cells obtained from human ovarian carcinomas [11]. Copper (II) complexes of thiosemicarbazones showed encouraging cytotoxic effect against HT-29 (human colon adenocarcinoma) cells [14]. The 2-furfural semicarbazone and thiosemicarbazone copper complexes demonstrate pronounced cytotoxic activity against human lung MB9812, colon SW480, ovary 1-A9 and uterine HeLa-S3 carcinomas [16].

It was found in our previous investigations that some copper (I, II) complexes with Mannich type ligands - N,N′-bis(4-antipyrylmethyl)-piperazine (BAMP) and N,N′-tetra-(antipyryl-1-methyl)-1,2-diaminoethane (TAMEN) exhibited antineoplastic effects *in vitro* on human (8-MG-BA) and animal (LSCC-SF-Mc29, LSR-SF-SR) tumour cell lines [7]. On the basis of their cytotoxic activity these copper (I, II) complexes were graded as follows: $Cu_2(BAMP)(NCS)_4 > Cu_2(BAMP)I_3 > Cu(TAMEN)(NO_3)_2$. In addition, it was also shown that applied at concentrations ranging from 1 to 200 μg/ml both ligands — BAMP and TAMEN, did not reduce significantly the viability and proliferation of tumour cells examined [10]. In order to continue the investigations in this field in the study presented here we report for the first time the data about synthesis, spectral and magnetic properties and antitumour potential *in vitro* of a mixed ligand copper (II) complex $Cu_2(BAMP)(dipy)Cl_4$, containing Mannich base BAMP and 2,2-dipyridyl as a coligand. The decision to start the investigations on biological activity of this compound namely on LSCC-SF(Mc29) chicken hepatoma cells was not occasional because this cell line was proved to be highly sensitive to the cytotoxic and cytostatic effects of different metal complexes [7, 8, 9, 10], alkaloids [1] and photosensitizers [5]. The results obtained revealed that $Cu_2(BAMP)(dipy)Cl_4$ expressed promising antitumour activity *in vitro*. This compound decreased significantly viability and proliferation of LSCC-SF(Mc29) cells in a time and concentration-dependent manner and induced DNA damages in the treated cells. $Cu_2(BAMP)(dipy)Cl_4$ was found to be much more effective than $Cu_2(BAMP)(NCS)_4$ and $Cu_2(BAMP)I_3$. For example, the IC_{50} (48 h) of $Cu_2(BAMP)(NCS)_4$ that reduced the neutral red uptake in chicken hepatoma cells was calculated to be 70 μg/ml ± 2.6 [7], whereas for $Cu_2(BAMP)(NCS)_4$ was 2.8 μg/ml 0.2. Copper complexes examined in the study presented here as well as in our previous experiments differ from each other in ligand (BAMP, TAMEN or BAMP + 2,2dipyridyl) and anion (NCS^-, I^-, NO_3^-, Cl^-). Each of these components (ligands and anions) as well as metal ions influences in different way physico-

chemical and biological properties of the complexes obtained which could explain the differences in their cytotoxic effects. A series of experiments with different copper complexes with Mannich type ligands are underway to study the relationship between the structure and physical and chemical properties of these compouns, and their biological activity. Additional investigations are also planned to clarify the potential antitumour properties of $Cu_2(BAMP)(NCS)_4$ on several tumour and nontumour human and animal cell lines as well as the mechanism(s) of action of this complex.

Acknowledgement. This study was supported by Grant CC 1402/2004, National Scientific Council, Bulgarian Ministry of Education and Science as well as by a bilateral project between Institute of Experimental pathology and Parasitology, Bulgarian Academy of Sciences, and Institute of Chemistry Timisoara of the Romanian Academy.

References

1. Alexandrova, R., T. Varadinova, M. Velcheva. I. Sainova, P. Genova. Cytotoxic effect of isoquinoline alkaloids on tumour cell lines. – Exp. Pathol. Parasitol., **4**, 2000, 8-14
2. Alexandrova, R. I., V. Ogneva, P. Jordanova. Tumor heterogeneity investigations in virus-induced transplantable tumor. – Int. J. Cancer, Suppl., **13**, 2002, p. 563.
3. Alexandrova, R., G. Rashkova, I. Alexandrov, W. Tsenova, R. Tudose, O. Costisor. Briefly about copper. – Exp. Pathol. Parasitol., **6**, 2003, No 12, 3-12.
4. Alexandrova, R. I., Y. Martinova, T. Popova, V. Todorova, M. Gabrashanska, S. Tepavitcharova. Effects of two basic salts of zinc and copper on viability and proliferation of tumor cell line LSR-SF-SR. – Compt. Rend. Acad. Bulg. Sci., **56**, 2003, No 2, 95-98.
5. Alexandrova, R., R.-M. Ion, E. Stoykova, S. Shurulinkov. *In vitro* investigation on cytotoxic activity of TS_4PP [5,10, 15, 20 — tetra (sulfophenyl) porphyrin]. – Proc. S.P.I.E., **5226**, 2003, 423-427.
6. Alexandrova, R., E. Nikolova. Metals as potential anticancer agents. – J. Bulg. Acad. Sci., **1**, 2004, 19-23.
7. Alexandrova, R., G. Rashkova, T. Popova, R. Tudose, S. Slavov, E.-M. Mosoarca, O. Costisor. Investigations on cytotoxic activity of three copper complexes with Mannich type ligands. – Exp. Pathol. Parasitol., **8**, 2004, No 2.
8. Alexandrova, R., T. Popova, G. Rashkova, S. Slavov, M. Alexandrov, M. Kirilova, G. Miloshev, Y. Martinova, E. Nikolova, D. Culita, L. Patron. Study on antitumor and antimicrobial effects of Zn(II), Cu(II), Co(II) and La(III) complexes with cholic acid in vitro. – In: Proceeding of 5th International Symposium on Trace Elements in Human: New Perspectives. 13-15 October, 2005, Athens, Greece. 233-241.
9. Alexandrova, R., G. Rashkova, T. Popova, R. Tudose, E.-M. Mosoarca, S. Slavov, O. Costisor. Preliminary investigations on cytotoxic activity of four nickel (II) complexes with Mannich type ligands on virus-induced tumor cell lines. – Acta Morphol. Anthropol., **11**, 2005.
10. Alexandrova, R. I., G. Rashkova, S. Slavov, E. Nikolova, M. Kirilova, G. Miloshev, E. M. Mosoarca, R. Tudose, O. Costisor. Cytotoxic and antiproliferative effects in vitro of iron complexes with Mannich type ligands. – In: Proceeding of 5th International Symposium on Trace Elements in Human: New Perspectives. 13 - 15 October, 2005, Athens, Greece. 242-250.
11. Andwancar, M. K., C. Wycliff, A. Samuelson. In vitro citotoxic effect of new diphenilphosphinoethane — copper(I) complexes on human ovarian carcinoma cells. – Ind. J. Exp. Biol., **35**, 1997, 810-814.
12. Barceloux, D. G. Copper. – J. Toxicol. Clin. Toxicol., **37**, 1999, 217-230.
13. Borenfreund, E., J. Puerner. Toxicity determination in vitro by morphological Iterations and neural red absorption. – Toxicol. Lett., **24**, 1985, 119-124.
14. Easmon, J., G. Purstinger, G. Heinisch, T. Roth, H. H. Fiebig, W. Holzer, W. Jager, M. Jenny, J. Hofmann. Synthesis, cytotoxicity, and antitumor activity of copper (II) and iron (II) complexes of (4)N-azabicyclo[3,2,2]nonane thiosemicarbazones derived from acyl diazines. – J. Med. Chem., **44**, 2001, 2164-2171.
15. Galanski, M., V. B. Arion, M. A. Jakuper, B. K. Keppler. Recent developments in the field of tumor-inhibiting metal complexes. – Curr. Pharm. Des., **9**, 2003, 2078-2089.
16. Hall, I. H., C. B. Lacke, T. D. Kistler, R. W. Durham Jr., E .M. Jouan, M. Khan, X. D. Thanh, S. Djebbar-Sid, O. Benadi-Baitich, G. M. Bonet. Cytotoxicity of copper and cobalt complexes of furfural semicarbazone and thiosemicarbazone derivatives in murine and human tumor cell lines. – Pharmazie, **55**, 2000, 937-941.
17. Olive P. L., J. P. Banath. Sizing highly fragmented DNA in individual apoptotic cells using the comet assay and a DNA crosslinking agent. – Exp. Cell. Res., **221**, 1995, 19-26.
18. Percival, S. S. Copper and immunity. – Am. J. Clin. Nutr., **67** (suppl), 1998, 1064S-1068S.
19. Zhang, C. H., S. J. Lippard. New metal complexes as potential therapeutics. – Curr. Opin. Chem. Biol., **4**, 2003, 481-489.

Institute of Experimental Morphology and Anthropology with Museum
Bulgarian Anatomical Society

Acta morphologica et anthropologica, 12
Sofia • 2007

Role of FGF1, FGF2 and FGF7 in the Development of the Pancreas of Diabetic Hamsters

M. Inchovska, V. Ogneva, Y. Martinova

Institute of Experimental Morphology and Anthropology with Museum, Bulgarian Academy of Sciences, Sofia

It has been established that in the early postnatal development after treatement with streptozotocin (STZ) the pancreas has the ability to regenerate B-cells. Little is known about the role of fibroblast growth factors (FGFs) in the development of the pancreas. That is why we have investigated the effects of FGF1, 2 and 7, *in vitro*, on proliferation and differentiation of the diabetic hamster pancreatic epithelial cells in the early postnatal development. The following methods have been used: cultivation, H.E. staining, P.A.F. staining and histoautoradiography. Our results have shown that in diabetic hamster pancreases at the age pnd 5 FGF2 acts as a strong stimulator of ductal epithelial cell proliferation and new islet formation.

Key words: fibroblast growth factors, diabetes, pancreatic cells, proliferative activity.

Introduction

Fibroblast growth factor receptor (FGFR) signalling has been implicated in processes of proliferation and differentiation in many organs, including the pancreas [12]. Numerous studies show that impairment of FGFR signalling in pancreatic β cells leads to diabetes, indicating that FGFR signalling plays a crucial role in controlling glucose homeostasis [1, 7, 8, 12].

It is well known that the formation of new β cells in the pancreas is a result of two processes: differentiation of ductal precursor cells that further assemble into islets, a process also called neogenesis, and proliferation of preexisting differentiated β cells [3, 10, 18]. It has been established that the injection of STZ at birth destroys 80% of the β cells thereby inducing a depletion of pancreatic insulin stores and a severe hyperglycemic state [2, 4, 14]. Various studies demonstrate that β cell regeneration that follows β cell destruction after STZ treatment involves both β cell proliferation and neogenesis [5, 9, 19]. It has not yet been established whether the new β cell masses display insulin secretion ability.

Studies in the field of recovery of pancreatic islet B cells after STZ treatment in the early postnatal development give us grounds to investigate the effect of FGF1, 2 and 7 on the development of diabetic hamster pancreas in this period.

Materials and Methods

We induced experimental diabetes in female hamsters during the first 24 hours after mating of female and male hamsters by intraperitoneal STZ administration at a dose of 65 mg/kg. For the study we used only these animals from the litter that had a blood glucose level above 11 mmol/l. We have studied three groups of diabetic hamsters: 20 hamsters at age pnd 1, 20 hamsters at age pnd 5, and 20 hamsters at age pnd 10. Pups were decapitated, their pancreases were dissected and cut into small segments. One or two segments from the isolated pancreases were cultivated in each well of 96 — well plates. For the preparation of organ cultures from pancreases we used Iscove's medium, supplemented with fetal bovine serum (FBS) and 100 U/ml penicillin and 100μg/ml streptomycin. In the three groups of hamsters incubation medium was additionally supplemented with 4, 10 and 100 ng/l FGF1, FGF2 and FGF7. We had also control wells in the present experiment in which pancreas segments were not treated with the fibroblast growth factors and STZ. The pancreatic pieces were incubated at 37 °C with 5% CO_2 for 48 hours. After 48 hours, the medium was supplemented with 3H-thymidine in concentration 2 μCi/ml for 8 hours. Then the pancreatic segments were fixed in Bouin's solution for 24 hours, embedded in paraffin, sectioned and stained with H.E. and P.A.F. according to routine procedures. After 14 days of exposure the autoradiographs were stained with haematoxilin — Bömer. The proliferative activity of pancreatic cells was determined by the labelling index (LI) according to the formula: LI (%) = number of labelled nuclei / number of counted nuclei × 100. From every slide of the experimental groups we estimated 200 cells. Statistical analysis was made by Student's t-test. The results are expressed as mean percentage ± S.E.

Results

The H.E. stained slides have shown well developed ductal epithelium on the periphery of the slides as well as acinar cells in the central part of slides obtained from pancreases of diabetic hamsters at age pnd 1 and treated with FGF1 at a concentration of 4 ng/l (Fig. 1). The histoautoradiographic study showed an increased proliferative activity of pancreatic epithelial cells in the three groups of diabetic hamsters — pnd 1, pnd 5 and pnd 10, and in all concentrations of the investigated FGFs. We have observed a large number of proliferating ductal cells as well as proliferating cells around the ducts on slides obtained from pancreases of the diabetic hamsters at age pnd 5 and treated with FGF2 at a concentration of 10 ng/l (Fig. 2). We have also observed proliferating exocrine cells on slides obtained from pancreases of the diabetic hamsters at age pnd 5 and after treatment with FGF1 at a concentration of 4 ng/l.

Slides stained with PAF provided additional knowledge about the role of FGFs in the early postnatal development of the pancreas of diabetic hamsters. We have observed insulin - synthesizing cells in the ductal epithelium on slides obtained from pancreases of the diabetic hamsters at age pnd 5 treated with FGF1 at a concentration of 4 ng/l as well as on slides obtained from pancreases of the diabetic hamsters at age pnd 10 and treated with FGF1 at a concentration of 10 ng/l (Fig. 3). Insulin-synthesizing cells scattered throughout the acinar cells have also been detected on slides obtained from pancreases of the diabetic hamsters at age pnd 5 and treated with FGF2 at a concentration of 4 ng/l (Fig. 4). We could also see insulin - positive islets of Langerhans on slides obtained from pancreases of the diabetic hamsters at age pnd 5 and treated with FGF1 at a concentration of 100 ng/l (Fig. 5).

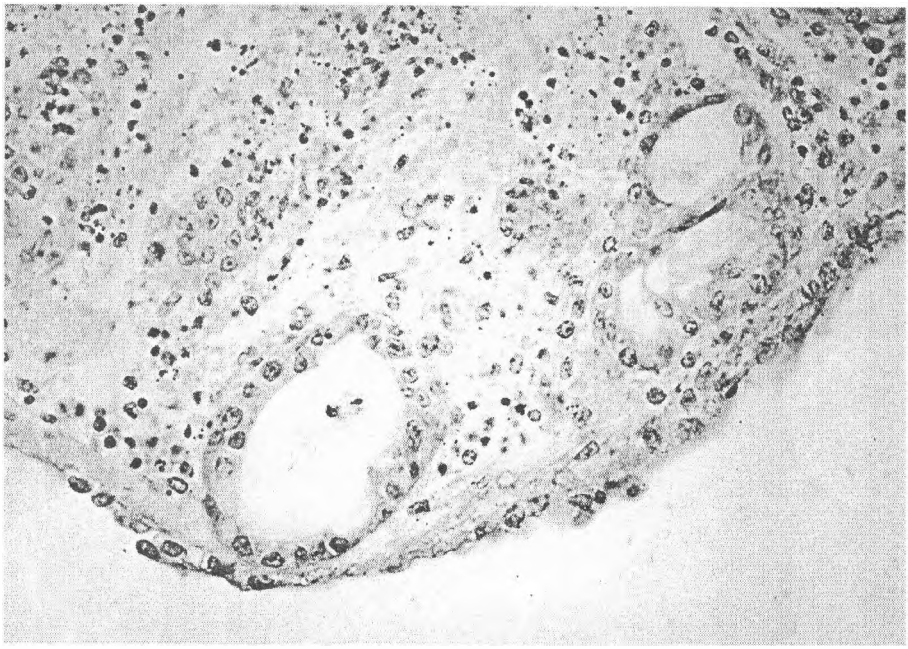

Fig. 1. Ductal epithelial cells in pancreas of diabetic hamsters at age pnd 1 after treatement with FGF1 at a concentration of 4 ng/l (× 25)

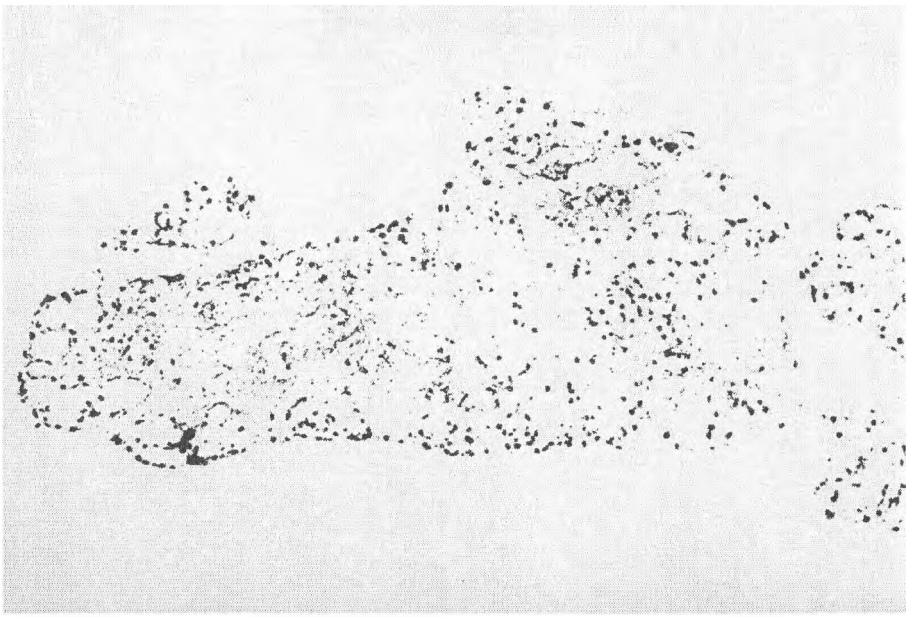

Fig. 2. Autoradiograph of diabetic hamster pancreas at age pnd 5 after treatement with FGF2 at a concentration of 10 ng/l (× 5)

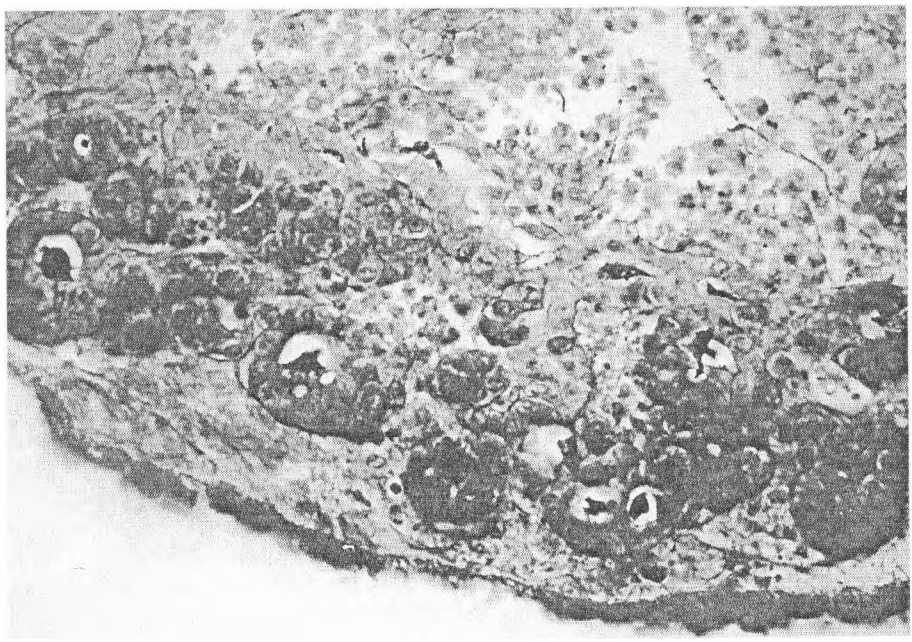

Fig. 3. Insulin - synthesizing cells in the ductal epithelium of diabetic hamster pancreas at age pnd 5 treated with FGF1 at a concentration of 4 ng/l (× 25)

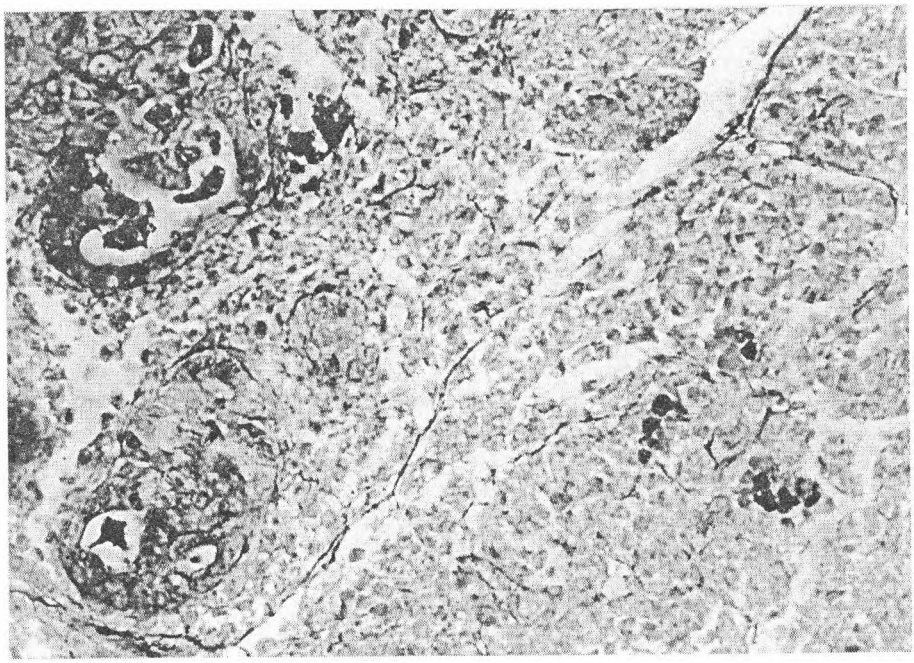

Fig. 4. Insulin - synthesizing cells scattered throughout the acinar cells in diabetic hamster pancreas at age pnd 5 after treatement with FGF2 at a concentration of 4 ng/l (× 25)

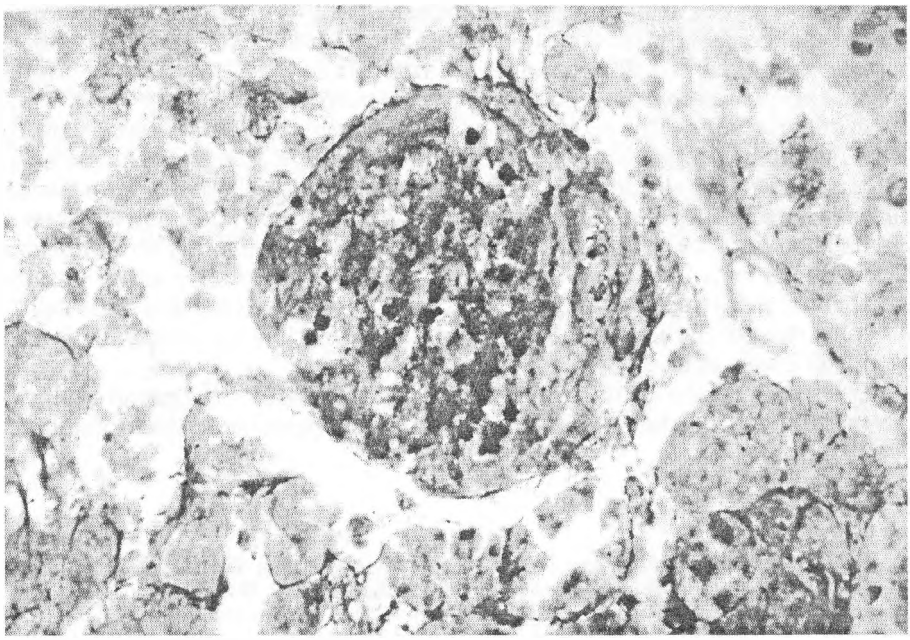

Fig. 5. Insulin - positive islets of Langerhans in diabetic hamster pancreas at age pnd 5 after treatement with FGF1 at a concentration of 100 ng/l (× 100)

We have determined the proliferative activity of pancreatic cells by the labelling index (LI). The control for experiments for pnd 1 had labelling index 4,2 ± 0,4%, control for experiments for pnd 5 had labelling index 6 %, control for experiments for pnd 10 had labelling index 6± 0,4%.

FGF1 has shown the strongest effect (18,7 ± 0,6%, $p< 0,05$ in comparison with the control) at age pnd 5 and at a concentration of 10 ng/l and the lowest mitogenic effect - (7 ± 1,6%) at pnd 1 and at a concentration of 100 ng/l. FGF2 has displayed the strongest mitogenic effect (26,2 ± 0,4%, $p< 0,01$ in comparison with the control) at a concentration of 10 ng/l and at age pnd 5 and the lowest (13± 0,4%, $p< 0,001$ in comparison with the control) — at a concentration of 4 ng/l and at age pnd 1. FGF7 has shown the strongest mitogenic effect (16,2 ± 0,6%, $p< 0,05$ in comparison with the control) at a concentration of 10 ng/l and at age pnd 5 and the lowest effect (5,5 ± 1,6%) — at a concentration of 100 ng/l and at age pnd 1.

The most prominent stimulatory effect (26, 2 ± 0,6 %, $p< 0,01$ in comparison with the control) was registered at a concentration of 10 ng/l of FGF2 and at age pnd 5 and the lowest mitogenic effect — (5,5 ± 1,6%) was registered at a concentration of 100 ng/l FGF7 at age pnd 1.

Discussion

It is generally admitted that the process of neogenesis mostly takes place during natal and early postnatal development. S t e i n e r et al., consider that B cells have a poor regenerative activity and that treatment with STZ leads to B cell destruction and irreversible diabetes [16]. Conversely, in rats treated with STZ at birth or at age pnd 2, 3 a destruction of the B cell mass causes diabetes followed by a rapid reappearance of B cell masses [2, 9, 14].

While data related to the development the pancreas accumulate, little is known about the factors that control the proliferation and differentiation of the B cells in normal and diabetic animals. It is established that FGF1, FGF2 and FGF7 are among the growth factors that are expressed in B cells. That is why the purpose of our study was to establish the effect of these FGFs in the early postnatal development of diabetic hamsters and to get a further insight into the process of regeneration of beta cells after treatment with STZ.

It is accepted that all endocrine cells of the Langerhans islets arise from the ductal epithelial stem cells through sequential differentiation [11, 15, 17]. Yamamoto et al. reported that most of the cells that had BrdU — positive nuclei after in vivo treatment with STZ were ductal cells, and only a few pancreatic islet cells showed positive reaction to BrdU. Therefore, division of ductal epithelial cells is promoted after loss of B - cells [20]. In our study most of the cells that had ^{3}H - thymidine marked nuclei after in vivo treatment with STZ were epithelial cells of ducts.

Our results have shown that in diabetic hamsters pancreases at age pnd 5 FGF2 acts as a strong stimulator of ductal epithelial cell proliferation and new islet formation.

References

1. Apelqvist, A., U. Ahlgren, H. Edlund. Sonic hedgehog directs specialized mesoderm differentiation in the intestine and pancreas. – Curr. Biol., 7, 1997, 801-804.
2. Bonner - Weir, S., D. F. Trent, R. N. Honey, G. Weir. Responses of neonatal rat islets to streptozotocin: limited B — cell regeneration and hyperglycemia. – Diabetes, **30**, 1981, 64-69.
3. Bonner - Weir, S., F. E. Smith. Islet cell growth and the growth factors involved. –Trends Endocrinol. Metab., **5**, 1994, 60-64.
4. Kato, S., K. Sekine. FGF — FGFR signalling in vertebrate organogenesis. – Cell. Mol. Biol., **45**, 1999,631-638.
5. Bonnevie - Nielsen, V., M. W. Steffes. A. Lernmark. A major loss in islet mass and B - cell function precedes hypeglycemia in mice given multiple low doses of streptozotocin. – Diabetes, **30**, 1981, 424-429.
6. Cantenys, D., B. Portha, M. C. Dutrillaux, E. Hollande, C. Roze, L. Picon. Histogenesis of the endocrine pancreas in newborn rats after destruction by streptozotocin: an immunocytochemical study. – Wirchows. Arch. (Cell Pathol.), **35**, 1981, 109-122.
7. Celli, G., W. J. La Rochelle, S. Mackem, R. Sharp, G. Merlino. Soluble dominant — negative receptor uncovers essential roles for fibroblast growth factors in multi — organ induction and patterning. – EMBO J., **17**, 1998, 1642-1655.
8. Cheon, H. G., W. J. La Rochelle, D. P. Bottaro, W. H. Burgess, S. A. Aaronson. High - affinity binding sites for related fibroblast growth factor ligands reside within different receptor immunoglobulin - like domains. – Proc. Natl. Acad. Sci. USA, **91**, 1994, 989-993.
9. Ferrand, N., A. Astesano, H. H. Phan, C. Lelong, G. Rosselin. Dynamics of pancreatic cell growth and differentiation during diabetes reversion in STZ — treated newborn rats. – Am. J. Physiol., **269**, 1995, 1250-1264.
10. Finegood, D. T., L. Scaglia, S. Bonner - Weir. Dynamics of B - cell mass in the growing rat pancreas: estimation with a simple mathematical model. – Diabetes, **44**, 1995, 249-256.
11. Hellerstrom, C., I. Swenne. Functional maturation and proliferation of fetal pancreatic beta - cells. – Diabetes, **40**, 1991, 89-93.
12. Itoh, N., T. Mima, T. Mikawa. Loss of fibroblast growth factor receptors in necessary for terminal differentiation of embryonic limb muscle. – Development, **122**, 1996, 291-300.
13. Kato, S., K. Sekine. FGF — FGFR signalling in vertebrate organogenesis. – Cell. Mol. Biol., **45**, 1999, 631-638.
14. Portha, B., C. Levacher, L. Picon, G. Rosselin. Diabetogenic effect of streptozotocin in the rat during the perinatal period. – Diabetes, **23**, 1974, 889-895.
15. Rosenberg, L., A. I. Vinik. Trophic stimulation of the ductular — islet cell axis: a new approach to the treatment of diabetes. – Adv. Exp. Med. Biol., **321**, 1992, 95-109.
16. Steiner, H., O. Oelz, G. Zahn, E. R. Froesch. Studies on islet regeneration, hyperplasia and intrinsular interrelations in long - lasting streptozotocin diabetes rats. – Diabetologia, **6**, 1970, 558-564.

17. S w e n n e, I. Pancreatic beta - cell growth and diabetes mellitus. – Diabetologia, **35**, 1992, 193-201.
18. V i n i k, A., G. R. P i t t e n g e r, L. R a f a e l o f f, W. R o s e n b e r g. Doguid. Determinants of pancreatic islet cell mass: a balance between neogenesis and senescence / apoptosis. – Diab. Rev., **4**, 1996, 235-263.
19. W a n g, R. N., L. B o w e n s, G. K l o p e l. Beta - cell proliferation in normal and streptozotocin treated newborn rats: dynamics and capacity. – Diabetologia, **37**, 1994, 1088-1096.
20. Y a m a m o t o, M., M. Y a s u d a, A. H o r i, K. A r i s h i m a, Y. E g u c h i. Recovery in the fetal pancreatic islet following fetal administration of streptozotocin in the rat in vivo and in vitro. – The Anatomical Record Part A, **281A**, 2004, 1319-1325.

Institute of Experimental Morphology and Anthropology with Museum
Bulgarian Anatomical Society

Acta morphologica et anthropologica, 12
Sofia • 2007

Fluorescent Histochemical Localization of Dipeptidyl Aminopeptidase IV Using a Newly Developed Substrate

R. Todorova, I. Ivanov, M. Dimitrova*

Institute of Experimental Morphology and Anthropology with Museum, Bulgarian Academy of Sciences, Sofia
**St. Kliment Ohridsky University of Sofia, Faculty of Biology, Sofia*

A new fluorogenic substrate for histochemical localization of dipeptidyl aminopeptidase IV / CD26 (DPP IV; EC 3.4.14.5) is synthesized — Gly-L-Pro-6-hydrazido-2-hexyl-1,8-naphthalimide and applied for the histochemical visualization of the enzyme in tissue sections of rat organs. Upon the enzyme action the substrate is hydrolyzed and the fluorochrome N-hexyl-6-hydrazino-1,8-naphthalimide is liberated, which reacts instantly with an aromatic aldehyde, e.g. piperonal (3,4-methylenedioxybenzaldehyde; PPL), presented in the incubation medium to form a water-insoluble orange hydrazone, which fluoresces in brilliant red when excited by green light (λexcit = 540 nm; λemiss = 620 nm). The enzyme locations are visualized by red fluorescence at a minimal or none background noise. The newly developed histochemical technique is used successfully for the fluorescent detection of DPP IV in all its locations, including the capillary bed endothelium, which has not been achieved by now.

Key words: Dipeptidyl aminopeptidase IV, naphthalimide derivatives, fluorescent histochemical methods, synthetic enzyme substrates, enzyme histochemistry.

Introduction

Dipeptidyl aminopeptidase IV (DPP IV, EC 3.4.14.5) is a serine type membrane-associated exopeptidase with ubiquitous expression. The enzyme hydrolyzes preferably X-Pro dipeptides from the amino-terminal of different oligo- and polypeptides at pH optimum 7.8 [5]. The enzyme is recognized as cell differentiation factor CD 26, expressed in T lymphocytes plasmalema [8] DPP IV plays an important role in regulatory processes such as T-cell activation, cell migration and invasiveness [10], digestion of proline containing peptides (mainly collagen) [1], etc. According to some present studies the enzyme was proposed as a specific marker for malignant transformations in the kidney [14]. Aberrant DPP IV expression was also detected in human hepatocellular carcinoma [15]. Obviously, the enzyme has a very important role in different biological processes and reasonably a lot of research groups are interested of it.

The histochemical visualization of DPP IV in normal and pathologically altered tissues is now performed exclusively by chromogenic methods [6]. There are also fluoro-

genic substrates, e.g. X—Pro-rhodamide 110 [11], Ala-Pro-2-cresyl violet [16] and Gly-Pro-4-methoxy-2-naphthylamide [7] but they are applicable for the enzyme detection only in cultured cells and not in tissue sections.

In the present paper we propose a new fluorogenic substrate for dipeptidyl aminopeptidase IV - Gly-L-Pro-6-hydrazydo-2-hexyl-1,8-naphthalimide, synthesized by us, and a novel fluorescent technique for the enzyme localization, based on it. Using the here presented histochemical method we visualized the enzyme in tissue sections of different rat organs.

Materials and Methods

Synthesis of the fluorochrome. The fluorochrome N-hexyl-6-hydrazino-1,8-naphthalimide (HHNI) was synthesized as follows: Acenaphthene (Merck, Germany) was brominated by N-bromosuccinimide in dimethylformamide after R o s s et al. [13]. The obtained 6-bromo acenaphthene was oxidized to 6-bromonaphthalanhydride by a standard procedure with sodium dichromate in acetic acid. The last compound was coupled with hexylamine by boiling it in absolute ethanol for 12 hours to give 6-bromo-N-hexyl-1,8-naphthalimide [2]. The fluorochrome — HHNI was obtained from the brom-containing compound and hydrazine monohydrate in dimethylsulphoxide at 60°C using potassium fluoride as auxiliary reagent and tetrabutylamonium sulfate as a catalyst by a novel procedure, which will be published elsewhere.

Synthesis of the substrate. The DPP IV substrate — Gly-L-Pro-6-hydrazido-2-hexyl-1,8-naphthalimide (Gly-L-Pro-HHNI) was synthesized from HHNI and Boc-Gly-L-Pro (Bachem, Switzerland) by N,N,N′,N′-Tetramethyl-O-(benzotriazol-1-yl)uronium tetrafluoroborate (TBTU) procedure [9]. The Boc-protection was cleaved in 4N HCl/ dioxane to obtain the substrate as hydrogen chloride salt.

Tissue treatment and incubation. Mature Wistar rats of both sexes were decapitated under ether anesthesia. Pieces of kidney, small intestine, epididymis, liver, heart and spleen were removed and frozen immediately in liquid nitrogen. Ten μm thin sections were cut on cryotome Reichert Jung (Nussloch, Germany) at –25°C and mounted on gelatinized glass slides. Half of them were covered with 0.75 % celloidin for one minute at room temperature; the other sections were left free of celloidin film. Both types of sections were incubated in liquid solutions, consisting of 0.25 to 0.5 mM of the substrate (Gly-L-Pro-HHNI) and 1 mg/ml aromatic aldehyde (piperonal, anizaldehyde, terephthalic aldehyde or antracen-9-carbaldehyde), dissolved in buffer (0.1 M HEPES, 0,1 M phosphate or 0,05-borax/boric acid), at pH 7.8. The incubation lasted for 60-120 min at 37°C, because of the different enzyme activity levels in the examined rat organs. All the samples were post-fixed in 4 % neutral formaldehyde and embedded in glycerol-jelly. Control sections were incubated only in buffered aldehyde (in the absence of the substrate).

The sections were studied under fluorescent microscope OPTON IM 35 with filter combination G 546 FT 580 LP 590. The photos were made on Konica Minolta (Japan) VX 200 colorful films.

Results and Discussion

6-Substituted-1,8-naphthalimides are highly fluorescent compounds, which are used as dyes for cotton, wool, silk, synthetic fibers and plastics [12]. The 6-hydrazino-2-alkyl-1,8-naphthalimides are found to possess unique electrochemical properties and, though recently synthesized, are already used in conducting and magnetic materials as well as in

nanotechnology [17]. They fluoresce in green when excited by blue light (λexcit = 430 nm, λemiss = 540 nm) [3], whereas their hydrazones with aromatic aldehydes, possessing an electron donor group at para-position show a large batochrome shift in the fluorescent spectra (λexcit = 540-580 nm, λemiss > 600 nm), i.e. they fluoresce in red when excited by green light. In the present study, we use the unique properties of these compounds to develop a novel fluorescent histochemical procedure for the visualization of dipeptidyl aminopeptidase IV on the basis of the substrate Gly-L-Pro-HHNI, synthesized by us. Our investigations show that the enzyme hidrolyzes the substrate, and as a result the fluorochrome 6-hydrazino-2-hexyl-1,8-naphthalimide, which is the primary reaction product, is liberated. Fluorescence of the last compound coincides with the tissue autofluorescence. To avoid this, we use aromatic aldehyde, as a coupling agent, to obtain orange hydrazone, which marks the places of enzyme activity. From the tested aromatic aldehydes, best results were achieved with piperonal. Its hydrazone shows stable red fluorescence, when excited with green light (λexcit 540-580nm). At this wavelength, tissue fluorochromes are not excited and we observed enzyme localization at the lack of background noise. The best visualization results were obtained in 0,1 M phosphate buffer. Sixty minutes of incubation was needed in organs where the enzyme activity is high (liver, kidney, small intestine). DPP IV activity was observed respectively in the glomeruli and in the brush-borders of convoluted tubules in kidney (Fig. 1), strictly in the brush border of small intestinal enterocytes (Fig. 2), and there is a reaction product in bile canaliculi and sinusoids in the liver (Fig. 3). In epididymis and spleen the enzyme activity is lower and ninety minutes of incubation period was necessary. DPP IV activity was visualized in the epididymis the reaction was seen in principal and basal cells of the channels (Fig. 4) and in the spleen the

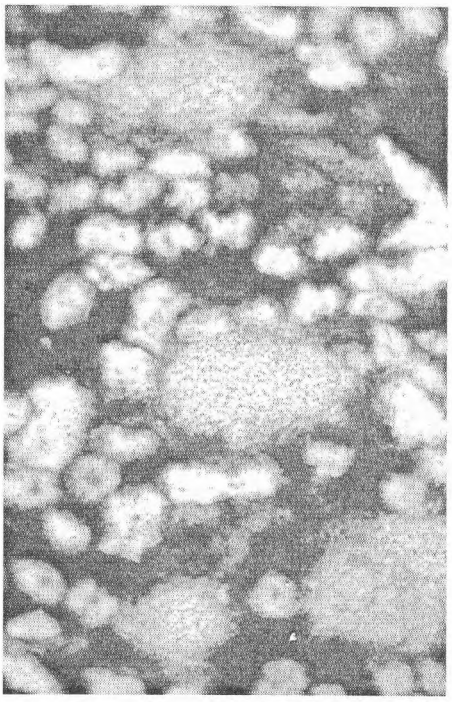

Fig. 1. Kidney. DPP IV activity in glomeruli and in the brush-border of convoluted tubules (× 200)

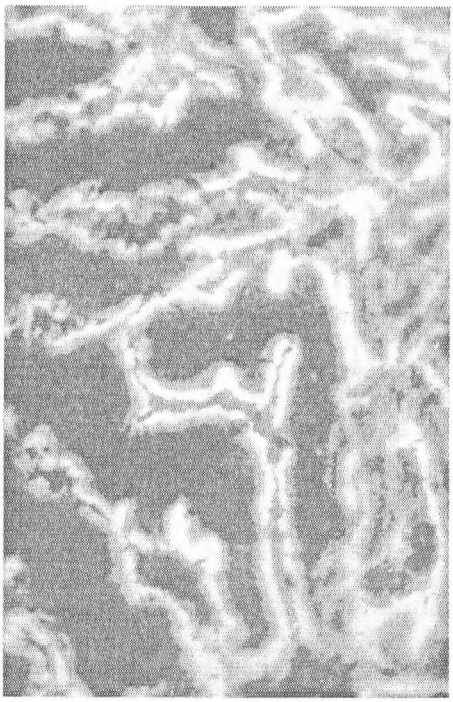

Fig. 2. Small intestine. The reaction product is strictly localized in the brush border of small intestinal enterocytes (× 200)

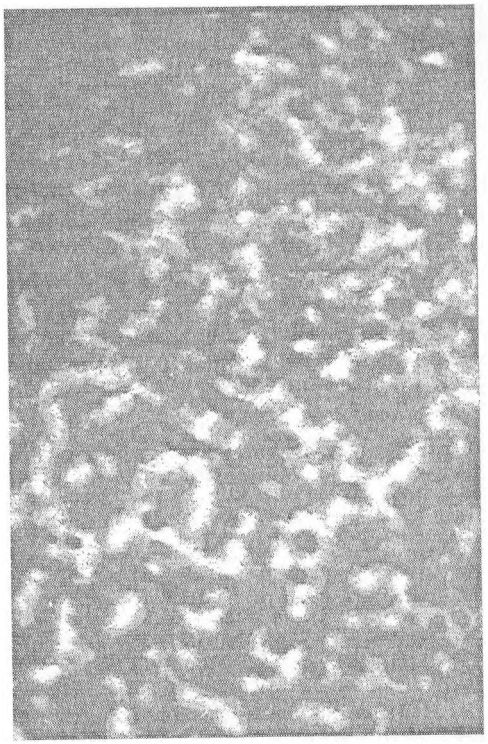

Fig. 3. Liver. Enzyme reaction in bile canaliculi and liver sinusoids (× 500)

Fig. 4. Epididymis. The reaction is seen in principal and basal cells of the channels (× 200)

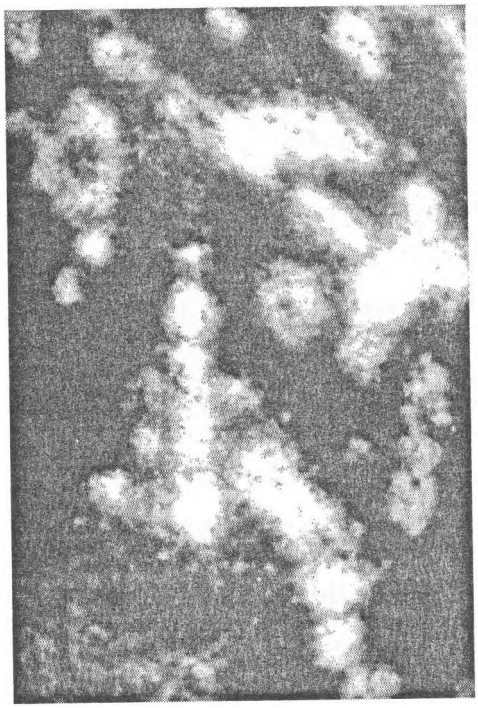

Fig. 5. Spleen. Reaction product in the sinusoids of the red pulp and in the surrounding lymphocytes, no reaction in the white pulp (× 500)

reaction product was localized in sinusoids of the red pulp and in the surrounding lymphocytes; no reaction was detected in the white pulp (Fig. 5).

In a previous paper [4], we proposed synthetic fluorescent substrate for amino peptidase N — L-Ala-6-hydrazido-2-butyl-1,8-naphthalimide in a similar visualization procedure, by which we obtained a strict visualization of the enzyme in all its locations. In comparison with this technique, the present substrate possesses a longer alkyl chain and the final reaction product — the hydrazone, has even more amorphous appearance. An important achievement of the here proposed synthetic fluorescent substrate is that it permits to visualize DPP IV activity in the glomeruli, sinusoid capillaries of spleen red pulp, liver sinusoids and bile canaliculi and in heart capillaries, which has not been done so far with the known fluorescent substrates [6].

The novel histochemical procedure for DPP IV visualization, proposed by us can be used to detect enzyme activity in all its locations and to compare qualitatively the enzyme levels in normal and pathologically altered tissues and organs.

Acknowledgement. This work was supported by the National Science Fund of Bulgarian Ministry of Education, grant No 1527/05.

References

1. Bermpohl, F., K. Loster, W. Reutter, O. Baum. Rat dipeptidiyl peptidase IV (DPP IV) exhibits endopeptidase activity with specificity for denaturated fibrillar collagens. – FEBS Lett, **428**, 1998, 152-156.
2. Bojinov, V., G. Ivanova, J. Chovelon, I. Grabchev. Photophysical and photochemical properties of some 3-bromo-4-alkylamino-N-alkyl-1,8-naphthalimides. – Dyes and Pigments, **58**, 2003, 65-71.
3. Chang, S-C., E. R. Utecht, D. E. Lewis. Synthesis and bromination of 4-alkylamino-N-alkyl-1,8-naphthalimides. – Dyes and Pigments, **43**, 1999, 83-94.
4. Dimitrova, M., R. Todorova, E. Georgieva, I. Ivanov. New fluorescent method for the visualization of aminopeptidase N activity. – Acta Morph. Anthr., **11**, 2005, 51-55.
5. Gossrau, R. Localization of DPP IV. Histochemical and biochemical study. – Histochemistry, **60**, 1979, 231-248.
6. Gossrau, R. Cytochemistry of membrane proteases. – Histochem. J., **17**, 1985, 737-771.
7. Gossrau, R. Investigation of proteinases in the digestive tract using 4-methoxy-2-naphtylamine (MNA) substrates. – J. Histochem. Cytochem., **29**, 1981, 464-480.
8. Kahne, T., U. Lendeckel, S. Wrenger, K. Neubert, S. Ansorge, D. Reinhold. Dipeptidyl peptidase IV: A cell surface peptidase involved in regulating T cell growth (Review). – Int. J. Mol. Med, **4**, 1999, 15-25.
9. Knorr, R., A. Trzeciak, W. Bannwarth, D. Gillssen. New coupling reagents in peptide chemistry. – Tetrahedron Lett., **30**, 1989, 19-27.
10. Lambeir, A. M., C. Durinx, S. Scharpe, I. de Meester. Dipeptidyi-peptidase IV from bench to bedside: An update on structural properties, functions, and clinical aspects of the enzyme DPP IV. – Crit. Rev. Clin. Lab. Sci., **40**, 2003, 209-294.
11. Mrestani-Klaus, C., W. Brandt, J. Faust, U. Hermanns, S. Lorey, K. Neubert. Structural studies of Rodamine 110 peptide derivatives representing a new class of fluorogenic substrates for dipeptidyl peptidase IV (DP IV). – Peptides, 1996, 663-665.
12. Nakaya, K., K. Funabiki, H. Muramatsu, K. Shibata, M. Matsui. N-Aryl-1,8-naphtalimides as highly fluorescent labeling reagents for carnitine. – Dyes and Pigments, **43**, 1999, 135-239.
13. Ross, S. D., M. Finkelstein, R. C. Petersen. Solvent effects in the reactions of N-bromosuccinimide with toluene, fluorene and acenaphthene. – J. Am. Chem. Soc., **80**, 1958, 4327-4330.
14. Stange, T., U. Kettmann, H. J. Holzhausen. Immunoelectron microscopic demonstration of the membrane proteases aminopeptidase N/CD13 and dipeptidyl peptidase IV/CD26 in normal and neoplastic renal parenchymal tissues and cells. – Eur. J. Histochem., **44**, 2000, 24-134.

15. S t e c a, B. A., B. N a r d o, P. C h i e c o, A. M a z z i o t t i, L. B o l o n d i, A. C a v a l l a r i. Aberrant dipeptidyl peptidase IV (DPP IV/CD26) expression in human hepatocellular carcinoma. – J. Hepatol., **27**, 1997, 337-345.
16. Van N o o r d e n, C., E. B o o n a c k e r, E. R. B i s s e l l, A. J. M e i j e r, J. Van M a r l e, B. S m i t h. Ala-Pro-cresyl violet, a synthetic fluorogenic substrate for the analysis of kinetic parameters of dipeptidyl peptidase IV (CD26) in individual living rat hepatocytes. – Anal. Biochem., **252**, 1997, 71-77.
17. W e i h o n g, Z., M. N o b u t s u g u, K. S a i d, Y. K i m. π - Chromophore — functionalized SWNTs by covalent bonding: substantial change in the optical spectra proving strong electronic interaction. – J. Mater. Chem., **14**, 2004, 1924-1926.

Institute of Experimental Morphology and Anthropology with Museum
Bulgarian Anatomical Society

Acta morphologica et anthropologica, 12
Sofia • 2007

A Case of Invasive Mola Hydatidosa in the Uterine Tube

S. Djambazova, M. Batinova, I. Hubavenska, M. Dimitrova***

Department of General and Clinic Pathology, Medical University, Plovdiv
**Department of Anatomy, Histology and Embryology, Medical University, Plovdiv*
***Department of Obstetrics and Gynecology, Medical University, Plovdiv*

We present a case of invasive hydatid mola as one of the forms of trophoblast proliferation of the chorial villi that vary in invasiveness and are classified under the common entity trophoblastic disease.
The case presented deserves interest as a rare localization of invasive hydatid mola in the uterine tube in an ectopic pregnancy. For the last 30 years (1994-2004) only 40 cases have been reported in literature.

Key words: hydatid mola, trophoblastic disease, ectopic pregnancy.

Introduction

Gestational trophoblastic disease is a collective notion which unites morphologically similar, but clinically diverse proliferative and other disruptions of the structure of the trophoblast. A portion of these pathological conditions belong to the tumour-alikes, while others are real tumours. Nosologically, the gestational trophoblastic disease includes *Endometritis Syncytiale*, *Mola Hydatidosa*, *Mola hydatidosa invasiva*, *Chorionepithelioma*, and trophoblastic pseudotumour at the site of placentary implantation. *Mola Hydatidosa* (MH) is a typical facultative precancerosis of the chorioepithelioma. The tubar localisation of MH is encountered extremely rarely and usually implies a diagnostic error. In this article we will describe one of our clinical cases to focus physicians' attention to this condition and to recall some clinical and non-clinical methods that assist in diagnosing it expediently and correctly.

Materials and Methods

A twenty-five-year-old single female admitted to the Clinic of Obstetrics and Gynecology at the University Hospital of Plovdiv with symptoms of acute abdomen. Status on admission: slightly swollen abdomen, peritoneal irritation in the right inguinal region, pale skin and mucosi. Gynecological status: uterus hardly palpable due to muscle defence. Uterine tubes and parameterium: without infiltrative changes, with palpatory tenderness on the

right. Cavum Douglasi: not swollen, painful. Ro: no free gas under the diaphragm dome; isolated hydroaeric shadows in the right abdominal half. Ultrasonography: uterus: no abnormality detected; dimensions of the right ovary: 23 mm/ 10 mm with doubts of amniotic sac in the area of the right uterine tube; left ovary and uterine tube without abnormalities. Presence of free liquid in cavum Douglasi. Puncture of the same: aspiration of blood and blood coagulates. The diagnosis - graviditas extrauterina, ruptura tuba dextra, haemoperitoneum — led to an emergency laparatomy. In situ: 800 ml free blood and blood coagulates in the abdominal cavity. Uterus: no abnormalities detected, left ovary and tube: no abnormalities detected, right uterine tube: ruptured in the isthmic section and necrotically altered. Classical salpingectomy was performed.

Results

Histopathological findings: the tissue material from the uterine tube was processed using a routine methodology and stained with haematoxylin and eosin (HE). The biopsy preparations (323-325/8.01.2001) provided histological verification: uterine tube with evidence of tubar pregnancy and tubar abortion — discrete decidual alterations in the mucose, presence of chorial villi in the lumen and wall. Haemorrage and rupture of the uterine tube wall.

Due to the retention of high levels of human choriongonadotropin (HCG) in the serum, in the postoperative period after the tubectomy, the physician in charge requested a second review of the histological preparations. The meticulous examination of the sections established the presence of villi with singnificantly increased volume; swelling; a decreased number of cells and avascularisation of the villi stroma; growth of the trophoblastic epithelium with manifestations of significant trophoblastic dysplasia (Figs. 1, 2, 3). At places, trophoblastic nuclei cluster and exceed 5-8 rows. They also exhibit significant changes in size, form, and colouration (polymorphism and hyperchromasia). The cytotrophoblast and the syncytiumtrophoblast exhibit significant cellular polymorphism and vascularisation (Figs. 2, 3). The tube wall is heavily stratified. A large number of trophoblastic cells, some with atypical, abnormal shape, and whole chorial villi migrate through the mucose and the muscle layer to the serous lining (Fig. 4). A group of villi are situated paravasally in the nearby paratubar tissue (Fig. 5).

On the basis of the stromal and trophoblastic manifestaions described above, we decided on tubar pregnacy with characteristics of MH. Regarding the topology of the process, the idiosyncrasies of the morphological course of the tubar pregnancy, and lack of evidence of invasion of molar structures in other genital organs, in the pelvis or extragenitally, we abstained from diagnosing invasive MH.

The patient was discharged in good condition, with recommendations for clinical monitoring and periodical follow-up of the HCG titer.

Discussion

The incidence of MH is 1 per 1400 pregnancies in Europe [1], so it is a relatively rare form of gestational trophoblastic disease. Ectopic tubar MH has been described in only 40 cases in world literature [3].

The most prominent risk factor discussed in the literature is the presence of a husband older than 40. The age of the mother is also important: women over 45 almost never develop MH. If the patient has had a previous MH, the risk increases by more than 25% [2]. Other risk factors are: previous abortions (regardless of whether they are spontaneous or induced), surgical intervention, oral contraceptives that have been taken for 2.5 to 10

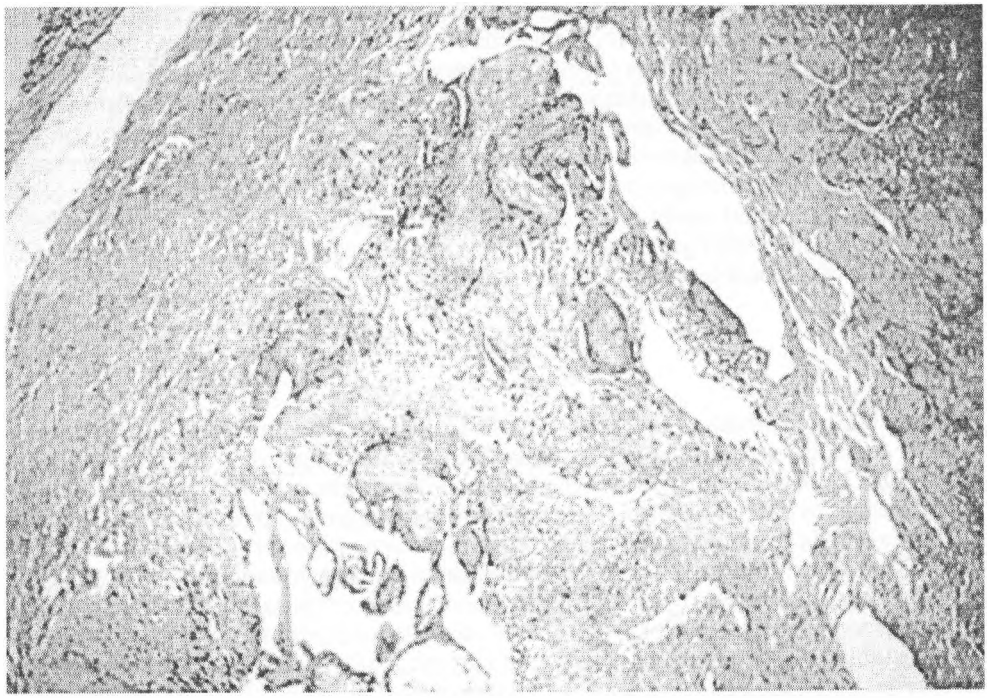

Fig. 1. Chorial villi with swelling and avascularisation of the stroma; trophoblast proliferation with considerable trophoblast dysplasia. HE staining (× 10)

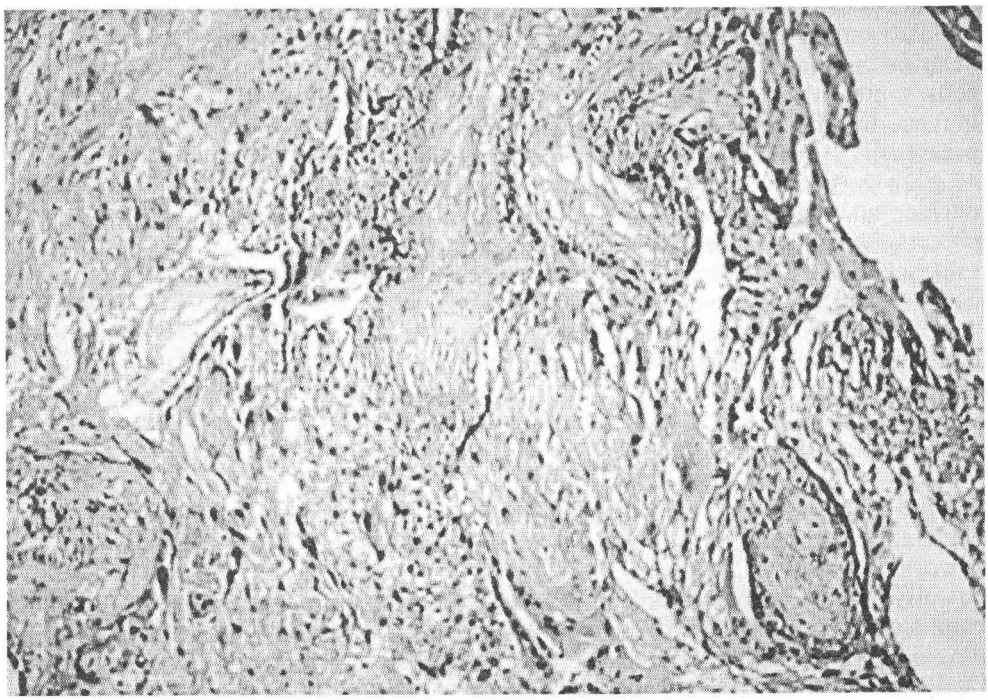

Fig. 2. Chorial villi with swelling, cell deprivation and avascularisation of the stroma; trophoblast proliferation. HE staining (× 40)

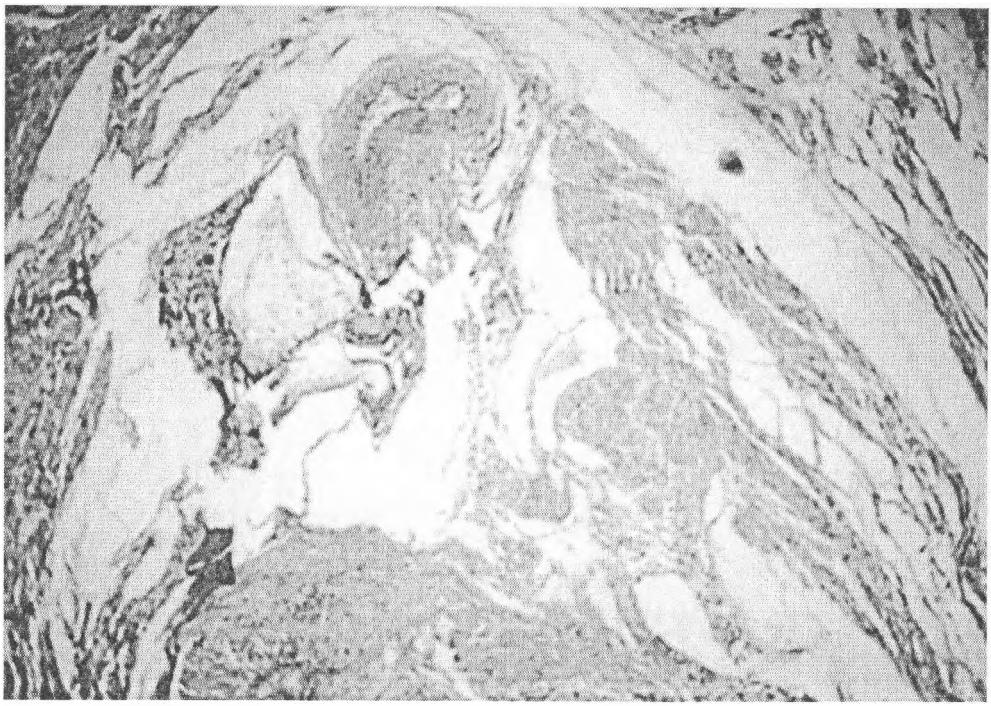

Fig. 3. Segment of a chorial villus with expressed swelling of the stroma, expressed trophoblast proliferation with dysplasia. HE staining (× 40)

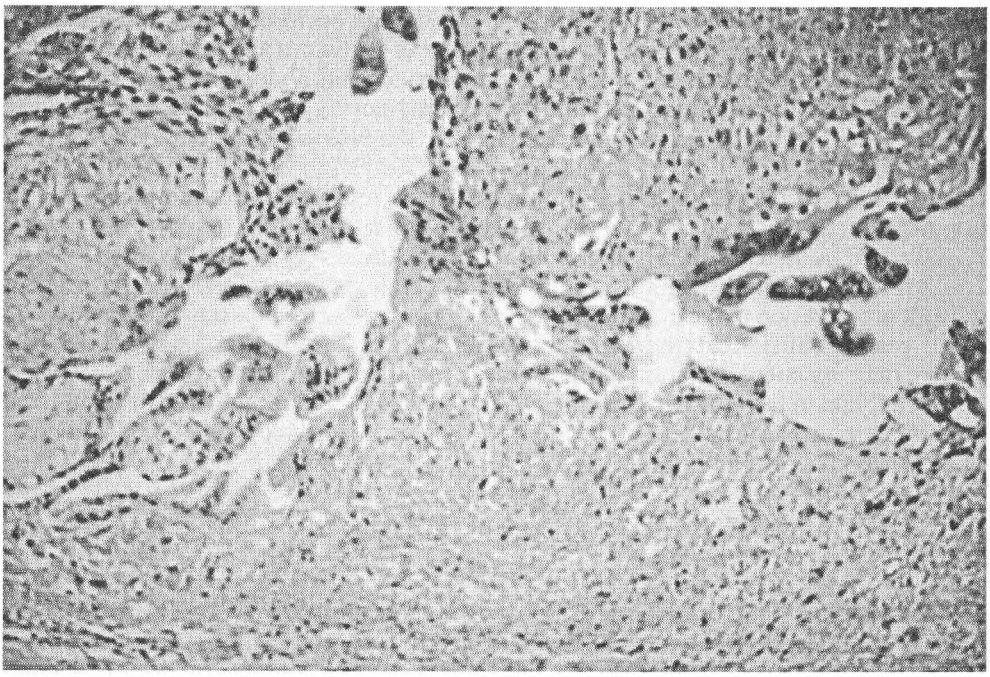

Fig. 4. A cluster of chorial villi resembling molar villi with perivasal localization in the adjacent paratubal tissue. HE staining (× 40)

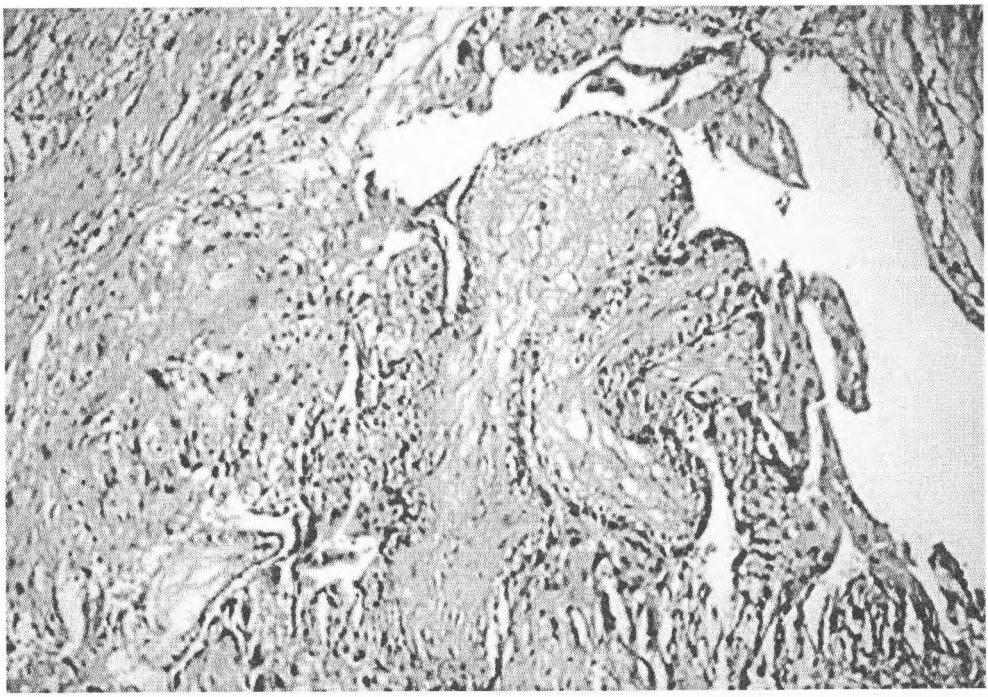

Fig. 5. Migration of a large number of atypical, abnormal cytotrophoblastic and syncytial cells in the uterine tube wall. HE staining (× 40)

years. Potential risk factors are: smoking, alcohol, dieting, socio-economic factors, infectious agents like the papilloma virus, and exposure to pesticides and herbicides [2].

Tubar MH can be expressed with the symptoms of acute abdomen, as in our case. To avoid misdiagnosis, the physician should consider anamnestic data of previous conditions, gynecological status, ultrasonographic findings, etc. An important characteristic of MH is the possibility of producing large quantities of HCG, although there are cases of ectopic tubar MH with low HCG levels [3]. As a noninvasive and repeatable method, a colour doppler examination can lead to a precise diagnosis in such unclear cases.

One DNA analysis shows that MH can become invasive [1].

MH and invasive MH should not be confused with choriocarcinoma despite the significant proliferation of the cytotrophoblast and the syncytiotrophoblast. There are no villi in the case of chorioncarcinoma [2]. Invasive MH also exhibits metastatic foci in the vagina, lung, ligamentum latum uteri several weeks after after its removal [4].

We found in the literature that mola hydatiosa forms as a result of fertilisation of an abnormal (anuclear) egg cell with a haploid 23X sperm cell, which then doubles (a complete MH has a 46XY or a 46XX karyotype).

Conclusion

The contribution of our research work is to demonstrate that MH developing in an ectopic tubar pregnancy is difficult to diagnose **clinically**. In such a case, the correct histopathological diagnosis is of primary importance. The case we described corroborates the challenges related to the diagnosis and the course of the disorder.

References

1. Altieri, A., S. Franceschi, J. Ferlay, J. Smith, C. La Vecchia. Epidemiology and aetiology of GTD. – Lancet Oncol., **4**, 2003, 670-678.
2. Asseryanis, E., B. Schurz, W. Eppel, R. Wenzl, N. Vavra, P. Husslein. Detection of an atypical invasive mole in an ectopic pregnancy by transvaginal color-flow Doppler. – Am. J. Obstet. Gynecology, **169**, 1993, No 6, p. 1656.
3. Burton, J., E. Lidury, A. Gillespie, J. Tidy, O. Smith, J. Lawry, B. Hancock, M. Wells. Over-diagnosis of hidatidiform mole in early tubal ectopic pregnancy. – Hystopathology, **38**, 2001, 409-417.
4. Danihel, L., M. Zaviacik, M. Korbel, I. Hatzibougias. Mola invaziva-Spetsial Form of GTD. – Gen Physiol.Biophys., **18**, 1999, 37-41.
5. Fourchardiere, A., A. Cassignol, L. Benkiran, R. Rudigoz, A. Gorgeon, M. Shisheboran. Mole Hydatiforme invasive chez une patiente menopausee. – Ann. Pathol., **23**, 2003, 443-446.

Institute of Experimental Morphology and Anthropology with Museum
Bulgarian Anatomical Society

Acta morphologica et anthropologica, 12
Sofia • 2007

Lichen Actinicus

Mary Gantcheva

Department of Dermatology, Medical Faculty, Sofia

Lichen actinicus is a sub-type of Lichen ruber planus, which occurs predominantly in dark-complexioned young adults after prolonged exposure to sun and has a distinct photodistribution. The histological findings are as variable as the morphology of the clinical lesions. They are only partly like those of classical Lichen planus. The constant findings are marked pigmentary incontinence and the lymphocytic infiltrate in the papillary dermis. We present a patient with Lichen actinicus with two different types of lesions. We discussed the morphological and histopathologic variants of the disease.

Key words: Lichen actinicus, Lichen ruber planus, morphological types, histopathological findings.

Introduction

Lichen actinicus (LA) is a disease of young people of Oriental extraction with a distinct photodistribution. The lesions develop on the face and on the upper part of the hands. They appear usually in the spring and summer with improvement and even complete remission in winter. The histologic changes are only partly like those as classical Lichen planus (LP). They are as variable as the morphology of the clinical lesions.

Emphasizing the role of sunlight the disease has been defined as a subtype of LP, called LA [1]. For a long time it was told to be confined to subtropical countries [1, 2, 3]. Eighty-three per cent of reported patients were of Oriental origin (Iraq, Egypt, North Africa, Afghanistan, Yemen, India, Turkey, Bukhara) [1]. From this point of view it was named Lichen planus subtropicus. Thirty to forty per cent of LP seen in the Middle East were of these subtype [2]. However, the original reports of this condition were clearly Italian in origin [4]. Other authors propose another name of the disease — Summertime actinic lichenoid eruption (SALE) [5]. The point that LP subtropicus only delineates a predominant and not unique geographic distribution and does not stress the role of light in the pathogenesis.

Materials and Methods

Our patient is a 32-year-old white woman. She complains of dark macules, distributed all over her face. The had appeared before one year, after sun exposure in August. She hasn't

pruritus but has been treated for 20 days with topical corticosteroid without effect. In the following winter months she has noticed an improvement as the pigmented lesions became grayish-white. After sun exposure next year the lesions became darker and larger and she also obtained violaceous papules on the dorsum of both hands. She has neither family history of skin disease nor internal disease. She doesn't take any medications. The patient followed laboratory investigations including complete blood counts, ESR, blood sugar, hepatorenal function test, HIV serology, urinalysis and immunological parameters including antinuclear antibodies, anti-Sm, anti-s DNA, anti-n DNA, anti-Ro, anti-La antibodies, C_3 and C_4 complement. Biopsies were taken from a macule on the face as well as the lichenoid papules on the hand. Direct immunofluorescence and phototesting were also performed.

Results

On physical examination it was observed that our patient has a skin phototype IV. Pigmented macules were seen all over her face — on forehead, nose and chin. Violaceous flat topped lichenoid papules arranged linear were distributed on the dorsa of the hands. The mouth, scalp and nails were normal. Routine investigations were in normal limits. Immunological parameters were negative except the antinuclear antibodies which were in titer 1:40. Minimal erythema dose was elevated in phototesting. Direct immunofluorescence was negative. Hematoxylin-eosin section from the face showed an epidermal atrophy, hyperkeratosis and smooth dermo-epidermal junction (Fig. 1). Melanin uncontinence was prominent. Lichenoid lymphocitic infiltrate could be seen in the papillary dermis. There was no deep dermal infiltrate or follicular plugging. The biopsy of the lichenoid papule from the hand revealed typical picture of so-called interface dermatitis (Fig. 2). Pseudoacantosis of the epidermis and obliterated dermo-epidermal junction could be seen. Some colloid bodies were present in the lower epidermis. A high-hugging lymphocitic infiltrate could be seen in the upper dermis obscuring the dermo-epidermal junction.

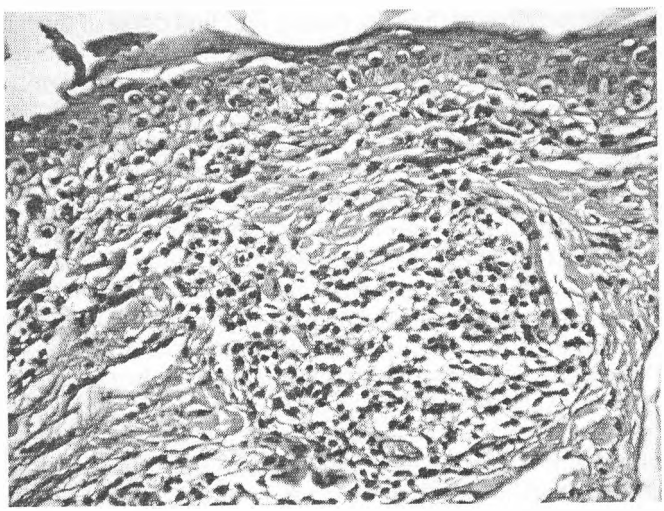

Fig. 1. Skin biopsy from lesion on the face: epidermal atrophy, hyperkeratosis, smooth dermo-epidermal junction, marked melanin uncontinence, Lichenoid lymphocitic infiltrate in papillary dermis (× 100)

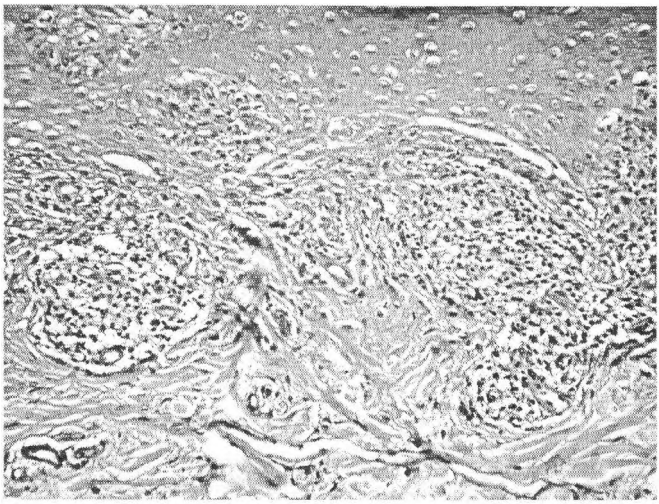

Fig. 2. Skin biopsy of the lichenoid papule from the hand: typical picture of so-called interface dermatitis (× 50)

The patient was treated with whitening lotion with cojic acid and a cream with Mexoryl XL for the lesions involving the face and with Methylprednisolon aceponat for the lesions distributed on the hands. Two months later she was slightly improved and she was recommended to use all the seasons photoprotecting cream.

Discussion

LA occurs or exacerbates after sun exposure, with recurrences in the spring and summer, and improvements or spontaneous remissions in the winter months. It affects almost exclusively the photoexposed parts of the skin, mainly face and dorsa of the hands. Morphologically, LA can be quite variable with several types of lesions:

1. Annular hyperpigmented plaques. This is the most common variety.
2. Pigmented form. This appears as chloasma-like lesions.
3. Dyschromic type. This consists of whitish pinhead papules with a tendency to coalesce.
4. Typical lichenoid papules. They are invariably present.

The histopathologic findings in LA differ according to the morphological type.

Typical lichen planus histology has been described in some of reported articles [2, 6, 7]. Some of the epidermal cell degenerated in so-called colloid bodies.

This change, which proceeded the formation of the dermal infiltrate, together with the liquefaction necrosis of the basal-cell layer, are the most characteristic features of early LP. Some colloid bodies are seen also in the biopsy specimen taken from the papules from the hand of our patient. According to K a t z e n e l l e n b o g e n [1] histologic features showed an overlap pattern between LP, lupus erythematosus, actinic dermatitis and irradiation dermatitis. In another group of patients lichenoid and non-specific inflammatory reactions were observed [8]. The only feature common to all types was marked pigmentary in continence. Our case confirmed this finding.

It is important to differentiate LA from lupus erythematosus and polymorphous light eruption as histologic differentiation may be somewhat more difficult. Microscopically

LA shows no thickening of the basement membrane, and the infiltrate is confined to the upper part of the dermis without involment of adnexal structures. LA differs from polymorphous light eruption by the absence of the papillary dermal edema and the deep dermal infiltrate seen on it later.

Having in mind the clinical and especially the histologic findings of LA it is more than clear that there is a close relationship between these disease and LP. More investigations will help us to understand why exactly the dark people suffer and what is the role of the light of the pathogenesis of this entity.

References

1. K a t z e n e l l e n b o g e n, I. Lichen planus actinicus (Lichen planus in subtropical counties). – Dermatologica, **124**, 1962, 10-20.
2. D i l i a m y, M. Lichen planus subtropicus. – Arch. Dermatol., **112**, 1976, 1251-1253.
3. V e r h a g e n, A., J. K o t e n. Lichenoid melanodermatitis: a clinicopathological study of fifty-one Kenyan patients with so called tropical lichen planus. – Br. J. Dermatol., **101**, 1979, 651-658.
4. Z a n c a, A. Lichen planus actinicus. – Int. J. Dermatol., **17**, 1978, 506-508.
5. I s a a c s o n, D., M. T u r n e r, M. E l g a r t. Summertime actinic lichenoid eruption (Lichen planus actinicus). – J. Am. Acad. Dermatol., **4**, 1981, 404-411.
6. B e e a f f e, D. Lichen planus actinicus. – Dermatology, **2**, 1979, 31-39.
7. J a n s e n, T., T. G a m b i c h l e r, L. K o b y l e t z k i, P. A l t e m e y e r. Lichen planus actinicus treated with acitretin and topical corticosteroids. – J. Europ. Acad. Dermatol. Venereol., **16**, 2002, 174-175.
8. P i n k u s, H. Lichenoid tissue reaction. – Arch. Dermatol., **107**, 1973, 840-846.

Institute of Experimental Morphology and Anthropology with Museum
Bulgarian Anatomical Society

Acta morphologica et anthropologica, 12
Sofia • 2007

Livedo Reticularis: A Clinico-Pathological Study

Mary Gantcheva

Department of Dermatology, Medical Faculty, Sofia

We studied a series of 10 patients with livedo reticilaris. Four of them were diagnosed as livedo vasculitis or so called segmental hyalinized vasculitis, two with idiopathic livedo reticularis and four of them were with Syndroma Sneddon. Histological examination of livedoid network disclosed in all cases the presense of thrombotic occlusion of venules and capillaries in papillary and reticular dermis, with occasional fibrinoid necrosis of the vascular wall, sparse perivascular lymphocytic infiltrate and variable extravasation of erythrocytes. In biopsy specimens obtained from areas adjacent to, but not involved by ulceration arteriolar thrombosis was also seen. Neither neutrophils nor nuclear dust were ever presented.

Our findings show that the capillary and venular thrombosis is the common histological hallmark of livedo reticularis, suggesting that vascular occlusion, but not leucocytoclastic vasculitis, is the primary event of the clinical condition: livedo reticularis.

Key words: Livedo reticularis, livedo vasculitis, Syndroma Sneddon, morphology, histopathology.

Introduction

Livedo reticularis (LR) is a persistent violaceous reticulated skin pattern usually found on the extremities and rarely trunk. Its coloration is due to the stagnation of blood in dilated superficial capillaries and venules, and implies pathologic changes in the deeper larger vessels. Normal skin areas are clearly demarcated from affected ones [1]. This type of lesion may occur on cold exposure in healty people or in a variety of pathologic states characterized either by blood hyperviscosity or by pathology in the arterioles, capillaries, or venules of the skin [2]. LR occurs in connective-tissue diseases such as systemic lupus erythematosus, thrombotic disorders such as thrombotic thrombocytopenic purpura, idiopathic thrombocytopenia. It is a main clinical sign of atheromatous vascular disease and occlusive vasculopathies, such as Livedo vasculitis (LV) [3, 4]. It could be found also in cerebrovascular thrombosis as Syndroma Sneddon [5] and antiphospholipid syndrome [1, 6].

Materials and Methods

We have reviewed the hystopathologic findings in 10 patients with skin manifestation of LR. Four patients carried a diagnosis of LV (3 females and 1 male, mean age 31 years). Clinically they were characterized by focal purpuric painful lesions of the lower legs (three

of the patients had necrotic ulcerations around the ankles), livedo like areas of hemosiderinic hyperpigmentation, reticulate of atrophie blance (stellate porcelain-white atrophic scars) and signs of LR.

Four patients (4 females, mean age 64 years) had Syndroma Sneddonps with LR distributed on the extremities, cerebrovascular accidents and negative anticardiolipine antibodies.

Two of the patients (2 females, mean age 25 years) included in the study were diagnosed as idiopathic LR as they had only the skin lesion of cyanotic discoloration of the legs (cutis marmorata). Ten skin biopsy specimens, taken from all the cases were examined. They were fixed in 10% neutral-buffered formaldehyde solution, processed routinely, and stained with hematoxylin-eosin.

Results and Discussions

The histological findings from the patients with LV showed results of microthromboses in dermal vessels. Some blood vessels in upper derma were with swollen endotel, some were dilated, as the others were with partly or totally obstructed lumen because of microthromboses (Fig. 1). The histopathological findings from the lesions from patients with LV were homogeneous,showing thromboses mostly in medium and upper dermal vessels, endothelial swelling, segmental signs of hyalinization, extravasated erythrocytes and a variable grade of perivascular lymphocyte imfiltration (Fig. 2). Idiopathic LR showed morphological changes consisted of thickned wall and endothelial cell oedema that were caused stenosis of the vessels. Sparse round-cell inflammatory infiltrate in the dermis round the vessel was presented (Fig. 3).

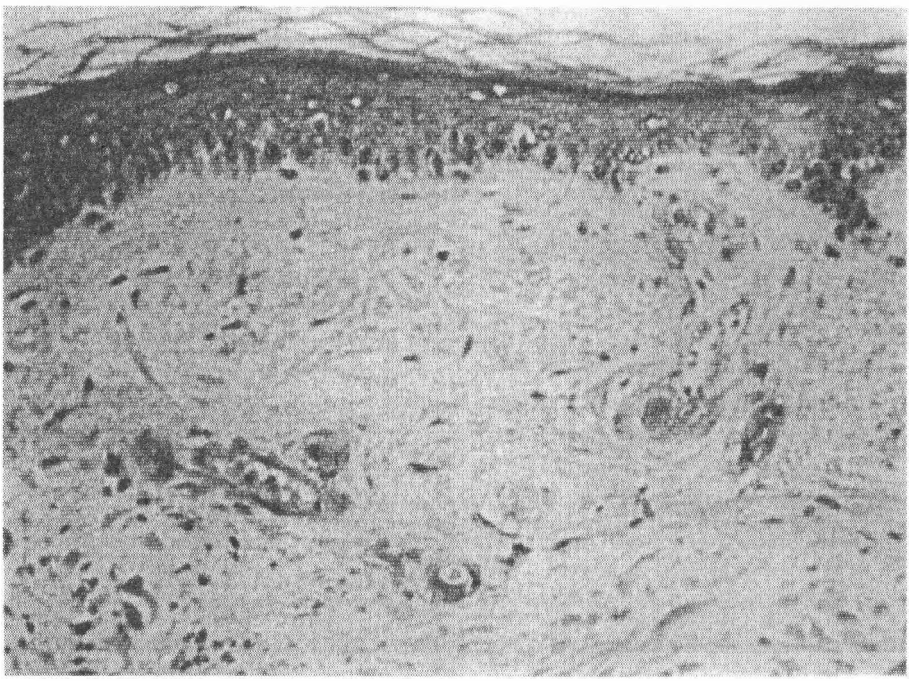

Fig. 1. Some blood vessels are with partly or totally obstructed lumen because of microthromboses. HE (×150)

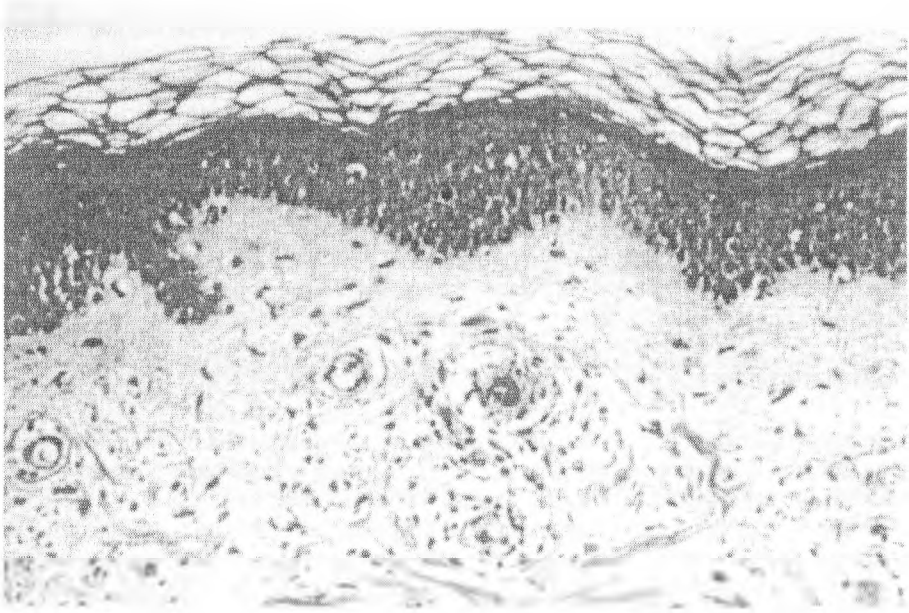

Fig. 2. Microvascular thromboses, slight perivascular lymphocytic infiltration in the upper dermis, without leucocytoclasis, segmental hyalinization of the dermal vessels. HE (× 80)

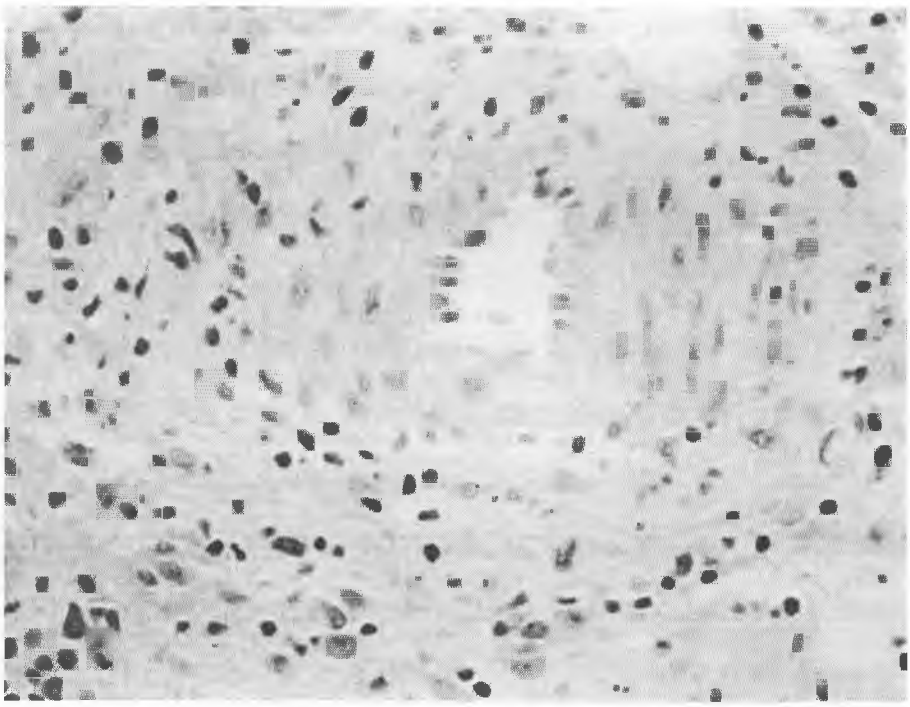

Fig. 3. Thickened wall and endothelial cell oedema that caused stenosis of the vessels, sparse roundcell inflammatory infiltrate. HE (× 250)

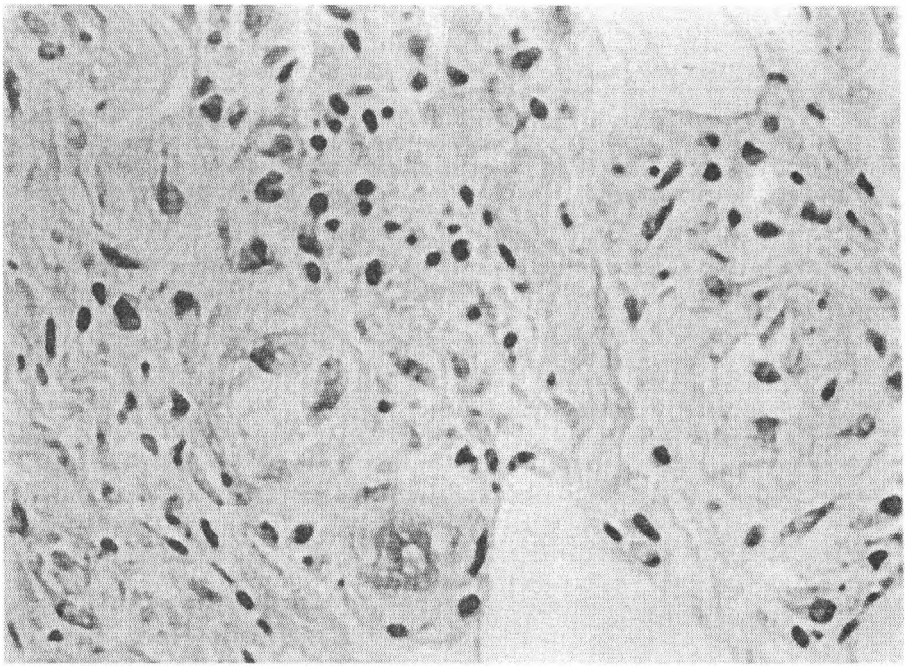

Fig. 4. Prominent endothelial cell oedema of capillares and post capillary venules. One of the capillaries is totally obturated with a plug by a thrombus. HE (× 250)

Thrombosis in the dermal vessels were found also in the biopsies from the lesions from patients with Syndroma Sneddon. It was seen that the capillary was with a totally plugged lumen as thrombosis existed. Prominent endothelial cell oedema of capillaries and post capillary venules was seen. One of the capillaries was totally obturated with a plug by a thrombus. Sparse round-cell infiltrate was seen round the vessels (Fig. 4).

Our findings show that capillary and venular thrombosis is the common histological hallmark of LR, suggesting that vascular occlusion, but not leucocytoclastic vasculitis, is the primary event of these clinical conditions. The mechanism of LR is unclear, but we think that the vasculopathy with occlusion is the main histopatological sign of LR. We didn't see the features of vasculitis. It could be demonstrated histologically when ulceration coexist with LR in systemic lupus erythematosus and neutrophils and nuclear dust could be seen [7].

Because of the histological absence of leucocytoclasia and the common finding of dermal vessel microthromboses, the hypothesis of a vasooclusive pathogenesis could be accepted.

References

1. G a n t c h e v a, M. Dermatological aspects in antiphosphoilipid syndrome. – Int. J. Dermatol., **36**, 1997, 173-180.
2. C o p e r m a n, P. Livedo reticularis: signs in the skin of disturbance of blood viscosity and of blood flow. – Br. J. Dermatol., **93**, 1975, 519-529.
3. P a p i, M., B. D i d o n a, O. De P i t a, M. G a n t c h e v a, L. C h i n n i. Purple (atrophie blance): clinical histological and immunological study of twelve patients. – J. Europ. Acad. Dermatol. Venerol., **9**, 1997, 129-134.
4. F r i t s c h, P., B. Z e l g e r. Livedo vasculitis. – Hautartz, **46**, 1995, 215-224.
5. G a n t c h e v a, M., N. T s a n k o v. Livedo reticularis and cerebrovascular accidents (Sneddon's syndrome) in the spectrum of antiphosphoilipid syndrome. – J. Europ. Acad. Dermatol. Venerol., **12**, 1999, 157-160.
6. G r o b, J., J. B u n e r a n d i. Cutaneous manifestations associated with the presence of the lupus anticoagulant. – J. Am. Acad. Dermatol., **15**, 1986, 211-219.
7. K u h n, A., P. L e h m a n n., T. R u z i c k a. Vasculitis and cutaneous lupus erythematosus. – In: Cutaneous lupus erythematosus. Berlin, Heidelberg, New York, Springer-Verlag, 2004, 156-160.

Institute of Experimental Morphology and Anthropology with Museum
Bulgarian Anatomical Society

Acta morphologica et anthropologica, 12
Sofia • 2007

Anthropology

Secular Changes of Physical Development in 19-20 Years Old Youths from the Beginning of the 20th Century till the Beginning of the 21st Century

N. Atanassova-Timeva

Institute of Experimental Morphology and Anthropology with Museum, Bulgarian Academy of Sciences, Sofia

The secular changes of physical development in 19-20 years old youths during 20th century are evaluated, and the specificity of physical development in students at this age at the beginning of the 21st century is characterized. Anthropometrically are studied 72 Bulgarian male students and 70 female ones during 2002 in Sofia City. The secular changes are assessed at universal body features: stature; body weight; chest measurements; biacromial and bicristal diameters. The secular trend is traced out using analogous data of youths at the same age from the beginning of the 20th century. The secular changes point out that the investigated in 2002 male and female youths are taller than the ones of previous generations lived during the 20th century. Deceleration of body weight and chest circumference is available after the 80s. A tendency for gracilization of body diameters is observed after the 80s, more strongly expressed among young females.

Key words: secular changes, physical development, anthropometry, youths.

Introduction

The human physical development is characterized by a complex of morphological and functional peculiarities on which normal human development and health depends during different ages. Indicators for physical development most often are the basic morphological and physiological features. Their realization after birth depends as on heredity, so on environmental factors — geographical, social, economical, etc. The changes of basic characteristics in human physical development that come in the course of time are denoted as "secular trend" and are well known to the experts who work in the field of anthropology and medicine. These changes affect as the increment and decrement of body measurements, so the rate and velocity of body and sexual maturation. During the past century

were discussed mainly the processes of increment in stature and body massiveness and of the speeded maturation, as well, i.e. the processes of acceleration. In last two decades, however, more and more experts gain results (published in many scientific papers), which make them to speak about acceleration delay and even about deceleration in some characteristics of human physical development. During 1993-2001 in the Department of Anthropology at the Institute of Experimental Morphology and Anthropology with Museum, Bulgarian Academy of Sciences was carried out a wide anthropological investigation including 7-14 years old schoolchildren from Sofia City. The data about secular changes in children from Sofia City, from the beginning till the end of the 20th century, show that the increment of stature, body weight and chest circumference has delayed between the 70s and 80s, while at the end of the century a tendency of gracilization is observed [8, 9]. In the symposium "Secular growth changes in Europe", edited by E. Bodzsár and C. Susanne, are summarized results of different investigations carried out in Europe during the last hundred years. S t o e v, Y o r d a n o v [12] have studied the secular changes in children, adolescents and adults in Bulgaria after literature data, emphasising mainly on the maturation terms and the brachycephalization process. The data about France display increment of mean stature during the period 1900-1990 (mainly between 60s and 80s), after which a tendency of deceleration is observed [3]. A study of children and youths in Sweden established acceleration delay at the end of the 20th century [6]. In Great Britain were carried out investigations (1974, 1980, 1994) for adults aged from 18 till 24 years that show increment of mean stature 12,5 cm for 18-year-old males, and 9,5 cm for 20-24 years old ones, while the increment for females is lower than 5.0 cm [10]. Š t e f a n č i č et al. [11] has established that secular increment of stature, body weight and biacromial diameter delayed around the 80s in 7-18-year-old children and adolescents from Ljubljana, concerning the period 1939-1992. In Russia the investigations from the end of 19th century till 1980 in children and adolescents aged 0-15 years and in adults (20-29 years) showed intensive secular changes till 1970, followed by stabilization and deceleration of somatic features [4]. In the closing paper [2] E. B. Bodzsár and C. Susanne summarised that greatest are the acceleration changes of growth and development in children and adolescents from Europe at the end of the 70s and the beginning of the 80s within the 20th century. After this period acceleration delay has been observed, while positive secular changes still are available.

In literature was not established purposeful anthropological study of young Bulgarians (19-20 years old) made after 1980 with a view to use this information for assessment of secular changes in this age group during the past century.

The aim of the present work is to evaluate the tendencies of secular changes in physical development of 19-20 years old youths during the 20th century and to characterize the specificity of physical development in same age students at the beginning of the 21st century.

Materials and Methods

In the period March-May 2002 were investigated anthropometrically 72 Bulgarian male students and 70 female ones aged 19-20 years from Saint Kliment Ohridski University of Sofia and Technical University, Sofia. The mean age is 19.49 years for males and — 19.57 years for females. The programme includes 20 directly measured features, 18 derivative ones, body proportions and indexes, and their distribution into rubrics and categories. In the present work secular changes of the following anthropometrical features are discussed: stature, body weight, bicristal and biacromial diameters, transversal and sagittal chest diameters and chest circumference. The anthropological characterization is made by the classical method of R. M a r t i n and K. S a l l e r [7]. Standard anthropometrical

instruments are used. The investigated by us sample claim not to be representative for the present generation of 19-20 years old Bulgarians, but still we expect to get a notion about specificity of physical development for this generation Bulgarians compared to data about different generations of their coevals lived during the past century.

To trace back the secular changes of physical development in 19 years old youths during the 20th century are used corresponding data from investigations of:

- St. V a t e v, a study carried out in 1907, published in 1939 [13];
- B. Y a n e v et al., a study carried out in 1960, published in 1965 [15];
- B. Y a n e v et al., a study carried out in 1970/72, published in 1982 [16];
- P. S l a n c h e v et al., a study carried out in 1980/82, published in 1992 [14].

Results and Discussion

Stature

The evaluation of metrical changes in stature during the past century shows that for the entire period (1907-2002), young men became 10.9 cm taller, and young women — 7.2 cm taller (Table 1, Fig. 1). During the first half of the 20th century till 1960, the increment is 3.7 cm in young males and 1.6 cm in young females. As a whole, the stature increment is bigger — respectively 7.2 cm in male youths and 5.6 cm in female ones since the second half of the past century till the beginning of the 21st one. Interesting information gives the analysis about stature changes made after decades concerning the second half of the past century. The acceleration observed at the beginning of the 20th century delayed between the 60s and 70s — the stature being almost the same in both sexes. In male youths this tendency is preserved till the 80s. In female youths is available slightly stature increment (2.6 cm) between the 70s and 80s. Greater are the acceleration changes for both sexes between 1980 and 2002, being more underlined for young men i.e. the 19-20 years old males have already stature of 178.78 cm and the females of 164.0 cm at the beginning of the 21st century. This data differ from the results obtained by many European scientists [3, 6] who established a delay of stature secular growth around the 80s of the past century. This difference, probably, could be due to the fact that we have investigated students in 2002, who distinguish by their higher stature, well known from the literature [1, 5]. Series of studies in students are carried out in Hungary (Debrecen town) during the period 1930-1992. B o d z s á r [1] observed stature decrease in the period 1942-1951, a fact explained mainly by the worsened social conditions of life after the World War II. The stature increased considerably after 1950, as for one decade only it raised at an average of 2.31 cm. In the Technology Institute, Budapest City, investigations of students are carried out during the period 1976-1985. G y e n i s [5] established stature increment of 2.17 cm in young women and of 2.81 cm in young men.

Table 1. Secular changes in basic anthropometrical features

Features		Males					Females				
		St. Vatev, 1907	B. Yanev et al., 1960	B. Yanev et al., 1970	P. Slanchev et al., 1980	Our data, 2002	St. Vatev, 1907	B. Yanev et al., 1960	B. Yanev et al., 1970	P. Slanchev et al., 1980	Our data, 2002
Stature	*n*	196	527	650	372	72	44	451	444	355	70
	mean	**167.9**	**171.6**	**171.3**	**172.3**	**178.8**	**156.8**	**158.4**	**158.8**	**161.4**	**164.0**
	SD		6.3	6.3	5.9	6.6		6.0	6.0	5.9	5.1
Biacromial diameter	*n*		528		372	72		451		355	70
	mean		**39.2**		**41.0**	**41.2**		**35.0**		**35.4**	**34.8**
	SD		2.3		2.4	2.0		1.9		2.9	1.9
Bicristal diameter	*n*		528		372	72		452		355	70
	mean		**28.4**		**29.0**	**27.2**		**27.7**		**27.4**	**25.4**
	SD		2.0		1.8	1.6		2.1		3.5	1.5
Transversal chest diameter	*n*		518		372	72		452		355	70
	mean		**27.9**		**28.9**	**29.5**		**24.8**		**25.2**	**24.9**
	SD		1.9		2.2	2.0		1.6		2.4	1.6
Sagital chest diameter	*n*		528		372	72		451		355	70
	mean		**20.0**		**20.8**	**20.9**		**18.0**		**17.8**	**17.7**
	SD		1.8		2.2	1.7		1.6		2.3	1.5
Chest circum-ference	*n*	579	528	658	372	72	34	450	446	355	70
	mean	**85.9**	**90.2**	**88.5**	**89.6**	**87.4**	**76.6**	**78.2**	**77.5**	**79.4**	**73.0**
	SD		4.7	5.2	5.4	5.8		5.5	6.9	7.2	4.4
Body weight	*n*	196	526	652	372	72	44	434	444	355	70
	mean	**58.8**	**67.0**	**67.6**	**71.2**	**70.4**	**53.2**	**57.4**	**57.8**	**58.4**	**52.4**
	SD		7.8	7.9	7.5	8.6		7.3	8.8	8.9	7.0

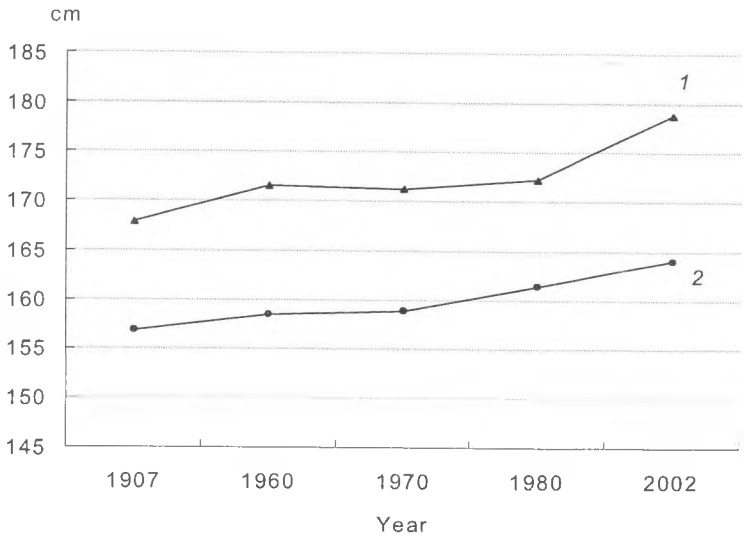

Fig. 1. Secular changes of stature
1 — males; *2* — females

Body weight

Body weight changes show that the young men studied by us are 11.6 kg heavier compared to their coevals investigated in 1907, while the young women are 0.8 kg lighter than their coevals examined at the beginning of the 20th century (Table 1, Fig. 2). Opposite to the stature, whose increment is more tangibly during the second half of the past century, the body weight growth is more significant for both sexes till 1960 — 8.2 kg in male youths and 4.2 kg in female ones. Body weight changes studied after decades concerning the second half of the 20th century show that similar to stature, between the 60s and 70s is available an acceleration delay for both sexes. In female youths this tendency remains till the 80s. In male youths, however, is established body weight increment (3.6 kg) between the 70s and 80s. It should be noted that body weight is greatest for both sexes during the 80s. After this period our data trace out a deceleration tendency that is more strongly expressed in females who have lowest body weight compared to all their coevals, as well. The males investigated in 2002 have mean body weight of 70.40 kg, being 0.8 kg lighter than the males examined during the 80s, and the females have respectively mean body weight of 52.4 kg being 6.0 kg lighter. The results obtained are in unison with the data by other European authors who reported about an acceleration delay in body weight established after the 80s.

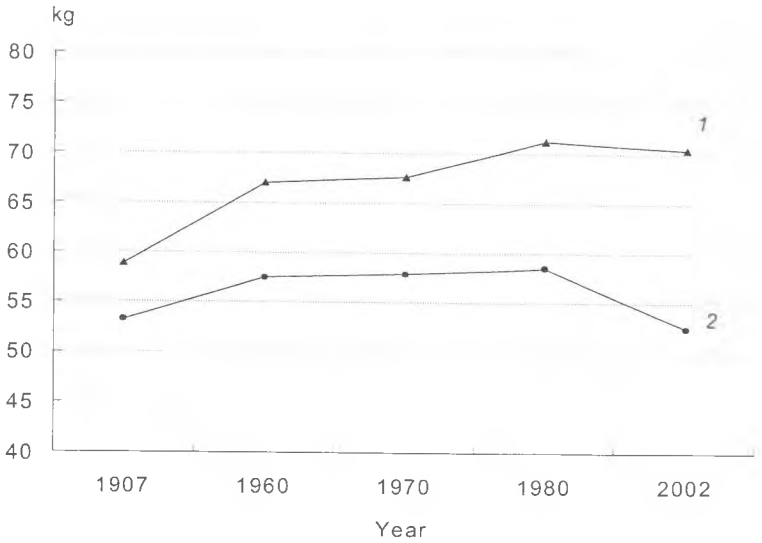

Fig. 2. Secular changes of body weight
1 — males; *2* — females

Chest circumference

The secular changes of chest circumference repeat to a great extent the ones of body weight but they are more slightly expressed (Table 1, Fig. 3). The investigated in 2002 male youths have 1.5 cm larger chest circumference compared to their coevals studied in 1907, while the females examined at the beginning of the 21st century have 3.6 cm smaller chest circumference. For the entire nearly hundred years period the investigated by us female students could be distinguished by smallest chest circumference. During the first half of the 20th century, an increment of chest circumference for both sexes is observed better expressed in young men (males — 4.3 cm; females — 1.6 cm). For the entire period under study (1907-2002), the male youths investigated in 1960 and the female ones examined in 1980 have greatest chest circumference. Analyzing the metrical changes of chest circumference after decades, concerning the second half of the past century, a certain decrement of chest circumference is established between the 60s and 70s (1.7 cm in male youths, and 0.7 cm in female ones), while it turned into poor increment between the 70s and 80s (1.1 cm in male youths, and 1.9 cm in females). The data about youths studied at the beginning of the 21st century compared to the youths examined during the 80s show considerably chest circumference decrement, better underlined in young women (2.2 cm smaller chest circumference in male youths, and 6.4 cm smaller — in female ones), i.e. a deceleration of this anthropometrical feature is available again after 1980 for the Bulgarian youths that is observed also in other European countries.

Chest diameters

The changes for both chest diameters — transversal and sagital, which determine also the chest form, are traced out in 20 years intervals: 1960-1980-2002 (Table 1, Figs. 4, 5). Smallest are the chest measurements in the 19 years old males studied during 1960. The chest diameters in young men increase consecutively till the end of the past century and the male youths, investigated at the beginning of the 21st century, have biggest chest mea-

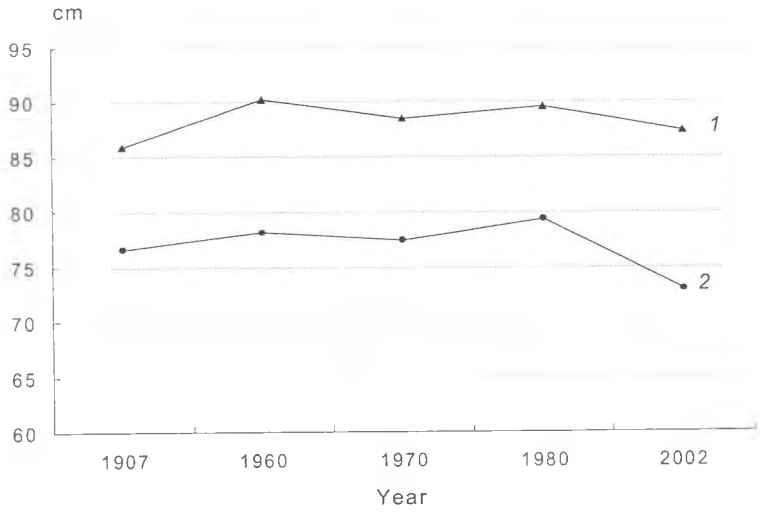

Fig. 3. Secular changes of chest circumference
1 — males; *2* — females

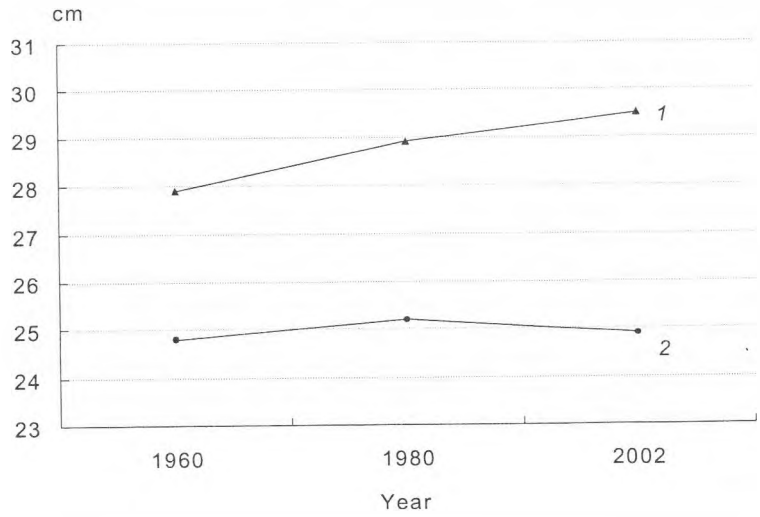

Fig. 4. Secular changes of transversal chest diameter
1 — males; *2* — females

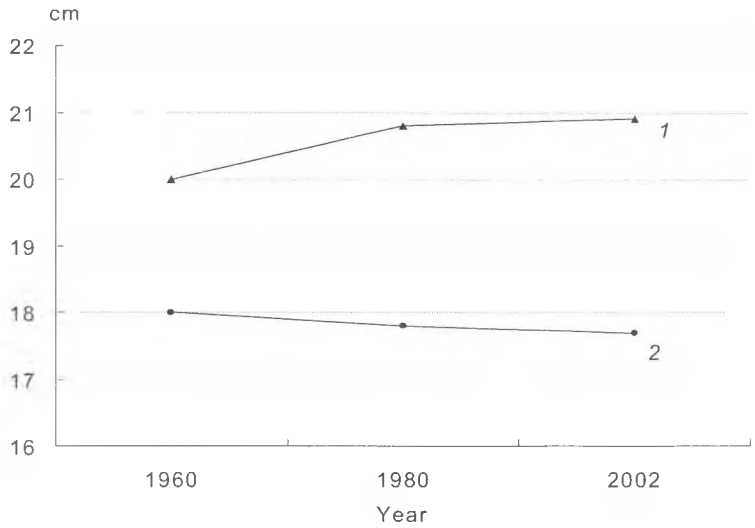

Fig. 5. Secular changes of sagital chest diameter
1 — males; *2* — females

surements. Differences in secular changes of transversal and sagital chest diameters are established in young women. From 1960 till 1980 the increment of transversal chest diameter is 0.4 cm for female youths, and throughout next 20 years it decreases and becomes equal to the transversal chest diameter for 19 years old women studied in the 60s. Opposite to the transversal diameter, the sagital chest diameter decreases, even very little (from 18.0 up to 17.7 cm) during the entire 40 years period.

Biacromial diameter

The analysis about this diameter is made again in 20 years intervals (Table 1, Fig. 6). The data show underlined sexual differences, similar to those for chest diameters. Narrowest shoulders have the young men investigated in the 60s. The male youths, researched in the 80s, have 0.8 cm bigger shoulder breadth compared to the previous generation. The young men studied by us (2002) have nearly the same biacromial diameter (41.2 cm) as the males examined during the 80s (41.0 cm), i.e. acceleration delay is available. In young women the biacromial diameter increases insignificantly (only 0.4 cm) between 1960 and 1980, while during the next 20 years period it decreases gradually, and the young women investigated at the beginning of the 21st century have smallest shoulder width (34.8 cm).

Bicristal diameter

The bicristal diameter increment is 0.6 cm for males from 1960 till 1980 (Table 1, Fig. 7). For the period under study (1960-2002), the bicristal diameter is biggest in young men examined during the 80s. Opposite to the males, in females the bicristal diameter decreases during the entire period under investigation, the decrement being more slightly expressed between the 60s and 80s (0.3 cm) and considerable between the 80s and the beginning of the 21st century (2.0 cm). It had to be underlined that bicristal diameter is significantly smaller in male and female youths studied at the beginning of the 21st century (mean bicristal diameter is 27.2 cm in male students and 25.4 cm in female ones), compared to their coevals born in the past century.

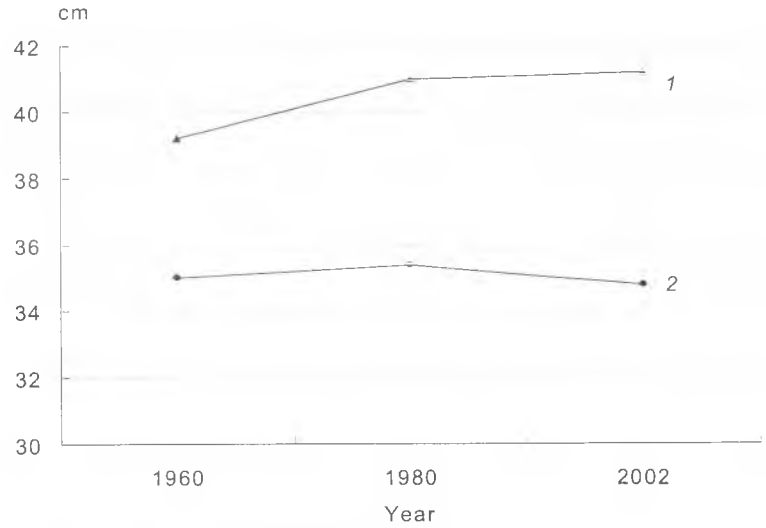

Fig. 6. Secular changes of biacromial diameter
1 — males; *2* — females

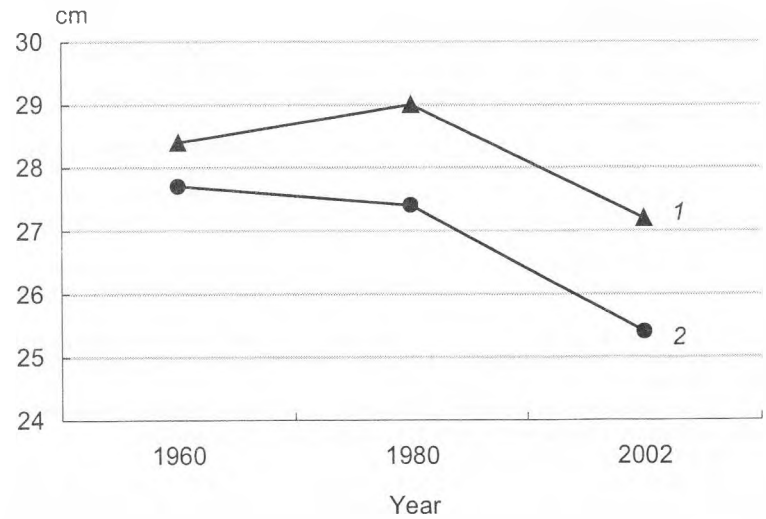

Fig. 7. Secular changes of bicristal diameter
1 — males; *2* — females

According to the summarized comparative analysis about body diameters is established a tendency of body gracilization after 1980 that is in unison to the results obtained in the Department of Anthropology at the Institute of Experimental Morphology and Anthropology with Museum, Bulgarian Academy of Sciences for 7-14-year-old children [8, 9]. It is obvious that at the end of the 20th century the decrement of body diameters during childhood and puberty retains in youth.

Conclusion

The results obtained about specificity of physical development in 19-20 years old students who are investigated at the beginning of the 21st century on the background of secular changes in their coevals examined during the 20th century show:

- a tendency of young males and females studied at the beginning of the present century to be taller than the ones examined during the 20th century;
- body weight and chest circumference to be smaller compared to these measurements in the generation researched in the 80s;
- a tendency of gracilization in body diameters after the 80s, more strongly expressed in females.

References

1. Bodzsár, E. Secular growth changes in Hungary. – In: Secular Growth Changes in Europe (Ed. E. Bodzsбr, C. Susanne). Budapest, Eötvös University Press, 1998, 175-207.
2. Bodzsár, E., C. Susanne. Secular growth changes in Europe: Do we observe similar trends? Considerations for future research. – In: Secular Growth Changes in Europe (Ed. E. Bodzsár, C. Susanne). Budapest, Eötvös University Press, 1998, 369-381.
3. Demoulin, F. Secular trend in France. – In: Secular Growth Changes in Europe (Ed. E. Bodzsár, C. Susanne). Budapest, Eötvös University Press, 1998, 109-134.
4. Godina, E. Secular changes in Russia and the Former Soviet Union. — In: Secular growth changes in Europe (Ed. E. Bodzsár, C. Susanne). Budapest, Eotvös University Press, 1998, 351-367.
5. Gyenis, G. Continuing positive growth chahges in height and weight of Hungarian university students. – Annals of Human Biology, **24**, 1997, 475-479.
6. Lindgren, G. Secular growth changes in Sweden. – In: Secular growth changes in Europe (Ed. E. Bodzsár, C. Susanne). Budapest, Eötvös University Press, 1998, 319-334.
7. Martin, R., K. Saller. Lehrbuch der Anthropologie in sistematischer Darstellung. Bd. I. Stuttgart, Gustav Fischer Verlag, 1957.
8. Nacheva, A., E. Lazarova, L. Yordanova. Physical development and secular trend in 7-13 years old schoolchildren from Sofia-town. – Journal of Anthropology, **3**, 2000, 7-30.
9. Nacheva, A., E. Lazarova, L. Yordanova. Specificity of the physical development in 7-14 years old schoolchildren from Sofia at the end of the 20th century — Basic body diameters and Circumferences. – Acta morph. et anthropol., **7**, 2002, 72-84.
10. Rona, R. Secular trend of stature and body mass index in Britain in the 20th century. – In: Secular Growth Changes in Europe (Ed. E. Bodzsár, C. Susanne). Budapest, Eötvös University Press, 1998, 335-351.
11. Štefančič, M., T. Tomazo-Ravnik. Fifty-two years of secular trend in Ljubljana schoolchildren. – In: Secular Growth Changes in Europe (Ed. E. Bodzsár, C. Susanne). Budapest, Eötvös University Press, 1998, 281-297.
12. Stoev, R., Y. Yordanov. Secular trend in Bulgaria. – In: Secular Growth Changes in Europe (Ed. E. Bodzsár, C. Susanne). Budapest, Eötvös University Press, 1998, 65-73.
13. Ватев, С. Антропология на българите. С., 1939.
14. Слънчев, П., Б. Янев, Ф. Генов, П. Щерев, П. Боев, Д. Сепетлиев, Б. Захариев. Физическо развитие, физическа дееспособност и нервно-психическа реактивност на населението на България (1980-1982). С., Национална спортна академия, 1992.
15. Янев, Б., П. Щерев, П. Боев, Р. Семерджиева, Д. Сепетлиев. Физическо развитие и дееспособност на населението в България от раждане до двадесет и шест години. Том I. Таблици. С., БАН, 1965.
16. Янев, Б., П. Щерев, П. Боев, Ф. Генов, Д. Сепетлиев, И. Попов, Б. Захариев. Физическо развитие, физическа дееспособност и нервно-психическа реактивност на населението в България от раждането до шестдесетгодишна възраст. С., Медицина и физкултура, 1982.

Institute of Experimental Morphology and Anthropology with Museum
Bulgarian Anatomical Society

Acta morphologica et anthropologica, 12
Sofia • 2007

Hand Clasping and Arm Folding in Bulgarians from South Bulgaria

Zl. Filcheva

Institute of Experimental Morphology and Anthropology with Museum, Bulgarian Academy of Sciences, Sofia

The incidence of the hand clasping and arm folding types has been studied in 1524 Bulgarians (711 males and 813 females) aged 30-39 from the three parts of South Bulgaria — South-West, South Central and South-East. In both sexes the L-type of hand clasping and arm folding is prevalent with its percentage dropping from the West to the East. The intersexual differences are statistically significant only with respect to the arm folding. The observed territorial varieties of the hand clasping and arm folding frequencies are statistically insignificant in both sexes. The relationship between both asymmetries is statistically insignificant.

Key words: functional asymmetry, hand clasping, arm folding, intersexual differences, territorial differences.

Introduction

Hand clasping (interlocking of the fingers of the hands) and arm folding (crossing over of the fore-arms in front of the chest) represent manifestations of the functional asymmetry of the upper limbs in the man. L u t z [17] was the first to describe both ways of crossing the fingers of the hands. In the first case the right thumb is situated over and is defined as the R-type whereas the other with the left thumb is placed over the thumb and is defined as the L-type. Analogous are the cases in the crossing of the fore-arms over the chest described by W i e n e r [25]. A number of authors show an interest in that problem starting from the beginning of the 20-th century and up till our day. The interest is directed mainly to the factors accounting for the development of these asymmetries, the relationship between them and the impact of sex, age and race. Even now there is no unified opinion about their character. Both L u t z [17] himself and a variety of other authors support the thesis of a genetic control over them [7, 8, 18, 19, 20, 26]. Other investigators assume that there is no adequate evidence for such a control [5, 25]. According to L o u r i e [16] arm folding in contrast to hand clasping is an anthropological marker of a lesser importance and that genetic control is more evident in hand clasping. L a i and W a l s h [13] suggest that more probably the habit formed at an early age rather than the genetic factors determine the hand clasping types. L e g u e b e [14] marks the combined impact of the factors determining hand clasping. According to some authors sex and age do not exert an influence on the asymmetries under study [2, 9] and according to others they do affect them

though to a lesser degree [18]. A number of authors do not find a correlation between hand clasping and arm folding or if they record one it is very weak [2, 22, 23, 25] while according to others such a link exists [11, 12, 15, 21]. S a r n a et al. [24] based on literature data prove by statistical analysis that the manifestation of these asymmetries is not a random phenomenon. These asymmetries together with other features are used in anthropological studies on different populations [1, 15].

The studies on that problem in our country are comparatively very scanty. B o e v and T o d o r o v [3] have investigated 238 individuals of both sexes from three ethnic groups and have found a very high percentage of the R-type of hand clasping especially in the Bulgarians. M u t a f o v [27] has studied a control group of 1500 schoolchildren where the L-type of hand clasping was predominant. K a r e v [10] has studied 2100 schoolchildren and has also found a higher per cent of the L-type in both asymmetries. F i l c h e v a [6] has carried out a research on 1511 Bulgarians from North Bulgaria where the L-type is dominant among males in both asymmetries while in women it is prevalent only in the case of arm folding.

The aim of the present study is to trace the incidence of the hand clasping and arm folding types in Bulgarians from the three regions of South Bulgaria — South-West, South Central and South-East and to look for intersexual and territorial differences as well as for an association between both asymmetries.

Material and Methods

A total of 1524 Bulgarians of both sexes (711 males and 813 females) aged from 30 to 39 years living and descending from the three parts of South Bulgaria — South-West, South Central and South-East were investigated. The regions under study encompass four administrative areas — Sofia, Plovdiv, Haskovo and Bourgas (according to the administrative ad territorial division of Bulgaria from 1987). The persons under study were living and originate from these regions. The study was carried out parallel to the National programme "Anthropological characteristics of the Bulgarian people" (1989-1993) realized by the department of Anthropology of IEMAM at the BAS. It was performed by the help of the conventional methods (4, 14) and the χ^2-test has been used in the comparative analysis.

Results and Discussion

Hand clasping

The L-type is prevalent in both sexes for the whole of South Bulgaria whose percentages are of close values (Table 1). This confirms the opinion of other authors that the L-type is prevailing in Europe [22]. The itersexual differences are statistically insignificant ($P>0.05$). In both sexes in the three regions of South Bulgaria the L-type is prevalent with a highest percentage in South-West Bulgaria especially in women and beginning to drop down from the West to the East (Table 2). The territorial differences observed are statistically insignificant ($P>0.05$).

Table 1. Per cent distribution of hand clasping types among a population of South Bulgaria

Sex	R — type		L — type		Total
	n	%	*n*	%	
Males	329	46.27	382	53.73	711
Females	384	47.23	429	52.77	813
Both sexes	713	46.78	811	53.22	1524

$\chi^2 = 0.14$, k = 1, $P > 0.05$

Table 2. Comparison of the frequencies of hand clasping types between populations from three regions of South Bulgaria

Region	Sex	R —type		L — type		Total	Comparison groups	χ^2 $k = 1$
		n	%	*n*	%			
1. South - West Bulgaria	Males	108	44.63	134	55.37	242	Males	
	Females	126	42.86	168	57.14	294	1 — 2	0.24
2. South Central Bulgaria	Males	125	46.82	142	53.18	267	1 — 3	0.37
	Females	146	49.83	147	50.17	293	2 — 3	0.02
3. South - East Bulgaria	Males	96	47.52	106	52.48	202	Females	
	Females	112	49.56	114	50.44	226	1 — 2	2.87
Total	Males	329	46.27	382	53.73	711	1 — 3	2.31
	Females	384	47.23	429	52.77	813	2 — 3	0.01

Arm folding

In both sexes for the entire South Bulgaria the L-type is predominant with a much higher percentage than that of the R-type especially in the males (Table 3). This fact is also in accord, as in the case of hand clasping, with the tendency for predomination of the L-type in Europe [19]. The intersexual differences are statistically significant ($P < 0.05$). In both sexes in the three regions of South Bulgaria the L-type is prevalent also in the men, being much more common than the R-type. By contrast to the hand clasping a clear-cut tendency

Table 3. Per cent distribution of arm folding types among a population of South Bulgaria

Sex	R — type		L — type		Total
	n	%	*n*	%	
Males	260	36.57	451	63.43	711
Females	347	42.68	466	57.32	813
Both sexes	607	39.83	917	60.17	1524

$\chi^2 = 5.92$, k = 1, $P > 0.05$

Table 4. Comparison of the frequencies of arm folding types between populations from three regions of South Bulgaria

Region	Sex	R —type		L — type		Total	Comparison groups	χ^2 $k = 1$
		n	%	*n*	%			
1. South - West Bulgaria	Males	89	36.78	153	63.22	242	Males	
	Females	122	41.50	172	58.50	294	1 — 2	0.14
2. South Central Bulgaria	Males	94	35.21	173	64.79	267	1 — 3	0.08
	Females	131	44.71	162	55.29	293	2 — 3	0.42
3. South - East Bulgaria	Males	77	38.12	125	61.88	202	Females	
	Females	94	41.59	132	58.41	226	1 — 2	0.62
Total	Males	260	36.57	451	63.43	711	1 — 3	0.00
	Females	347	42.68	466	57.32	813	2 — 3	0.50

in the percent distribution for the region is not observed in this type of asymmetry (Table 4). The found territorial differences are statistically insignificant ($P > 0.05$).

The per cent distribution of the combinations between the R-types and the L-types of hand clasping and arm folding was traced. In both sexes for South Bulgaria as a whole the per cent of the combination between the L-type of hand clasping and the L-type of arm folding is of highest values (LL). Ranking second is the combination between the R-type of hand clasping and the L-type of arm folding (RL). The per cent of the combination between the R-type hand clasping and R-type arm folding is of lowest values ((RR) (Table 5). The intersexual differences are statistically insignificant ($P > 0.05$). This tendency in the combination between both asymmetries is preserved with respect to their territorial distribution in both sexes where the differences are statistically insignificant (Table 6). The sought association between both asymmetries is statistically insignificant (Table 7). Compared with the data of Filcheva [6] about Bulgarians from North Bulgaria significant differences were established only with respect to arm folding and in the case of the males at that ($\chi^2 = 9.44$, $k = 1$, $P < 0.05$).

Table 5. Per cent distribution of hand clasping / arm folding combinations among a population of South Bulgaria

Sex	RR		RL		LR		LL		Total
	n	%	n	%	n	%	n	%	
Males	115	16.18	213	29.96	145	20.39	238	33.47	711
Females	171	21.03	213	26.20	174	21.40	255	31.37	813
Both sexes	286	18.77	426	27.95	319	20.93	493	32.35	1524

$\chi^2 = 7.23$, $k = 3$, $P > 0.05$

Table 7. Relationship between hand clasping and arm folding among a population of South Bulgaria

Hand clasping	Arm folding		
	Right	Left	Total
Right	286	426	712
Left	319	493	812
Total	605	919	1524

$\chi^2 = 0.12$, $k = 1$, $P > 0.05$

Conclusion

The incidence of the hand clasping and arm folding types in Bulgarians from South Bulgaria corresponds to the parameters typical of the Europoid race. The L-type prevails in both sexes and in both types of asymmetry, especially in arm folding. The intersexual differences are statistically significant only in the case of arm folding. The observed territorial variations in both types of asymmetry are statistically insignificant. The most common combination between than in both sexes is LL where the intersexual differences are also statistically insignificant. The study of these types of asymmetry adds to the morpho-functional characteristics of the individuals under study and they deserve their position in the complex anthropological characterization of modern Bulgarian population.

T a b l e 6. Comparison of the frequencies of hand clasping / arm folding combinations among the three regions of South Bulgaria

Region	Sex	RR		RL		LR		LL		Total	Comparison groups	χ^2 $k = 3$
		n	%	*n*	%	*n*	%	*n*	%			
1. South - West Bulgaria	Males	36	14.88	71	29.33	52	21.49	83	34.30	242	Males	
	Females	54	18.37	72	24.49	68	23.13	100	34.01	294	1 — 2	1.21
2.South Central Bulgaria	Males	43	16.10	82	30.71	52	19.48	90	33.71	267	1 — 3	0.78
	Females	68	23.21	78	26.62	61	20.82	86	29.35	293	2 — 3	0.37
3. South - East Bulgaria	Males	36	17.82	60	29.70	41	20.30	65	32.18	202	Females	
	Females	49	21.68	63	27.88	45	19.91	69	30.53	226	1 — 2	3.27
Total	Males	115	16.18	213	29.96	145	20.39	238	33.47	711	1 — 3	2.38
	Females	171	21.03	213	26.20	174	21.40	255	31.37	813	2 — 3	4.75

References

1. Apostolou, M., Ts. Minkov, V. Angelova. Anthropological characteristic of the contemporary population from the Thessally region (Greece) in respect of the anthropological traits. – Annuaire de L′ Universite de Sofia "St. Kl.Ohridski", Faculte de Biologie, Livre 1 – Zoologie, No 93-94, 2003, 99-106.
2. Beckman, L. R. Elston. Data on bilateral variation in man: handedness, hand clasping and arm folding in Swedes. – Human Biol., **34**, 1962, 99-103.
3. Boev, P., V. Todorov. Hand clasping bei den Bulgaren. – Anthropologie, **11**, 1973, No 1, 2, 91-93.
4. Collins, E. The concept of relative limb dominance – Human Biol., **33**, 1961, 293-319.
5. Dahlberg, G. Twin Births and Twins from a Hereditary Point of View. Stockholm, Bokforlags A. B. Tidens Tryckeri, 1926.
6. Filcheva, Zl. Functional asymmetry of the upper limbs in Bulgarians from North Bulgaria – Acta Morphol. et Anthropol., **8**, 2003, 115-121.
7. Freire-Maia, N., A. Quelce-Salgado, A. Freire-Maia. Hand clasping in diffrent ethnic groups. – Human Biol., **30**, 1958, 281-291.
8. Freire-Maia, A., N. Freire-Maia, A. Quelce-Salgado. Genetic analysis in Russian immigrants. – Am. J. Phys. Anthropol., **18**, 1960, 235-240.
9. Freire-Maia, A., J. de Almeida. Hand clasping and arm folding among African Negroes. - Human Biol., **38**, 1966, 175-179.
10. Karev, G. B. Arm folding, hand clasping and dermatoglyphic asymmetry in Bulgarians. – Anthrop. Anz., **51**, 1993, No 1, 69-76.
11. Kawabe, M. A study on the mode of clasping the hands. – Trans. Sapporo Nat. Hist. Soc., **18**, 1949, 49-52.
12. Kobyliansky, E., S. Micle, B. Arensburg. Handedness, hand clasping and arm folding in Israeli males. – Annals of Human Biol., **5**, 1978, 247-251.
13. Lai, L. Y., R. J. Walsh. The patterns of hand clasping in different ethnic groups. – Human Biol., **37**, 1965, 312-319.
14. Leguebe, A. Hand clasping: Étude anthropologique et genetique. – Bull. Soc. Roy. Belge Anthrop. Prehist., **78**, 1967, 81-107.
15. Lianbin, Z., A. Zhiyi, W. Jiying, L. Shunhua, H. Zaizhu. Study on potical type, palmar and plantar digital formulae, hand clasping, arm folding, handedness, leg folding and stride type in the Daur population, China. – Anthrop. Anz., **57**, 1999, No 4, 361-369.
16. Lourie, J. A. Hand clasping and arm folding among Middle Eastern Jews in Israel. – Human Biol., **44**, 1972, 329-334.
17. Lutz, F. E. The inheritance of the manner of clasping the hands. – Am. Nat., **42**, 1908, 195-196.
18. Pons, J. Hand clasping (Spanish data). – Ann. Hum. Genet., **25**, 1961, 141-144.
19. Reiß, M. Armeverschranken — eine Übersicht. – Anthrop. Anz., **56**, 1998, No 2, 163-178.
20. Reiss, M. The genetics of hand-clasping — a review and a familial study. – Annals of Human Biol., **26**, 1998, No 1, 49-62.
21. Reiss, M. Genetic associations between lateral signs. –Anthrop. Anz., **57**, 1999, No 1, 61-68.
22. Reiß, M. Handefalten - eine Übersicht - Anthrop. Anz., **57**, 1999, No 2, 165-184.
23. Rhoads, J., A. Damon. Some genetic traits in Solomon Island population. II. Hand clasping, arm folding and handedness. – Am. J. Phys. Anthropol., **39**, 1973, 179-184.
24. Sarna, J., A. Siniarska, A. Wokroj. Hand clasping, arm and leg folding in populations of Poland and other countries. – Coll. Antropol., **4**, 1980, No 1, 37-44.
25. Wiener, A. S. Observations on the manner of clasping the hands and folding the arms. – Am. Nat., **66**, 1932, 365-370.
26. Yamaura, A. On some hereditary characters in the Japanese race including the Tyosenese (Coreans). – Jap. J. Genetics, **16**, 1940, 1-9.
27. Мутафов, Ст. Психо-физически особености на децата с аномалии. С., Медицина и физкултура, 1981.

Institute of Experimental Morphology and Anthropology with Museum
Bulgarian Anatomical Society

Acta morphologica et anthropologica, 12
Sofia • 2007

Correlations Between Basic Anthropological Features in Fullterm and Preterm Newborn Infants

I. Yankova

Institute of Experimental Morphology and Anthropology with Museum, Bulgarian Academy of Sciences, Sofia

The aim of the study is to assess comparatively the degree and direction of correlations between anthropometrical features in fullterm and preterm newborn infants. During 2001 and 2003 a total of 219 healthy fullterm and 60 conditionally healthy preterm newborns in Sofia are investigated anthropometrically. In this paper, the relationships among 17 from 42 directly measured anthropometrical features are analyzed. The relationships' degree is estimated according to correlation coefficient's values, while direction — according to their sign. The generalized results from comparative evaluation of correlation structures in the investigated two groups of newborn show that the regular dependencies between anthropometrical features, which ensure optimum control over the impending metrical growth changes in fullterm infants, are already formed after birth. The formation of these dependencies in the preterm newborns is still not completed at their birth.

Key words: anthropometrical features, fullterm newborns, preterm newborns, correlation's degree, correlation's direction.

Introduction

The detailed characterization of human physical development during the prenatal and postnatal period is a basis for estimation of norm and its deviations along the specific for every ontogenetic stage processes of the organism's growth and development [1, 5].

The harmonious body development and mainly the proportionality between body dimensions in postnatal ontogenesis are based on dependences between different anthropometrical features ensuring optimum control of their growth and development. The last weeks of intrauterine growth and the period immediately after birth are most important for the formation of these dependencies. The correlations between investigated anthropometrical features are discussed rarely in the publications about physical development of newborns [2, 3, 6, 7].

The aim of the present study is to assess comparatively the degree and direction of correlations between different anthropometrical features in fullterm and preterm newborn infants, with a view to enrich the knowledge of physical development specificity in both groups of newborns.

Material and Methods

A total of 219 healthy fullterm babies (38-42 g.w.) — 110 boys and 109 girls and 60 conditionally healthy newborns (30 boys and 30 girls) of 1st grade prematurity defined by a body weight (between 2500 g and 2000 g) and morphological maturation of 34 - 37 g. w. are studied anthropometrically. The investigation was carried out between 2001 and 2003 in the section of Neonatology at 2nd SOGHAT "Sheynovo" — Sofia.

In this paper, the correlations among 17 from 42 directly measured anthropometrical features are analyzed for boys and girls from both newborns' groups. The relationships' degree is estimated by correlation coefficients' values, according to the scale proposed by K a l i n o v [4]: "very low" correlation ($r \leq 0.29$), "low" ($r = 0.30 \div 0.49$), "moderate" ($r = 0.50 \div 0.69$) and "high" and "very high" correlation ($r \geq 0.70$). The significance of correlation coefficients is reported at $P < 0.01$ and $P < 0.05$.

Results

The existence, direction and degree of correlations between anthropometrical features in boys and girls from both newborns' groups are presented in eight correlation matrices (Tables 1-8). The significance of dependencies between the studied features is given on tables 1, 3, 5, 7. Tables 2, 4, 6 and 8 demonstrate the degree and direction of the significant correlations between each couple of features, as the lower coefficients than 0.30 are not marked.

Significance of the correlations

The statistical significant coefficients between couples of anthropometrical features are a basis for the assessment of biological information concerning the specificity of awaited relationships between them.

Almost all correlation coefficients of fullterm boys and girls are statistically significant (Tables 1, 3). That's why the relationships between anthropometrical features of fullterm newborns are already formed ensuring their independent development.

The correlation structure of the significant dependencies in preterm newborns is quite different. The statistically significant correlations in both genders are relatively rare (Tables 5, 7): in boys 22.22 % or 34 from a total of 153 correlations and in girls 18.95 % or 29 from a total of 153.

Marked sexual differences in the structure of significant correlations in both groups of newborns are not established but differences between groups are very well expressed.

Degree of the correlations

At this stage of the analysis will be estimated the correlations' degree between four anthropometric features, considered as the most important and informative characteristics of newborns' physical development, and other studied features (Tables 2, 4, 6 and 8).

The **stature** in fullterm newborns correlates positively by high significance ($P < 0.01$) with all anthropometric features included in the correlation matrix and correlations' strength is of "low" to "high" degree. The bigger stature in both genders goes along with bigger body weight (correlation of "high" degree), longer torso and extremities, and bigger bitrohanterial breadth and body and extremities circumferences (correlation of "moderate" degree). In fullterm boys the correlation ("moderate" degree) of stature with biacromial and bicristal diameters and of stature with body mass index (BMI) is stronger, compared with girls ("low" degree).

Table 1. Correlation structure of the dependences between investigated features in fullterm boys - graphical image

Insignificant coefficients of correlation
Significant coefficients of correlation in $P < 0.05$
Significant coefficients of correlation in $P < 0.01$

Features	Head breadth	Head circumf.	Stature	Torso length	Biacr. breadth	Chest breadth	Bicr. breadth	Bisp. breadth	Bitroh. breadth	Chest circumf.	Upper extr. length	Lower extr. length	Arm circumf.	Thigh circumf.	Body weight	BMI	Sum of 6SF
Head breadth																	
Head circumf.																	
Stature																	
Torso length																	
Biacr.breadth																	
Chest breadth																	
Bicr.breadth																	
Bisp.breadth																	
Bitroh.breadth																	
Chest circumf.																	
Upper extr. length																	
Lower extr. length																	
Arm circumf.																	
Thigh circumf.																	
Body weight																	
BMI																	
Sum of 6SF																	

T a b l e 2. Correlation structure of the dependences' degree between investigated features in fullterm boys

Features	Head breadth	Head circumf.	Stature	Torso length	Biacr. breadth	Chest breadth	Bicr. breadth	Bisp. breadth	Bitroh. breadth	Chest circumf.	Upper extr. length	Lower extr. length	Arm circumf.	Thigh circumf.	Body weight	BMI	Sum of 6SF
Head breadth	1	**0.71**	0.49	0.34	0.34	0.37	0.39	0.39	0.32	0.43	0.33	0.34	0.42	0.41	*0.59*	0.48	0.34
Head circumf.	**0.71**	1	*0.51*	0.44	0.47	0.48	0.48	0.44	0.46	*0.57*	0.42	0.49	0.49	0.45	**0.71**	*0.65*	0.44
Stature	0.49	*0.51*	1	*0.60*	*0.50*	0.49	*0.55*	0.48	*0.59*	*0.69*	*0.64*	*0.59*	*0.55*	*0.60*	**0.78**	0.37	0.49
Torso length	0.34	0.44	*0.60*	1	0.41	0.43	*0.55*	0.39	*0.58*	*0.59*	0.42	0.46	*0.52*	0.49	**0.70**	*0.57*	0.43
Biacr.breadth	0.34	0.47	*0.50*	0.41	1	*0.62*	*0.68*	**0.75**	*0.56*	*0.59*	0.37	*0.54*	*0.53*	*0.57*	*0.64*	*0.57*	0.48
Chest breadth	0.37	0.48	0.49	0.43	*0.62*	1	*0.59*	0.48	*0.52*	**0.71**	0.37	0.36	*0.59*	*0.66*	**0.72**	*0.68*	*0.66*
Bicr.breadth	0.39	0.48	*0.55*	*0.55*	*0.68*	*0.59*	1	**0.80**	**0.70**	*0.68*	0.46	*0.52*	*0.61*	*0.68*	**0.78**	**0.72**	*0.68*
Bisp.breadth	0.39	0.44	0.48	0.39	**0.75**	0.48	**0.80**	1	*0.54*	*0.54*	0.31	*0.53*	*0.51*	*0.56*	*0.62*	*0.54*	0.47
Bitroh.breadth	0.32	0.46	*0.59*	*0.58*	*0.56*	*0.52*	**0.70**	*0.54*	1	*0.64*	*0.50*	*0.58*	*0.59*	*0.62*	**0.75**	*0.64*	*0.57*
Chest circumf.	0.43	*0.57*	*0.69*	*0.59*	*0.59*	**0.71**	*0.68*	*0.54*	*0.64*	1	*0.55*	*0.51*	*0.69*	**0.77**	**0.88**	**0.76**	*0.62*
Upper extr. length	0.33	0.42	*0.64*	0.42	0.37	0.37	0.46	0.31	*0.50*	*0.55*	1	*0.57*	0.39	0.44	*0.60*	0.39	0.36
Lower extr. length	0.34	0.49	*0.59*	0.46	*0.54*	0.36	*0.52*	*0.53*	*0.58*	*0.51*	*0.57*	1	0.41	0.44	*0.59*	0.42	0.29
Arm circumf.	0.42	0.49	*0.55*	*0.52*	*0.53*	*0.59*	*0.61*	*0.51*	*0.59*	*0.69*	0.39	0.41	1	**0.81**	**0.78**	**0.71**	*0.68*
Thigh circumf.	0.41	0.45	*0.60*	*0.50*	*0.57*	*0.66*	*0.68*	*0.56*	*0.62*	**0.77**	0.44	0.44	**0.81**	1	**0.81**	**0.72**	**0.74**
Body weight	*0.59*	**0.71**	**0.78**	**0.70**	*0.64*	**0.72**	**0.78**	*0.62*	**0.75**	**0.88**	*0.60*	*0.59*	**0.78**	**0.81**	1	**0.87**	**0.75**
BMI	0.48	*0.65*	0.37	*0.57*	*0.57*	*0.68*	**0.72**	*0.54*	*0.64*	**0.76**	0.39	0.42	**0.71**	**0.72**	**0.87**	1	**0.71**
Sum of 6SF	0.34	0.44	0.49	0.43	0.48	*0.66*	*0.66*	0.47	*0.57*	*0.62*	0.36	0.29	*0.68*	**0.74**	**0.75**	**0.71**	1

Table 3. Correlation structure of the dependences between investigated features in fullterm girls - graphical image

Insignificant coefficients of correlation
Significant coefficients of correlation in $P < 0.05$
Significant coefficients of correlation in $P < 0.01$

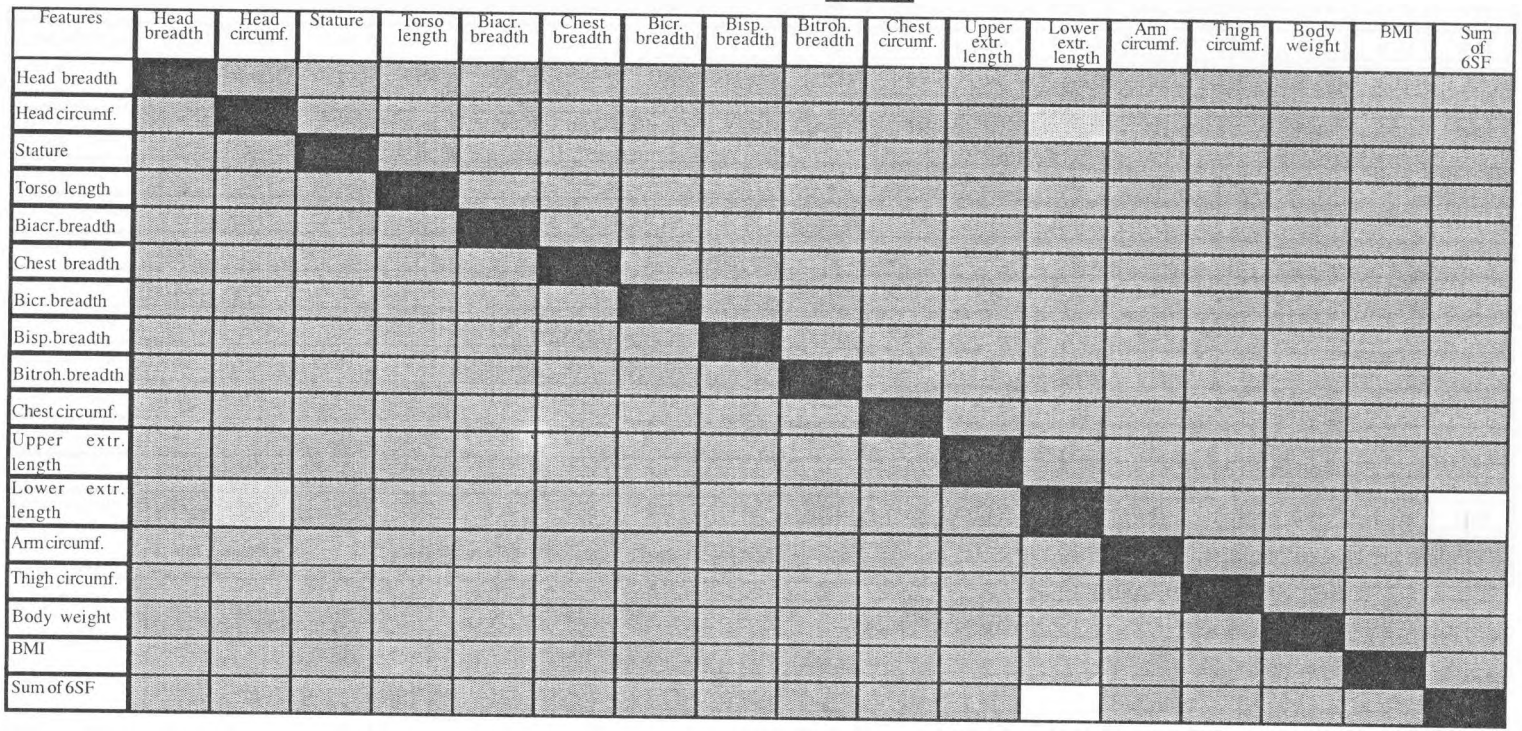

T a b l e 4. Correlation structure of the dependences' degree between investigated features in fullterm girls

Features	Head breadth	Head circumf.	Stature	Torso length	Biacr. breadth	Chest breadth	Bicr. breadth	Bisp. breadth	Bitroh. breadth	Chest circumf.	Upper extr. length	Lower extr. length	Arm circumf.	Thigh circumf.	Body weight	BMI	Sum of 6SF
Head breadth	1	0.75	0.48	0.38	0.30	0.38	0.41	0.29	0.42	0.53	0.37	0.34	0.42	0.48	0.65	0.55	0.44
Head circumf.	0.75	1	0.53	0.40	0.31	0.45	0.41	0.34	0.41	0.57	0.35	0.25	0.50	0.47	0.67	0.55	0.51
Stature	0.48	0.53	1	0.60	0.38	0.43	0.47	0.43	0.54	0.63	0.59	0.50	0.56	0.54	0.76	0.28	0.42
Torso length	0.38	0.40	0.60	1	0.35	0.43	0.48	0.44	0.58	0.51	0.49	0.38	0.48	0.50	0.66	0.47	0.41
Biacr.breadth	0.30	0.31	0.38	0.35	1	0.54	0.61	0.63	0.45	0.53	0.45	0.48	0.47	0.53	0.57	0.54	0.38
Chest breadth	0.38	0.45	0.43	0.43	0.54	1	0.57	0.53	0.57	0.70	0.39	0.32	0.60	0.52	0.62	0.55	0.55
Bicr.breadth	0.41	0.41	0.47	0.48	0.61	0.57	1	0.83	0.65	0.71	0.39	0.47	0.66	0.69	0.75	0.71	0.53
Bisp.breadth	0.29	0.34	0.43	0.44	0.63	0.53	0.83	1	0.59	0.65	0.38	0.50	0.61	0.65	0.68	0.64	0.40
Bitroh.breadth	0.42	0.41	0.54	0.58	0.45	0.57	0.65	0.59	1	0.70	0.50	0.45	0.63	0.69	0.76	0.67	0.52
Chest circumf.	0.53	0.57	0.63	0.51	0.53	0.70	0.71	0.65	0.70	1	0.54	0.47	0.76	0.76	0.88	0.77	0.62
Upper extr. length	0.37	0.35	0.59	0.49	0.45	0.39	0.39	0.38	0.50	0.54	1	0.64	0.36	0.42	0.60	0.39	0.30
Lower extr. length	0.34	0.25	0.50	0.38	0.48	0.32	0.47	0.50	0.45	0.47	0.64	1	0.37	0.43	0.52	0.35	
Arm circumf.	0.42	0.50	0.56	0.48	0.47	0.60	0.66	0.61	0.63	0.76	0.36	0.37	1	0.85	0.82	0.73	0.71
Thigh circumf.	0.48	0.47	0.54	0.50	0.53	0.52	0.69	0.65	0.69	0.76	0.42	0.43	0.85	1	0.84	0.78	0.64
Body weight	0.65	0.67	0.76	0.66	0.57	0.62	0.75	0.68	0.76	0.88	0.60	0.52	0.82	0.84	1	0.83	0.65
BMI	0.55	0.55	0.28	0.47	0.54	0.55	0.71	0.64	0.67	0.77	0.39	0.35	0.73	0.78	0.83	1	0.60
Sum of 6SF	0.44	0.51	0.42	0.41	0.38	0.55	0.53	0.40	0.52	0.62	0.30		0.71	0.64	0.65	0.60	1

Table 5. Correlation structure of the dependences between investigated features in preterm boys - graphical image

Insignificant coefficients of correlation
Significant coefficients of correlation in $P < 0.05$
Significant coefficients of correlation in $P < 0.01$

Features	Head breadth	Head circumf.	Stature	Torso length	Biacr. breadth	Chest breadth	Bicr. breadth	Bisp. breadth	Bitroh. breadth	Chest circumf.	Upper extr. length	Lower extr. length	Arm circumf.	Thigh circumf.	Body weight	BMI	Sum of 6SF
Head breadth																	
Head circumf.																	
Stature																	
Torso length																	
Biacr.breadth																	
Chest breadth																	
Bicr.breadth																	
Bisp.breadth																	
Bitroh.breadth																	
Chest circumf.																	
Upper extr. length																	
Lower extr. length																	
Arm circumf.																	
Thigh circumf.																	
Body weight																	
BMI																	
Sum of 6SF																	

Table 6. Correlation structure of the dependences' degree between investigated features in preterm boys

Features	Head breadth	Head circumf.	Stature	Torso length	Biacr. breadth	Chest breadth	Bicr. breadth	Bisp. breadth	Bitroh. breadth	Chest circumf.	Upper extr. length	Lower extr. length	Arm circumf.	Thigh circumf.	Body weight	BMI	Sum of 6SF
Head breadth	1	*0.55*													0.48		
Head circumf.	*0.55*	1	0.44							0.38	0.42	0.47			*0.64*		
Stature		0.44	1	*0.51*						0.43	*0.65*	0.47			0.49	*-0.58*	
Torso length			*0.51*	1							0.41		-0.42				-0.42
Biacr.breadth					1												
Chest breadth						1				0.36			0.40		0.39	0.42	
Bicr.breadth							1	**0.77**	**0.76**							0.41	
Bisp.breadth							**0.77**	1	0.41								
Bitroh.breadth							**0.76**	0.41	1			*-0.51*				0.37	
Chest circumf.		0.38	0.43			0.36				1					*0.59*		
Upper extr. length		0.42	*0.65*	0.41							1	**0.72**			*0.51*		
Lower extr. length		0.47	0.47						*-0.51*		**0.72**	1					
Arm circumf.				-0.42		0.40							1	*0.65*		0.38	*0.62*
Thigh circumf.													*0.65*	1	0.46		
Body weight	0.48	*0.64*	0.49			0.39				*0.59*	*0.51*			0.46	1	0.42	
BMI			*-0.58*			0.42	0.41		0.37				0.38		0.42	1	
Sum of 6SF				-0.42									*0.62*				1

Table 7. Correlation structure of the dependences between investigated features in preterm girls - graphical image

Insignificant coefficients of correlation
Significant coefficients of correlation in $P < 0.05$
Significant coefficients of correlation in $P < 0.01$

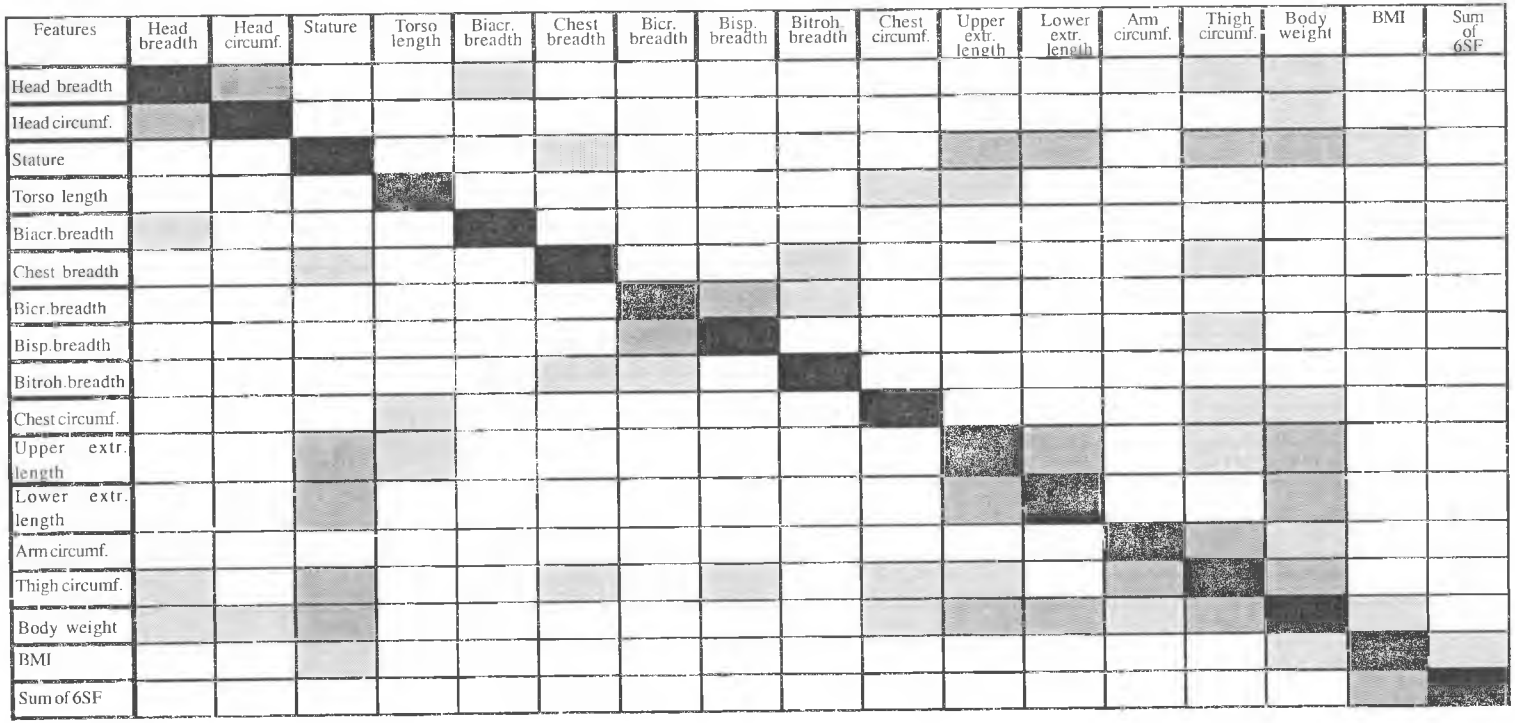

Table 8. Correlation structure of the dependences' degree between investigated features in preterm girls

Features	Head breadth	Head circumf.	Stature	Torso length	Biacr. breadth	Chest breadth	Bicr. breadth	Bisp. breadth	Bitroh. breadth	Chest circumf.	Upper extr. length	Lower extr. length	Arm circumf.	Thigh circumf.	Body weight	BMI	Sum of 6SF
Head breadth	1	*0.62*			0.40									0.45	0.46		
Head circumf.	*0.62*	1													0.40		
Stature			1			0.43					*0.64*	*0.61*		*0.54*	*0.64*	-0.40	
Torso length				1						0.40	0.40						
Biacr.breadth	0.40				1												
Chest breadth			0.43			1			0.43					0.44			
Bicr.breadth							1	**0.84**	0.45								
Bisp.breadth							**0.84**	1						0.37			
Bitroh.breadth						0.43	0.45		1								
Chest circumf.				0.40						1				0.38	0.36		
Upper extr. length			*0.64*	0.40							1	*0.56*		0.41	*0.69*		
Lower extr. length			*0.61*								*0.56*	1			0.48		
Arm circumf.													1	0.47	0.44		
Thigh circumf.	0.45		*0.54*			0.44		0.37		0.38	0.41		0.47	1	**0.75**		
Body weight	0.46	0.40	*0.64*							0.36	*0.69*	0.48	0.44	**0.75**	1	0.44	
BMI			-0.40												0.44	1	0.47
Sum of 6SF																0.47	1

In preterm newborns, the **stature** correlates significantly with fewer features, as some coefficients of correlation are negative. The stature correlates with body weight by a strength of relationship of "moderate" degree ($r = 0.64$) only in girls. In preterm boys this correlation is at the borderline between "low" and "moderate" degree ($r = 0.49$). The bigger stature in both genders goes along with longer upper extremity, while in the girls also with longer lower extremity and bigger thigh circumference. The stature in boys has relationship of "moderate" degree with torso length ($r = 0.51$).

Body weight is another basic characteristic of individual's physical development, which in fullterm newborn infants correlates significantly and positively with all measured anthropometrical features. Correlations of "high" degree are established for both genders between body weight and stature, torso length, head circumference, chest circumference, extremities' circumference, BMI and the two pelvis diameters — bicristal and bitrohanterial. In boys with higher degree is still the correlation between bigger body weight and thicker subcutaneous fat tissue (SFT). This correlation is of "moderate" degree in girls.

The dependences of "moderate" degree have lower values of correlation coefficients in girls than in boys. In the fullterm newborns from both genders, the body weight correlates by "moderate" degree with the sizes of head, with biacromial and bispinal diameters, chest breadth, as well as with the sizes of upper and lower extremities.

In preterm newborns the established relationships between **body weight** and other features are lower, and the correlations' degree is mostly "low" and rarely "moderate", than in fullterm babies. Correlation of "high" degree exists only between body weight and thigh circumference in girls ($r = 0.75$). In both genders body weight correlates by "moderate" degree with upper extremity length. In preterm boys, body weight correlates by "moderate" degree with head and chest circumferences also, and in girls — with stature. The correlations between body weight and all the rest features are of "low" degree.

The other two basic features **head circumference and chest circumference** for the assessment of newborns' physical development in fullterm newborns correlate also with all the measured metrical features.

The bigger **head circumference** in both genders is related by "high" degree with the bigger head breadth. Correlation of "high" degree in boys is observed still with body weight ($r = 0.71$), while in girls the strength of this dependence is of "moderate" degree ($r = 0.67$). In both genders the head circumference correlates by strength of "moderate" degree with stature, chest circumference and BMI, and in girls with arm circumference and total quantity of SFT, too. The strength of relationships between head circumference and torso length, body diameters and extremities' circumference is of "low" degree.

In the correlation matrices of preterm newborns are observed considerably less number of significant correlations being only two in girls.

In contrast to fullterm babies, the strength of relationship between **head circumference** and its breadth for preterm is of "moderate" degree. The correlation with body weight ($r = 0.64$) in boys is of "moderate" degree too, while in girls the strength of this relationship is of "low" degree ($r = 0.40$). In preterm boys the head circumference correlates with stature, chest circumference and lengths of upper and lower extremities too, and the strength of relationships is of "low" degree.

The **chest circumference** in fullterm babies correlates positively with the anthropometrical features included in correlation matrices, as the coefficients are predominantly of a "moderate" degree. The bigger chest circumference in both genders goes along with bigger chest breadth, circumferences of extremities, body weight, BMI and SFT thickness ("high" correlation), as the correlation with body weight ($r = 0.88$) is highest. In girls the relationships of "high" degree exist with bicristal and bitrohanterial diameters also, while in boys these correlations are of "moderate" degree. The chest circumference size in fullterm newborns for both genders is more weakly related ("moderate" correlation) to the

sizes of stature, torso length, and upper extremity's length, head circumference, biacromial and bispinal diameters. Except the described dependences, in fullterm boys correlations of "moderate" degree of chest circumference with lower extremity's length and arm circumference are observed also. In girls the chest circumference correlates with same strength with head breadth, as well.

In preterm newborns between **chest circumference** and other anthropometrical features few significant correlations are established, and they are mainly of "low" degree. Only the relationship between chest circumference and body weight in girls is of "moderate" degree ($r = 0.59$), while in boys it is of "low" degree ($r = 0.36$).

In fullterm newborns the relationships between the rests anthropometrical features are positive having mainly "moderate" degree, while in preterm babies they are predominately "low" and negative correlation coefficients are established. For both groups of newborns the correlations between the three pelvis diameters are of "moderate" to "high" degree. In fullterm boys and girls the correlations between pelvis breadth and other metrical features, as well as the correlations between body and extremities circumferences, body weight, BMI and thickness of SFT are of the same degree. This type of dependencies reflects the relationships between body weight and SFT thickness, as well as its accumulation on body and extremities and the increment of their circumferences. In preterm newborns these correlations are mainly of "low" degree. In regard to the thickness of SFT, the significant correlation's coefficients are less. These results show that the formation of relationships between body weight, body and extremities circumferences and SFT thickness in preterm newborns is still not completed, while in fullterm babies these dependencies are already formed.

Discussion

In fullterm newborns from both genders, all relationships between the features are significant, while in preterm babies the significant correlations are about five times rarer. High significance of relationships between head circumference, stature and sitting heigh in fullterm newborns are reported by K a r a p e t r o v [2], and significant correlations between stature and body weight and between head circumferences and chest circumferences are established by D u n d o v a [3].

The correlations between separate couple of features in fullterm babies are very well presented in the three degrees — "low", "moderate" and "high". The tendency to higher coefficients of correlation, although weakly manifested, is observed in boys, than in girls. In this attitude, our results confirm these received by other authors [5]. The preterm newborns have less significant correlations and its degree is lower. The relations of "low" degree are most, these of "moderate" degree are rarer and relationships of "high" degree are single.

The established correlation structures between basic anthropometrical characteristics of physical development and other studied features describe tendencies to mutually related processes of anthropometrical features' growth and development after birth.

In fullterm newborns the body and extremities' lengths correlate by "moderate" strength, as well as between themselves, and with the relevant breadths and circumferences. These relations are a basis for future development of body proportionality. The established values of correlation coefficients between the features mentioned above are close to these described by S e m e r d j i e v a et al. [6] and K a r a p e t r o v [2].

In preterm newborns the body and extremities' lengths correlate between themselves mainly. The relations between lengths, breadths and circumferences, which determine their proportional development, are either missing or very slightly manifested.

The body and extremities' breadths and circumferences in fullterm newborns correlate by "moderate" and "high" strength, as between themselves, so with body weight, with SFT thickness and body nutritional status (BMI).

In preterm newborns the small number of the established significant correlation coefficients about body and extremities' breadths and circumference characterizes mainly the relationships between features of close topical belonging. This result shows that in preterm newborns the formation of relationships between breadths and circumferences and other metrical features is not completed, yet.

Conclusion

The generalized results from the comparative assessment of correlation structures in fullterm and preterm newborn infants allow the following conclusions to be made:

- In fullterm newborns, the regular dependencies between anthropometrical features, which ensure optimum control over the impending metrical growth changes, are already formed at birth. This correlation structure is a basis for future harmonious and proportional body development.
- In preterm babies, the formation of these dependencies ensuring optimum control over the impending metrical growth changes is not completed at their birth, yet.

References

1. Falkner, F., J. M. Tanner. Human Growth (2nd Edition). New York and London, Plenum Press, 1987, 1-537.
2. Karapetrov, Gr. Corrélations entre le périmètre de la tête, la stature et la taille assis pendunt la croissance. – Bull. De l´Assoc. des Anatomistes, 54e Congrès, Sofia, № 146, 536-538.
3. Дундова, Р. Лонгитудинално проучване растежа на деца от 0 до 3-годишна възраст (канд. дис.). 1978, 1-158.
4. Калинов, К. Статистически методи в поведенческите и социалните науки. София, НБУ, 2001, 79 с.
5. Резлер, Х., Х. Эггерс, И. Кюльц, Е. Курт, К. Вагнер. Критерии и нормативы нормального соматического развития от периода новорожденности до окончания периода созревания. – В: Проблемы постнатального соматопсихического развития. М., Медицина, 1974, 49-107.
6. Семерджиева, Р., Й. Венедикова, П. Божиков. Физическо развитие на деца до 3-годишна възраст в България. – Информационен бюлетин, 1, 1972, 1-195.
7. Цировски, М. Медико-антропологично изследване на деца от периодите кърмачество и ранно детство (канд. дис.). 1986, 1-298.

Institute of Experimental Morphology and Anthropology with Museum
Bulgarian Anatomical Society

Acta morphologica et anthropologica, 12
Sofia • 2007

Subcutaneous Fat Tissue in Children Aged from 3 till 6 Years (preliminary report)

Y. Zhecheva

Institute of Experimental Morphology and Anthropology with Museum, Bulgarian Academy of Sciences, Sofia

The development of Subcutaneous Fat Tissue (SFT) is morphological characterization with high ecological sensitivity and specificities connected with age and sex. The aim of the present work is to characterize the age and sexual differences of subcutaneous fat tissue thickness and its distribution in children aged from 3 to 6 years. The data presented are part of a detailed anthropological investigation started in June 2004 in Sofia kindergartens. Data about 440 children (210 boys and 230 girls) at 3, 4, 5 and 6 years are included. The thickness of 9 standard skinfolds and the total quantity of SFT are analyzed. The total quantity of SFT in all the examined ages is larger in girls. The age differences show that SFT accumulation happens basically during the periods 3-4 and 5-6 years. Sexual differences of total quantity SFT are biggest in 5 years old children and smallest at the age of 3.

Key words: subcutaneous fat tissue, skinfolds, sexual differences, age differences, children.

Introduction

From birth till adulthood in the anthropometrical characterization occur great changes, which accompany the morphological maturation of human body [3]. The changes themselves are connected with individual's sex and his physiological status. The Subcutaneous Fat Tissue (SFT) thickness is an important morphological characterization for the assessment of physical development in children. It possesses great eco-sensitivity and age-sexual specificity, and gives valuable medico-anthropological information about physical and health status of the growing up organism [2, 4].

The aim of the present work is to characterize the age and sexual differences of subcutaneous fat tissue thickness and its distribution in children aged from 3 to 6 years.

Material and Methods

The data presented are part from a detailed anthropological investigation started in June 2004 and carried out till now in kindergartens in Sofia City. The report includes data about 440 children (210 boys and 230 girls) at the age of 3, 4, 5 and 6 years.

The thickness of 9 standard skinfolds (in mm) and the total quantity SFT presented by the 9 skinfolds' sum are analyzed.

The skinfolds are measured with Holtain skinfold caliper, by the WHO standardized method approved in 1987 and published in 1989 [1].

The sexual differences are evaluated quantitatively by the Index of Sexual Differences (ISD), expressed in Index Units (IU) and computed by the formula:

$$ISD = 2 \times [(\bar{x}\,\text{boys} - \bar{x}\,\text{girls}) \times 100] / (\bar{x}\,\text{boys} + \bar{x}\,\text{girls}).$$

The zero ISD value shows absence of sexual differences. The positive values point out priority for boys and the negative — priority for girls.

The metrical data are statistically computed and the established differences are assessed by the t-test of Student at $P<0.05$.

Results

The statistical data about each skinfold on body and extremities and the sexual differences and their reliability are presented in Tables 1, 2, 3 and Figs. 1, 2, 3; while about the sum of 9 skinfolds in Tables 1, 2, 3 and Fig. 4.

Subscapular skinfold. The subscapular skinfold thickness concerning the 3 years old children is 5.29 mm for boys and 5.23 mm for girls. It increases up to 5.61 mm in the 6-year-old boys and up to 6.43 mm in the 6-year-old girls. The inter-age comparison shows that the changes of SFT thickness on back during 3-6 years are similar for both sexes. Throughout the periods 3-4 years and 5-6 years the subscapular skinfold increases for both sexes more tangible in girls, throughout the period 4-5 years it remains nearly the same for boys and girls and even a slightly decrement have been observed for both sexes. The sexual comparisons indicate almost equal SFT thickness on back for both sexes at 3 years of age but girls have always thicker subscapular skinfold from 4 till 6 years of age. The ISD data pointed out that the sexual differences increase in the ages, being 1.14 IU at 3 years (little priority of boys over girls) and it rises already to 13.62 IU at 6 years — priority of girls over boys. The sexual differences are not statistically significant in any of the studied age groups.

X-th rib skinfold. The X-th rib skinfold thickness is nearly equal for both sexes at 3 years of age, being insignificantly thicker in boys (boys — 4.12 mm, girls — 3.93 mm). There are small changes of the X-th rib skinfold in the ages for both sexes that are more strongly expressed in girls. The skinfold thickness increases in boys, although slightly, during the entire studied period. The accumulation of SFT on chest is more clearly displayed in girls throughout the periods 3-4 and 5-6-years, compared to boys for the same periods. In girls the SFT thickness decreases between the 4th and 5th year, at the age of 5 boys and girls have equal skinfolds, and girls at 6 have already thicker X-th rib skinfold than boys (boys — 4.45 mm, girls — 5.12 mm). Most intensive is the accumulation of SFT on this area in boys between 4 and 5 years, and in girls — between 5 and 6 years.

The sexual differences assessed by ISD data are smallest, practically missing, at 5 years of age (0.69 IU) and biggest with priority for girls at 6 years of age (–14.22 IU). The differences are not statistically significant.

Abdomen skinfold and suprailiac skinfold. The SFT quantity on abdomen area is determined by the abdomen and suprailiac skinfolds. At 3 years of age they are practically equal for both sexes: in boys respectively 6.81 mm and 3.77 mm, and in girls respectively

Table 1. Data about skinfolds' thickness in boys

Age	*n*	Subscapular		X-th Rib		Suprailiac		Abdominal		Triceps		Biceps		Forearm		Thigh		Calf		Sum of
		$\bar{x}$	SD	$\bar{x}$	SD	$\bar{x}$	SD	$\bar{x}$	SD	$\bar{x}$	SD	$\bar{x}$	SD	$\bar{x}$	SD	$\bar{x}$	SD	$\bar{x}$	SD	9 SF
3	44	5.29	1.16	4.12	0.86	3.77	0.89	6.81	2.20	10.03	2.36	4.87	1.10	5.99	1.17	10.25	2.60	9.22	2.26	60.35
4	62	5.39	1.92	4.16	1.31	4.07	2.00	7.31	3.32	9.91	2.84	4.76	1.50	5.62	1.13	10.88	4.58	9.26	3.52	61.36
5	59	5.20	2.72	4.35	2.97	3.75	1.34	6.78	2.84	9.68	2.52	4.41	1.04	5.04	0.79	10.42	4.02	8.94	2.72	58.57
6	45	5.61	2.85	4.44	2.23	4.41	2.32	8.17	4.74	9.90	3.14	4.67	1.84	5.06	1.13	11.77	4.91	9.60	3.08	63.63

Table 2. Data about skinfolds' thickness in girls

Age	*n*	Subscapular		X-th Rib		Suprailiac		Abdominal		Triceps		Biceps		Forearm		Thigh		Calf		Sum of
		x	SD	x	SD	x	SD	x	SD	x	SD	x	SD	$\bar{x}$	SD	x	SD	x	SD	9 SF
3	48	5.23	1.16	3.93	0.91	3.89	1.01	6.82	2.16	10.35	1.96	4.74	1.15	6.19	1.26	11.3	2.75	10.08	2.25	62.53
4	69	5.90	1.70	4.42	1.23	4.78	1.82	8.13	3.00	11.42	2.80	5.14	1.27	5.89	1.24	13.41	4.50	11.15	3.46	70.24
5	70	5.70	2.02	4.32	1.12	4.71	1.64	8.44	3.34	10.94	2.58	5.02	1.32	5.43	1.30	13.25	4.04	10.97	2.84	68.78
6	43	6.43	3.66	5.12	3.13	5.34	3.12	9.10	4.49	11.12	3.38	5.46	2.06	5.24	1.48	14.76	6.00	10.91	3.64	73.48

Table 3. Sexual differences according to the ISD data and the statistical significance by Student's t-test

Age	Subscapular skin fold		X-th Rib skin fold		Suprailiac skin fold		Abdominal skin fold		Triceps skin fold		Biceps skin fold		Forearm skin fold		Thigh skin fold		Calf skin fold		Sum of 9 SF
	ISD	t-test	ISD	t-test	ISD	t-test	ISD	t-test	ISD	t-test	ISD	t-test	ISD	t-test	ISD	t-test	ISD	t-test	ISD
3	1.14	0.24	4.72	1.04	-3.13	-0.62	-0.15	-0.03	-3.14	-0.71	2.70	0.56	-3.28	-0.79	-9.74	-1.88	-8.91	-1.83	-3.55
4	-9.03	-1.62	-6.06	-1.17	-16.04	-2.12*	-10.62	-1.50	-14.16	-3.08*	-7.68	-1.61	-4.69	-1.30	-20.83	-3.19*	-18.52	-3.09*	-13.50
5	-9.17	-1.19	0.69	0.09	-22.70	-3.58*	-21.81	-3.01*	-12.22	-2.79*	-12.94	-2.88*	-7.45	-2.02*	-23.91	-3.98*	-20.39	-4.13*	-16.03
6	-13.62	-1.17	-14.22	-1.19	-19.08	-1.58	-10.77	-0.95	-11.61	-1.76	-15.60	-1.92	-3.50	-0.64	-22.54	-2.56*	-12.77	-1.82	-14.37

* Statistically significant differences ($P< 0.05$)

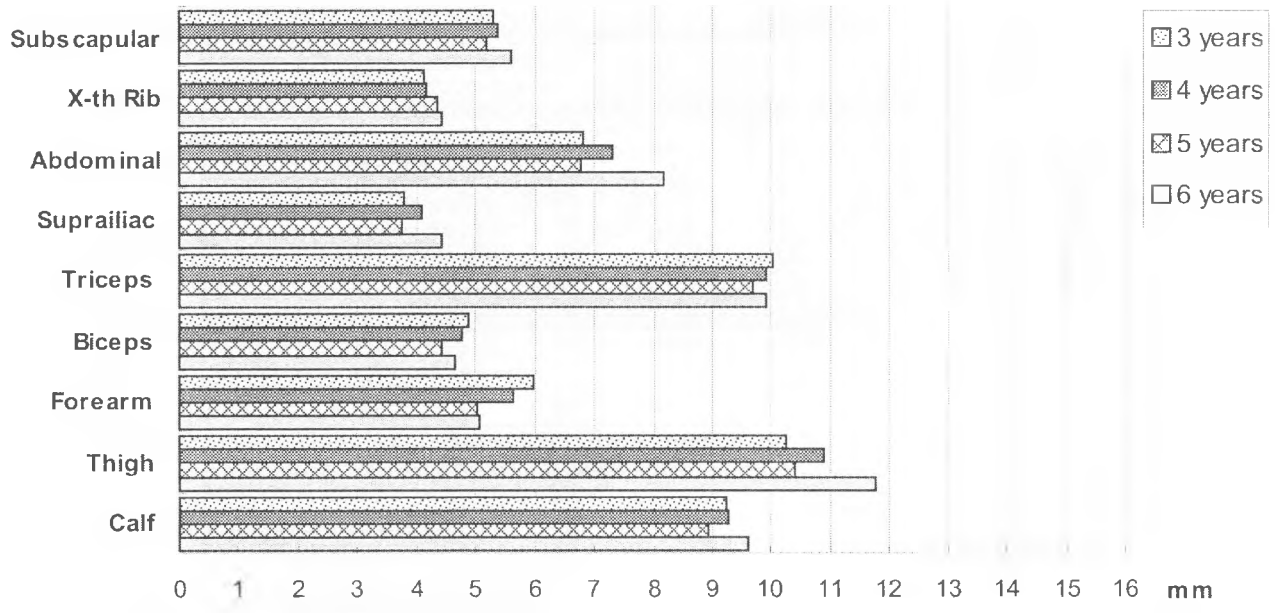

Fig. 1. Data about skinfolds thickness in boys

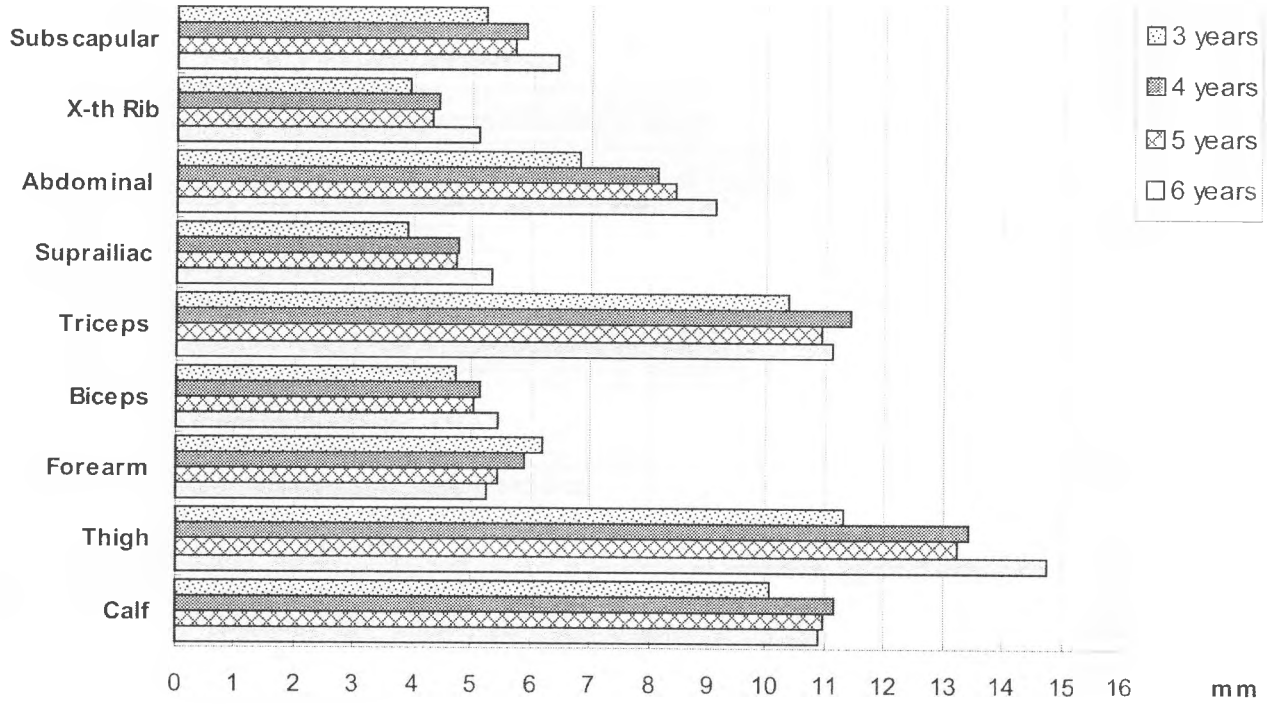

Fig. 2. Data about skinfolds thickness in girls

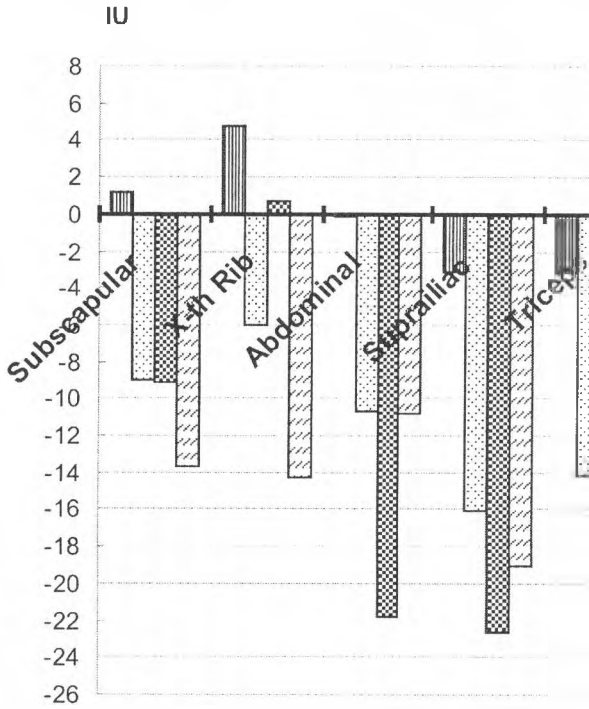

Fig. 3. Intersexual differences according to the ISD data

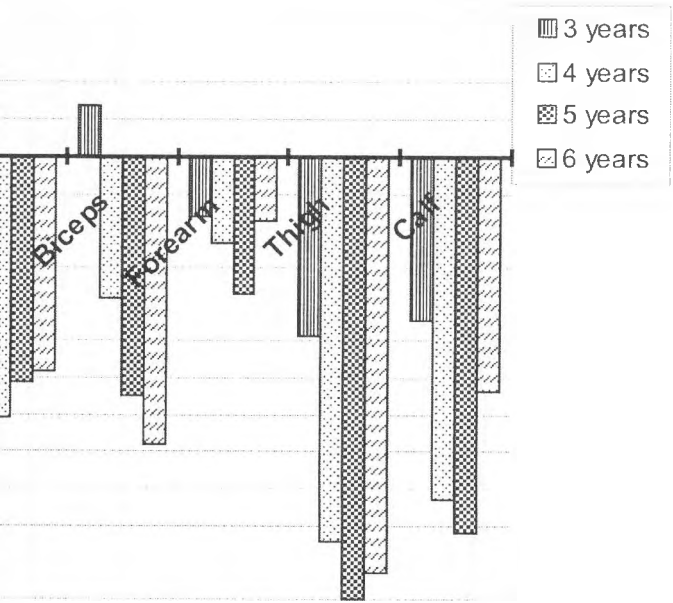
3 years
4 years
5 years
6 years
Biceps
Forearm
Thigh
Calf

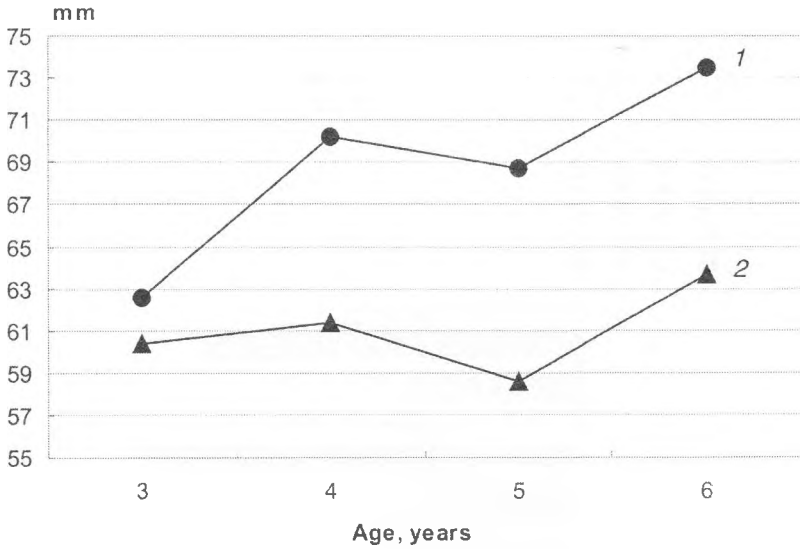

Fig. 4. Sum of the measured 9 skinfolds thickness
1 — girls; *2* — boys

6.82 mm and 3.89 mm. For boys at 6 the abdomen skinfold thickness is 8.17 mm and the suprailiac skinfold — 4.41 mm. Girls at the same age have thicker skinfolds (abdomen skinfold — 9.10 mm, supailiac skinfold — 5.34 mm). The inter-age comparisons show that more intensive is the accumulation of SFT on abdomen area between 5th and 6th year in boys, and between 3rd and 4th year in girls. Throughout the period 4-5 years, the thickness of both skinfolds decreases in boys, in girls the abdomen skinfold increases insignificantly and the suprailiac skinfold remains nearly the same.

The sexual comparison displays nearly equal thickness of both skinfolds for the 3 years old boys and girls. Further till 6 years their mean values are bigger in girls. The ISD data display an increment of sexual differences till 5 years of age when the ISD values are highest (-21.81 IU for abdomen skinfold and —22.70 IU for suprailiac skinfold). Statistically significant are the differences of abdomen skinfold at 5 years and of suprailiac one — at 4 and 5 years. At 6 years of age, the sexual differences are smaller and this decrement is better expressed for the abdomen skinfold.

Triceps skinfold. The SFT thickness on back-arm area (triceps skinfold) in the 3-year-old children have similar values for both sexes — in boys it is 10.03 mm and in girls it is 10.35 mm. The age changes of triceps skinfold are of a different nature for both sexes. For boys in the period 3-5 years it decreases, between 5 and 6 years it slightly increases being 9.90 mm for the 6 years old boys, but it reaches not the value for the 3-year-old boys. For girls the triceps skinfold thickness increases reliably between 3rd and 4th year and achieves its maximum for the entire period under study at the 4-year-old ones (11.42 mm). A decrement of the triceps skinfold is observed during the period 4-5 years. Between the 5th and 6th year the triceps skinfold thickness increases again, at 6 it is 11,12 mm but it is not so high as for the 4-year-old girls.

The sexual differences of triceps skinfold are smallest at 3 and biggest at 4 years, after which they gradually decrease remaining considerably high. Statistically significant are the differences for the 4 and 5-years-old boys and girls. For all studied age groups the SFT thickness on triceps area is higher for girls.

Biceps skinfold. The mean value of SFT on frontal-arm area (biceps skinfold) is 4.87 mm for 3-year-old boys and 4,74 mm for 3-year-old girls. At 6 years of age the biceps skinfold decreases up to 4.67 mm for boys, and vice versa it increases for girls up to 5.46 mm. The age changes of biceps skinfold for boys are similar to the ones of triceps skinfold, and more clearly expressed are: the biceps skinfold decrement between 3rd and 5th year and its increment after the 5th year. The age changes of biceps skinfold for girls are similar to those of triceps skinfold, but it reaches its maximal mean value at 6 years of age.

The ISD data display that sexual differences of biceps skinfold increase in the ages. They are smallest, not statistically significant at the age of 3 (2.70 IU) in favor for boys. After this age till 6, girls have permanently thicker biceps skinfold but statistically significant are only the differences at 5 years of age (—12.94 IU).

The age changes of SFT thickness on arm (biceps skinfold and triceps skinfold) tended to a SFT distribution that is characteristic for adults, i.e. for boys the tendency is commonly toward a decrease of the SFT thickness on arm, while for girls — it is toward an increase.

Forearm skinfold. The SFT quantity on forearm site during the period 3-5 years gradually decreases for both sexes. Throughout the 5th and 6th year forearm skinfold thickness remains the same in boys and it continue to decrease in girls. The forearm skinfold decreases in boys from 5.99 mm to 5.06 mm and in girls — from 6.19 mm to 5.24 mm during the period 3-6 years.

Thicker is the SFT thickness on forearm site in girls about all age groups. ISD data show that sexual differences are smallest at 3 years of age (—3.28 IU) but they are biggest and statistical significant at 5 years of age (—7.45 IU). After this age the sexual differences become smaller and at the age of 6, being —3.50 IU, they are near to the differences for the 3-year-old children.

Thigh skinfold. Highest is the SFT thickness on thigh site (thigh skinfold) for both sexes in all age groups. For the 3-year-old children it is 10.25 mm in boys, and 11.30 mm in girls. At 6 years the thigh skinfold is already 11.77 mm in boys and 14.76 mm in girls. The age changes are nearly the same for both sexes. Throughout the 4th and 5th year the thigh skinfold becomes slightly lower in both sexes and in girls — even unnoticeably. After 5 years of age, the SFT thickness on thigh site increases again for both sexes, more intensively in girls.

The sexual comparison displays that for all investigated ages, girls have larger quantity of SFT on thigh. The sexual differences are smallest at 3 years and only at this age they are not statistically significant (—9.74 IU). Biggest are they in the 5-year-old children (—23.91 IU) and at the age of 6 the sexual differences slightly diminish.

Calf skinfold. The thickness of calf skinfold is 9.22 mm in 3-year-old boys and 10.08 mm in 3-year-old girls. At 6 years of age it is 9.60 mm for boys and 10.91 mm for girls. In the age, the changes of this skinfold thickness are different for both sexes. In boys between 3rd and 4th year the calf skinfold practically didn't modify, between 4th and 5th year it decreases, and between 5th and 6th year it increases noticeably. Girls accumulate larger quantity of subcutaneous fat tissue on calf site in the period 3-4 years and after this age till 6 the calf skinfold thickness slightly decreases.

The intersexual differences assessed quantitatively are smallest for the 3-year-old children (—8.91 IU), as it is for the rest skinfolds, and they increase till the 5th year when the differences are most clearly expressed (—20.39 IU). At 6 years of age the sexual differences become smaller, in view of the fact that the calf skinfold thickness decreases in girls and it increases in boys.

Sum of 9 skinfolds thickness. The total quantity of measured SFT thickness is presented by the sum of 9 skinfolds. The tendency and intensity of age differences are comparatively equal for both sexes. The accumulation of SFT happens basically during the periods 3-4 and 5-6 years, as the total quantity of SFT increases throughout the 3rd and 4th year more noticeably in girls than in boys. Between 4th and 5th year a tangible change in the total quantity of SFT is not observed. The sum of 9 skinfolds for boys aged 6 years is about 5.43% higher compared to this for the boys aged 3 years, and for girls the percentage is three times higher — 17.51%.

The results described could be explained by the first physiological extension, mainly of the extremities, that could be observed during the period 4-6 years (in girls it happens one year earlier) [3].

The results about sexual comparison of the 9 skinfolds thickness sum display that girls have larger quantity of SFT than boys in all studied age groups. The intersexual differences assessed by the ISD data are smallest in the 3-year-old children (—3.55 IU) and biggest — in the 5-year-old ones (—16.03 IU).

Conclusions

1. The total quantity of SFT thickness in the period 3-6 years of age is greater in girls compared to boys.
2. The inter-age differences display that the accumulation of SFT happens mainly in the periods 3-4 and 5-6 years of age in both sexes.
3. The sexual differences of total quantity SFT are biggest at the 5 years old children and smallest at 3 years old ones.

References

1. Measuring Obesity — Classification and Description of Anthropometric Data. Report on a WHO Consultation on the Epidemiology of Obesity. Warsaw, World Health Regional Office for Europe, 1987, 1-22.
2. Nacheva, A., E. Lazarova, L. Yordanova. Development of Subcutaneous Fat Tissue in 7-17 years old schoolchildren from Sofia. – Acta morphologica et anthropologica, 9, 2004, 118-127.
3. Бобев, Др., Е. Генев. Педиатрия. София, 2000.
4. Начева, А., М. Колева, Особености в количеството и разпределението на подкожната мастна тъкан при израснали. – Journal of Anthropology, 2, 1999, 58-67.

Institute of Experimental Morphology and Anthropology with Museum
Bulgarian Anatomical Society

Acta morphologica et anthropologica, 12
Sofia • 2007

Age at Menarche and Somatotype in Young Adults

R. Stoev

Institute of Experimental Morphology and Anthropology with Museum, Bulgarian Academy of Sciences, Sofia

An attempt is made to correlate age at menarche with the somatotype in young adults. Data of 542 university students in Sofia, mean age 22,1 at the investigation (1986) are analysed according the permanent residence place. Somatotype is evaluated after Heath-Carter, age at menarche — by recalled age method. The results show high differences between students from towns (higher mean age at menarche, higher mesomorphy and endomorphy) and cities (lower mean age at menarche, lower mesomorphy and endomorphy). The differences can be traced also in their curves of correlation age at menarche-somatotype. These curves are opposed one to the other. The results set the limits of normal age at menarche in city residents from 11.25 to 14.24 years and show that the connection age at menarche-somatotype is more complicated than usually accepted.

Key words: age at menarche, somatotype, university students, young adult age, city-town differences.

Introduction

The interrelations of sexual maturation and somatotype have been object of various studies [1, 2, 6]. In such studies usually is looked for these relations in adolescence period. In present study an attempt is made to correlate age at menarche with the somatotype in young adults, when the processes of growth, development and maturation are more or less over. The interrelations of age at menarche and somatotype have been traced on the background of the urbanization level.

Material and Methods

For the purpose of this study the individual data of 542 young female students in Sofia universities (mean age 22.1 years in the moment of investigation — spring 1986) are analysed according the permanent residence place. They were near 9 years since their menarche (mean age at menarche 13.2 years). The students were classified according the population and the status of their residence place in 1975 census (the most close to their adolescence). The following groups have been used:

1) villages;
2) small towns (less than 25 thousands);
3) big towns (25 — 100 thousands);
4) cities (above 100 thousands);
5) Sofia — migrants (since it is possible that some of them have reported the place of temporary residence as a place of permanent);
6) Sofia — native born (born in Sofia).

Students' somatotype is evaluated after Heath-Carter's schedule [9, 12]. Data of age at menarche are collected by the recalled age method (retrospective). The crude mean values of the separate somatotype components by age groups have been adjusted by the method of moving average [10].

Results and Discussion

The analysis of the material has found significant differences between the subsamples as in the mean age at menarche (from 12.95 to 13.61 years, $p \leq 0.01$) but also in the separate components of the somatotype (endomorphy from 4.26 to 4.90, $p \leq 0.05$; mesomorphy from 3.46 to 4.40, $p \leq 0{,}001$; ectomorphy from 1.76 to 2.45, $p \leq 0.01$). As the reader can see, these differences are most sharply expressed in the mesomorphy (Table 1, Fig. 1). On the basis of these differences the investigated students can be divided in two major groups — girls from the towns and girls from the cities (including Sofia and the migrants in it). The students from towns show higher mean age at menarche combined with higher mesomorphy and endomorphy (Table 2) — mean somatotype mesomorph-endomorph. The students from cities show lower mean age at menarche combined with lower mesomorphy and endomorphy — mean somatotype mesoendomorph. These significant differences are present also if the somatotype is traced by age at menarche according the residence (Fig. 2). The curves of correlation between age at menarche and somatotype in city and town girls, which have been found, were completely different and opposed one to the other.

Table 1. Age at menarche and somatotype in the investigated students by residence

Residence	*N*		Age at menarche	Somatotype — components			Somatotype
				Endo-morphy	Meso-morphy	Ecto-morphy	
Village	36	M	**12.95**	**4.90**	**4.12**	**1.76**	Mesoendomorph
		SD	1.67	1.70	1.19	1.03	
Small town	59	M	**13.61**	**4.47**	**4.40**	**1.95**	Mesomorph-endomorph
		SD	1.30	1.37	1.08	0.98	
Big town	148	M	**13.35**	**4.55**	**4.52**	**2.18**	Mesomorph-endomorph
		SD	1.42	1.19	1.09	1.13	
City	93	M	**13.04**	**4.40**	**3.46**	**2.20**	Mesoendomorph
		SD	1.26	0.96	0.92	1.15	
Sofia (migrants)	72	M	**12.95**	**4.26**	**3.47**	**2.45**	Mesoendomorph
		SD	1.17	1.39	0.96	1.08	
Sofia (native born)	134	M	**12.97**	**4.54**	**3.52**	**2.28**	Mesoendomorph
		SD	1.25	1.43	1.12	1.18	
Total	542	M	**13.15**	**4.50**	**3.91**	**2.19**	Mesoendomorph
		SD	1.34	1.37	1.15	1.13	

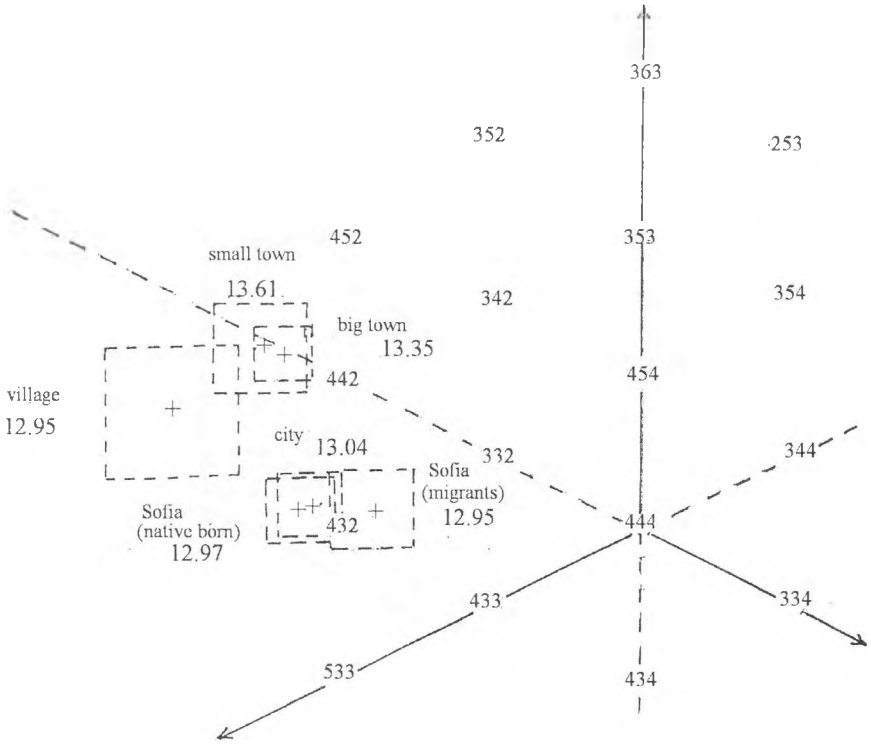

Fig. 1. Mean somatotype (M±m) and mean age at menarche by residence

T a b l e 2. Age at menarche and somatotype in the investigated students by united groups

Residence	*N*		Age at menarche	Somatotype — components			Somatotype
				Endo-morphy	Meso-morphy	Ecto-morphy	
Village	36	M	**12.95**	**4.90**	**4.12**	**1.76**	Mesoendomorph
		SD	1.67	1.70	1.19	1.03	
Town	207	M	**13.42**	**4.53**	**4.49**	**2.11**	Mesomorph-endomorph
		SD	1.39	1.24	1.06	1.09	
City	299	M	**12.99**	**4.43**	**3.49**	**2.30**	Mesoendomorph
		SD	1.23	1.29	1.02	1.15	
Total	542	M	**13.15**	**4.50**	**3.91**	**2.19**	Mesoendomorph
		SD	1.34	1.37	1.15	1.13	

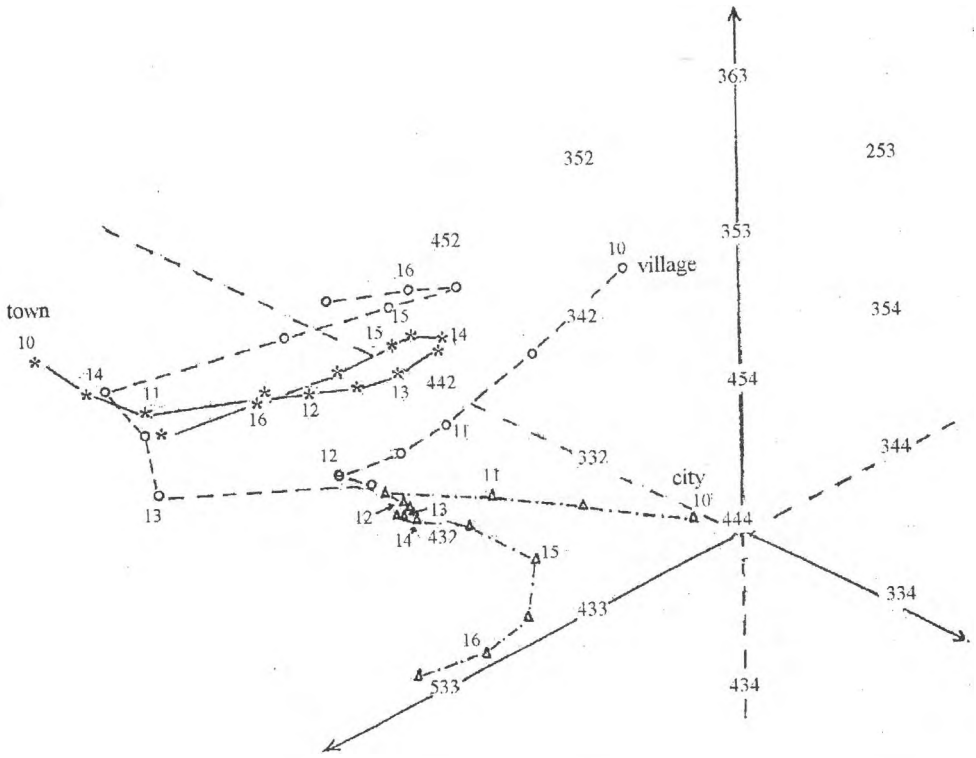

Fig. 2. Somatotype by age at menarche and residence

The small subsample of students — rural residents has an intermediate position. They are closer to the city residents in mean age at menarche (12.95 years) and in the general description of their somatotype (mesoendomorph), but in the values of every separate somatotype component are closer to the town students (Table 2). The composition of this subsample has some specific peculiarities, which have been discussed in details in our former paper and explain the early upset of menarche [11]. It can be presumed that the similarity of their somatotype to the somatotype of city students is due to the reasons discussed in the cited paper. If we analyse the somatotype by age at menarche in village students, we come to a curve similar to the curve in city students, but shifted to the curve in town students.

It is interesting that the city residents with age at menarche from 11.5 to 14 years (more strictly from 11.25 to 14.24 years) show practicalle the same somatotype — 4.56 : 3.52 : 2.20 (Table 3, Fig. 2). Variations can be found only in students with earlier or later age at menarche. These both cases present lower endomorphy and higher ectomorphy. In author's opinion these are the limits of the normal age at menarche in a city population (11.25 to 14.24 years). Around the middle of this interval (12.75 years) concentrate the data of mean age at menarche in city and well urbanised populations in Bulgaria and in whole Eastern Europe in the last quarter of 20th century [4, 7, 8].

Table 3. Periodisation of the age at menarche and somatotype in the investigated students by united groups

Residence	Age at menarche	*N*		Somatotype components			Somatotype
				Endo-morphy	Meso-morphy	Ecto-morphy	
City	< 11.24	25	M	**3.80**	**3.52**	**2.70**	Mesomorph-endomorph
			SD	1.20	0.81	1.05	
	11.25-14.24	232	M	**4.56****	**3.52**	**2.20***	Mesoendomorph
			SD	1.43	1.04	1.15	
	14.25 <	42	M	**4.05***	**3.30**	**2.57***	Mesoendomorph
			SD	1.29	1.01	1.12	
Town	< 11.24	14	M	**5.89**	**4.46**	**1.32**	Mesoendomorph
			SD	1.46	1.31	0.64	
	11.25-13.24	75	M	**4.64***	**4.33**	**2.12*****	Mesomorph-endomorph
			SD	1.14	1.56	1.05	
	13.25-15.24	101	M	**4.20***	**4.66**	**2.30**	Endomesomorph
			SD	1.13	1.02	1.12	
	15.25 <	17	M	**4.88***	**4.15(*)**	**1.62***	Mesoendomorph
			SD	1.24	1.07	1.02	
Village	< 12.74	15	M	**4.10**	**3.77**	**2.00**	Mesomorph-endomorph
			SD	1.50	1.03	1.07	
	12.75-14.24	13	M	**6.00****	**3.96**	**1.08****	Mesoendomorph
			SD	1.65	1.42	0.61	
	14.25 <	8	M	**4.62***	**5.06***	**2.44****	Endomesomorph
			SD	1.25	0.42	0.94	

* — $P < 0.05$; ** — $P < 0.01$, *** — $P < 0.001$, (*) — $P < 0.10$ in comparison to the former subsample by age at menarche

As far as city residents cluster in three subgroups (with early, medium and late menarche), in town residents can be traced four subgroups. These with early menarche (less than 11.24 years) present a strongly expressed endomorphy (5.89) and their mean somatotype is mesoendomorph. In students with menarche from 13.25 to 15.24 (named conventionally "later than medium") is very typical that the mesomorphy is more expressed than the endomorphy (besides the lower endomorphy). Thus their mean somatotype is endomesomorph. Such predomination of the mesomorphy is not typical for the female somatotype in general. It distinguishes them from the group with menarche "earlier than medium" (11.25 to 13.24 years) with mean somatotype mesomorph-endomorph. At last in town residents with menarche later than 15.25 years can be found a higher endomorphy.

Despite their small number, village residents divide also in three subgroups with statistically significant differences between them: with early (less than 12.74 years), medium (12.75-14.24 years) and late menarche (over 14.25 years). They are similar to the city residents in this fact that in the medium group can be found again the girls with the highest endomorphy and the lowest ectomorphy and mean somatotype mesoendomorph, and in the girls with early menarche the mean somatotype is mesomorph-endomorph. In the group of village girls with late menarche, however, a similarity to the town girls with menarche "later than medium" can be found (a mesomorphy higher than endomorphy and mean somatotype endomesomorph).

In the literature usually is given a simple relation between age at menarche and somatotype — earlier maturation correlates higher endomorphy [1]. The somatotype of students with early menarche in both early maturing samples (city and village residents — mesomorph-endomorph) deviates from such type of relationship. The somatotype of the late maturing girls from the towns (mesoendomorph) also falls out of such relationship.

Such a relation cannot explain also the differences in the somatotype and in the age at menarche according the residence. The results of present study show that the connection between age at menarche and somatotype is more complicated than usually accepted. It is possible that the correlation is under social environment influence too. The Heath-Carter schedule (according its authors themselves) belongs to the group of somatotyping methods which estimate the phenotypic (i.e. present) somatotype, and not to the methods, which attempt to assess the constitutional, unchanging pattern of somatotype [3]. Probably no significant differences should be found by urbanisation level if a somatotype schedule assessing the stable ecologically constitution has been used, for example the schedule of Shtefko-Ostrovsky or of K a d a n o f f — J o r d a n o v [5]. A higher mesomorphy in town and village girls than in city ones has been found in this study. A similar phenomenon has been found for this period in a comparison of the somatotypes of adolescents from Sofia and Smolyan and explained on the base of the higher motor activity of the children and youth in the smaller town [6].

As a conclusion, the author considers that the relationship between social environment, sexual maturation terms and somatotype (in adolescence and after its termination) needs additional studies.

References

1. B o d z s a r, E. B., J. P a p a i. Maturation and body composition. – Humanbiologia Budapestinensis, **19**, 1989, 215-218.
2. B o d z s a r, E. B., J. P a p a i. 1994. Secular trend in body proportions and composition. – Humanbiologia Budapestinensis, **25**, 1994, 245-254.
3. C a r t e r, J. E. L., B. H. H e a t h. Somatotyping — Development and Applications. Cambridge, Cambridge University Press, 1990, 70-71.
4. D a n k e r — H o p f e, H. Menarcheal age in Europe. – Yearb. Phys. Anthrop., **29**, 1986, 81-112.
5. K a d a n o f f, D., J. J o r d a n o v. Bestimmung des Konstitutiontyps beim Menschen. — Comptes rendues de l'Academie bulgare des Sciences, **34**, 1:119-122.
6. S t o e v, R. Somatotype in adolescents from a big city and a smaller town. Papers on anthropology (Tartu, Estonia), **XIV**, 2005, 344-352.
7. S t o e v, R., Y. Y o r d a n o v. Secular trend in Bulgaria. – In: Secular Growth Changes in Europe (Eds. B. E. Bodzsar, Ch. Susanne, C). Budapest, Eotvos University Press, 1998, 65-73.
8. Г о д и н а, Е. З. Ауксология человека — наука XXI века: проблемы и перспективы. – В: Антропология на пороге III тысячелетия (ред. Т. И. Алексеева, Е. В. Балановская, Е. З. Година, Н. А. Дубова). Москва, Росийское отделение ЕАА, 2003, Т. 2, 529-566.
9. М а р т и р о с о в, Э. Г. Методы исследования в спортивной антропологии. Москва, Физкультура и спорт, 1982, 104-111.
10. П л о х и н с к и й, Н .А. Биометрия. Москва, Изд. Московского университета, 1970, 220-226.
11. С т о е в, Р., Цв. К а з а к о в а, Л. Ж е л к о в а, Л. Ц а ч е в а. Възраст при менархе и някои специфични за човека екологични фактори при студентки в град София. – В: Младежка научна конференция „Приносът на младите научни работници при решаването на екологичните проблеми", Враца. 1—2 декември. 1988, 151-156.
12. Х и т, Б. Х., Дж. Е. Л. К а р т е р. Современные методы соматотипологии, ч. II – Модифицированный метод определения соматотипов. — Вопросы антропологии, **33**, 1969, 60-79.

Institute of Experimental Morphology and Anthropology with Museum
Bulgarian Anatomical Society

Acta morphologica et anthropologica, 12
Sofia • 2007

Graphical Method for the Assessment of Eco-sensitivity in the Components of Human Somatotype

*M. Toteva, A. Nacheva**

National Sports Academy, Sofia
**Institute of Experimental Morphology and Anthropology with Museum, Bulgarian Academy of Sciences, Sofia*

The aim of the present work is to present a new method ensuring possibility for individual assessment of portion between the values of three somatotype components, for evaluation of their eco-sensitivity, for comparison of somatotype data in different studies, and to show the results of its application in sportive-medical practice. The method offered is an original illustrative addition to Heath-Carter's somatotype method. Our method visualizes three-dimensionally the portion between somatotype components' value. The graphic method is elaborated and applied on representative data by M. Toteva in 353 individuals studied longitudinally and 4001 athletes studied transversally. The results from comparative somatotype studies in not engaged in sports children and adolescents, young but already trained beginners and top-class sportsmen in different sport disciplines are shown as an illustration of the graphic method offered. The new method is applicable in morphological control for the assessment of physical development in adolescents and in sportive-medical practice.

Key words. somatotype components, eco-sensitivity, individual assessment, growing up individuals, sportsmen.

Introduction

Somatotype is a complex morphological characterization that is considerably genetically determined [4, 5, 10], while its separate components undergo through different changes during the ontogenetic development [1, 11]. Its eco-sensitivity reflects mainly the type of physical activity in labor, the way of life and sport, the nutritional specificity and nutritional habits, the different diseases, etc. [3, 6, 7, 8, 9].

All purposeful investigations till now show that ages couldn't affect essentially the basic somatotype and their changes remain in the same somatotype zone during whole life. The established changes in the ages express themselves only by moving into neighboring somatotype categories [2, 11]. It depends on the changes of three-somatotype components during different age periods that reflect the age dependent eco-sensitivity of different body tissues and systems.

We didn't found in the special literature purposeful studies giving prominence to the objective evaluation of eco-sensitivity in the separate somatotype components.

The **aim** of the present work is to present a new method ensuring possibility for individual assessment of portion between the values of three somatotype components; for evaluation of their eco-sensitivity; for comparison of somatotype data in different studies; and to show the results of its application in sportive-medical practice.

Material and Methods

The method offered is an original illustrative addition to Heath-Carter's somatotype method [2] by which could be visualized three-dimensionally the values of the three-somatotype components, and comparatively medico-biological information to be gain, as well. It gives possibility for eco-sensitivity of each somatotype component separately to be assessed as connected with age and sex, so dependent to the effect of different factors.

The construction of graphical somatotype models is done on the basis of values (individual or group) for the three-somatotype components. Values are marked on the axes of three-dimensional system at 120 grades centigrade, which system is a base in Heat-Carter's somatotype card, as well. Outwards from center on the left axis are marked the values of endomorph component, on the vertical axis — of mesomorph component, and on the right axis — the ectomorph component. By the connection of points on the three axes is formed a triangle. Fig. 1A illustrates a graphic model of somatopype arbitrarily chosen; being in this case mesomorph-ectomorph (En 2.44 — M 3.81 — Ec 4.01). Comparatively is presented also the Heath-Carter's somato-card of the same somatotype (Fig. 1B). The triangle received by somatotype graphic model gives possibility of portions between the three-somatotype component values to be visualized. This illustrative method gives also possibilities of the results from studies containing data of multiple observations during childhood and adolescence to be compared, a period during which the individual somototype characteristics are more changeable stimulated by the active growth. Such comparisons could be made by/or the selection and health morphological control during training process in sportive-medical practice, as well.

The graphic method is elaborated and applied on representative data elaborated by M. T o t e v a [11] in a longitudinal investigation of not engaged in sports (non-athletic) schoolchildren (7-14 years old), advanced young sportsmen (12-17 years old) who are representatives of 11 sports, and top class sportsmen (mean age: ♀ - 20.2; ♂ - 23.4) representatives of 20 sports. Totally 353 individuals from both sexes are studied longitudinally and 4001 ones — transversally.

Results

As an illustration of the informative possibilities of the graphical method are presented results from comparative somatotype investigations in not engaged in sports children and adolescents (Table 1), beginners but advanced athletes (Table 2) and elite sportsmen engaged in different sports (Table 3).

A

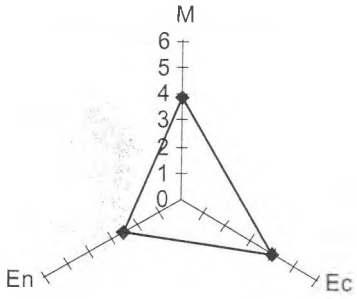

B

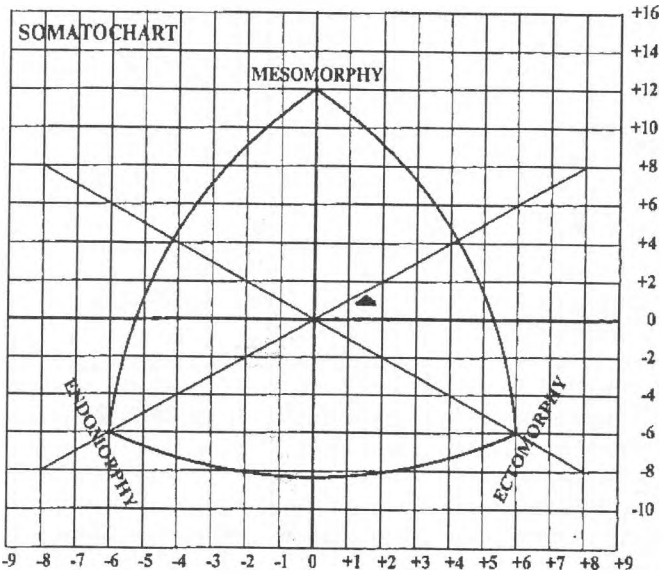

Fig. 1. Illustration of somatotype graphical method according to data about 14 years old not engaged in sports boys Mesomorph-ectomorph somatotype (En 2.44 — M 3.81 — Ec 4.01)
A — Our somatotype graphical model; *B* — Somato-card by Heath-Carter

The longitudinal results of boys and girls not engaged in sports show that for boys aged from 7 till 12 years the mean somatotype is balanced mesomorph, at 13 years — ectomorph-mesomorph, and at 14 years — mesomorph-ectomorph. In girls at 7 years of age the mean somatotype is central, between 8 and 11 years it is balanced mesomorph, and at 14 years — again central.

The construction of our somatotype graphic models gives possibility for the age changes of total somatotype in adolescents established by Heath-Carter's method to be worked out in detail that reflect spatially the quantitative changes in separate components. Illustrated in such manner, the age changes of separate somatotype components could be connected with the quantitative changes in body constitution of the growing up and sexually maturating organism.

Table 1. Somatotype of not engaged in sports 7-14 years old children (longitudinal data)

Sex	Boys								Girls							
Age	7	8	9	10	11	12	13	14	7	8	9	10	11	12	13	14
En	2.66	2.69	2.88	2.90	2.89	2.90	2.81	2.44	3.04	3.09	3.27	3.21	3.30	3.42	3.48	3.52
M	4.34	4.43	4.66	4.46	4.53	4.35	4.20	3.81	3.94	4.37	4.36	4.18	4.40	4.18	3.62	3.55
Ec	3.05	2.91	2.92	2.90	3.21	3.32	3.51	4.01	3.20	2.77	3.12	2.92	3.01	2.82	3.00	3.04

Table 2. Somatotype of 12-17 years old sportsmen

Sex	Boys											
Sport	*Football players*						*Weight lifters*					
Age	12	13	14	15	16	17	12	13	14	15	16	17
En	1.86	1.63	2.08	2.25	2.40	2.30	2.08	2.35	2.50	2.06	2.71	2.25
M	4.52	4.66	4.92	5.05	4.85	4.92	4.78	5.26	5.73	5.41	5.31	5.48
Ec	4.27	4.00	3.17	3.00	3.20	3.25	2.50	2.16	2.25	2.43	3.00	1.50
Sex	Girls											
Sport	*Field and track athletes*						*Academic rowing*					
Age	12	13	14	15	16	17	12	13	14	15	16	17
En	2.33	2.85	2.93	3.50	3.50	3.94	4.10	3.79	4.59	4.75	4.67	4.68
M	3.19	3.59	3.60	3.93	3.31	3.53	3.42	3.32	4.02	3.38	3.86	4.82
Ec	4.12	3.97	3.58	3.14	3.44	2.69	3.40	3.61	3.11	2.85	2.64	2.92

Table 3. Somatotype of top class sportsmen

Sex	Men			Women	
Sport	*Weght lifters*	*Acrobats*	*Body builders*	*Rhythmic gymnasts*	*Weight lifters*
En	2.90	2.50	1.70	1.53	3.82
M	6.90	5.48	7.15	2.89	6.09
Ec	1.00	2.08	0.94	4.91	0.88

For greater clarity we shall illustrate our results only by the somatotype graphic models of boys and girls at 7 and 14 years of age. In Figures 2A and 2B are presented the somatotype differences in the ages separately for boys and girls, which reflect also the sexual differences in this ages.

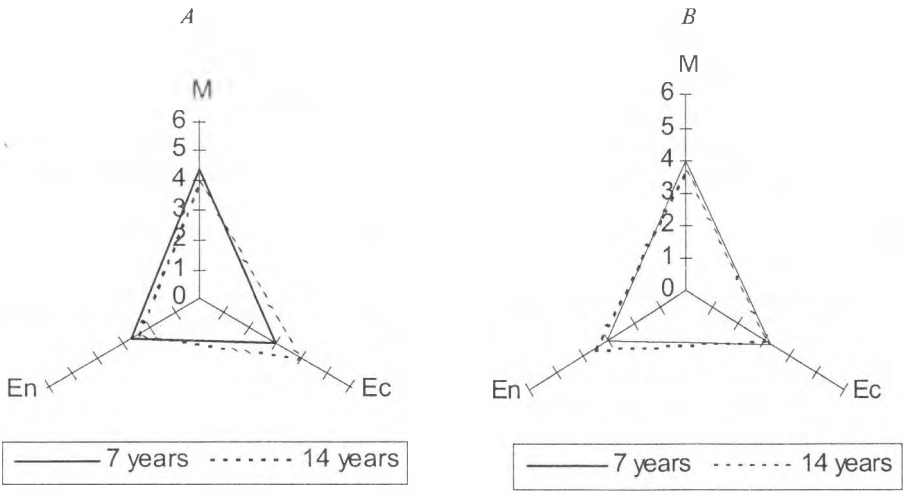

Fig. 2. Somatotype graphical models of not engaged in sports 7-14 years old schoolchildren (longitudinal data)
A — boys; *B* — girls

The analyses of detailed data (Table 1) show that in boys at 7 and 9 years is available slightly increase of endomorphy and mesomorphy, while the ectomorphy decreases. During 9 and 14 years of age, however, the endomorphy and mesomorphy already decrease, if only very few at the expense of the ectomorphy considerable increment.

For girls in the ages, the changes of somatotype components are more slightly expressed. Between 7 and 9 years, the endomorphy and mesomorphy in them slightly increase, and the ectomorphy remains nearly the same. Between 9 and 14 years the values of endomorphy and mesomorphy still increase and the values of ectomophy decrease.

By means of our somatotype graphical models are visualized also the specific sexual differences in somatotype characterization throughout the period 7—14 years. During childhood — 7 years of age, both sexes have relatively equal ectomorphy, the endomorphy being greater for girls and the mesomorphy — for boys. At 9 years (pre-puberty) the sexual differences are similar to those at 7 years. At 14 years of age, however, the sexual differences of somotottype components values are underlined better — the endomorphy in girls is already considerably greater, while ectomorphy is considerably smaller compared to boys.

The somatotype characterization being a routine method in sportive-medical practice is very important for the selection of beginners in sport, and for the morphological control during training process, as well. By the application of our somatotype graphic models a precondition for quantity assessment in the differences between somatotype components of beginners and top class sportsmen could be created. In this respect as example we show the results of somatotype graphic models analysis in 12 years old beginners and 17 years old sportsmens who were supposed beening trained at least 5 years the respective sport. Boys are football-players (Fig. 3A) and weight lifters (Fig. 3B); girls are track-and-field athletes — runners (Fig. 4A) and academic rowers (Fig. 4B).

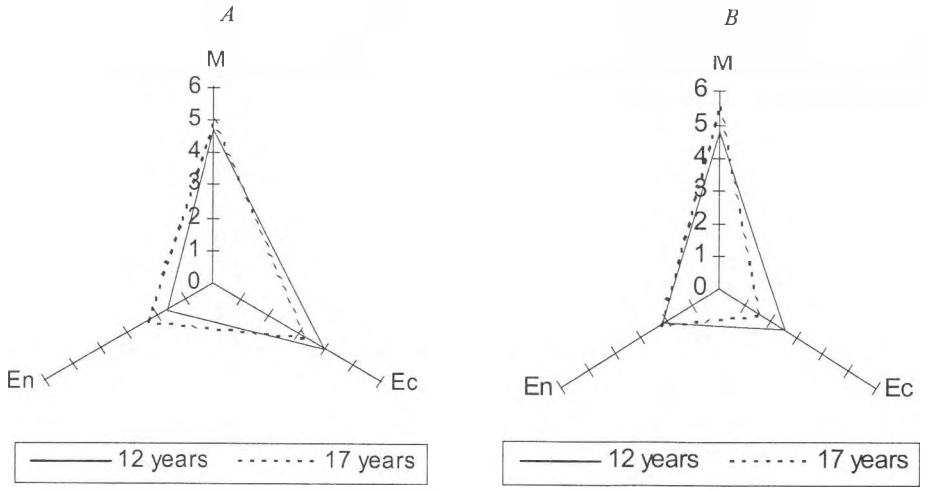

Fig. 3. Somatotype graphical models of 12-17 years old athletes — boys
A — football-players; *B* — weight lifters

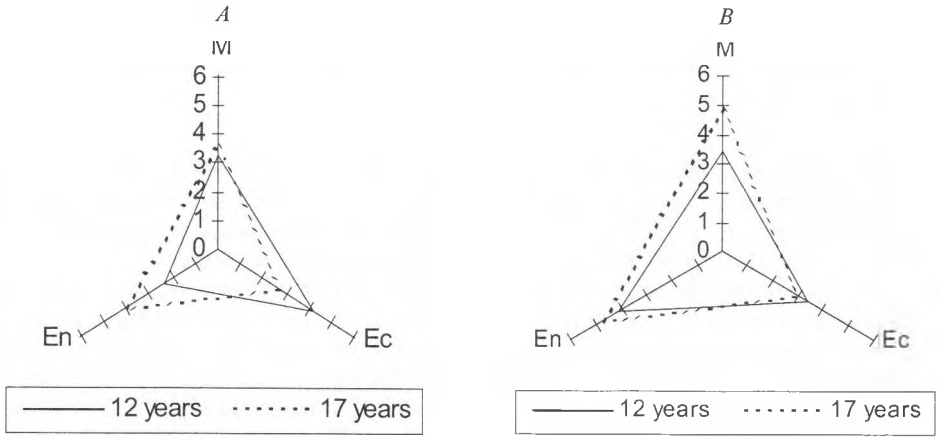

Fig. 4. Somatotype graphical models of 12-17 years old athletes — girls
A — track and field athletes; *B* — academic rowers

Mesomorph-ectomorph is the mean somatotype of the football-players — beginners, and ectomorph-mesomorph of the 17 years old male football-players. Balanced mesomorph is the mean somatotype of the weight lifters — beginners, and endomorph-mesomorph of the 17 years old weight lifters.

In track-and-field female athletes the mean somatotype is mesomorph-ectomorph at 12 years of age, and for the 17 years old ones it is endomorph-mesomorph. In girls academic rowers the mean somatotype is central at 12 years of age, and for the 17 years old ones it is endomorph-mesomorph.

Summarizing the analysis of somatotype graphic models in these sportsmen, it becomes immediately obvious that in boys (football-players and weight lifters) the proportion of ectomorph component inside the complete somatotype decreases in the ages, oppo-

site to those for not engaged in sport boys, by who was established that the proportion of the ectomorph component increases in the ages during the growing up period. For not engaged in sport girls was established that the ectomorphy didn't change in the ages, while for the girl-athletes, as it is for boy-athletes, the ectomorphy decreases in the course of ages.

In male football players, parallel with the decrease of ectomorphy, the values of endomorphy and mesomorphy increase, but in male weight lifters the decrease of ectomorphy is accompanied with mesomorphy increase.

In female track and field athletes the decrease of ectomorphy is accompanied by increase of endomorphy and mesomorphy in the ages, while in female academic rowers the increase of endomorphy is on a small scale and the increase of mesomorphy is considerable.

From sportive-medical point of view it is well known that the athletes' somatotype is of a great importance for their sportive achievements. On the other hand, the somatotype serves as a basis when good evaluation whether someone is appropriate to train the desired by him sport had to be given. This assessment is based on the somatotype model's data of top class sportsmen, by which model on the other hand the morphological control during training process could be supported.

The presentation of the somatotype for top class sportsmen by our somatotype graphic models extends the quantitative base of somatotype assessment used in the sportive-medical practice. It could be realized creating standard somatotype graphic models under sports on the basis of data for respective somatotypes about top class athletes. These models visualize the information about optimal proportion between the values of separate somatotype components in mean somatotype for top class sportsmen engaged in the respective sport, and could be used as evaluation criteria in the sportive-medical practice.

In the present paper we present some exemplary standard somatotype graphic models of top class sportsmen.

The mean somatotype of top class male weight lifters is endomorph-mesomorph (Fig. 5A). Their standard somatotype graphic model shows that the optimal formula concerning the proportion between values of the three components is **3En: 7M: 1Ec.**

The mean somatotype of male acrobats is balanced mesomorph (Fig. 5B), the optimal proportion between each components' value is of the type **2.5En: 5.5M: 2Ec.**

The best illustration about merit and necessity of the presented graphic somatotype model to be applied is the one elaborated for top class male body builders (Fig. 5C).

Their mean somatotype is endomorph-mesomorph. The optimal proportion between values of the three components shows that mesomorphy is 7 times higher than ectomorphy, and nearly 4 times higher than endomorphy — **1.7En: 7M: 1Ec.**

The standard somatotype graphic model of female top class rhythmic gymnasts (Fig. 6A) shows that the mean somatotype is mesomorph-ectomorph, by which ectomorphy dominates nearly twice over mesomorphy, whish on its side dominates nearly two times over endomorphy, i.e. the proportion is of the type **1.5En: 3M: 5Ec.**

In female top class weight lifters (Fig. 6B) the mean somatotype is endomorph-mesomorph. The optimal proportion between its somatotype components is of the type **3.8En: 6M: 0.9Ec.**

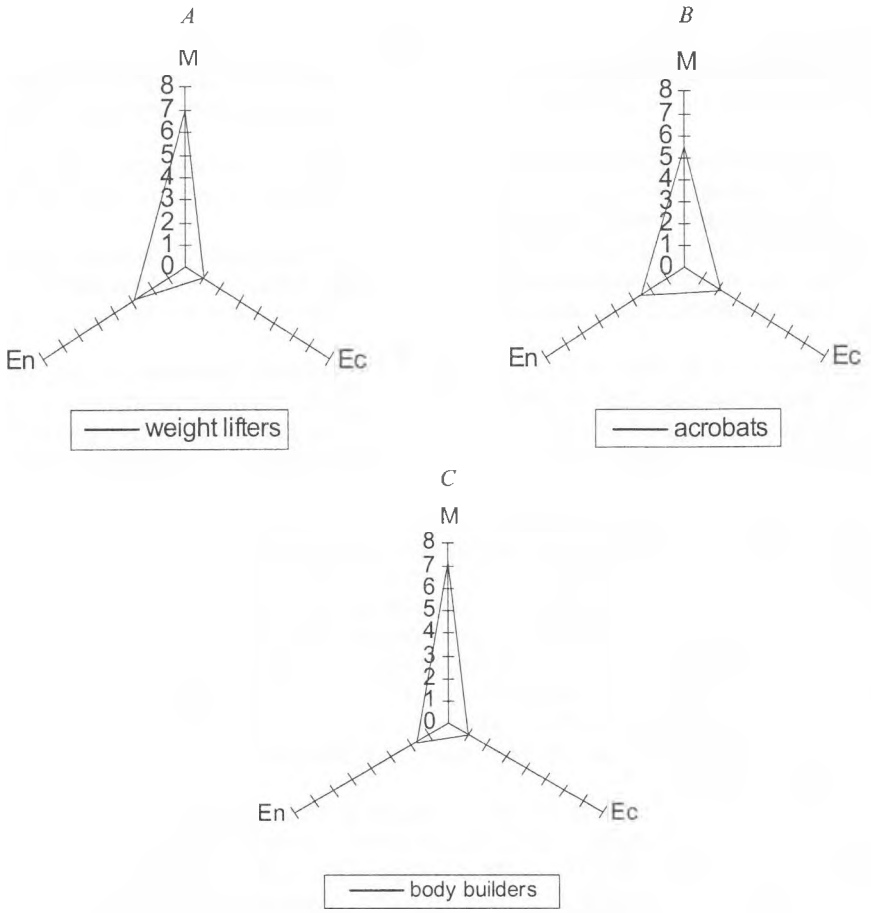

Fig. 5. Standard somatotype graphical models of top class athletes — men
A — weight lifters; *B* — acrobats; *C* — body builders

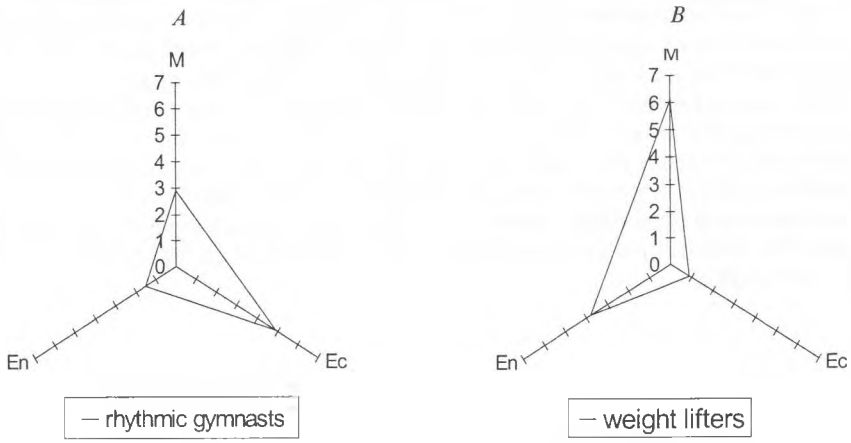

Fig. 6. Standard somatotype graphical models of top class athletes — women
A — rhythmic gymnasts; *B* — weight lifters

By way of example applying our somatotype graphical method is presented the somatotype assessment of beginners weight lifter (En 2.08 — M 4.78—Ec 2.50) and of top class weight lifters (En 2.90 — M 6.90 —Ec 1.00) (Fig. 7). In young weight lifters the endomorph component values are smaller compared to those in top class weight lifters, and the ectomorph component is bigger. The differences are characteristic for the values of both somatotype components. Clearly could be seen the model of body form and structure towards which initially had to be directed the selection of beginners weight lifter, and later their training process. Obviously, the suitable training rules for the selected and turned to this sport individual had to be such that enlarges the mesomorph and lessens the ectomorph component realized by the increment of muscles mass and skeletal massiveness.

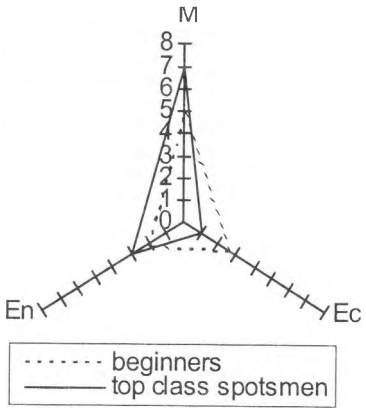

Fig. 7. Application of somatotype graphical models when comparing the somatotype of beginners and top class weight lifters. Somatotype of beginners (2.08 — 4.78 — 2.50);
standard somatotype model (2.90 — 6.90 — 1.00)

Conclusion

The somatotype graphic model and the described results by way of example about its application show that it can be used as in the preventive medical, so in the sportive-medical practice.

Evaluating the physical development of children and adolescents by the somatotype graphical models, the specific interconnected changes of the three-somatotype components could be visualized, which attend the sexual body maturation during this dynamic period on human ontogenesis.

In sportive-medical practice the method ensures objective biometrical data for selection, assessment and control of athletes' morphological constitution.

As an original illustrative addition to Heath-Carter's somatotype method, our graphical method is easy for application and gives direct visual spatial information in self-dependant or comparative investigations.

References

1. Beunen, G., A. Claessens, J. Lefevre, R. Renson, J. Simons, D. Van Gerven. Somatotype as related to age at peak velocity in height, weight, and static strength. – In: Kinanthropometry II (Ed. T. Reilly, J. Watkins, J. Borms). London, Spon, 1986, 68-72.

2. Carter, J. L., B. H. Heath. Somatotyping — Development and Applications. New York, Cambr. Univ. Press, 1990, 1-503.
3. Chovanová, E. The problems of the selection of talented downhill skiers from the somatic point of view. – Teorie a Praxe Tělesné Výchovy, **29**, 1981, No 4, 18-212.
4. Chovanová, E., P. Bergman, R. Štukovský. The share oh heredity on forming a somatotype. – In: Sbornik VR UV CSTV, Sport (Bratislava). Vol. **12**, 1981, 21-218.
5. Chovanová, E., P. Bergman, R. Štukovský. Genetic aspects of somatotypes in twins. – Modern Man Anthropos, Brno, **22**, 1982 a, 5-12.
6. Claessens, A., G. Beunen, J. Lefevre, G. Matrens, R. Wellens. Body structure, somatotype, and motor fitness of top-class Belgian judoists and karateka: a comparative study. – In: Kinanthropometry III (Ed. T. Reilly, J. Watkins, J. Borms). London, Spon, 1986 a, 7-53.
7. Eiben, O., P. Bösze, J. Lászly, J. Buday, M. Gaál. Somatotype of patients with streak gonad syndrome. – In: Physique and Body Composition (Ed. O. Eiben). Vol. **16**, Budapest, Human Biologia Budapestinensis, 1985, 53-64.
8. Meleski, B. W., R. F. Shoup, R. M. Malina. Size, physique, and body composition of competitive female swimmers 11 through 20 years of age. – Human Biology, **54**, 1982, 25-609.
9. Sharma, S. S., N. K. Dixit. Somatotype of athletes and their performance.–International Journal of Sport Medicine, **6**, 1985, 2-161.
10. Walker, R. N., J. M. Tanner. Prediction of adult Sheldon somatotypes I and II from ratings and measurements at childhood ages. – Annals of Human Biology, 7, 1980, 24-213.
11. Тотева, М. Соматотипология в спорта. НСА, 1992, 1—338.

Institute of Experimental Morphology and Anthropology with Museum
Bulgarian Anatomical Society

Acta morphologica et anthropologica, 12
Sofia • 2007

Genealogical and Dermatoglyphic Investigations of Families with Hemophilia[1]

*G. Karev, R. Mishkova**

Institute of Experimental Morphology and Anthropology with Museum, Bulgarian Academy of Sciences, Sofia
**Medical University – Varna, Deparretment of Internal Diseases, Clinics of Hematology*

Five large families with hemophilia were investigated. For each propositus a circumstantial family anamnesis was taken and a detailed genealogical tree of each family was drawn and analyzed. In all the genealogical trees the typical characteristics of the illness as a X-linked recessive defect were established. On the other hand, our analysis demonstrated that, despite the genetics of hemophilia and the manner of its hereditary transmission have been elucidated long ago, the genealogical analysis in hemophilic families is far of having exhausted its possibilities. In our sample, it allowed to make both social and genetic conclusions. The social applications concern the Muslim hemophilic families and their behavior concerning the *circumcision*. The genetic findings allow to hypothesize that the gene of hemophilia could show its effect with different expressivity. Among dermatoglyphic findings, the increased asymmetry in hemophilic patients should be noted and this concerns both finger and palm dermatoglyphics.

Key words: hemophilia, genetics, pedigree analysis, dermatoglyphics, social applications.

Introduction

The only study of dermatoglyphics of hemophilic patients which we found in foreign and Bulgarian literature [8] reported dermatoglyphic peculiarities in certain patients, but it reminded somewhat isolated, probably because of the lack of statistical significance of most of the findings. On the other hand, numerous studies reported the importance of the X-chromosome for dermatoglyphic traits. As early as forty years ago P a r s o n s [5] assumed that the higher dermatoglyphic variability in women is due to different proportions between mother's and father's X-chromosomes remaining active after inactivation of one of them accordingly to Lyon's hypothesis. Although dermatoglyphic traits are mainly autosomically determined [6], the possibility for a considerable impact of the sex-chromosomes was also widely accepted [3, 4]. What is more, it was concluded that additional X-chromosomes strongly reduce the finger ridge counts [1, 2, 7].

[1] This article is dedicated to the memory of Professor Dr. Rumiana Mishkova.

The current study was devoted to dermatoglyphic and genealogical analysis of families with hemophilia A and B.

Since the genes of hemophilia are X-linked, it could be expected that dermatoglyphic examination of hemophilic patients would reveal relationships , if any, between the two packages of genetic information: this determining the lack of blood coagulation factor VIII or IX and that governing dermatoglyphic patterns and ridge counts as well as their asymmetry.

Material and Methods

Five large families with hemophilia were investigated, four of them with hemophilia A (factor's VIII deficiency) and one with hemophilia B (factor's IX deficiency), the latter belonging to the Turkish ethnical community in Bulgaria. The propositi varied in age between 13 and 30 complete years. They themselves, as well as some of their hemophilic relatives have been hospitalized and treated many times in the Clinics of Hematology at the Department of Internal Diseases, Medical University (at the time — High Medical Institute) — Varna. Among the clinical findings, hemorrhages and posttraumatic intra-articulation bleedings of retarded type prevailed. A circumstantial family anamnesis was taken of each patient and a detailed genealogical tree was drawn. Complete dermatoglyphic analysis was carried out in seven patients (all of them Bulgarians with hemophilia A) whose clinical and laboratory investigation had undoubtedly confirmed the diagnosis. All the dermatoglyphic findings were compared to criteria elaborated by the first of us [9] on a large sample of Bulgarians from the same region.

Results

All the pedigrees under analysis showed the typical peculiarities of the hemophilia as a X-linked recessive defect of the blood coagulation. In most of the cases all the patients belonging to a given family have received the pathologic gene from a common progenitor — female heterozygous career.

Fig. 1 presents the pedigree of a Turkish family with 7 hemophilic patients; in three of them the diagnosis has been clinically approved and the death of the remaining four at age between 7 and 12 years because of blooding after *circumcision* makes the diagnosis more than probable. The transmission of the pathologic gene could be traced between all the hemophilic persons in the family and their common progenitor, I — 1, Seniha. The family member III -3, Ravie, is an object of particular interest here. She has suffered a heavy haemorrhage syndrome, with clinics practically identical to those in the hemophilic men in the same family. Despite Ravie has been hospitalized and treated a lot of times, the clinics of the illness has become more and more heavier and she committed suicide at age of 23 years.

Concerning the second pedigree, presented in Fig. 2, the hemophilia of the propositus Todor (III — 3) and in his nephew Krasimir (IV -1) could be easily explained with the presence of hemophilic gene in the heterozygous career Nedialka (II — 1). However, there are another six hemophilic men in the same family : the propositus' father and five other father's line relatives. Evidently, all these cases have to do with the very rare accidental coincidence of two heterozygous careers in the same family; in our case those are Neda (I — 1) and her daughter-in-law (II — 1), Nedialka.

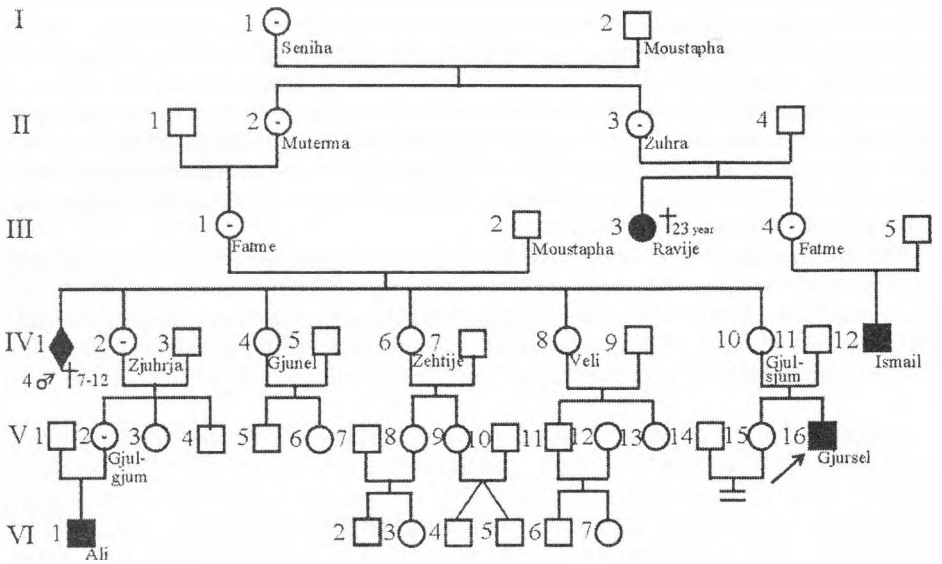

Fig. 1. Pedigree of a Turkish family comprising seven hemophilic patients, four of them deceased after *circumcision* and three of them clinically confirmed. All have received the pathologic gene from a common progenitor, I — 1, Seniha

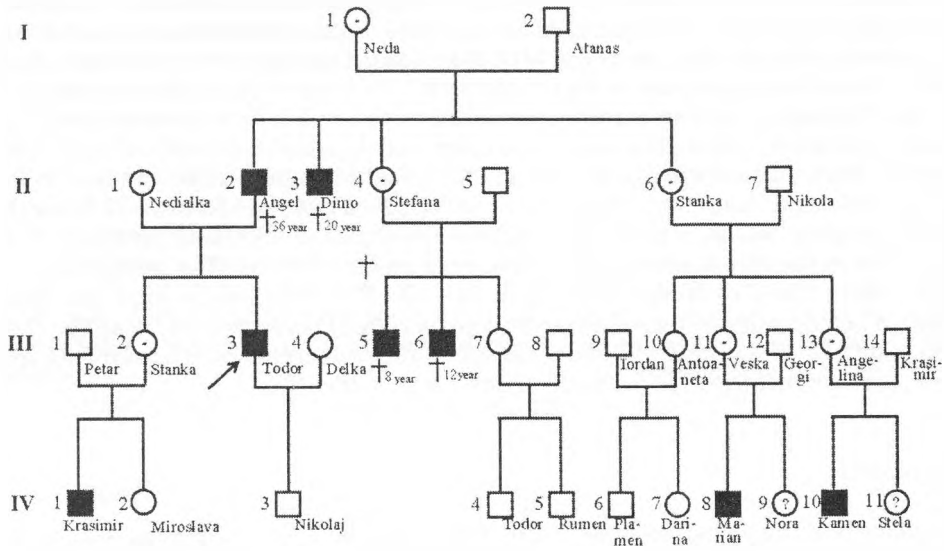

Fig. 2. Pedigree with eight hemophilic men. The transmission of the hemophilic gene could be traced to two distinct progenitors : I — 1, Neda and II — 1, Nedialka

Dermatoglyphic analysis showed that three out of four values of the finger ridge count of hemophilic patients demonstrated statistically significant differences as compared to the corresponding values in healthy men. The difference is especially expressed in the total finger ridge count (TFRC) : mean values of 169.29 versus 145.64. Of course, the question arises as to the different contributions of the separate fingers to this difference. The comparisons realized finger-by-finger showed that, except the fifth fingers of both hands, all the remaining fingers participle in the total difference with almost equal contributions. As far as the TFRC is an indicator of the model size, it is evident that bigger finger patterns prevail in hemophilic patients.

The absolute finger ridge count (AFRC) is also higher in the hemophilic patients; the difference between the latter and the healthy men being especially expressed concerning its internal structure, i.e. concerning the relationship between its two components, the radial (RFRC) and the ulnar (UFRC) ridge counts. We found a significantly lower UFRC and significantly higher RFRC in the hemophilic patients in comparison with the healthy controls.

Undoubtedly, the question arises as to whether these differences are caused by an unusual proportion between the radially and ulnarly directed finger patterns. Assessment of the radio-ulnar index [9] evidenced that such is the case. Except the first three fingers of the right hand, a decrease of this index was observed on all the rest fingers. As a result, its mean value was 0.21 in the hemophilic patients versus 0.25 in the healthy men. Consequently, the changed proportion between the ulnar and the radial finger ridge counts is due to an "ulnarization" of the finger patterns — much more expressed preponderance of the ulnar patterns over the radial ones in the hemophilic patients as compared to the healthy men.

Concerning the palm dermatoglyphics, the only our finding which corroborated the corresponding finding of K a l e v a et al. [8] was the increased occurrence of radial loops on the hypothenar. Significant differences were found neither in the localization of the palm triradii, nor in the values of the atd-angle. Neither significant deviations were established concerning two of the main palm lines, A and D, and, since the sum of the fields of their endings gives the main line index, MLI, the values of the latter were practically equal in the hemophilic patients and in the healthy men (14.14 versus 14.04, correspondingly). On the other hand, considerable differences were established in the other two main lines, B and C. The line C ended abortively much more often in hemophilic patients than in the controls. Such an ending was observed in 28.37 % of the hands (right and left) in the patients versus the normal proportions of 6.85 % for the right hand and 14.37 % for the left one. In other words, in hemophilic patients this configuration was observed 4-fold more often on the right hand and two-fold more often on the left hand as compared to the healthy men. The proportions of the field 5 (5′ and 5″) ending of the main line B are higher in hemophilic patients than in the controls (28.57% versus 22.63% on the right hand and in 71.43% versus 42.73% on the left one). Concerning both lines mentioned above, the asymmetry is considerably increased in the patients.

Discussion

The analysis of the pedigrees shown in all of them all the typical characteristics of the hemophilia as a X-linked recessive pathologic trait. On the other hand, our analysis demonstrated that, although the manner of genetic transmission of hemophilia has been established a long time ago, the genealogical analysis is very far from having exhausted its possibilities and perspectives concerning the illness under discussion. In the case of our study, it allowed us to made contributions in two respects — a social and a genetic ones.

The social factors should be carefully examined in every single one of the pedigrees with hemophilia, since they influence considerably the time and the manner of its phenotypic occurrence and, still more importantly, the outcome of the illness. Thus, the pedigree of the Turkish family showed that not so much ago even the death of three boys in a given family because of *circumcision* was not a contra-indication for the parents to perform this procedure on the fourth boy and to lose him in this way. It is known that in the Jewish population, where the same tradition also exists, despite the different religions, the fanatic application of the procedure in question is surmounted long ago and the boys having male mother's line relatives with hemorrhages are discharged from subjection to this manipulation. At the same time, in the younger families from the same pedigrees a considerable effect of the insisting medical advices are observed in this respect. On the other hand, the increased survival and expected longevity of the hemophilic men address new social and medical problems to the society.

Among the findings in finger dermatoglyphics, the most important were the increase of the TFRC in hemophilic patients, as an expression of the augmented finger pattern size, as well as the deviation in the proportion between the UFRC and RFRC, and correspondingly in the proportion between the ulnar and the radial patterns, expressed by the radial-ulnar index. This is a specific and very interesting change in the finger asymmetry. Concerning the palm dermatoglyphics, the findings about the lines B and C in hemophilic patients are oriented in the same direction on the right and the left hand; but, being very different in their extent, the differences increase considerably the palm dermatoglyphic asymmetry in hemophilic patients. Thus, the endings of the line B in the field 5 is augmented by 5.94% on the right hand versus 28.70% on the left and this increases the asymmetry with nearly 23%. The same event is still more prominent about the main line C, whose abortive ending showed a 4-fold increase on the right hand versus a 2-fold increase on the left one.

The finger ridge count is polygenically determined, but it is known that X-linked genes decrease its values. This explains the lower values in females than in males, as well as its decrease in X-chromosome polisomies. The observed higher values in hemophilic patients as compared to the healthy men allow to hypothesize a relationship between the genes coding the blood coagulation factors and those inhibiting the finger ridge counts, in which the pathologic condition of the former suppresses the effects of the latter.

Another finding, still more interesting from a genetic point of view, is Ravie (see III — 3 in Fig. 2), who committed suicide at age of 23 years, exhausted by repeated very heavy hemorrhage accidents. Theoretically, her complaints could be due to causes other than her belonging to a hemophilic family, but such a coincidence seems quite improbable. If so, two other possibilities should be hypothesized, both of them connected with an unusual expressivity of the gene of hemophilia. First, if the gene has been of very low expressivity in Ravie, she could be homozygous by such a gene, and because of its marginally low expressivity, the homozygous combination had not caused the usual letal effect during the embryogenesis. Secondly, if the gene was of very high expressivity, it had not been dominated by the normal one and thus has caused a phenotypic expression quite similar to that observed in hemizygous hemophilic men belonging to the same family.

Conclusion

Our results show that the genealogical analysis is far from having exhausted its possibilities concerning the hemophilia. Its application in the present study allowed to hypothesize two quite probable genetic mechanisms and to make important medico-social recommendations. The findings concerning the increased dermatoglyphic asymmetry in hemophilic patients with hemophilia A are more than promising in both theoretical and diagnostic respects.

References

1. Barlow, P. The influence of inactive chromosomes on human development. – Humangenetik, **17,** 1973, 105-136.
2. Hunter, H. Finger and palm prints in chromatin-positive males. – J. Med. Genet., **5,** 1968, 112-117.
3. Matsunaga, E., E. Matsuda. Sexual variation in finger pattern types and ridge counts. – Ann. Rep. Nat. Inst. Genet., **18,** 1968, 120-121.
4. Matsunaga, E., E. Matsuda, H. Schade. Sexual variation in finger pattern type and ridge counts in Germans. – Ann. Rep. Nat. Inst. Genet., **20,** 1970, 100-101.
5. Parsons, P. A. Finger-print pattern variability. – Acta Genet., **14,** 1964, 201-211.
6. Penrose, L. S. Medical significance of finger-prints and related phenomena. – Brit. Med. J., **2,** 1968, 321-325.
7. Penrose, L. S., D. Loesch. The effect of sex chromosomes on some characteristics of dermal ridges on palms and fingertips. – Genet. Polon., **10,** 1969, 328-331.
8. Калева, А., Ш. Ниньо, В. Спасов. Дерматоглифски проучвания при деца, болни от хемофилия. – Педиатрия, **13,** 1974, 88—94.
9. Карев, Г. Нормален дерматоглифски статус на българите от Североизточна България (канд. дис.). София, 1979. 216 с.

Institute of Experimental Morphology and Anthropology with Museum
Bulgarian Anatomical Society

Acta morphologica et anthropologica, 12
Sofia • 2007

Sex Determination of Human Humerus in Bones and Bone Fragments — New Suggested Formula

*A. Katsarov, Y. Yordanov, E. Tasheva-Terzieva**

Institute of Experimental Morphology and Anthropology with Museum, Bulgarian Academy of Sciences, Sofia
**Department of Zoology and Anthropology, Faculty of Biology, Sofia University, Sofia*

Sex determination of bones in findings is essential for the anthropological and forensic investigations. It is possible only with adolescent or adult skeletons because there is not so well expressed sexual dimorphism in preadolescent children.

In present study we suggest new formula for sex determination of bones based on the measuring of distal humerus.

Key words: determination, sex, distal humerus, bones, formula.

Introduction

Bone remains give us the possibility to determine the age, sex and even body posture. Undoubtedly if we make detailed morphometric characteristic of the contemporary human skeleton we can create standards leading us in evaluation of bone remains from the past.

The problem of sex determination of bone remains, especially when it is connected with sex determination of the humerus or parts of it, is still disputable.

If the investigated bones belong to contemporary people the possibility for exact sex determination is more significant than in bone findings from the ancient times or those belonging to evolutionary relatives [5].

Many authors present different methods of sex determination of humeral bone remains and for its distal part [2, 4].

Most of them think that there are no significant differences in applying these methods of investigating in contemporary remains and fossils. Others have different opinion [1, 3].

These different methods of sex determination are based on statistic calculations. Most used are the Discriminant and Cluster Analysis.

Step Discriminant Analysis is statistical method used to determine which variables discriminate between two or more naturally occurring groups.

Computationally, discriminant function analysis is very similar to analysis of variance (ANOVA).

Material and Methods

Our study is based on the measuring of 218 distal humera. A number of 138 bones are taken from cadavers and 80 bones from the ossuary of the Military Museum - Sofia.

Bones are cut at 15 cm proximally from the distal part of the humerus. At the time of the study we determined more than 30 linear and 10 angular signs. We also created 20 indexes divided into two big groups — common and special.

Results

Measurements are done by conventional anthropometric measuring devices.

First step of our study is to define the signs of division of men and women. Fig.1 is a point diagram of the signs which differs most of all the groups in common. Canonic variables I and II are shown at the axes of the diagram. It is seen higher level of differentiation of cases at the right side of the graphic Where the distance between the separate frequencies is bigger.

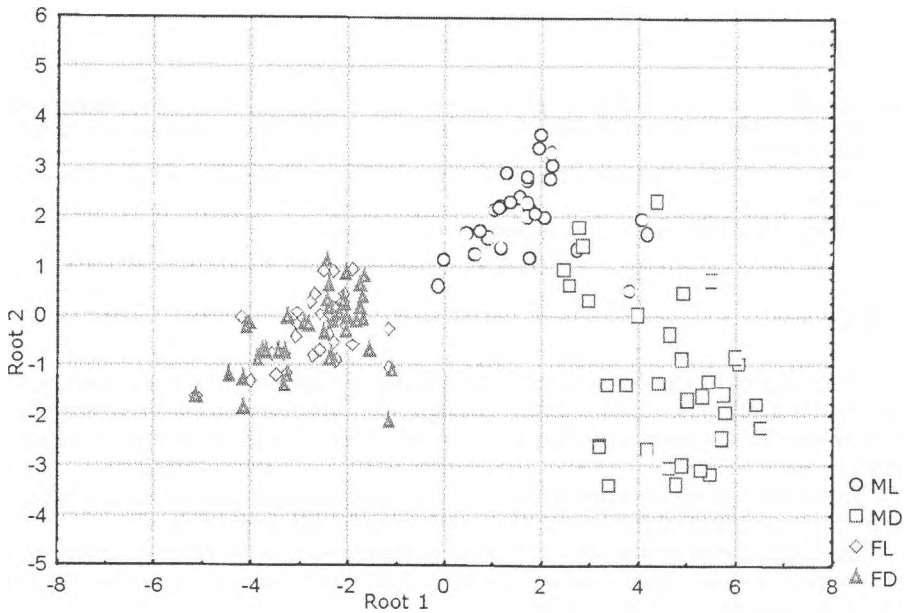

Fig. 1. Spatial distribution of the frequences by sex and lateralization for man-left (ML), men-right (MD), women-left (FL), women-right (FD)

The data from the point diagram are confirmed absolutely by the 3 D graphic of the first three canonic variables (Fig. 2). The difference here is abrupt which confirms 100% the distribution of the signs in the classification matrix.

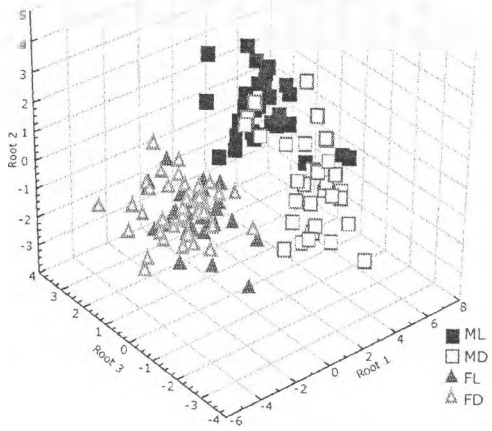

Fig. 2. Spatial distribution of the groups male left (ML), male-right (MD), women-left (FL), women-right (FD) in the frame of reference of the first 3 canonic variables

Fig. 3 presents the distribution of the group middle values in the frame of reference of the first three canonic variables.

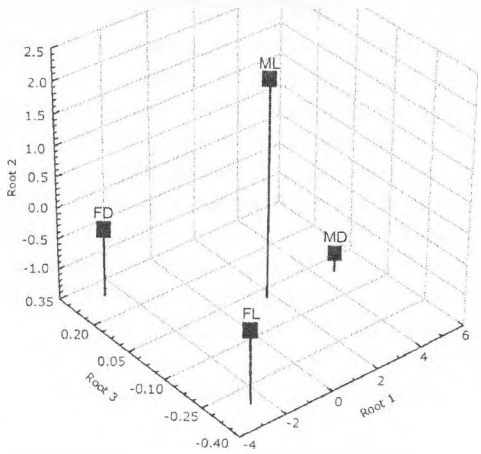

Fig. 3. Spatial distribution of the group middle values in the frame of reference of the first 3 canonic variables for groups male left (ML), male-right (MD), women-left (FL), women-right (FD)

In the study concerning division of the signs and indexes by sex, 100% division is find out in 2 signs — Length of the Lateral Column (LCL), Length of the Medial Column (MCL) and 5 indexes — Index of the Lateral Trochlear Ridge (LPI), Index of the Medial

Trochlear Ridge (MPI), Length - Thickness Index of the Lateral Column (LLI), Length - Thickness Index of the Medial Column (MLI) High — Length Index of Capitulum (HCI) (Fig. 4).

SIGN	M	F
INDEX	p=0.45652	p=0.54348
LCL	31.91133	28.38091
LPI	251.3068	352.8643
MCL1	14.53383	13.03371
LLI	293.5373	255.6207
HCI	299.5184	280.4488
MPI	1774.45	1710.998
MLI	436.3304	395.6075
CONSTANT	−2118.08	−1827.34

Fig. 4. Signs and indexes of 100% division by sex

Such distribution is positive and confirms the division by sex, because as much as the listed signs are, the bigger is the similarity and more difficult is the division.

Even the first sign divides man and women in 100% in such division.

Additional calculations only of anthropologic signs, with the help of software program, showed significant percentage of reliability of the study. This fact gave us the possibility to suggest a formula for sex determination of the individual which bones are found, using the sign Length of the Lateral Column (LCL) of the distal humerus.

This anthropometric sign is measured with the help of gliding caliper at the dorsal surface of the distal humerus. The longitudinal axis of the column needs to be determined first. LCL is the distance from the top of the lateral epicondyle with the cross point of the corresponding longitudinal axis of the medial column.

If a bone or a bone fragment is found and we need a sex determination, we measure the LCL sign of the bone. The measured value is multiplied with 38.52956009 and added with —1046.280762 (constant for males). If the result is nearer to the group constant, the conclusion is that the bone or the fragment belongs to male (X*38.52956009—1046.280762).

By analogy the value of LCL is multiplied with 34.86389923 and added with — 856.6347046. If the result is nearer to the group constant for women, the conclusion is that the bone or the fragment belongs to female (X*34.86389923—856.6347046).

For example – the measured value of LCL is 55.00 mm.

1. LCL = 55 mm — the initial value.

2. 55*38.52956009—1046.280762 = 1072 — multiplication with the constant for male and addition.

3. 55*34.86389923—856.6347046 = 1060 — multiplication with the constant for female and addition.

The bigger from two values is closer to the value of the constant for males, therefore the bone belongs to male.

It is possible to create formulas with all the signs and indexes listed above (MCL, LPI, LLI, HCI, MPI, MLI), having in mind the calculated constants.

Discussion

Determination of sex is crucial for any analysis of unidentified human remains, because all techniques of assessment of age and calculation of stature are different for male and females.

Suggested formula could take place in sex determination of individuals by found humeral bones and is of importance in fragment bone findings of the distal humerus.

With the help of Step Discriminant Analysis of signs inclusion in the discriminant functions it is shown the statistical significance of the discrimination of the aggregates. The classification matrices are the percentage of right determined variations by the chosen model.

Classification functions are used exceptionally in creating formulas for sex determination.

The reliability of the suggested formula is more than 95%. It depends on the correct determination of the column axes.

We believe that it could be used in sex determination of skeletal remains and bone fragments and could have applications in archaeology, anatomy, paleontology and forensic medicine.

References

1. H a g e r, L. D. Sex differences in the sciatic notch in great apes and modern humans. – Am. J. Phys. Anthropol., **99**, 1996, 287-300.
2. J u n g e r s, W. L, T. M. C o l e, T. M., D. W. O w s l e y. Multivariate analysis of relative growth in the limb bones of Arikara Indians. – Growth Dev Aging., **52**, 1988, No 2, 103-107.
3. L e e, S. H. Prz. Antropology. – Anthropol. Rev., **64**, 2001, 21-39.
4. M c H e n r y, H. M., R. S. C o r r u c c i n i. Distal humerus in hominoid evolution illus. – Folia primatologica, **23**, 1975, No 3, 227-244.
5. T a g u e, R. G., C. O. L o v e j o y. AL 288-1— Lucy or Lucifer: gender confusion in the Pliocene. – J. Hum. Evol., **35**, 1998, 75-94.

Institute of Experimental Morphology and Anthropology with Museum
Bulgarian Anatomical Society

Acta morphologica et anthropologica, 12
Sofia • 2007

Quantitative Characterization on the Dermatoglyphics of the Fingers and Palms of Male Bulgarians

S. Tornjova-Randelova, P. Borissova, D. Paskova-Topalova

Institute of Experimental Morphology and Anthropology with Museum, Bulgarian Academy of Sciences, Sofia

Finger and palm ridge count for both hands in representative group of 1161 healthy men from 116 settlements in Bulgaria are determined. Computed are: ridge count on each finger, summed finger ridge count on both hands separately, total finger ridge count; ridge count on each interdigital area, summed palm ridge count on both hands separately, total palm ridge count. Descendent formulae about ridge count on fingers and interdigital areas are elaborated. The studied individuals are distributed according to summed finger and summed palm ridge count, and total finger and total palm ridge count too. Correlations between ridge count on single fingers and between ridge count on palm interdigital areas are computed. Highest is the correlation between ridge count on homologous fingers and between ridge count on homologous interdigital areas in right and left hand. Data could be used as norm in clinical and medico-anthropological investigations with theoretical and scientific applied purpose.

Key words: dermatoglyphics, finger ridge count, palm ridge count, correlation dependencies, Bulgarian men.

Introduction

The dermatoglyphic characterization of man is a part of his complete anthropological characteristics. The dermatoglyphic investigations could be differentiated conditionally in two sections: the first covering studies of variability in dermatoglyphic features for healthy populations, and the next investigating the genetic aspects of dermatoglyphics and its application in the clinical practice. It is taken for granted that dermatoglyphic features are determined polygenic but during the early stages of embryogenesis the influence of environmental factors hadn't to be neglected. Dermatoglyphics could be used for the differentiation of inherited and acquired pathology in different diseases. The dermatoglyphic status of healthy population had to be known when the diversions of dermatoglyphic characterization are evaluated in different diseases.

The finger and palm ridge count are quantitative dermatoglyphic features used more rarely than the papillary patterns by themselves. In Bulgaria are available data only about finger and palm ridge counts of healthy persons from Northeast Bulgaria [7] and some data about dermatoglyphic investigations of control groups when studying different diseases [9, 10].

The aim of the present study is to investigate the finger and palm ridge counts on both hands in representative group healthy Bulgarian men.

Material and Methods

Object of the study are the dermatoglyphic prints for both hands of 1161 healthy men from 116 settlements in the country. The digital and palm ridge counts are elaborated after P e n r o s e [5] and H o l t [3] methods. The analysis includes: the digital ridge count on each finger, the summed finger ridge count separately for both hands, the total finger ridge count; the palm ridge count on each interdigital area, the summed palm ridge count separately for both hands and the total palm ridge count for both hands. Correlations between ridge count on the single fingers and between ridge count on the single palm interdigital areas are computed by the coefficient of P e a r s o n [8]. The bilateral differences are evaluated by the t-criterion of Student at $P < 0.05$.

Results and Discussion

Finger ridge count

As it is well known the values of finger ridge count are conditioned by the frequency of model type finger papillary patterns. The highest ridge count corresponds to the whorl patterns (that's why they exert greatest influence to the total finger ridge count), followed by ulnar and radial loops. Highest is the mean ridge count on I-st digit in right (18.44 ± 0.17), and lowest — on II-nd digit in left (10.60 ± 0.20) (Table 1, Fig. 1). The descendent formula is identical for both hands — I>IV>V>III>II. So, the results obtained corresponds to the high frequency of whorls and loops on I-st and IV-th digits and to the high frequency of arches on II-nd digits in right and left hand of the investigated Bulgarian men [6]. The average ridge count is higher on all fingers in right, excepting the III-rd digit by which the difference is 0.11 in favor of left. Statistically significant is the bilateral difference for I-st and II-nd digits ($t = 8.58$ and $t = 4.11$ respectively) while the difference for the rest three fingers is very small. Considerably higher is the mean summed ridge count in right (71.12 ± 0.72) compared with its values in left (67.44 ± 0.71) ($t = 3.64$) (Table 1, Fig. 2). We calculated also the percent distribution of individuals according to the summed ridge count on both hands separately, i.e. whether the ridge count is equal on both hands, or it is higher in favor for right or in favor for left. Equal is the summed ridge count in right and in left for 4.67% of the persons. At 61.22% of the men the summed ridge count is higher in right, and at 34.11% of them it is higher in left. These data are in unison with these published by Holt in 1954 for 254 English males — 3.9%, 63.4% 32.7% respectively [after 3].

T a b l e 1. Statistical parameters of the ridge count on single fingers and Total ridge count in Bulgarian males

Statistics	Right hand						Left hand						Total both hands
	I	II	III	IV	V	I – V	I	II	III	IV	V	I – V	I – X
n	1091	1081	1104	1098	1112	960	1114	1085	1109	1104	1121	990	858
$\bar{x}$	18.44	11.75	11.98	16.03	13.35	71.12	16.38	10.60	12.09	15.69	13.09	67.44	137.84
S	5.60	6.69	5.85	5.50	4.83	22.38	5.79	6.63	5.96	5.54	4.48	22.37	43.55
$S_{\bar{x}}$	0.17	0.20	0.18	0.17	0.15	0.72	0.17	0.20	0.18	0.17	0.13	0.71	1.49
v	30.36	56.95	48.86	34.30	36.17	31.47	35.37	62.54	49.31	35.30	34.26	33.16	31.60
min	0	0	0	0	0	0	0	0	0	0	0	2	4
max	35	30	31	30	25	127	44	29	29	32	27	139	260

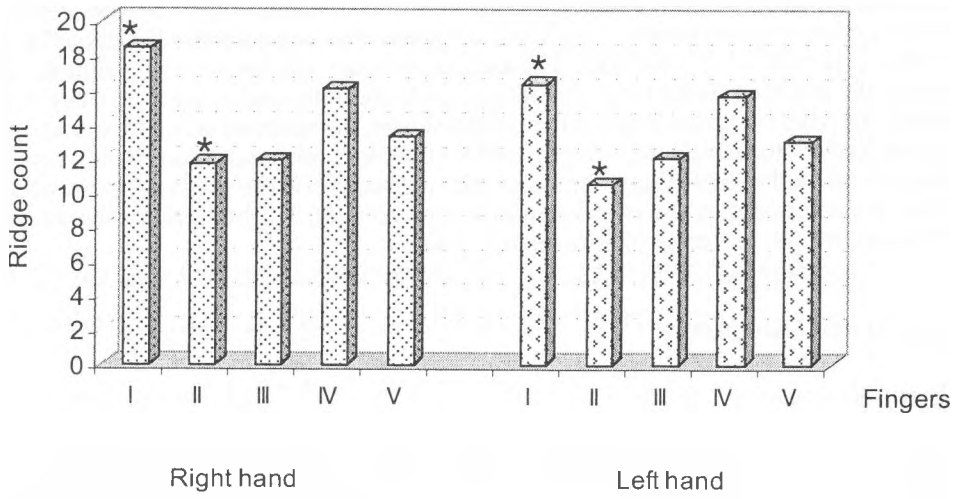

Fig. 1. Ridge count on separate fingers
* — $P < 0.05$

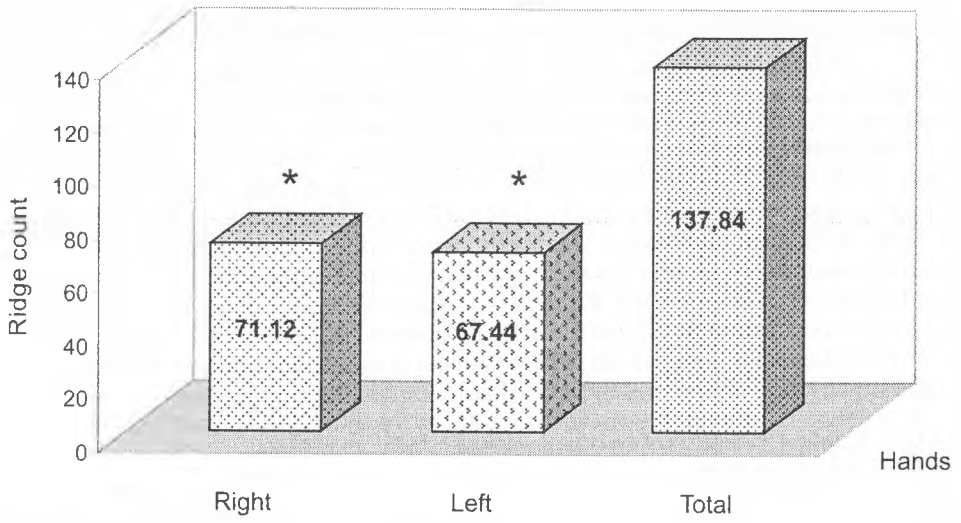

Fig. 2. Fife fingers' ridge count and total ridge count
* — $P < 0.05$

The distribution of individuals according to the summed ridge count from I-st to V-th digits shows that most of the males come into the interval 71 — 80 ridges in right, which coincide with the calculated mean value (x — 71.12 ± 0.72). In left again most are the individuals who have summed ridge count from I-st to V-th digits getting into the interval 71-80, but the average value falls into the former interval 61 — 70 ridges (x — 67.44 ± 0.71). The frequency distribution of summed ridge count is moved in left, or negatively skewed for both hands. The non-normality is better expressed in left hand compared with the right one (Fig. 3).

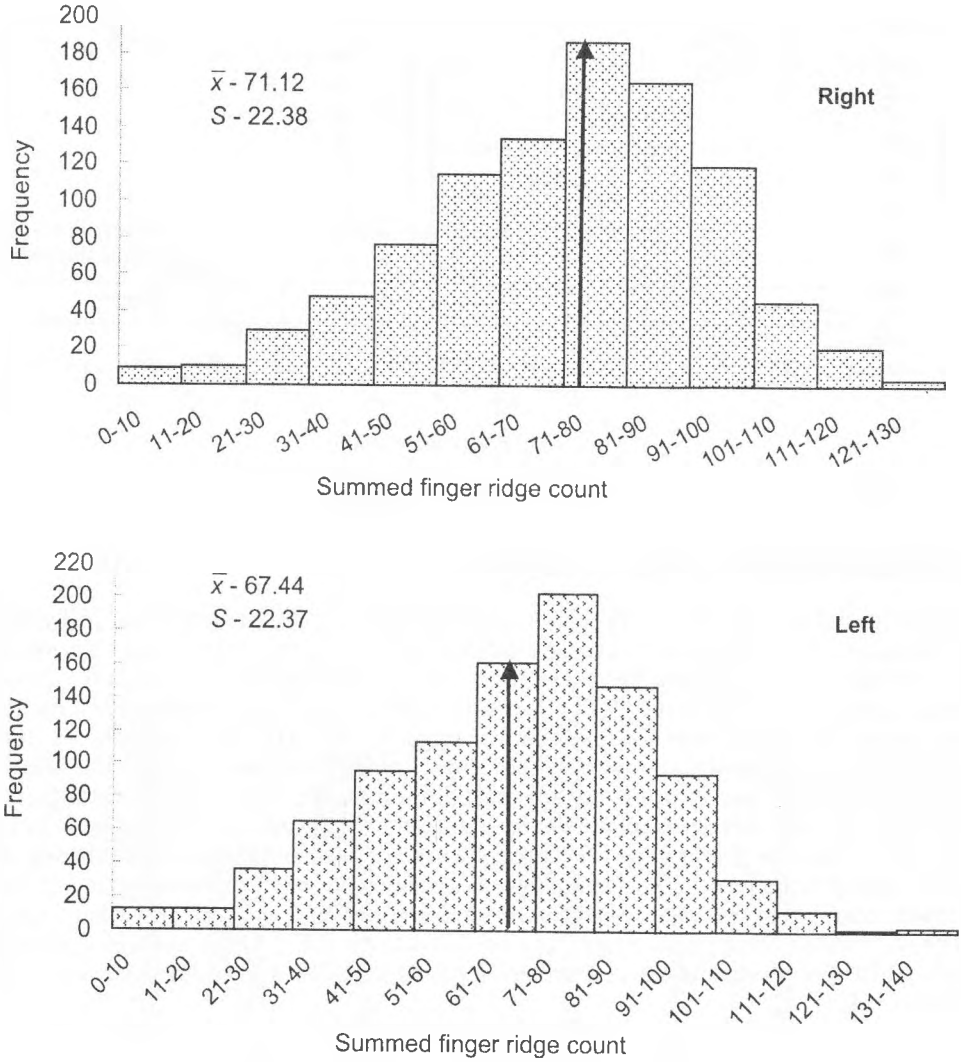

Fig. 3. Distribution of the individuals according to their summed finger ridge count

The obtained total finger ridge count (TFRC) for both hands of the investigated males is 137.84 ± 1.49 (Table 1). The distribution of the individuals according to their TFRC is asymmetrical, moved in left (Fig. 4). This result is probably determined by the distribution of summed ridge count in left hand. Analogical are the results in the investigations of Holt, 1955 for 825 English males [after 3] and Karev, 1979 for 1065 Bulgarian males [8]. The negative skewness in the frequency distribution is accepted by Holt as an indicator for the influence of comparatively small genes number over TFRC determination. In the case when big number of genes has an appreciable effect on the TFRC determination, the curve of frequency distribution had to be similar to the Gaussian one [3].

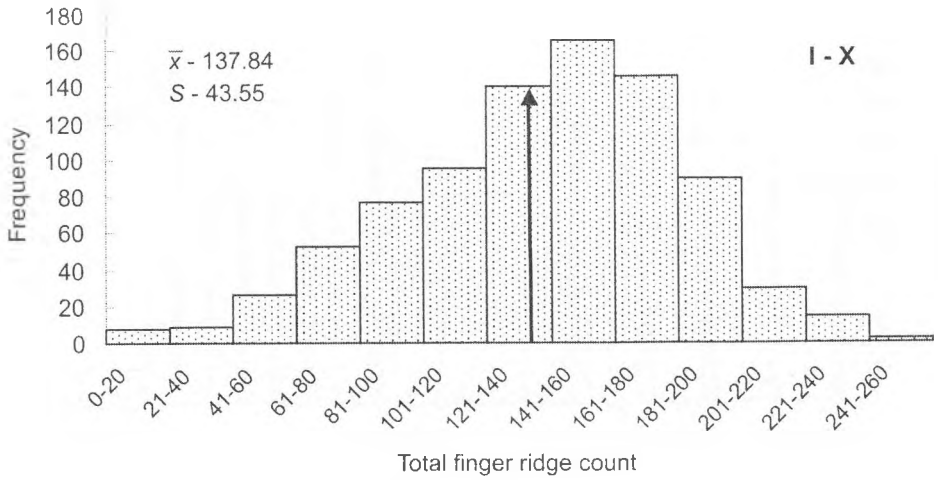

Fig. 4. Distribution of the individuals according to their total finger ridge count

Correlation between ridge count on single digits

The values of correlation coefficients about finger ridge count are presented in Table 2. The highest correlation coefficients are established between the ridge count on homologous fingers in right and left. The correlation coefficients range from $r = 0.725$ for the I-st finger pair to $r = 0.786$ for the IV-th finger pair. High correlation dependence but moderate degree was established for the neighbor finger pair (II-III, III-IV and IV-V). Such dependence was found about the neighbor fingers of the same hand, as well as about the fingers of different hands within the same pair, as for instance, II-nd left — III-rd right, etc. We suppose that the results obtained are in unison with the advanced hypothesis by De W i l d e [1] for the presence of one complete system of finger ridges, which during the early stage of hand formation in embryogenesis period continue from one digit to another. Lowest correlation was established between ridge count on the thumb and other fingers. The correlation coefficients range from $r = 0.364$ to $r = 0.473$. Other authors have published also similar results about correlation dependence between ridge count on single digits [3, 4].

T a b l e 2. Correlation coefficients between the finger ridge counts

Finger		Right					Left				
		I	II	III	IV	V	I	II	III	IV	V
Right	I	1.000	0.453	0.442	0.426	0.473	0.725	0.434	0.428	0.414	0.452
	II	-	1.000	0.657	0.525	0.511	0.435	0.744	0.685	0.552	0.496
	III	-	-	1.000	0.585	0.517	0.401	0.600	0.761	0.600	0.493
	IV	-	-	-	1.000	0.636	0.364	0.503	0.617	0.786	0.626
	V	-	-	-	-	1.000	0.417	0.472	0.516	0.616	0.778
Left	I	-	-	-	-	-	1.000	0.443	0.418	0.379	0.431
	II	-	-	-	-	-	-	1.000	0.655	0.519	0.482
	III	-	-	-	-	-	-	-	1.000	0.656	0.524
	IV	-	-	-	-	-	-	-	-	1.000	0.623
	V	-	-	-	-	-	-	-	-	-	1.000

Palm ridge count

The results about palm ridge count show that biggest is the number of papillary ridges found on II Interdigital Area (IA) (between triradii **a - b**) in both hands, followed after a descendent order by IV IA (**c - d**) and III IA (**b - c**). Higher are the mean values of **a - b** ridge count on left hand in comparison to right one, while the **c - d** ridge count is higher on right hand compared to left one. Both differences are statistically significant ($t = 3.16$ and $t = 5.88$ respectively) (Table 3, Fig. 5).

T a b l e 3. Statistical parameters of the palmar interdigital ridge count and Total ridge count in Bulgarian males

Sta-tis-tics	Right hand				Left hand				Total both hands
	a-b	b-c	c-d	a-d	a-b	b-c	c-d	a-d	a-d
n	1088	1030	1023	978	1111	1025	995	972	885
x	37.29	24.88	34.55	97.03	38.05	24.48	33.02	95.74	193.37
S	5.94	5.55	5.78	13.13	5.62	5.42	6.23	13.28	25.45
Sx	0.18	0.17	0.18	0.42	0.17	0.17	0.20	0.43	0.86
v	15.93	22.30	16.72	13.54	14.77	22.14	18.86	13.87	13.16
min	20	8	13	55	9	8	8	45	100
max	66	46	58	154	60	40	51	141	295

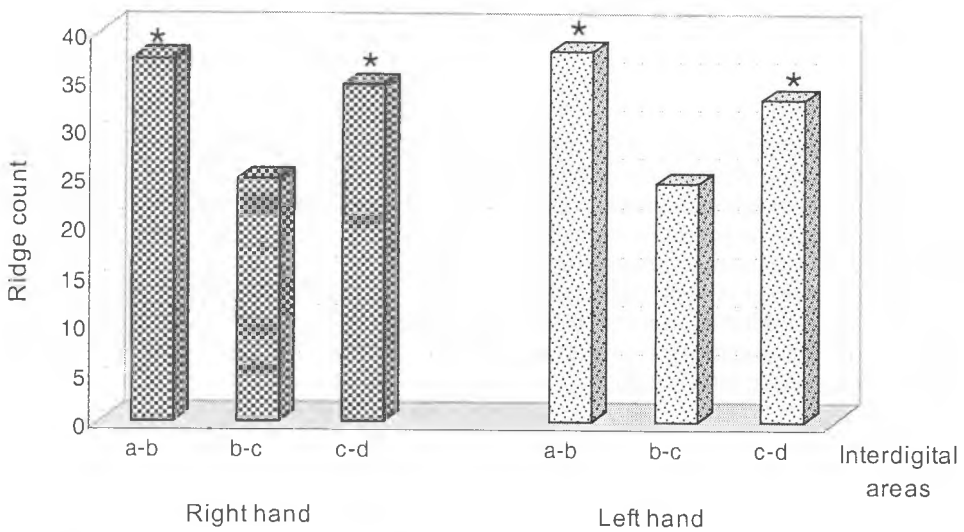

Fig. 5. Palm ridge count on separate interdigital areas
* — $P < 0.05$

Considering the three IA, the summed ridge count **a-d** is higher in right hand (97.03 ± 0.42) than it is in left hand (95.74 ± 0.43) ($t = 2.15$) (Table 3, Fig. 6). The values of summed ridge count range from 55 ridges to 154 ridges in the right hand and from 45 to 141 ridges in the left one. As about finger ridge count, we calculated also the per cent

distribution of individuals who have equal ridge count on both hands, or higher ridge count in favor for right or in favor for left. The summed palm ridge count is higher on the right hand for most of the males (54.01%). Least are the individuals having equal summed ridge count on both hands (6.33%), and 39.66% have higher summed ridge count in left hand.

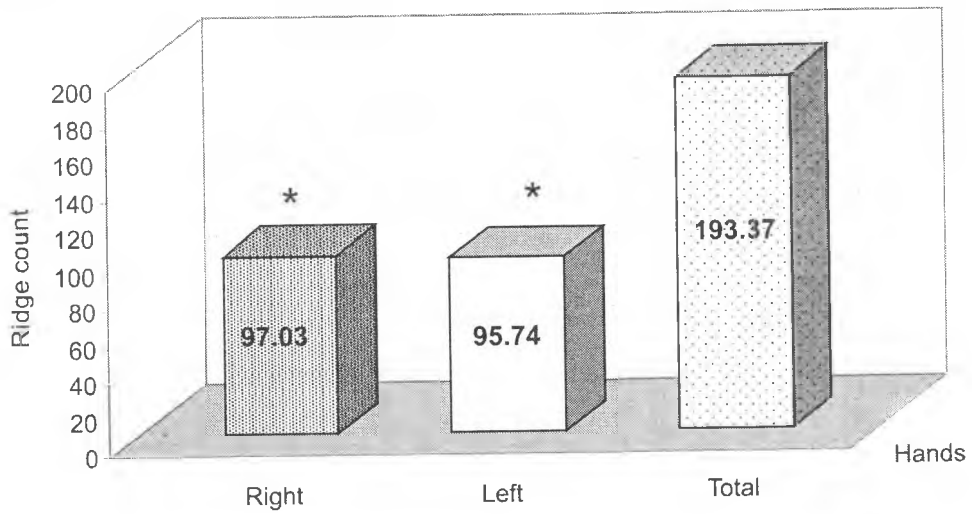

Fig. 6. Palm ridge count on right, left and both hands
* — $P < 0.05$

The distribution of individuals after summed palm ridge count **a-d** shows that most of them have ridge count within the interval 91 — 100 on both hands. These results coincide with the established mean values for both hands. The frequency distribution of the summed palm ridge count is practically symmetrical in contrast to the frequency distribution of the summed finger ridge count (Fig. 7).

The mean value of total palm ridge count (TPRC) for both hands is 193.37 ± 0.86 (Table 3). The established minimal total ridge count is 100, and the maximal is 295. The frequency distribution of the individuals according to their TPRC is almost symmetrical but slightly moved in left (Fig. 8).

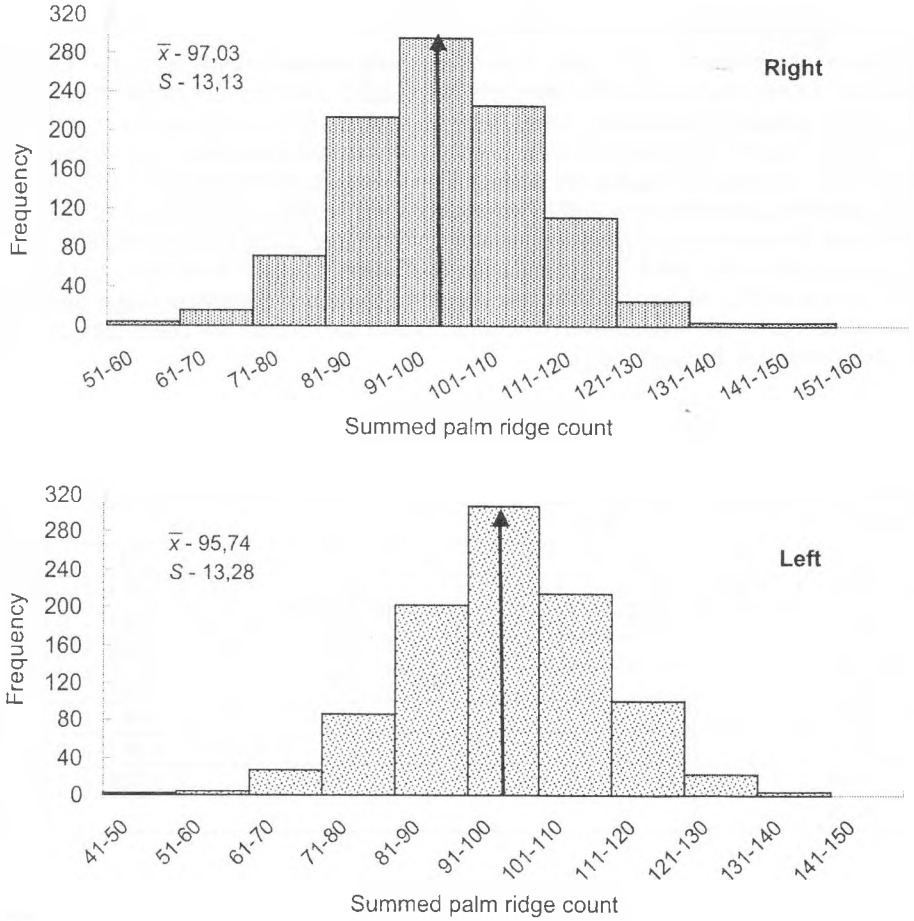

Fig. 7. Distribution of the individuals according to their summed palm ridge count

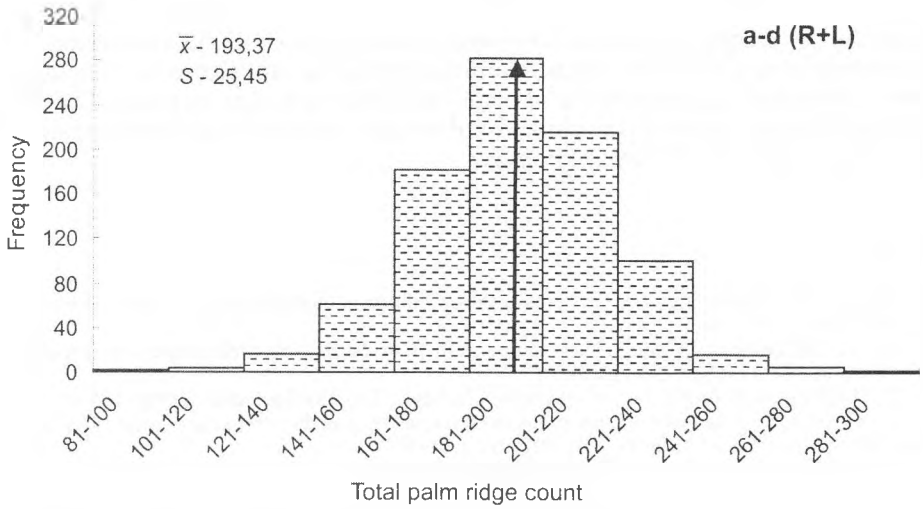

Fig. 8. Distribution of the individuals according to their total palm ridge count

Correlation between ridge count on single interdigital areas

The values of correlation coefficients about palm ridge count are presented in Table 4. Highest are the correlation coefficients between ridge counts on the single interdigital areas and the summed palm ridge count (**a-d**) on same hand, as well as, the correlation coefficients between ridge counts for the homologous interdigital areas on left and right hand (with the exception of **c-d** ridge count). The values range between $r = 0.736$ to $r = 0.852$. Moderate correlation ($\mathbf{r} = 0.688$) was established between **c-d** ridge count for right and left hand. Lowest is the correlation between palm ridge count for the neighbor interdigital areas on the same hand. The correlation coefficients range between $r = 0.314$ to $r = 0.417$. G. Floris and G. M. Sanciu have investigated 116 men of Sardinian origin and have established similar to our correlation dependences and coefficients for the ridge count on interdigital areas **a-b**, **b-c** and **c-d** [2].

Table 4. Correlation coefficients between the palm ridge counts of interdigital areas

Hand		Right				Left			
		a-b	b-c	c-d	a-d	a-b	b-c	c-d	a-d
Right	a–b	1.000	0.391	0.400	0.795	0.744	0.395	0.373	0.647
	b–c	-	1.000	0.314	0.736	0.393	0.759	0.445	0.680
	c–d	-	-	1.000	0.752	0.421	0.305	0.688	0.621
	a–d	-	-	-	1.000	0.688	0.632	0.657	0.852
Left	a–b	-	-	-	-	1.000	0.376	0.417	0.768
	b–c	-	-	-	-	-	1.000	0.397	0.748
	c–d	-	-	-	-	-	-	1.000	0.802
	a–d	-	-	-	-	-	-	-	1.000

Conclusion

The results in the present representative investigation together with the elaborated and published data by us till now for another dermatoglyphic features give notion about the entire morphological characterization of hands' skin relief in Bulgarian males. The data could be used also as a norm in the clinical and medico-anthropological investigations with theoretical and scientific applied purpose.

References

1. De Wilde, A. G. Reflections on ridge systems or the development of glyphologics. – Coll. Anthropol., **6**, 1982, No 2, 111-120.
2. Floris, G., G. M. Sanciu. I conteggi intertriradiali palmari nei Sardi: Nota preliminare. – Antropologia Contemporanea, **12**, 1989, No 1-2, 51-55.
3. Holt, S. The genetics of dermal ridges. – Illinois, Charles C. Thomas, Springfield, 1968. 195 p.
4. Kobyliansky, E., S. Micle. Finger patterns characteristics as determinants of total ridge count variability. – Inter. J. of Anthripol., **1**, 1986, No 1, 49-58.
5. Penrose, L. S. Memorandum on Dermatoglyphic Nomenclature. – Birth Defects Original Article Series, **4**, 1968, No 3, 1-12.

6. Tornjova-Randelova, S., D. Paskova-Topalova. Dermatoglyphics in Bulgarians – Finger Patterns. — Acta Morhol. et Anthropol., **6**, 2001, 137-143.
7. Калинов, К. Статистически методи в поведенческите и социалните науки. С., НБУ, 2001. 445 с.
8. Карев, Г. Нормален дерматоглифски статус на българите от Североизточна България (канд. дис.). София, 1979. 216 с.
9. Сивков, С. Сравнително антропологично проучване на шизофренно болни от гледна точка на невроонтогенетичната хипотеза за шизофренията. (канд. дис.). Пловдив, 2000. 140 с.
10. Торньова-Ранделова, С. Дерматоглифика при здрави деца и деца със зрителна, слухова и интелектуална недостатъчност (канд. дис.). София, 1986. 214 с.

Institute of Experimental Morphology and Anthropology with Museum
Bulgarian Anatomical Society

Acta morphologica et anthropologica, 12
Sofia • 2007

An Anthropological Study of the Skeleton from "A Grave with a Collective Finding of Ornaments in a Pot", Veliki Preslav, Site "Administrative Building"

Y. Yordanov, Br. Dimitrova

Institute of Experimental Morphology and Antropology with Museum, Bulgarian Academy of Sciences, Sofia

We carried out an anthropological research of the skeleton from "A grave with a collective finding of ornaments in a pot", site "Administrative Building", Veliki Preslav. After the pelvis characterization and the skull features, the sex was determined as male. According to the suture ossification, the age of the buried individual can be assigned to the beginning of "maturus" (about 40 years of age). In accordance with the metric and scopic characterizations of the skull, the buried individual belongs to the Europeoid anthropological type.

Key words: anthropology, skull, Middle Ages.

On December 17th 2004 in the Laboratory of Plastic Anthropological Reconstruction at the Institute of Experimental Morphology and Anthropology the bones from a grave with a collective findings of ornaments in a pot, Veliki Preslav, site "Administrative Building" were brought to be investigated. According to data of the archaeologists Georgi Maistorski and Tonka Mihailova the grave is single, i.e. it is not in the framework of a necropolis. Beside the skull to the right a pot is placed in which a number of woman's adornment have been found. This fact has misled the archaeologists to determine the sex of the buried individual as female. The skeleton is orientated to the west with the cranium, and lower limbs to the east. The lower legs and the feet are cut off in the excavation works. The legs a parallel. The body is stretched downwards from the neck. The cervical vertebrae are twisted in a curve to the left. The skull is facing north, i.e. to the left. Underneath and around the skeleton animal bones, an animal tooth and pieces of charcoal are found. The archaeologists date the finding back to 13th-14th century. In the anthropological study carried out mainly by the classical method of R. M a r t i n and K. S a l l e r (1957) [1] the following was established:

Cranial fragments and bones from the post-cranial skeleton of the individual are discovered.

The sex determined after the pelvic profile is male.

The long bones of the limbs are massive, of a well-pronounced relief, i.e. in his life the person has displayed a well-developed musculature. The lengths of the following bones were measured with the aim of calculating the height:

— right femur — 46.3 cm;
— left femur — 46.4 cm;
— right humerus — 32.2 cm;
— left humerus — 31.6 cm;
— right radius — 24.8 cm;
— left radius — 24.6 cm.

The height of the living individual was calculated to have been 175 cm using the Trotter-Gleser formula and after Pearson-Lee it amounted to 166 cm [4].

A thickening of the edges of the bodies of the cervical and thoracal vertebrae together with an emergence of exostoses of the lumbar ones is observed [5].

The handle of the sternum is separated.

After a thorough cleansing and washing of the cranial fragments the skull was restored almost reaching the degree of "cranium" with the skull basis, the zygomatical arches and the right joint protrusion of the mandible are missing. In its characteristics the skull confirms the belonging of the individual to the male sex. According to the degree of ossification of the skull sutures the age was established to have been in the age group of matures (about 40 years).

Of the taken skull measures [2] the length of the mandible proves to be very big; also big are the width of occipital bone, the full facial and the upper face height, the orbital height, nasal height, the length and width of the alveolar arch, the angular width of the mandible; of medium size are the skull length and width, the circumference of the skull taken by glabella, the orbital width, the palatal length , the smallest width of the ramus of the mandible; small are the smallest width of the forehead, the nasal width, the palatal width, the frontal width of the mandible, the height of the ramus of the mandible and the mandibular angle.

According to the calculated indexes the skull is brachycranic, stenometopic, hypsiconchic, leptorrhinic, mesocranic and mesostaphylinic (Table 1).

The vertical skull norm is ovoid. The occipital norm is roof-like and the transition of the bones of the skull vault in profile is smooth. The occipital bone is moderately convex with a strong relief. The mastoid processes are massive, of a very strong relief, pointed forward and inward. The frontal bone is comparatively poorly tilted, low and narrow. The glabella is poorly expressed (degree 2 of the 6-degree scale of P. Broca) and supraorbital arches are of degree 1 after the 4-degree scale of P. Broca [4]. The frontal elevations are very poorly expressed.

The shape of the face is a pentagonal one. The orbits are square-shaped, with smooth angles. The nasal bones are narrow, symmetrical and concave. The shape of the nasal orifice in irregularly heart-like. Its lower end is anthropina. The zygomatical bones are slightly jutting out and moderately to the sides. The canine pit is shallow and of a good relief. The mandible is big, moderately massive, of a very strong relief and of a low bit wide ramus. The chin is triangular on a broad basis and moderately protruding. The bite is a psalydontic one (Figs. 1, 2). The tooth formula is:

$$\frac{87\ \ 54321|12345678}{8\ \ \ 43\ \ |\ 2345\ \ 78}$$

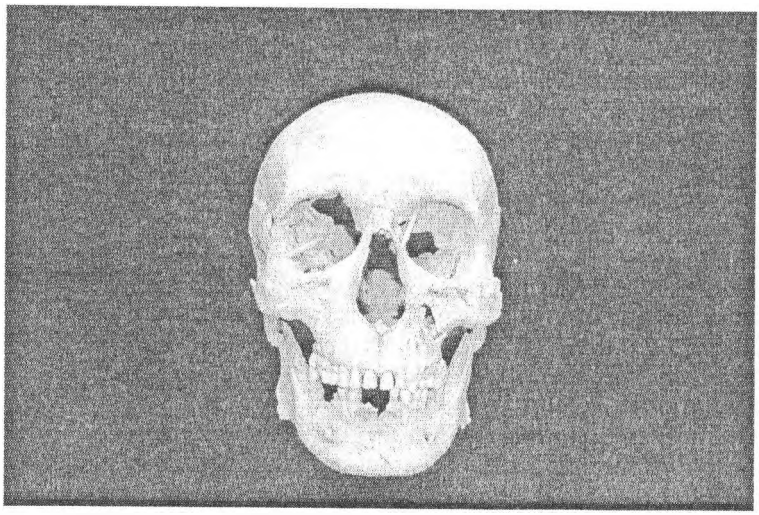

Fig.1. A skull from "A grave with a collective finding of ornaments in a pot", Veliki Preslav, site "Administrative building", 13th — 14th century, male, maturus (about 40 years of age). Norma frontalis

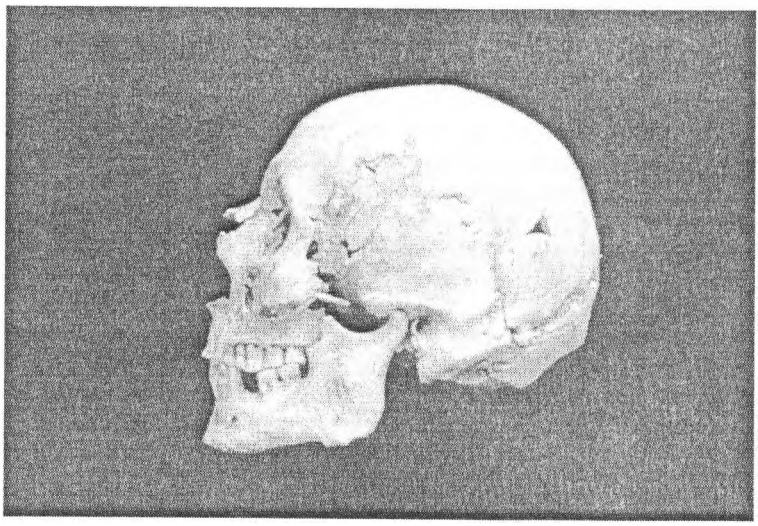

Fig. 2. A skull from "A grave with a collective finding of ornaments in a pot", Veliki Preslav, site "Administrative building", 13th — 14th century, male, maturus (about 40 years of age). Norma lateralis sinistra

Table 1. Metric characterization of the skull from "A grave with a collective finding of ornaments in a pot", Veliki Preslav, site "Administrative Building". Male, Maturus (~ 40)

No	No after Martin	Dimensions	Values	Category
1	1	Skull length	179	average
3	8	Skull width	144	average
4	9	Smallest width of forehead	93	small
5	12	Occiput width	115	large
8	23	Skull circumference throught glabella	522	average
12	47	Full facial height	124	large
13	48	Upper facial height	75	large
14	50	Maxillofrontal width	20	
15	51	Orbital width	42	average
16	52	Orbital height	37	large
17	54	Nasal width	24	small
18	55	Nasal height	56	large
22	60	Alveolar arch length	58	large
23	61	Alveolar arch width	65	large
24	62	Palate length	45	average
25	63	Palate width	37	small
26	66	Mandible angle width	105	large
27	67	Mandible front width	44	small
28	68	Mandible length - projectional	90	very large
30	70	Mandible branch height	56	small
31	71a	Mandible branch smallest width	34	average
36	79	Mandibular angle	111°	small
		Indices		
42	1(8:1)	Skull width-length	80.45	brachycranic
47	13(9:8)	Transverse frontal-sincipital	64.58	stenometopic
51	42(52:51)	Orbital	88.09	hypsiconchic
52	48(54:55)	Nasal	42.86	leptorrhinic
53	54(61:60)	Alveolar	112.07	mesouranic
54	58(63:62)	Palatal	82.22	mesostaphylinic

The first and second lower molars to the right together with the first lower molar and the first upper right molar have been lost in life-time. The crown of the second lower right premolar is completely destroyed from the tooth-decay process in life to the degree of radix. The rest of the missing teeth have fallen out post mortem.

The teeth attrition (abrasio) is strong (degree 3 after A. Zubov) [3]. Periodontal alterations are found on the alveolar projection [5].

Based on a total number of skeletal features it can be asserted with certainty that these skeletal remains belong to a male of the age of "maturus" (about 40 years). The anthropological type is Europeoid. No traits typical of the Mongoloid race have been recorded.

The data from the anthropological study of the bone remains categorically prove the male sex of the buried person. The finds of woman's decoration placed in the pot cannot be interpreted with relation to the sex.

References

1. Martin, R., K. Saller. Lehrbuch der Anthropologie, I-IV. Stuttgart, Gustav-Fischer Verlag, 1957-1966.
2. Алексеев, В., Г. Дебец. Краниометрия. М., Наука, 1964
3. Зубов, А. Одонтология. М., Наука, 1968.
4. Йорданов, Й. Наръчник по антропология. С., УИ „Св. Климент Охридски", 1997.
5. Рохлин, Д. Болезни древних людей. М.-Л., Наука, 1965.

Institute of Experimental Morphology and Anthropology with Museum
Bulgarian Anatomical Society

Acta morphologica et anthropologica, 12
Sofia • 2007

Computed Tomographic Features of Feline Prostate Gland

*R. Dimitrov, Y. Toneva**

Department of Veterinary Anatomy, Histology and Embryology
Faculty of Veterinary Medicine, Trakia University, Stara Zagora, Bulgaria
**Department of Physics, Biophysics, Roentgenology and Radiology,*
Faculty of Medicine, Trakia University, Stara Zagora, Bulgaria

The aim of the present study was to determine some anatomo-topographic features of feline prostate gland using computerized axial tomography (CAT). The study was performed in 7 sexually mature European shorthair male cats at the age of 1-2 years weighing 2.8-4.0 kg, anaesthetized prior to the examination. The positive contrast material (Ultravist 300) was applied via both the venous and the urethral routes. The study was performed with a TOMOSCAN-CX/Q scanner. The pelvis was transversally cut between the L6 lumbar segment and the pelvic arc. The distance between CT scanograms and the thickness of cross-section was 2 mm. The feline prostate was visualized dorsally in the section between the 1st and the 2nd coccygeal vertebrae, laterally in the section of hip joints and femoral diaphyses and caudally to the cranial branch of pubic bones. Three glandular dimensions were determined: length, width and height. Feline prostate gland is an oval, homogenous, relatively hyperdense structure with the radiodensity of soft tissue (from 43 HU in native scans to 54 HU with contrast enhancement).

Key words: tomcat, prostate, computed tomography.

Introduction

Feline prostate gland is situated far behind the urinary bladder. The species-specific long preprostatic urethra is located over the anterior symphyseal rim. The gland is situated behind the cranial border of pelvic symphysis under the ventral wall of the rectum. Both glandular lobes embrace the prostatic urethra dorsolaterally and are separated by a dorsomedian sulcus [6].

Initially, a computed tomographic study of healthy prostate was performed in human male [12, 13]. In men, the gland appeared as a homogenous oval structure with a radiodensity similar to that of soft tissue, length of 2-4 cm, located behind the pelvic symphysis just under the rectum. Via CT, the prostate is well visualized and its three dimensions could be precisely determined. In 30-year-old men, the craniocaudal diameter of the gland (length) was 3 cm, the anterior-posterior (height) – 2.3 cm and the lateral (width) – 3.1 cm.

Human prostate is visualized on CT as a homogenous, oval, infravesical soft tissue structure whose dimensions increased with age. Its height increased from 2.5 to 3 cm and

the length and width – from 3 to 5 cm. Its soft tissue radiodensity was between 40 and 65 HU [14].

M i r o w i t z and H a m m e r m a n [9] performed a CT depiction of zonal anatomy of human prostate by dividing it into peripheral zone and central zone.

O z d e m i r et al. [10] performed a CT study of human prostate gland on the distance between: anterior and posterior glandular surface, the base and the apex, left and right surface, anterior surface and symphysis, posterior surface and rectum.

M i l o s e v i c et al. [8] reported the CT localization of prostatic apex in men and comparing it to the topography obtained via magnetic resonance imaging and urethrography, they observed differences in apex visualization depending on method used.

H u g u e t [5] and R o r v i k [11] studied the normal male pelvis and the prostate gland via magnetic resonance imaging and computed tomography, suggestign that MR imaging was more accurate than CT.

Mc L a u g h l i n [7] used computed tomography and MRI for male prostate visualization, determining three glandular zones: internal, external and anterior fibromuscular.

E v e l y n et al. [3] achieved a precise imaging of prostate in men using computed tomography, MRI and three-dimensional ultrasonography.

In a CT and ultrasonographic study, A t a l a n et al. [1] determined the length of prostate gland in the dog and its ratio vs the distance from the sacral promontory to the pelvic symphysis. A prostate length > 70% of this distance was assessed as enlarged and < 70% as normal.

The insufficient literature data referring to CT imaging of normal prostate gland in domestic carnivores, especially in cats, motivated our study. Our results could be used as reference data in the diagnostic imaging and the differentiation between normal and pathologic feline prostate glands.

Material and Methods

Seven sexually mature, male European shorthair cats at the age of 1–2 years, weighing 2.8–4 kg were studied. Prior to the investigation, the image intactness of the prostate glands was evidenced via ultrasonography.

The animals were anaesthetized with 0.03 mg/kg atropine sulfate s.c. (Atropinum sulfuricum, Sopharma), followed by 2 mg/kg xylazine i.m. (Alfazan) after 15 min and 15 mg/kg ketamine (Alfazan) i.m. after another 15 min [2].

In two cats, the CT study was done without contrast enhancement whereas in the other, a positive contrast material (Ultravist, Schering, Germany, 300 mg I/ml) was applied slowly intravenously at a dose of 3 ml/kg.

The urinary bladder was catheterized for the intraurethral application of contrast (1 ml/kg) and 3 ml/kg isotonic physiological saline (Natrii Chloridum 0.9%, Balkanpharma).

The study was done using an axial computer tomograph TOMOSCAN — CX/Q with a table height of 149 cm and FOV = 250. The scan time was 4.5 s, filter 1, 120 kV anode power and a 100 mA current. A high resolution mode and CT index of 0.5 were used.

The animals were positioned in dorsal recumbency.

In the computed tomography study, the pelvis was cut transversally from the L6 lumbar segment and the pelvic arc with section thickness of 2 mm.

Some of obtained images are presented.

Results and Discussion

The topography of feline prostate was determined using the following bone markers: the respective vertebra (dorsally), the hip joints (laterally) and the pelvic symphysis (ventrally).

The CT transverse image of feline pelvis, scanned through the third sacral vertebrae (Fig. 1, S3 level), depicts the cranial parts of hip joints and the pelvic brim that ventromedially is scarcely detectable (cranially, it is completely visualized). The non-contrasted preprostatic urethra is observed dorsomedially to the anterior border of the symphysis, ventromedially to the hip joints and ventrally to the rectum. Its lumen was hypodense, and the wall – relatively hyperdense and homogenous. The image of Fig. 1 allowed us to assume that the CT localization of feline preprostatic urethra was in the transverse plane through the third sacral vertebra, the cranial parts of hip joints and the anterior border of the symphysis.

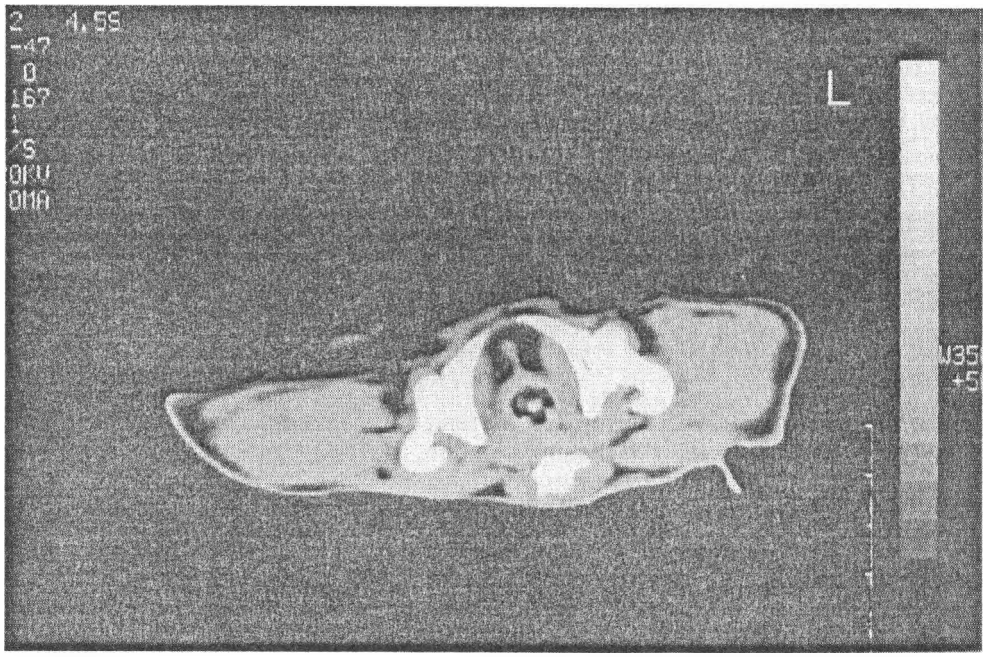

Fig. 1. Transverse CT image of feline pelvis through the 3rd sacral vertebra (section thickness 2 mm)

Fig. 2 (at the level of C1) depicts the image of cranial parts of the prostate, evident by the thickened urethral wall ventrally, laterally and especially dorsolaterally under the rectum. The lumen of prostatic urethra was contrasted (hyperdense) and prostatic areas were relatively hypodense compared to urethral and rectal walls. The gland was well differentiated from the adjacent soft tissues. The feline prostate image appeared from scanning in the transverse plane passing through the first coccygeal vertebra and proximal femoral diaphyses and caudodorsally to the cranial branch of pubic bones.

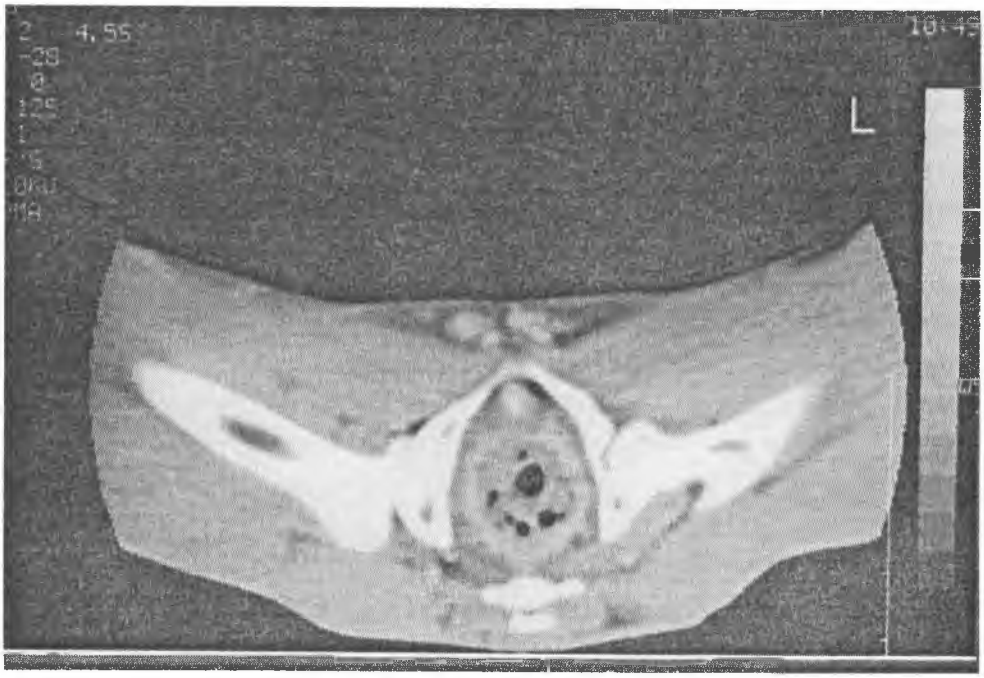

Fig. 2. Transverse CT image of feline pelvis through the 1st coccygeal vertebra (section thickness 2 mm)

The complete CT image of prostate is shown in Fig. 3 (at the level of C1-C2) where the lumen of prostatic urethra was also contrasted (hyperdense) and glandular lobes were visulaized dorsolaterally to the urethra under the ventral rectal wall, that is hyperdense than the prostate itself. The feline gland is a oval, homogenous and relatively hyperdense structure on the background of adjacent soft tissues (with the exception of urethral and rectal walls). It is observed during the transverse scanning of the pelvis between the 1st and the 2nd coccygeal vertebrae (dorsally), the hip joints with femoral diaphyses (laterally) and caudally to the cranial branch of pubic bones. Its margins are adequately distinguished from adjacent soft tissue structures.

The radiodensity of feline prostate is a soft tissue one (43 HU — native and up to 54 HU — wit contrast enhancement). The gland width (lateral dimension) is 9,7 mm, the height (dorsoventral) — 3.1 mm (Fig. 3) and the length (craniocaudal) — 8 mm.

Caudally, the scan between 2nd and 3rd coccygeal vertebrae, the caudal parts of hip joints and over the caudal parts of pubic bones, the initial part of membranous urethra is observed. Its lumen is contrasted (hyperdense) and its wall — comparatively thinned (Fig. 4). At this level, there is no image of the prostate.

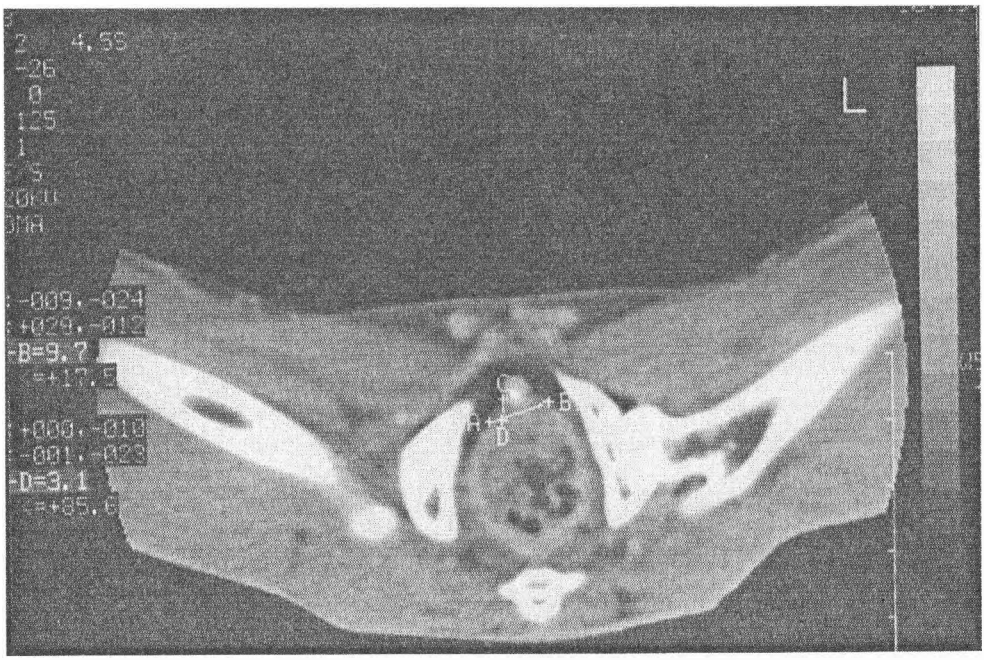

Fig. 3. Transverse CT image of feline pelvis between the 1st and the 2nd coccygeal vertebrae (section thickness 2 mm)

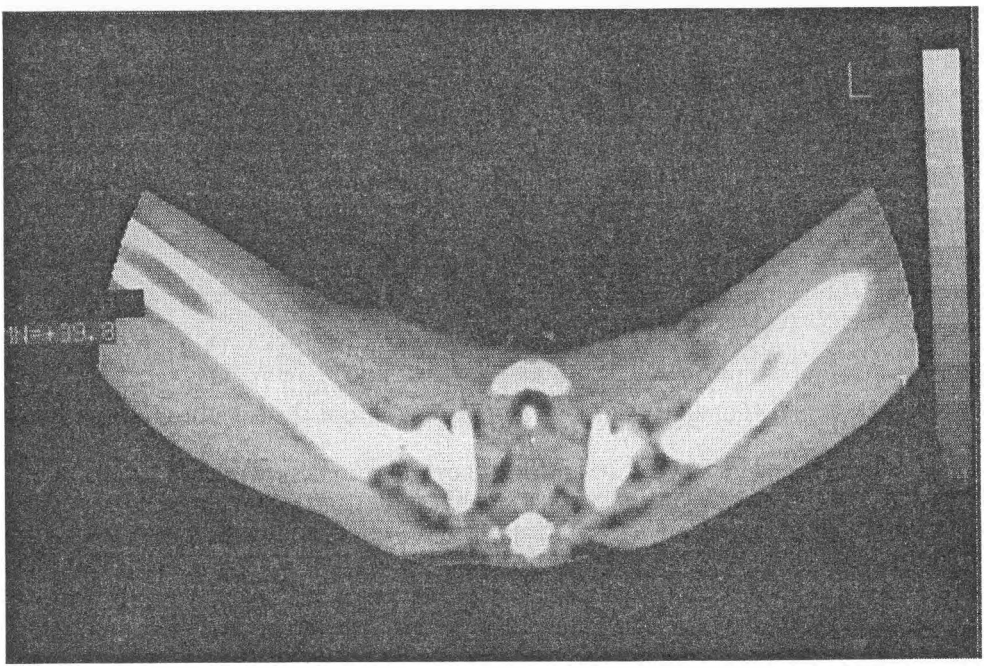

Fig. 4. Transverse CT image of feline pelvis between the 2nd and the 3rd coccygeal vertebrae (section thickness 2 mm)

The soft tissue density of feline prostate gland is similar to that in men [14]. Unlike men, however [7, 9], no glandular zones are present on CT images of male cats.

The glandular dimensions are not analogous to those of human prostate because of the size of the studied species itself [10].

Unlike human prostate [8], feline prostate lacks an apex and such a finding is not observed.

Compared to Atalan [1], who defined the length of the gland in dogs and its ratio to pelvic height, we present the three dimensions of prostate — width, height and length.

Conclusions

The CT image of feline prostate appears during the scanning in the transverse plane through the first coccygeal vertebra, the hip joints with the proximal femoral diaphyses and caudodorsally to the cranial branch of pubic bones.

An entire image of prostate is seen during the transverse scan of the pelvis between 1st and 2nd coccygeal vertebrae (dorsally), the hip joints with femoral diaphyses (laterally) and caudally to the cranial branch of pubic bones.

Feline prostate gland is an oval, homogenous, relatively hyperdense structure with the radiodensity of soft tissue (from 43 HU in native scans to 54 HU with contrast enhancement), visulaized dorsolaterally to the prostatic urethra under the ventral rectal wall and well differentiated from the adjacent soft tissues in the pelvis.

The gland width (lateral dimension) was 9.7 mm, the height (dorsoventral) — 3.1 mm (Fig. 4) and the length (craniocaudal) — 8 mm.

At scan of pelvis in the planes through the 3rd sacral vertebra and the 2nd and the 3rd coccygeal vertebra, the prostate gland is not visualized.

References

1. Atalan, G., F. Barr, P. Holt. Comparison of ultrasonographic and radiographic measurements of canine prostate dimensions. – Vet. Radiol.Ultrasound, **40**, 1999, No 4, 408-412.
2. Dinev, D., B. Aminkov. Veterinary Anaesthesiology, Stara Zagora, 1999. 117 p.
3. Evelin, A., Wei Chen, S. Wesarg. Registration of 3D U/S and CT images of the Prostate. – In: CARS (Ed. Lemke, M., K. Vannier, A. Inamura, G. Farman, K. Doj & J. Reiber). Germany, Plenium Pres, 2002, 156-163.
4. Hans Henrik, H. The history of interstitial brachytherapy of the prostatic cancer. – In: Seminar in Surgical Oncology, **13**, 1998, No 6, 431-437.
5. Huguet Panella, M. Magnetic resonance of the male pelvis. – Arch. Esp. Urol., **54**, 2001, No 6, 511-518.
6. McClure, R., M. Dallman, P. H. Garret. – In: Cat Anatomy. Philadelphia, Lea & Febiger, 1973, 158-162.
7. McLaughlin, P., S. Troyer, S. Berri, V. Narayana, A. Meirowitz, P. Roberson, J. Montie. Functional anatomyof the prostate: Implications for treatment planning. - International Journal of Radiation Oncology Biology Physics, **36**, 2005, 128-135.
8. Milosevic, M., S. Voruganti, R. Blend, H. Alasti, P. Warde, M. McLean, P. Catton, C. Catton, M. Gospodarowicz. Magnetic resonance imaging (MRI) for localization of the prostatic apex: comparison to computed tomography (CT) and urethrography. – Radiother. Oncol., **47**, 1998, No 3, 277-284.
9. Mirowitz, S., A. Hammerman. CT depiction of prostatic zonal anatomy. – J. Comput. Assist. Tomogr., **16**, 1992, No 3, 439-441.

10. O z d e m i r, B., H. S u r u c u, A. O t o, H. C e l i c. Anatomy of the prostate examined by CT imaging of 100 patient. – In: BACA/SAE. Plenium Pres, Barcelona, 2002, 95-99.
11. R o r v i k, J., S. H a u k a a s. Magnetic resonance imaging of the prostate. – Curr. Opin. Urol., **11**, 2001, No 2, 181-188.
12. T h o e n i, R. Computed tomography of the pelvis. – In: Computed Tomography of the Body. (Ed. A. Moss, G. Gamsu, K. Genand). San Francisco, W. B. Saunders Company, 1983, 987-993.
13. Van E n g e l s h o v e n, J., L. K r e e l. Computed tomography of the prostate. – J. Comput. Assist. Tomogr., 3, 1979, No 1, 45-51.
14. W e g e n e r, H. The Prostata. – In: Whole Body Computed Tomography. Philadelphia, W. B Saunders Company, Second Edition, 1996, 425-430.

Institute of Experimental Morphology and Anthropology with Museum
Bulgarian Anatomical Society

Acta morphologica et anthropologica, 12
Sofia • 2007

Basic Anthropometric Characteristics of Wrist Bones in the Wrist Joint Complex with Os Lunatum Types I and II

S. Dyankova, G. Marinov

Department of Anatomy, Histology and Embryology,
Varna Medical University "Prof. Dr Paraskev Stoyanov", Varna, Bulgaria

The aim of the present study is to determine the possible differences in the anthropometric characteristics of the wrist bones when they articulate in the wrist joint complex with os lunatum type I, or type II. Thirty six sets of macerated bones were studied scopically and anthropometrically after Martin, Saller (1957). 936 measurements were taken and 864 indices were calculated separately for wrist bones with os lunatum type I and type II. Wrist bones in the wrists with the lunate bone type II are bigger than those with type I. The enlargement for the proximal wrist row is mainly in proximo-distal direction, and for the distal wrist row — mainly in dorso-volar direction. The differences between the wrists with os lunatum types I and II show that there are two types wrist joint complexes: with and without hamate-lunate joint. They also differ from each other anthropometrically which also affects their biomechanics.

Key words: anthropometry, wrist bones, os lunatum, types.

Introduction

The variations of the anthropometric characteristics of the wrist bones are of great interest for the explanation of the complicated biomechanics [2, 17] of the wrist joint complex [7, 9, 11, 14]. In the last decade special attention is given to the variations of the lunate bone. This is due to its central position within the wrist joint complex. For this reason the lunate bone is often described as a "nucleus of the wrist joint" [6] or as a "key to a Roman arch" [13].

It is well known that the lunate bone has two main types — os lunatum type I and os lunatum type II [15]. In the literature there are great differences in the occurrence ratios between type I and type II os lunatum [15] — from 27:73 to 50:50 [5, 12, 16]. However, in the literature there is no data if the variations in the anthropometric characteristics of the lunate bone type I and type II correlates with the variations of the anthropometric characteristics of the other wrist bones. The research on this problem is important for the distinction of the biomechanics in the wrist joint complexes with different types of the lunate bones. The complexity of the problem deepens because of the fact that every main type of os lunatum has two corresponding sub-types [5], thus greatly enhancing the possible variations of the wrist bones.

The aim of the present study is to determine the possible differences in the anthropometric characteristics of the wrist bones when they articulate in the wrist joint complex with os lunatum type I, or os lunatum type II.

Material and Methods

Thirty six sets of macerated wrist bones form the collection of the Department of Anatomy, Histology and Embryology, Varna Medical University "Prof. Dr Paraskev Stoyanov", Varna, Bulgaria were studied following all the ethical rules of work on cadaver material. The type of os lunatum was determined scopically according the V i e g a s et al. (1990) [15] classification using magnifying glass (×3). The scopical observation of the lunate bone revealed that 16 out of 36 wrist bone sets had os lunatum type I, and 20 had type II.

Anthropometrical examination. The anthropometrical measurement included the basic anthropometric characteristics of the wrist bones — length, width and height. All the wrist bones were measured anthropometrically by the method of M a r t i n and S a l l e r (1957) [10] by using calliper-gauge with possible variation of up to 0.1 mm as follow: the length was measured in proximo-distal direction, the width — in radio-ulnar direction and the height — in dorso-volar direction. Totally 936 linear measurements were taken. In addition 864 indices were calculated, separately for the wrist bones from the wrists with the lunate bone type I and for the wrist bones from the wrists with the lunate bone type II.

Statistical analysis. The data was analyzed in Microsoft Office Excel 2000. The following statistical methods were used:

- Analysis of variance
- Nonparametric analysis (Pearson × 2)

The statistically significant differences were evaluated by the Student's t-test. The level of significance was accepted at $p<0.05$.

Results and Discussion

The anthropometrical measurements revealed that the basic metrical characteristics of the wrists with the lunate bone type I and type II differ (Tables 1-8).

The basic anthropometrical measurements of the scaphoid bone of the wrists with the lunate bone type II are greater than the same measurements of types I. The bone is greater in proximo-distal direction and in radio-ulnar direction. Index 1 is greater and indices 2 and 3 are smaller (Table 1).

T a b l e 1. Basic metrical characteristics and indices of os scaphoideum

Indicators and indices after Martin, Saller (1957)	No	Mean and standard error in the wrists with	
		os lunatum type I (n=16)	os lunatum type II (n=20)
Greatest length of os scaphoideum	1	24.63 ± 0.61	**26.42 ± 0.64***
Width of os scaphoideum	2	14.7 ± 0.40	**15.82 ± 0.49***
Greatest width of os scaphoideum	2a	15.96 ± 0.39	**17.01 ± 0.49**
Height of os scaphoideum	3	10.51 ± 0.27	**10.63 ± 0.39**
Greatest height of os scaphoideum	3a	13.13± 0.40	**13.98± 0.43**
Index length - width of os scaphoideum	1	59.78 ± 1.17	**60.11 ± 1.71**
Index length - height of os scaphoideum	2	**43.07 ± 1.56**	40.46 ± 1.43
Index height - width of os scaphoideum	3	**72.10 ± 2.37**	67.88 ± 2.53

*$p<0.05$

The basic anthropometrical measurements of the lunate bone type II are greater than the same measurements of types I. The bone is longer in proximo-distal, wider in radio-ulnar and higher in dorso-volar direction. Indices 1, 2 and 3 are greater (Table 2).

Table 2. Basic metrical characteristics and indices of os lunatum

Indicators and indices after Martin, Saller (1957)	No	Mean and standard error in the wrists with	
		os lunatum type I (n=16)	os lunatum type II (n=20)
Length of os lunatum	1	15.29 ± 0.48	**16.71 ± 0.40****
Greatest width of os lunatum	2	12.96±0.43	**14.21±0.38*****
Greatest height of os lunatum	3	16.53±0.42	**17.91±0.35*****
Index length - width of os lunatum	1	84.90±1.59	**85.16±1.46**
Index height - length of os lunatum	2	92.58±1.82	**93.27±1.19**
Index height - width of os lunatum	3	78.53±2.09	**79.31±1.38**

**p<0.025; ***p<0.0125

The basic anthropometrical measurements of the triquetral bone of the wrists with the lunate bone type II are greater than the same measurements of types I except indicator No. 3 "Greatest height of os triquetrum", which is the same with the corresponding size on wrists with the lunate bone type I. The bone is wider in radio-ulnar direction and longer in proximo-distal direction. Index 2 is greater and indices 1 and 3 are smaller (Table 3).

Table 3. Basic metrical characteristics and indices of os triquetrum

Indicators and indices after Martin, Saller (1957)	No	Mean and standard error in the wrists with	
		os lunatum type I (n=16)	os lunatum type II (n=20)
Greatest length of os triquetrum	1	17.19 ± 0.46	**17.86 ± 0.43**
Greatest width of os triquetrum	2	12.89 ± 0.38	**13.95 ± 0.44***
Greatest height of os triquetrum	3	**14.22 ± 0.45**	**14.22 ± 0.29**
Index width - length of os triquetrum	1	**134.15±3.39**	129.5±3.62
Index height - length of os triquetrum	2	121.70±2.86	**126.23±3.21**
Index width - height of os triquetrum	3	**110.59±2.51**	103.03±2.43

*p<0.05

Two lineal parameters of os pisiforme in the wrists with the lunate bone type II are greater than the same measurements of types I. The bone is higher in dorso-volar direction and longer in proximo-distal direction. Index 1 is greater and indices 2 and 3 are smaller (Table 4).

Table 4. Basic metrical characteristics and indices of os pisiforme

Indicators and indices after Martin, Saller (1957)	No	Mean and standard error in the wrists with	
		os lunatum type I (n=16)	os lunatum type II (n=20)
Greatest length of os pisiforme	1	13.94 ± 0.50	**14.2 ± 0.52**
Greatest width of os pisiforme	2	**10.18 ± 0.42**	9.85 ± 0.29
Greatest height of os pisiforme	3	9.8 ± 0.33	**10.43 ± 0.28**
Index width - length of os pisiforme	1	138.23±3.86	**144.23±2.61**
Index height - length of os pisiforme	2	**142.92±4.34**	136.09±3.21
Index width - height of os pisiforme	3	97.97±3.99	**106.80±2.63**

The basic anthropometrical measurements of os trapezium in the wrists with the lunate bone type II are greater than the same measurements of types I. The bone is bigger in all directions, but biggest in dorso-volar direction. Indices 1 and 3 are greater and index 2 is smaller (Table 5).

Table 5. Basic metrical characteristics and indices of os trapezium

Indicators and indices after Martin, Saller (1957)	No	Mean and standard error in the wrists with	
		os lunatum type I (n=16)	os lunatum type II (n=20)
Greatest length of os trapezium	1	15.4±0.38	**16.56±0.39****
Greatest width of os trapezium	2	20.27 ± 0.37	**21.28 ± 0.40***
Greatest height of os trapezium	3	15.46 ± 0.46	**16.86 ± 0.52***
Index width - length of os trapezium	1	76.02±1.41	**78.12±1.88**
Index height - length of os trapezium	2	**100.34±2.60**	99.01±2.23
Index width - height of os trapezium	3	76.53±2.54	**79.33±1.02**

*p<0.05; **p<0.025

The basic anthropometrical measurements of os trapezoideum of the wrists with the lunate bone type II are greater than the same measurements of types I. The bone is bigger in all directions, but biggest in dorso-volar direction. Indices 1 and 2 are greater and index 3 is smaller (Table 6).

Table 6. Basic metrical characteristics and indices of os trapezoideum

Indicators and indices after Martin, Saller (1957)	No	Mean and standard error in the wrists with	
		os lunatum type I (n=16)	os lunatum type II (n=20)
Greatest length of os trapezoideum	1	11.51±0.39	**12.74±0.47***
Greatest width of os trapezoideum	2	13.89±0.31	**15.12±0.32****
Greatest height of os trapezoideum	3	16.11±0.3	**17.67±0.29*****
Index width - length of os trapezoideum	1	83.11 ± 2.60	**85.05 ± 3.82**
Index height - length of os trapezoideum	2	71.40 ± 1.72	**72.18 ± 2.31**
Index height - width of os trapezoideum	3	**86.30 ± 1.43**	85.74 ± 1.28

*p<0.05; **p<0.0125; ***p<0.0025

The basic anthropometrical measurements of os capitatum of the wrists with the lunate bone type II are greater than the same measurements of types I. The bone is bigger in all directions, but biggest in dorso-volar direction. Indices 4, 5 and 6 are greater (Table 7).

Table 7. Basic metrical characteristics and indices of os capitatum

Indicators and indices after Martin, Saller (1957)	No	Mean and standard error in the wrists with	
		os lunatum type I (n=16)	os lunatum type II (n=20)
Greatest length of os capitatum	1	21.99 ± 0.43	**23.06 ± 0.43***
Greatest width of os capitatum	2	13.82 ± 0.28	**15.0 ± 0.45****
Greatest height of os capitatum	3	18.44± 0.33	**19.63± 0.43****
Index length - width of os capitatum	4	63.06 ± 1.32	**64.94 ± 1.38**
Index length - height of os capitatum	5	84.07 ± 1.44	**85.17 ± 1.20**
Index height — width of os capitatum	6	75.28 ± 1.90	**76.51 ± 1.96**

*p<0.05; **p<0.025

The basic anthropometrical measurements of os hamatum of the wrists with the lunate bone type II are greater than the same measurements of types I. The bone is bigger in all directions, but biggest in dorso-volar and radio-ulnar direction. Indices 1 and 3 are greater and index 2 is smaller (Table 8).

Table 8. Basic metrical characteristics and indices of os hamatum

Indicators and indices after Martin, Saller (1957)	No	Mean and standard error in the wrists with	
		os lunatum type I (n=16)	os lunatum type II (n=20)
Greatest length of os hamatum	1	20.79±0.59	**21.52 ± 0.46**
Greatest width of os hamatum	2	14.82±0.24	**16.4±0.39*** **
Greatest height of os hamatum	3	20.88±0.40	**23±0.43*** **
Index length - width of os hamatum	1	71.91 ± 1.76	**76.63 ± 2.05**
Index height - length of os hamatum	2	**99.46 ± 1.60**	93.88 ± 1.99
Index height - width of os hamatum	3	71.22 ± 1.30	**71.27 ± 0.95**

***p<0.0025

In conclusion our data present that:

1. Wrist bones of the lunate bone type II:

A. The basic anthropometrical measurements of the wrist bones are greater except indicator No 3 "Greatest height of os triquetrum", which is the same with the corresponding size on wrists with the lunate bone type I and indicator "Greatest width of os pisiforme" which is greater in wrists with the lunate bone type I.

B. Differences in the measurements in "A" are in the following directions:

— In os scaphoideum — mainly in proximal — distal and radio — ulnar direction;
— In os lunatum is greater in all direction;
— In os triquetrum — mainly in radio — ulnar and proximal — distal direction;
— In os pisiforme — mainly in dorso-volar and proximal — distal direction;
— In os trapezium — mainly in dorso-volar and proximal — distal direction;
— In os trapezoideum — mainly in dorso-volar direction;
— In os capitatum - mainly in dorso-volar and radio — ulnar direction;
— In os hamatum- mainly in dorso-volar and radio — ulnar direction.

2. The significant anthropometric differences of the wrist bones according to the type of os lunatum in the corresponding wrist joint complex give us the reason to distinguish them in two types:

— with lunate-hamate joint;
— without lunate-hamate joint.

Each type has a specific biomechanics and therefore a specific pathology.

The enlargement of the wrist bones of the wrists with os lunatum type II for the proximal wrist row is mainly in proximo-distal direction, and for the distal wrist row — mainly in dorso-volar direction.

The anthropometric differences between the wrists with os lunatum types I and II show that all the wrist bones with the presence of hamato-lunate joint are larger than those without it. This fact is very important, because these differences can affect the biomechanics, as well as pathology of the wrist bones and the wrist joints. Because of this the future examinations of the differences in the wrist joints with os lunatum types I and II can contribute for the better understanding of a biomechanics and the pathophysiology of the diseases in the wrist, which in very important in occupational and recreational human activities [1, 2, 3, 4, 8].

References

1. Aufauvre, B., G. Herzberg, J. Garret, E. Berthonneaud, J. Dimnet. A new radiographic method for evaluation of the position of the carpus in the coronal plane: results in normal subjects. – Surg. Radiol. Anat., **21**, 1999, 383-385.
2. Cerezal, L., F. Abascal, R. Garcia - Valtuille, F. Del Pinal. Wrist MR arthrography: how, why, when. – Radiol. Clin. North Am., **43**, 2005, 709-731.

3. Craigen, M. A. C., J. K. Stanley. Wrist kinematics. Row, column or both?. – J. Hand Surg., **20B**, 1995, 165-170.
4. Crisco, J. J. S., W. Wolfe, C. P. Neu, S. Pike. Advances in the in vivo measurement of normal and abnormal carpal kinematics. – Orthop. Clin. North America, **30**, 2001, 219-231.
5. Dyankova, S. Lunate bone — types and morphological characteristics. – Acta Morphol. Anthropol., **10**, 2005, 304-308.
6. Gupta, A., N. M. Al — Moosawi. Lunate morphology. – J. Biomech., **35**, 2002, 1451-1457.
7. Kapandji, A. Biomechanik des Carpus und des Handgelenkes. – Orthopade, **15**, 1986; 60-73.
8. Koebke, J. Anatomical and clinical aspects of the wrist joint area. – Scr. Sci. Med. (Varna), **36**, 2004, suppl. 1, p.24.
9. Linscheid, R. L. Kinematic considerations of the wrist. – Clin. Orthop. Rel. Research, **202**, 1986, 27-39.
10. Martin, R., K. Saller. Lehrbuch der Anthropologie. Bd.I-II. Stuttgart, G. Fischer Verl. 1957-1958.
11. Palmer, A. K., F. W. Werner. Biomechanics of the distal radioulnar joint. – Clin. Orthop. Rel. Research, **187**, 1984, 26-35.
12. Pfirrmann, C. W. A., N. H. Theumann, C. B. Chung, D. J. Trudell, D. Resnick. The hamatolunate facet: characterization and association with cartilage lesions — magnetic resonance arthrography and anatomic correlation in cadaveric wrists. – Skeletal Radiol., **31**, 2002, 451-456.
13. Sommelet, P., P. Hahn, D. Schmitt, M. Jandeaux, M^me Large. L'allongement du cubitus dans le traitement de la maladie de Kienbock. — Rev. Chir. Orthop. et reparat. dApp. Mot. (Paris), **56**, 1970, 731-743.
14. Tubiana, R. Rheumatische Läsionen am Carpus. - Orthopädie, **15**, 1986, 135-149.
15. Viegas, S. F., K. Wagner, R. Patterson, P. Peterson. Medial (hamate) facet of the lunate. – J. Hand Surg., **15A**, 1990-b, 564-571.
16. Viegas, S. F., R. M. Patterson, J. Hokanson, J. Davis. Wrist anatomy: incidence, distribution, and correlation of anatomic variations, tears, and arthrosis. – J. Hand Surg., **18A**, 1993, 463-475.
17. Viegas, S. F. Advances in the skeletal anatomy of the wrist. – Hand Clin., **1**, 2001, 1-11.

Institute of Experimental Morphology and Anthropology with Museum
Bulgarian Anatomical Society

Acta morphologica et anthropologica, 12
Sofia • 2007

Dynamic of the Changes in the Thickness of the Wall of the Main Leg Vessels during the Prenatal Ontogenesis. Quantitative Analysis

S. Pavlov, S. Kirilova, G. Marinov

Departament of Anatomy, Histology and Embryology,
University of Medicine "Prof. Dr Paraskev Stoyanov", Varna

The structure and development of the lower limb vessels are subject to elevated scientific interest due to the varied heavy pathology affecting these. Histotopographic slices from 16 lower limbs of eight 135 mm to 388 mm long fetuses and longitudinal and transverse slices of isolated main vessels from the lower limbs of six mature still-born human fetuses were studied. To characterize quantitatively the vessel wall development two indexes are suggested: average week increment for the investigated period (shows the average speed of the vessel wall growth in μm/week) and growth index of the increment (shows the average increase of the vessel wall per mm increase of the crown-heel fetal length in μm/mm). Both indexes show common dynamics and render the investigated cases comparable. The comparative morphometric analysis allows substantiating the divergence in the prenatal histogenesis of the wall of the arteries and of the deep and the superficial veins of the lower limb.

Key words: prenatal development, vessel wall, chronic arterial insufficiency, chronic venous insufficiency.

Introduction

The vascular systems of the upper and the lower limb of the human show principally the same structure. They are affected, however, by considerably different in character, occurrence, duration and severity pathological processes. When compared to the vessels of the upper limb, the analogical arterial, venous and lymphatic vessels of the lower limb suffer more often and much earlier from systemic vascular diseases, as well as from specific local disorders. The Chronic Arterial Insufficiency of the Lower Limb (CAILL) and the Chronic Venous Insufficiency of the Lower Limb (CVILL) are leading amongst the latter.

The pathological processes affecting the lower limb develop progressively and cause irreversible changes in the arterial, venous and lymphatic vessel wall. The treatment, in the best case, slows down the process, but does not stop it [2, 10, 12, 13, 14, 20, 28]. The reasons for these differences are probably complex. The opinion is formed, however, that the leading cause is the insufficient adaptation of the lower limb vascular system in the process of evolution towards upright posture and bipedal locomotion [5, 19, 24]. The

lower limb vessels are in unfavorable position even during the prenatal ontogenesis, because before birth they are supplied by blood with lower oxygen contents. The anticipating in size and mass growth of the lower limb during postnatal life sets higher demands in front of its arterial system. On the other hand, the haemodynamic conditions in its venous system worsen through the high hydrostatic pressure. These circumstances burden the adaptation mechanisms of the lower limb vasculature. Sometimes these mechanisms turn out inadequate and the respective parts of the lower limb vasculature — arterial, venous or lymphatic, decompensate. The proof of this hypothesis needs considerable widening of the insufficient literature data about the mechanisms and dynamics of the discrete changes in wall of the main lower limb vessels during the phylo- and ontogenesis [6, 7, 8, 25]. Clarification of these changes could give valuable criteria for discrimination between normal mechanisms of adaptation and the initial pathological changes [9, 26, 27]. Consequently, the objective of this investigation is to clarify and compare the dynamic of the changes in the thickness of the wall of the main arterial and venous leg vessels during the prenatal ontogenesis.

Material and Methods

The study was carried out on cadaver material from the fund of the department of anatomy, histology and embryology at the University of Medicine "Prof. Dr Paraskev Stoyanov", Varna, following all the ethical rules for work on cadaver material. Subject of the examination were:

— histotopographical slices from proximal, middle and distal third of the legs of 16 lower limbs taken from 8 human foetuses with crown-heel lengths of 135 mm, 140 mm, 198 mm, 200 mm, 256 mm, 257 mm, 306 mm and 388 mm;

— longitudinal and transverse slices mostly from the middle third of the legs from 6 lower limbs from 6 full-term human still-borns.

The average age was calculated after the rule of Haase. Slides were stained with hematoxilin-eosin, orcein, after van Gieson and with the combined method of Weigert-Mallori. The following vessels were examined:

I group — main arteries of the leg: *a. tibialis anterior* (Ata), *a. tibialis posterior* (Atp);

II group — deep main veins of the leg: *v. tibialis anterior* (Vta), *v. tibialis posterior* (Vtp);

III group — superficial main veins of the leg: *v. saphena magna* (Vsm), *v. saphena parva* (Vsp).

The observation was carried out with Olympus BX50 microscope. Representative areas of the vessel wall were photographed with Ikegami ICD-840P and Olympus Camedia 5.1 digital cameras. With the help of the programs ImageTool 3.0 [17] and ImageJ 1.35d [1, 15] the digital images were processed and the common media-intima thickness of every captured vessel was measured. On the examined histotopographical slides the border between adventitia and surrounding connective tissue was quite unclear, therefore the latter wasn't measured.

Results were analized statistically by means of Student test and factorial analysis of variance (ANOVA) and parameters of the dynamic changes of the vessel wall thickness were calculated.

Results and Discussion

The examined vessels were divided in 6 age groups (Table 1).

Table 1. Length and age of the examined fetuses

Lunar Month (LM)	Number of fetuses, crown-heel length (mm)
III 3/4	Two fetuses, 135 mm and 140 mm
IV 1/2	Two fetuses, 198 mm and 200 mm
V	Two fetuses, 256 mm and 257 mm
VI	One fetus, 306 mm
VII 3/4	One fetus, 388 mm
X	Six full-term still-borns

The measurement results are displayed on an extended scatter diagram (Fig. 1). According to the factorial ANOVA the greatest influence upon the dispersion belongs to the factor "crown-heel length", which is linked to the fetal age, F=115.26 (F_{crit} = 2.76 for p=0.01); second in importance is the factor "vessel type" (artery, deep vein or superficial vein) — F=99.20 (F_{crit} = 4.75 for p=0.01). Lack of data renders impossible to estimate statistically adequate the influence of the factor "level of measurement" (proximal, middle or distal third of leg) on the dispersion. We eliminate the influence of this factor by averaging of the results from different measurement levels for every investigated vessel of every fetus (Table 2, Fig. 2).

Table 2. Average results according to the age and investigated vessel

Fetal crown-heel length (mm)	Average age of the fetuses in months (weeks) after Haase	Mean common intima-media thickness in μm					
		arteries		deep main veins		main superficial veins	
		Ata	Atp	Vta	Vtp	Vsp	Vsm
135	III ¾ (15 weeks)	6.53	7.06	2.70	3.46	-	4.10
140	III ¾ (15 weeks)	8.02	6.43	2.87	3.99	7.08	6.19
198	IV ½ (18 weeks)	13.00	11.39	9.84	10.49	11.62	13.44
200	IV ½ (18 weeks)	9.13	9.49	11.05	11.26	12.92	14.80
256	V (20 weeks)	11.12	12.67	12.66	12.61	15.37	19.16
257	V (20 weeks)	12.00	17.52	13.30	16.64	-	16.29
306	VI(24 weeks)	13.51	17.47	15.63	17.56	21.11	38.96
388	VII ¾ (31 weeks)	22.14	25.04	15.17	16.52	67.90	57.63
500	X (40 weeks)	47.52	46.47	-	17.72	87.08	63.48

The Student test does not show any statistically meaningful differences in the variance between the vessels from the same group — t_{art}=0.4228, $t_{deep\ veins}$ =0.2433, $t_{superf.\ veins}$=0.3352 (t_{crit}= 2.92, for p=0.01). The effect of the internal casual and individual aspects was eliminated by means of averaging of the results from the vessels of the respective groups for every age (Fig. 3). Two periods can be distinguished on this diagram. Between III and V LM (Crown-heel length 135-257 mm) the three vessel groups follow common hardly different linear trend in the increment of the common intima-media thickness. In VI LM (306 mm) the wall thickness of the superficial veins increases harshly followed in VII lm (388 mm) by a shift in the development of the arterial wall. Between VI lm and X lm the common intima-media thickness of the wall of the deep veins remains almost unchanged.

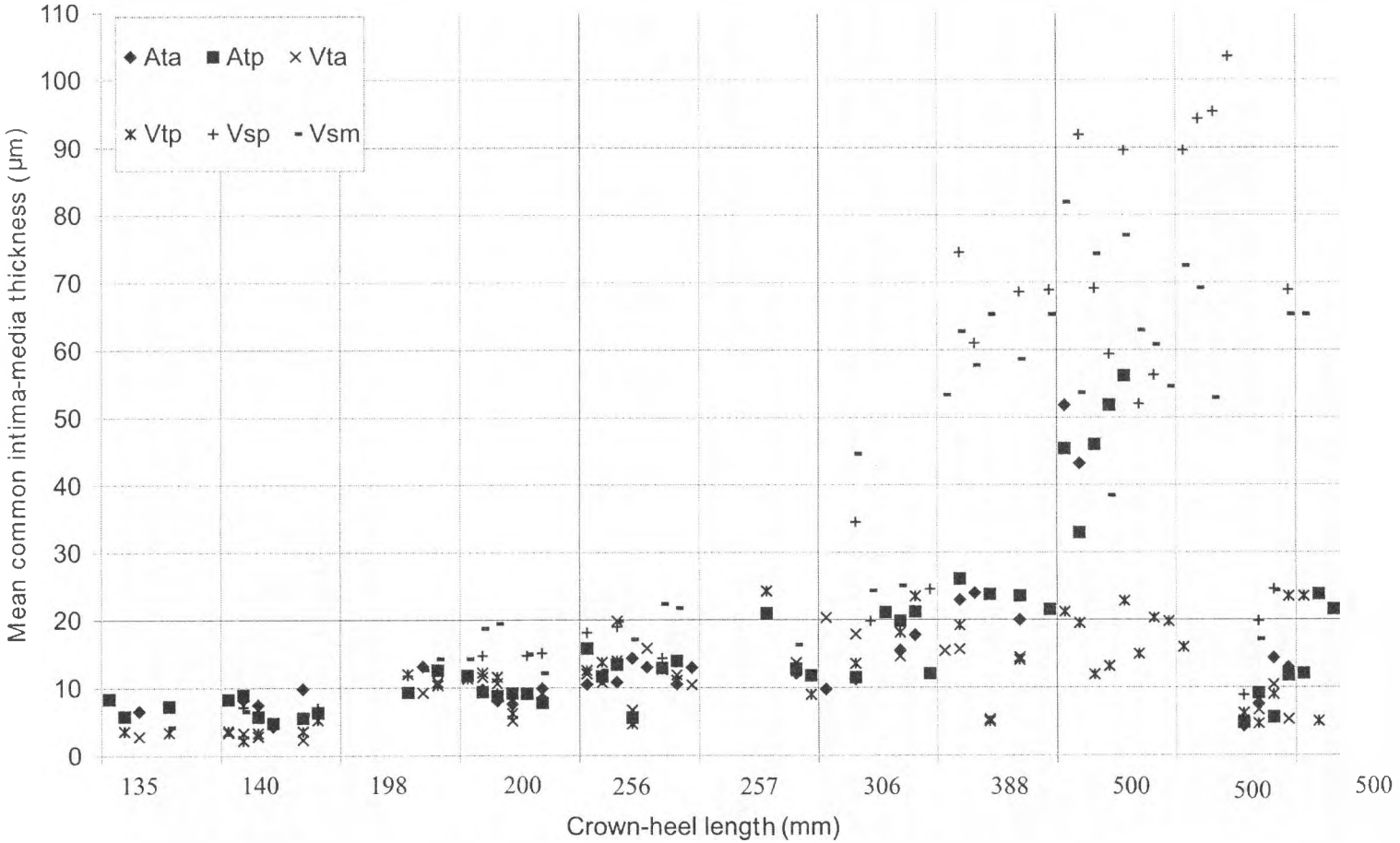

Fig. 1. Scatter diagram of the initial results

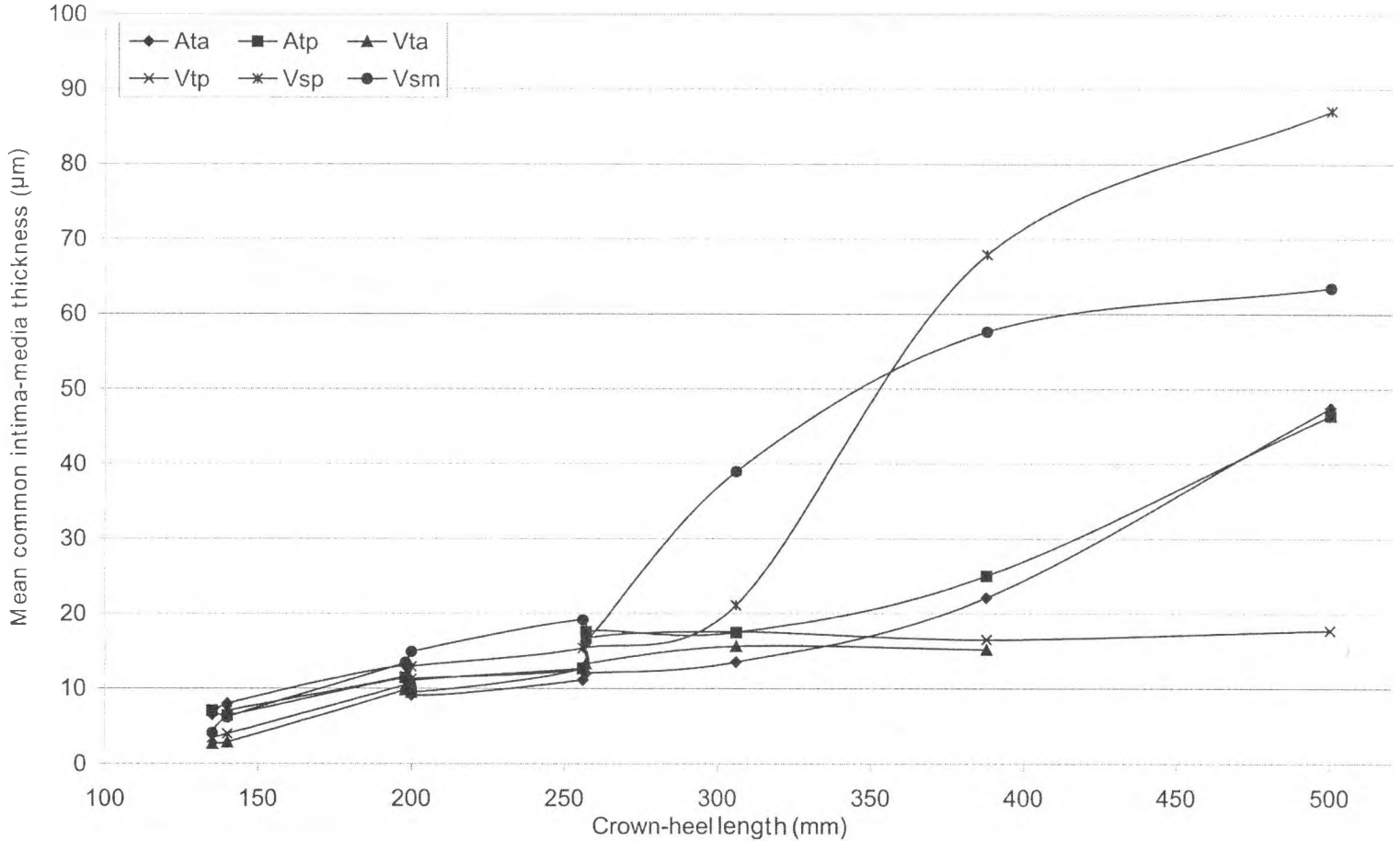

Fig. 2. Dynamic in the growth of the mean common intima-media thickness (μm) relative to the crown-heel length

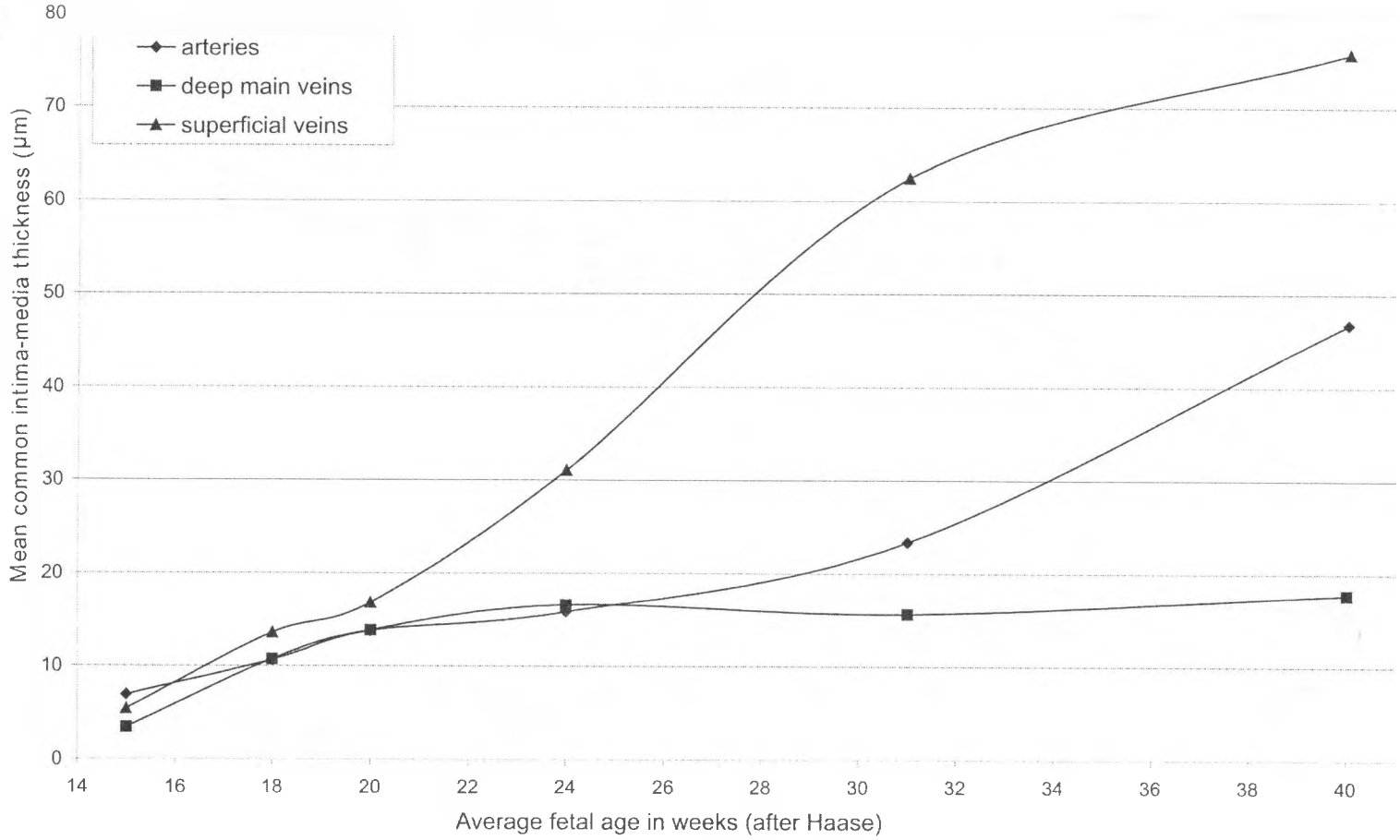

Fig. 3. Age related dynamic of the growth of mean common intima-media thickness (μm) in the different vessel groups

The found minimal variance is probably due to casual and individual peculiarities.

We calculated two indexes, to characterize the dynamic of the common intima-media thickness during the prenatal development:

— average week increment for the investigated period — the absolute growth of the mean intima-media thickness of the vessels between two neighboring age groups, divided by the difference in the average fetal age in weeks; the resulting numbers express the mean week growth of the investigated parameter (common intima-media thickness) for the respective period (μm/week) (Fig. 4);

— index of the increment — the absolute growth of the mean intima-media thickness of the vessels between two neighboring age groups, divided by absolute growth in the crown-heel length. This index shows the change in the investigated parameter for 1 mm change in the fetal crown-heel length (μm/mm) (Fig. 5).

Both indexes express common dynamic throughout the investigated period — 15 - 40 weeks from gestation. In the beginning (15-18 weeks) the growth speed of the intima-media thickness is relatively high for all of the three vessel groups and eventually decreases. A second peek in the growth speed can be observed during 20-31 week for the superficial veins and during 24-40 week for the arteries. In both cases this growth acceleration is connected to increase in the quantity of smooth muscle cells in the media [11, 22].

In our opinion, one of the most plausible causes for the harsh increment of the wall thickness of arteries and superficial veins is the increased burden of the vessel wall. In arteries this is connected to the increment of the arterial transmural blood pressure [3, 4]. In superficial veins the increased load of the vessel wall is probably due to deteriorated through the posture venous drainage — in the last trimester the lower limbs of the fetus are flexed in the hip and sometimes also in the knee joint. The altered rheological properties of the fetal blood — physiological erythrocytois and macrocytosis, elevated hematocrit and decreased erythrocyte sedimentation rate by the pregnancy term, also contribute to the increase of the vessel wall load [3, 4, 16, 21]. These factors, however, do not exert their influence upon the wall of the deep main veins of the leg. This could be explained through the effect of two factors, which are absent in the superficial veins:

1) in this period of the pregnancy the muscle pump is already functional;

2) through the arterial wall pulsations the transmural arterial blood pressure is acting upon the deep veins from the outside in the area where they touch the arteries and renders the drainage easier. A proof for this is the decrease of the wall thickness of the deep veins of the leg in the same area [23, 22].

The established fluctuation in the developmental dynamic of the main arterial and venous leg vessels in the prenatal ontogenesis represent undoubtedly an interesting fact. Especially interesting are the "accelerated growth periods". The discovered in our previous investigations qualitative changes in the vessel wall structure in these periods show, that they are based upon increase in the active contractile elements (smooth muscle cells) and in the passively elongated elastic fibers [11, 22]. This shows that even in these early developmental stages the vascular system of the lower limb is evolving and adapting to the changing hemodynamics. This adaptation must be observed in the light of different specific peculiarities of position and interaction of the arterial and venous vessels with other surrounding structures in the leg region. What is the potential possibility in time for adequate adaptation of the vessel wall to the constantly changing with age hemodynamic conditions, is a question that still awaits its answer.

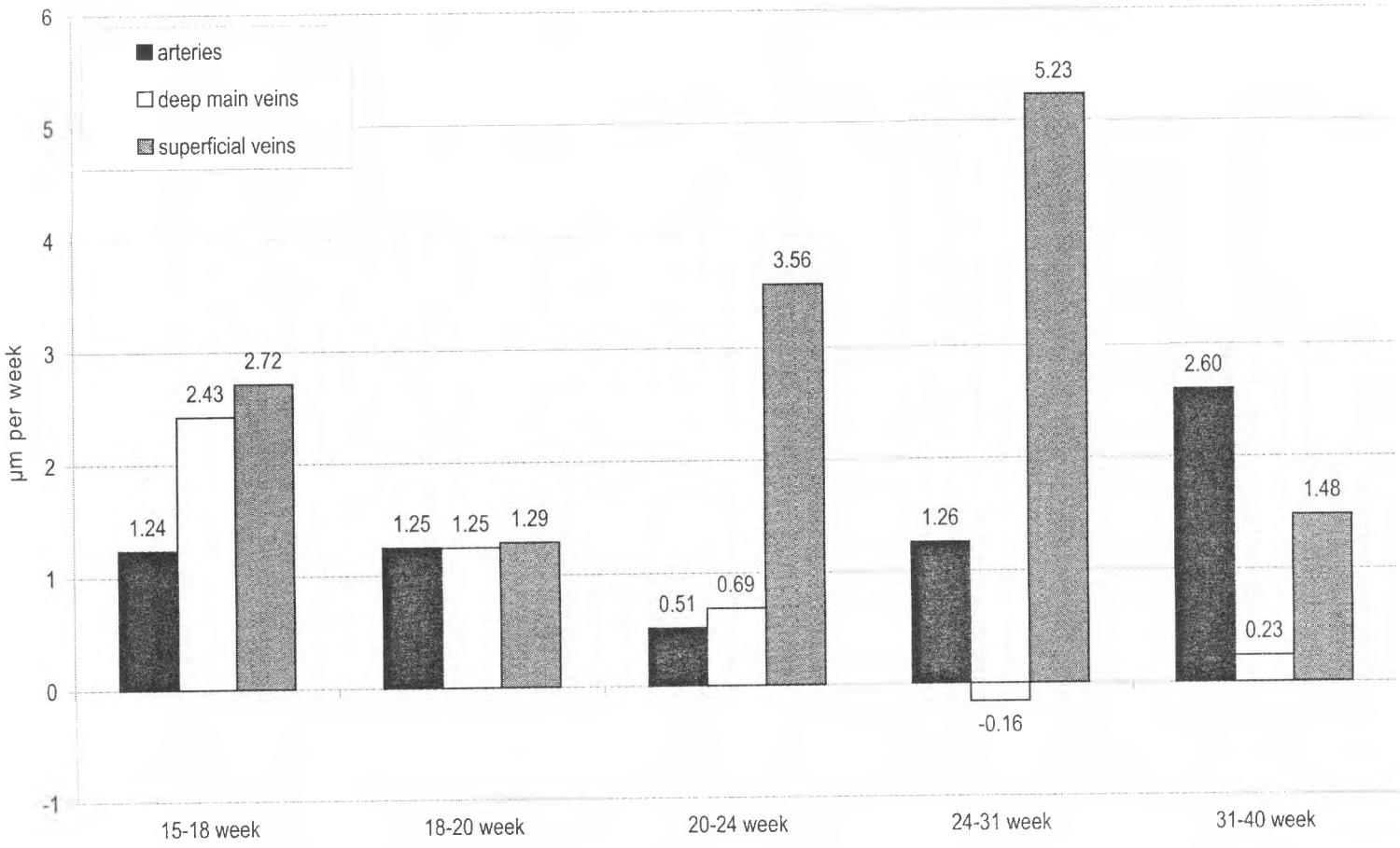

Fig. 4. Average week increment of the mean common intima-media thickness (µm) for the investigated period

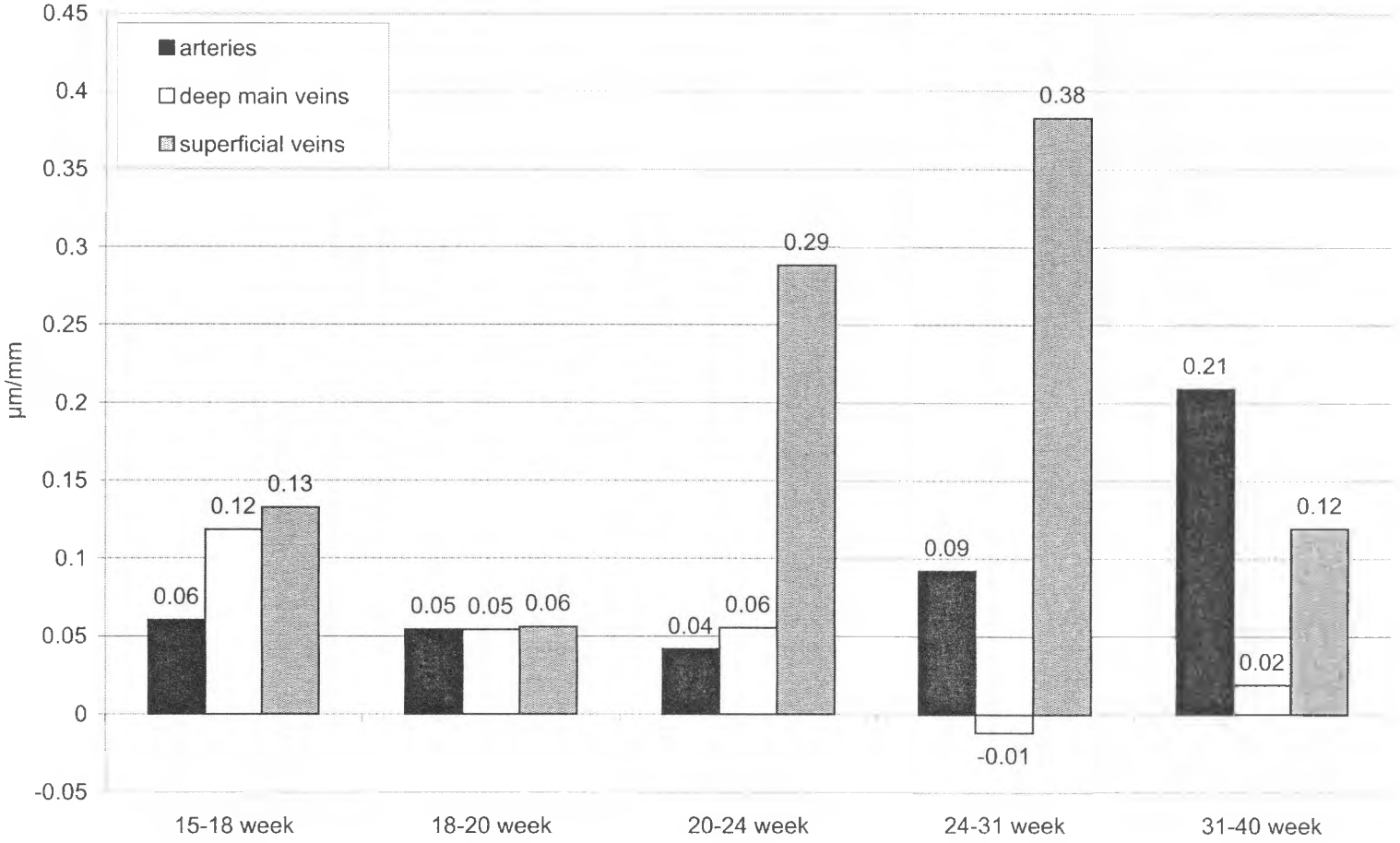

Fig. 5. Index of the increment of the mean common intima-media thickness (µm)

References

1. A b r a m o f f, M. D., P. J. M a g e l h a e s, S. J R a m. Image Processing with Image – J.Biophotonics International, **11**, 2004, No 7, 36-42.
2. B a d i e r - C o m m a n d e r, C., T. V e r b e u r e n, C. L e b a r d, J. B. M i c h e l l e, M. P. J a c o b. Increased TIMP/MMP ratio in varicose veins: a possible explanation for extracellular matrix accumulation. – J. Pathol., **192**, 2000, 105-112.
3. C a r o, C., T. P e d l e y, R. S c h r o t t e r, W. S e e d. The Mechanics of Circulation. Oxford, Oxford University Press, 1978. Москва, Мир, 1981.
4. G u y t o n, A. C., J. E. H a l l. Textbook of Medical Physiology. Philadelphia-London-Toronto, W. B Saunders Company, 2005.
5. K o c o v a - P e c h a k o v a, J. Development of the venous wall in the extremities of sheep. – Pilzen Lek Sborn, **33**, 1970, 5-13.
6. K o c o v a, J. Development of the vascular wall in the human limb. – Folia Morphol. (Praha), **20**, 1972, No 3, 265-267.
7. K o c o v a, J. Histogenesis of the vascular wall in the limbs. – Folia Morphol. (Praha), **26**, 1978, No 2, 194 -196.
8. K o c o v a, J., Z. T e s a r. The development of the vascular system in man. – Cor Vasa, **21**, 1979, No 2, 124-127.
9. M a r i n o v, G. R., T. T a b a k o v. Medial and medio-intimal thickening and atherosclerosis. A light microscopical study on the lower limb arteries. – Verh. Anat. Ges., **76**, 1982, 291-292.
10. M a r i n o v, G., V. V a n c o v. Early changes of the smooth muscle cells (SMC) and extracellular matrix in the wall of the varicose veins. – Verh. Anat. Ges. 84 Anat. Anz. (Jena), Suppl., **168**, 1991, 99-100.
11. P a v l o v, S., G. M a r i n o v. Prenatal morphogenesis and remodeling of the wall of the main arteries of the leg and foot. – Acta. Morphol. Anthropol., **10**, 2005, 110-113.
12. P o r t o, L.C., P. R. M. da S i l v e r i a, J. L. D e C a r v a l h o, M. D. B. P a n i c o. Connective tissue accumulation in the muscle laer in normal and varicose saphenous veins. – Angiology, **46**, 1995, 243-249.
13. P o r t o, L. C., M. A. P. F e r r e i r a, A. M. A. C o s t a, P. R. M. de S i l v e i r a. Immunolabeling of type IV collagen, laminin, and alpha-smooth muscle actin cells in the intima of normal and varicose saphenous veins. — Angiology, **49**, 1998, 391-398.
14. P o r t o, L.C., M. A. A. A z i z i, M. P e l a j o - M a c h a d o, P. R. M. de S i l v e i r a, H. L. L e n z i. Elastic fibers in saphenous varicose veins. – Angiology, **53**, 2002, 131-140.
15. R a s b a n d, W. S. J. Image. http://rsb.info.nih.gov/ij/. U. S. National Institutes of Health, Bethesda, Maryland, USA, 1997-2005.
16. T c h e r n i a, G. Erythropoiesis and erythrocytes in children, physiology and standards. – Rev. Prat., **39**, 1989, No 24, 2111-2116.
17. W i l c o x C. D., S. B. D o v e, W. Mc D a v i d, D. B. G r e e r. UTHSCSA ImageTool V. 3.0. http://ddsdx.uthscsa.edu/dig/itdesc.html. San Antonio, Texas, 1996-2002.
18. А в т а н д и л о в, Г. Г. Морфометрия в патологии. Москва, Медицина, 1973.
19. В а н к о в, В., Г. М а р и н о в. Анатомични особености на клапния апарат по протежение на венозната магистрала бедрена-външна хълбочна вена у Macacus rhesus. – В: Сборник доклади „Юбилейна научна сесия на ВМИ–Варна (1961–1971)". III св. 1971, 124–127.
20. В а н к о в, В. Морфология на вените. София, Медицина и физкултура, 1989. 208 с.
21. Г а т е в, В. Морфологична и физиологична характеристика на детския организъм. София, Медицина и физкултура, 1988.
22. К и р и л о в а, С., С. П а в л о в, Г. М а р и н о в. Ремоделиране на стената на магистралните вени на подбедрицата и ходилото в пренаталната онтогенеза. – Известия на съюза на учените — Варна, **2**, 2003, № 1, 2004, 3–8.
23. М а р и н о в, Г. Строеж и васкуларизация на вените на подбедрицата и задколянната яма (канд. дис. м. н.). Варна, 1969. Автореферат, Варна, 1969. 20 с.
24. М а р и н о в, Г., С. Б а к ъ р д ж и е в а Някои анатомични особености на венозните съдове в задните крайници на Macacus rhesus. – В: Сборник доклади „II Научна сесия на младите научни работници, ВМИ–Варна, 3–6 VI 1971". 1971, 11–16.

25. М а р и н о в, Г. Възрастови особености в структурата на стената на магистралните артерии на долния крайник. – Медико-биологични проблеми, МА, София, V, 1977, 49–57.
26. М а р и н о в, Г., Т. Т а б а к о в. Структура и локализация на ранните интимални разраствания в стените на магистралните артерии на долния крайник в пренаталната онтогенеза. – Медико-биологични проблеми, МА, София. VIII, 1980, 42–50.
27. М а р и н о в, Г. Ранни задебеления на артериалната стена – класификация и роля в развитието на артеросклеротичния процес. – В: Научни доклади на „X Юбилейна сесия на ВМИ–Варна. 31 X 1981, Варна“, 1982, 31–34.
28. С т а в р е в, Д., Г. М а р и н о в, В. К н я ж е в. Ремоделиране на стената на vena saphena magna при облитериращa атеросклероза на долния крайник. – Ангиология и съдова хирургия, **IV**, 2003, № 1, 30–39.
29. С е п е т л и е в, Д. Медицинска статистика. София, Медицина и физкултура, 1976.

Institute of Experimental Morphology and Anthropology with Museum
Bulgarian Anatomical Society

Acta morphologica et anthropologica, 12
Sofia • 2007

A Bicuspid Construction of the Pulmonary Valve of the Heart

A. Petrova

Department of Anatomy, Histology and Embriology,
Medical University of Varna, Varna

A case of congenital bicuspid pulmonary valve was found in a cadaver of a male in the age of about 70 years. The valve was found closed and the valve sinuses were filled with blood. So, the heart had been fixed in the phase of diastolic closure of the pulmonary valve. The valve described shows a normal position of an outflow valve of the right ventricle. The right leaflet of the valve is smaller than the left one. There is no evidence for valve incompetence. The biophysical analysis shows that in this moment both cusps are overloaded — the pressure on them is to be 50% more than on the normal tricuspid pulmonary valve. Evidently, this is the reason for strongly manifested fibrosis of the cusps.

Key words: pulmonary valve, bicuspid construction, male.

Introduction

In the literature during recent time are to be found only a few cases of bicuspid pulmonary valve in humans without any other damage of the heart [5, 1]. E m u r a et al. [2] describe in a men without heart failure a pulmonary valve consisted of two leaflets - the right one is smaller than the left one. In major cases the bicuspid pulmonary valve was in coexistence of Fallot's tetrology or ventricular septal defect [4]. K a d r i et al. [3] describe pulmonary incompetence in an adult due to the congenital absence of anterior leaflet of the pulmonary valve.

An exceptional case of congenital bicuspid pulmonary valve in the neart of a male was observed. The valve is not combined with other lesions of the heart.

Material and Methods

The heart was discovered during dissecting practice at Medical University of Varna (Petrova, 2000) in a 70-year-old male. The pulmonary valve was examined macroscopically. Both leaflets were cut into histological slides and stained with hematoxylin-eosin (HE), orcein, Azan.

Results and Discussion

The valve was found closed and the valve sinuses were filled with blood. So, the heart had been fixed in the phase of diastolic closure of the pulmonary valve. No evidence of heart failure was found.

The valve described shows a normal position of an outflow valve of the right ventricle. As regard the construction, it differs greatly from normal tricuspid pulmonary valve. The cusps are right (RC) and left (LC), intercuspid commissures are anterior and posterior. The cusps are attached by their convex margins to double-scalloped fibrous thickening in the wall of pulmonary trunk at its junction with the ventricle. In the region of the valve there are two prominent dilatations of the vessel wall - sinuses (S), corresponding to the cusps. The upper margin of each sinus is limited by well-defined supravalval ridge, situated considerably beyond the level of the free border of the cusps.

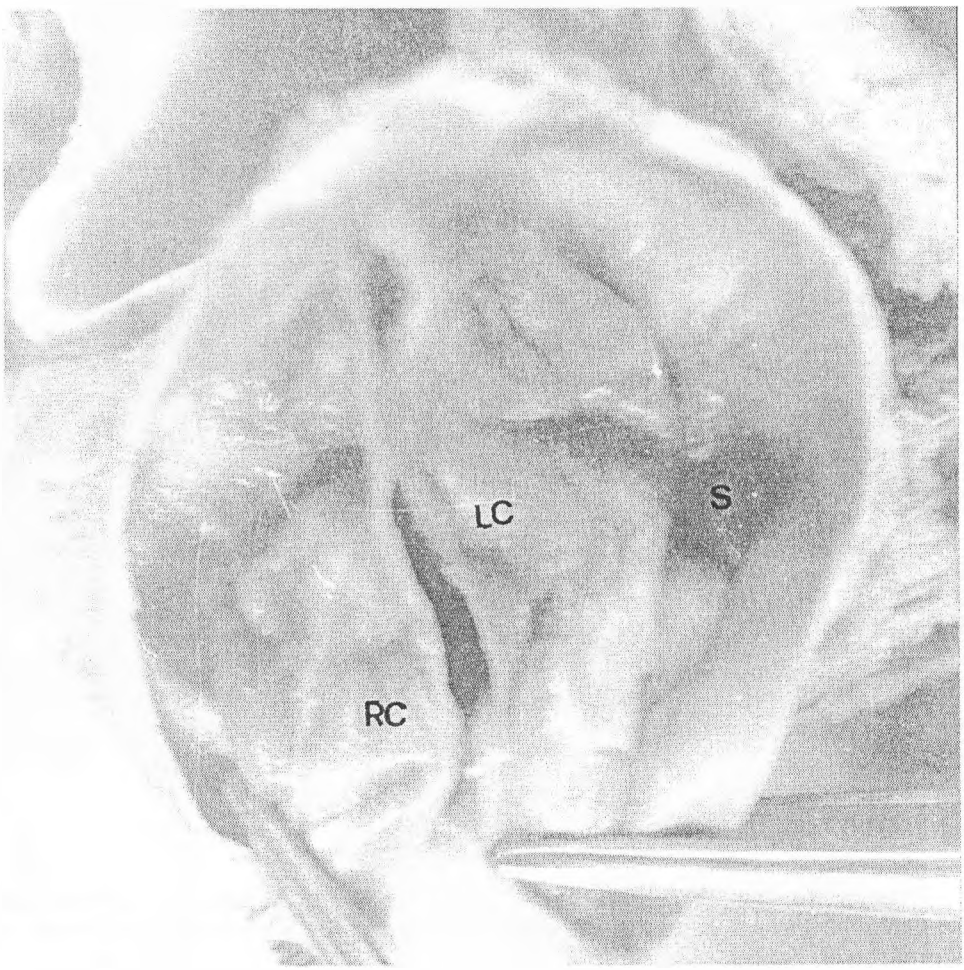

Fig. 1. Bicuspid pulmonary valve
RC — right leaflet; LC — left leaflet; S — sinuses

The right leaflet of the valve described is smaller than the left one. The concave free border (FB) is 5.4 vs. 5.9 cm long and 2.0 vs. 2.7 cm high (vertical size in the middle of the leaflet). The anterior half of the free border of the right leaflet is unevenly thickened; the posterior half is thin and smooth. As a whole the anterior part of the leaflet is thicker than that of the posterior one. In the central part of the leaflet at a distance of 3 — 4 mm from the free border there is a fibrous nodular formation (NF). The left leaflet of the valve, which is bigger than the right one shows similar morphological features, but the thickenings of the free border and the leaflet as a whole are better expressed. A strongly prominent central thickening (fibroma — F) is located at a distance of 8 mm from the free border. In the rest of the leaflet small protuberances are seen.

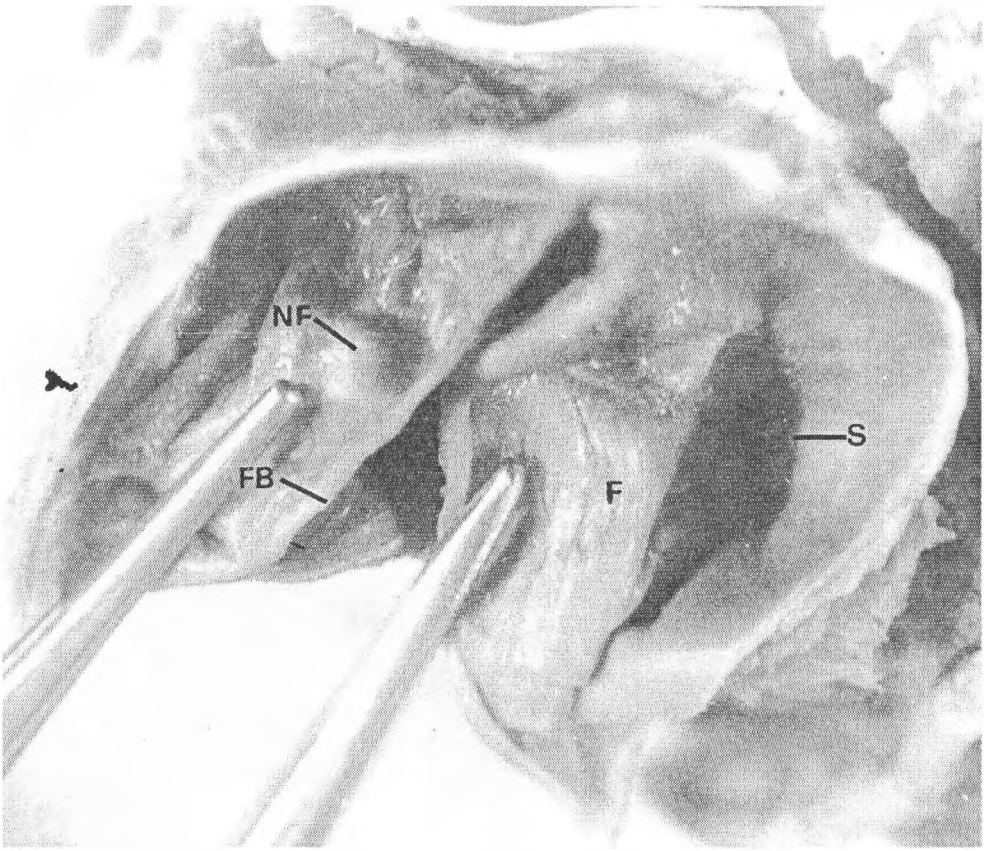

Fig. 2. Bicuspid pulmonary valve
FB — free border; NF — nodular formation; F — fibroma

In spite of that, there is no evidence for valve incompetence; the size of the right ventricle (RV) as regard to the left ventricle (LV) and the thickness of their walls are approximately normal.

Aortic valve of the heart was a normal tricuspid valve.

Histological investigation shows that the layers of the leaflets are unevenly developed from place to place. In the thickenings, especially in the central tuberal ones, stratum

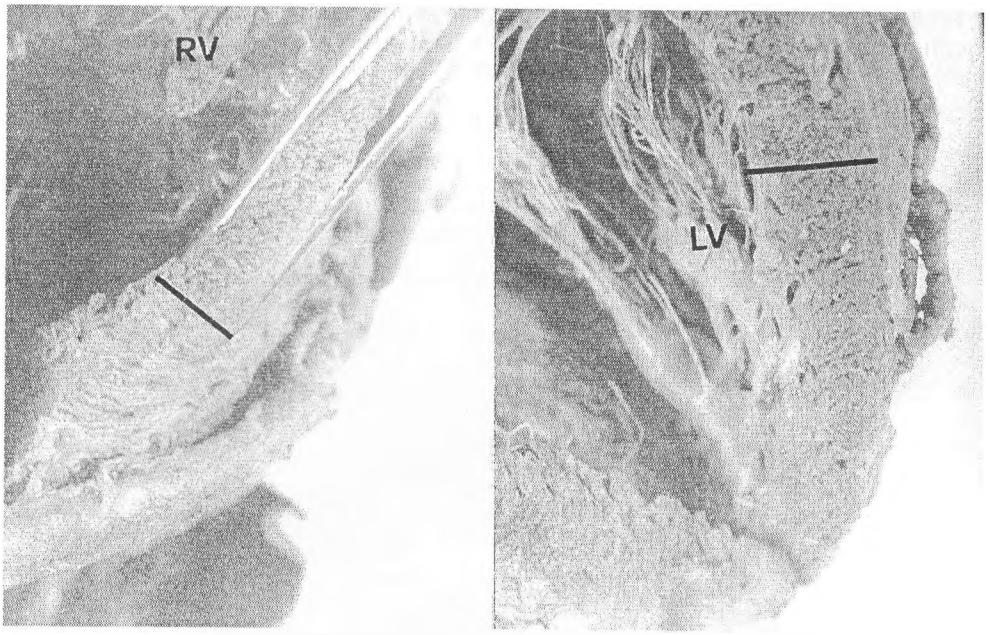

Fig. 3. Right ventricale (RV), left ventricale (LV)

ventriculare is better developed, stratum fibrosum is degeneratively altered, stratum spongiosum is with fibrosis. Homogenisation of the structural components and subsequent hialinisation are seen.

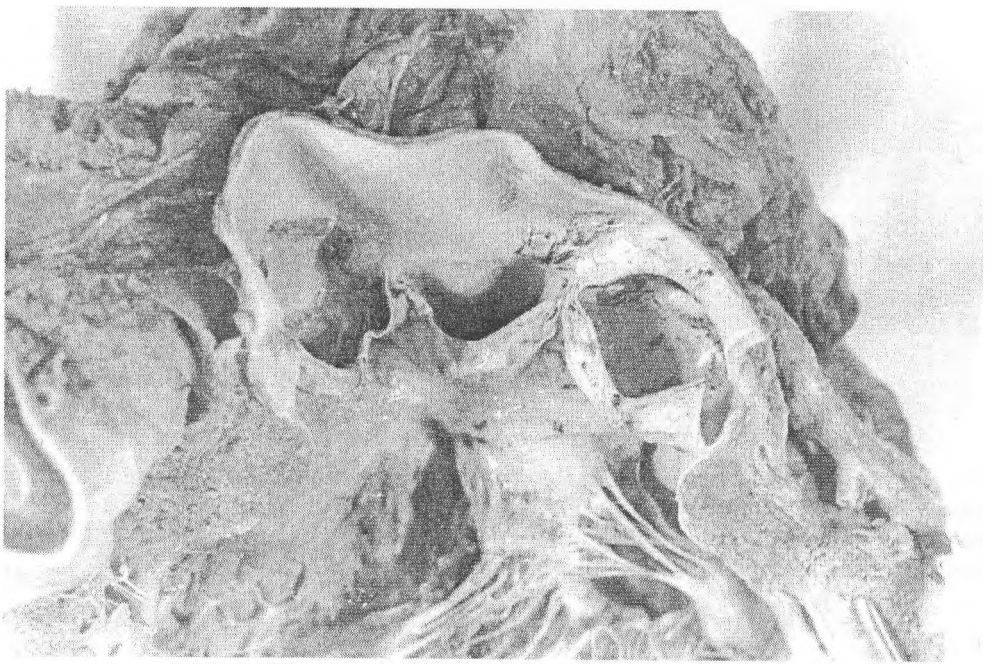

Fig. 4. Aortic valve

The construction of the bicuspid pulmonary valve described shows that during the ejection phase of the right ventricular sistole both cusps are moved to the wall by the ejected blood; during the diastolic closure both valvular pockets are filled with blood and

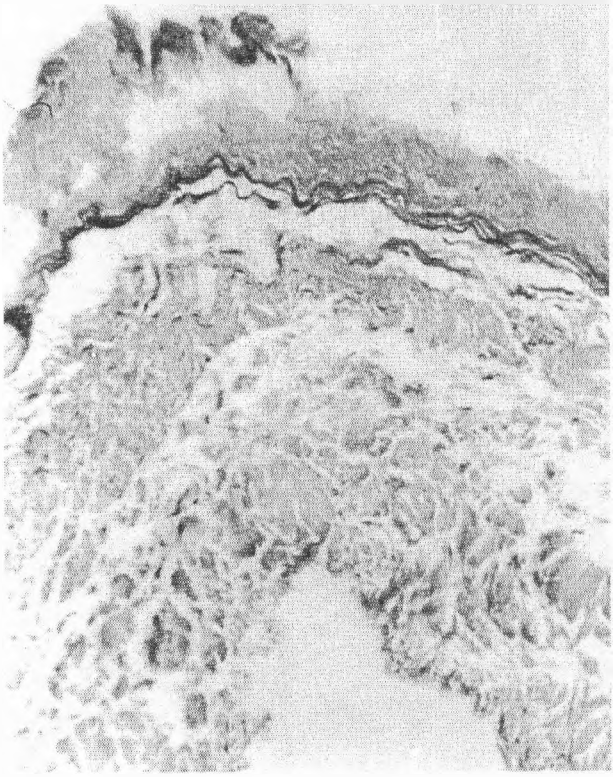

Fig. 5. Leaflet of the pulmonary valve. Hematoxylin-eosin (× 200)

the free borders of the cusps are tightly apposed to each other. The biophysical analysis shows that in this moment both cusps are overloaded - the pressure on them is to be 50% more than that on the cusps of the normal tricuspid pulmonary valve. Evidently, this is the reason for strongly manifested fibrosis of the cusps.

References

1. B i g o t t i, A., F. L e o n a r d o. Bicuspid pulmonary valve. – Minerva Cardioangiol., **12**, 1976, 873-880.
2. E m u r a, S., S. S h o u m u r a, M. U t s u m i, H. C h e n, T. Y a m a h i r a. A case of congenital bicuspid pulmonary valve. – Kaibogaku Zasshi, **65**, 1990, 381-382.
3. K a d r i, M., R. L a z z a r a, B. Mc L e l l a n. Repair of congenital pulmonary incompetence by bicuspidization of the pulmonary valve. – Ann. Thorac Surg., **63**, 1997, 1482-1483.
4. R o m e r o - C a r d e n a s, A., M. V i l l g a s, M. R y l a a r s d a m, F. A t t i e, C. K e i r n s, R. D e l o n g. Two dimensional and Doppler echocardiographic diagnosis of bicuspid pulmonary valve. – Arq. Bras. Cardiol., **57**, 1991, 245-247.
5. S h i m a d a, Y. 2 cases of pulmonary valve anomaly. – Kaibogaku Zasshi, **50**, 1975, 138-140.

Institute of Experimental Morphology and Anthropology with Museum
Bulgarian Anatomical Society

Acta morphologica et anthropologica, 12
Sofia • 2007

Review Article

The Secret of Epigenesis and its Implication for Cell Therapy

M. Anastassova-Kristeva

Institute of Experimental Morphology and Anthropology with Museum, Bulgarian Academy of Sciences, Sofia

New molecular mechanism for cell differentiation essential for epigenesis is uncovered. The massive transcription of all meiotic chromosomes along the side-elements of the synaptonemal complex has not been explained till now. The messengers transcribed are packed with "translation repressor proteins" into mRNP particles and stored in the ovoplasm, known as "maternal inheritance". The significance of this immense ovoplasmic genetic information was not understood. It is logical to admit that during embryonic development the highly conservative deblocking proteins are transported by the mRNAs to the nascent DNA strands of the corresponding genes. A stable DNA- protein complex is formed, selectively deblocking the genes and transforming the heterochromatin into active euchromatin.

In this aspect the ovoplasmic mRNP particles play the role of morphogenes designed to unlock selectively new genes during epigenesis, which in and of itself represents the molecular mechanism of cell differentiation.

New avenues are thereby introduced, helping to resolve many unsolved questions concerning the biology of cell differentiation. A new kind of in vitro gene engineering will make possible the unlocking of desired genes and create specific cells for the purposes of regenerative medicine.

Key words: epigenesis, cell differentiation, cell therapy.

The molecular basis of cell differentiation is one of the fundamental and most challenging unsolved problems in the biological sciences. A historical survey shows that during the "post genomic era" the efforts of researchers to resolve cell differentiation have been focused on transcriptional mechanisms and substances that switch genes on and off. The Sanger Institute in Cambridge, UK, and Epigenomics, a Berlin-based Corporation have focused their research on gene on/off switches, the main goal of their 'Human Epigenome Project' being to study and map DNA methylation, or 'epigenetic' changes across the entire human genome [5]. David Allis from the University of Virginia believes that the "histone methylation switch" is probably responsible for gene expression or lack of expression [5]. Histone methylation affects genes packed in nucleosomes in the inactive heterochromatin. Such type of gene stimulation for transcription is not equivalent to cell

differentiation [4]. Under normal circumstances a cell has to be already differentiated to respond to stimuli switching on the gene for function.

All differentiated cells possess specific deblocked structural genes in their active euchromatin. These genes must receive a signal to activate the promoter, so that RNA polymerase can begin transcription. At this point, the gene is switched on for *function* or gene expression. After transcription is terminated, the gene is switched off but the cell remains differentiated because the gene is deblocked and ready to respond again to the next starting signal. *Gene deblockage occurs only once during embryonic development and results in DIFFERENTIATION. Activation of deblocked genes in differentiated cells is repeated and results in FUNCTION [4], see Stem Cells and Self Renewal).* "There are two distinct levels of regulation in mammalian somatic cells. One level is concerned with genomic commitment (i.e. determination) and the other level with the expression of tissue specific proteins" [1], p. 247. Hence, *it is critical when considering epigenesis not to confuse gene deblockage and the processes of differentiation with gene on/off switches and the processes of gene expression or function.*

M o r g a n [25] established that gene activity in the earliest embryonic development is influenced by the ovoplasmic heterogeneity. During cleavage, a variety of ovoplasmic substances surround the nuclei and activate specific genes. This process, generally termed nucleo-cytoplasmic induction, has been confirmed repeatedly, as acknowledged by H o p p e r and H a r t [17] who note that " Basically, the interplay between nucleus and cytoplasm is considered to be the force that moves the cell along a specific pathway of differentiation and is thus responsible for development."

Morgan and his followers made tremendous strides in defining the maternal mRNAs in the sea urchin ovocytes [7, 10]. In spite of the large quantities of rRNAs and of other repeated RNA sequences, these investigators established that there are longer transcripts packed with special proteins of unknown chemical composition. These proteins prevent the translation of the messengers in the ovoplasm. These messenger ribonucleoprotein particles (mRNPs), described in the literature as 'masked mRNAs', 'long lived ribonucleoproteins', maternal mRNA and oogenetic messenger RNPs [18, 19, 24, 30, 31], are thought to carry the maternal inheritance. It is very probable that Vogt's fate maps [29] depend on the specific order in which the RNP particles are distributed in the ovoplasm.

The mRNP particles have been separated and analyzed, but the time and mechanism of their origin are not known. D a v i d s o n et al. [11] believe that the mRNPs are translated after fertilization but that other possibilities exist as well, i.e., a regulatory function is considered but has not been found.

During my extensive investigations of ovopoiesis in amphibia, birds and mammals I have become intimately familiar with the details of egg maturation, from oogonium to ovulation and particularly meiosis [2]. Initially, oogonia multiply by simple mitosis, but after a last DNA replication mitotic division stops and the oogonium enters the prophase of the first meiotic (reduction) division, thereby becoming a primary oocyte in leptotene stage. During zygotene and pachitene the duplicated homologous chromosomes fuse as bivalents or tetrads, at which time segments are exchanged between two non-sister chromatids (crossing over), a process responsible for a substantial part of the diversification of the species.

Under the electron microscope, bivalents show a central element and two lateral elements, a structure termed a "synaptonemal complex". The central element is involved in the crossing over. The lateral elements of the synaptonemal complex develop thousands of DNA side loops (as many as 20000/chromosome in some animals, e.g., salamanders), which are involved in active transcription of the entire genome. During the next meiotic phase (diplotene), the bivalents stretch and form "Lampbrush chromosomes" [15], which continue to transcribe all types of mRNAs. This unique phenomenon needs further exam-

ination. Translation does not occur in the ovoplasm, because the mRNAs are packed with special nonhistone proteins found in the nuclei, called *translation repressor proteins* (TRP) or Hox proteins, which prevent translation [1], p. 593. Messenger RNAs packed with TRP do not undergo processing, splicing of introns, or attaching to ribosomes. Instead they are accumulated in large quantities as long-lived messengers (mRNP particles) in the egg cytoplasm.

Some nuclear proteins are synthesized by genes, which contain a homeobox (a sequence of about 180 nucleotide pairs). Homeobox (Hox) containing genes have been found in many species including man [16]. The homeobox sequence has been conserved at the protein level throughout (over) 500 million years of evolution. "These proteins, localized in the cell nucleus suggest direct involvement in the control of gene expression" [1], p. 937.

Recently more data accumulate indicating that Hox proteins cause morphological diversity and contribute to body-plan evolution [16, 24, 26]. However, the exact mechanism remains obscure.

The experiments of De Robertis and his school [6,8] indicate the role of homeodomain proteins in specifying the identity of cells, tissues and body regions. It is in general assumed that these proteins bind directly specific DNA sequences. However, "Gooscoid and bicoid proteins can bind to similar target sequences" [6], but do not have the ability to recognize and bind directly DNA of a given structural gene. The conservation of these special proteins over millions of years is an indication that in combination with mRNAs they participate in a very important process, essential for epigenesis and for the conservation of the cytoplasmic genetic memory.

Two main groups of nuclear proteins have evolved during evolution:

1) Histones (basic) to protect and keep genes blocked.

DNA + histones = nucleosomes = heterochromatin = inactive.

Histones don't recognize gene sequences.

2) Hox proteins (acidic) [16, 26], bind with mRNAs (RNPs), to unlock the genes.

DNA + Hox proteins = no nucleosomes = euchromatin = active.

Chromosome banding clearly shows the localization of hetero- and euchromatin in the condensed metaphase chromosomes. Giemsa C-banding stains the basic histones dark purple, while the acidic Hox proteins in the euchromatin remain unstained.

The rDNA, which is permanently bound with acidic proteins, appears as secondary constriction in the satellite chromosomes 13, 14 ,15, 21 and 22 of the human karyotype [3]. The genes belonging to the housekeeping genome are as well permanently bound with acidic proteins and are located as tiny light segments in the metaphase chromosomes. In interphase nuclei, the heterochromatin appears as dark patches while the euchromatin is dispersed in the nuclear matrix.

Under normal circumstances a structural gene packed with histones cannot be transcribed and belongs to the inactive heterochromatine. It is the complex DNA-Hox proteins that make the gene accessible to RNA polymerase and thus transcribable, as it belongs now to the active euchromatin.

Some attempts have been made to explain the connection between nucleohistones and the acidic nonhistone proteins. The *histone displacement model* of S t e i n et al. [28], for example, proceeds from the assumption that genomic DNA is permanently bound with histones. However, the variety of different models connecting nucleohistones and nonhistone proteins suggests that we are far from understanding the transition from inactive to active chromatin.

The big question is, do histones and nucleosomes exist in the euchromatic synthetically active genes? F r a n k e et al. [14], using the spreading technique of M i l l e r and B e a t t y [23], and electron microscopic observations unequivocally show that the DNA

of actively transcribed regions is not packed into nucleosomal particles. This is a morphological proof that during differentiation acidic proteins replace the histones in an inactive gene, and so prevent the formation of nucleosomes on the level of the newly syntesized gene, which is now deblocked and open for transcription. It is generally accepted that epigenesis is the gradual deblockage of specific genes during embryogenesis.

If histones and nucleosomes are not present in the transcribing genes, methylation and acetylation cannot interact with them, but would interact with inactive histone-bind DNA only. An attempt to explain such interaction [13] does not make clear how the nucleosomes are displaced from DNA and how they get re-formed. Similar mechanism might cause the massive genome transcription of bivalents during meiotic prophase, but further research is necessary.

While observing lampbrush chromosomes in various contexts over the years, I repeatedly wondered why all the genes are transcribed if the egg follicle does not need their products. Why are these messengers packed with specific proteins that prohibit translation? What is the role and significance of the mRNP particles, containing so much genetic information stored in the ovoplasm?

If the genes of sperm are protected to prepare them for the long trip outside the male body, blocked by histones and protamines against extraneous damaging factors, and the genes in the egg nucleus are blocked as well, then it follows that there must be a natural mechanism to deblock the specific genes after fertilization. Then it suddenly flashed upon me that the mRNPs *are designed to deblock their own blocked genes by a positive feedback mechanism. I enjoyed discovering how simple, logical and smart this secret of the Nature is.*

After fertilization the mRNP particles remain inactive, as long as the early embryonic rapid cell cycles are under the control of cyclin-dependent protein kinases [9], and under the high concentration of histones in the ovoplasm. During the rapid replications, the newly synthesized DNA adopts the histones and the genes remain blocked. This control changes markedly as the embryo undergoes gastrulation (species specific differences are possible). The mRNP particles, depending on their ovoplasmic distribution enter the nuclei and unfold to read the sequences of their complementary DNAs at the time of replication. The complementary RNA, synthesized during meiosis recognizes its template and selectively attaches the deblocking proteins (Fig. 1) to the newly synthesized DNA strand forming a stable DNA/ Hox protein complex. Thus the gene passes from a blocked to an unblocked state. Heterochromatin turns into euchromatin, and the gene is permanently deblocked and accessible for RNA polymerase. The embryonic cell, now committed to transcribe and translate the deblocked gene is differentiated.

The role of mRNA as chaperone and mediator gives answer to the question how the deblocking Hox proteins find and bind selectively the corresponding genes.

The mRNP particles stored in the ovoplasm appear now to represent the substrate caring the *CYTOPLASMIC GENETC MEMORY*, or *the MORPHOGENES*, which unlock selectively new genes. In adult somatic cells, nontranslatible mRNPs encoded by the active genes specific for the given cell, maintain the differentiated state in the long term. The same compounds interact with the genes of transplanted nuclei. For instance if a nucleus from a differentiated cell is injected in the cytoplasm in another differentiated cell, it acquires the characteristics of the host cell [1], p.900.

Recent experiments with RNA interference show that "killing the messenger" [12] stops embryonic development [27], and the embryos die. These observations confirm the important role of the mRNPs in cell differentiation during embryogenesis. Moreover the total genome transcription during egg maturation takes on now a new and important significance in understanding epigenesis, for it explains the exact and selective deblockage of genes, which cannot be achieved by methylation or other similar procedures. Instead, *the oocyte displays a remarkable feedback mechanism to selectively unlock new genes*

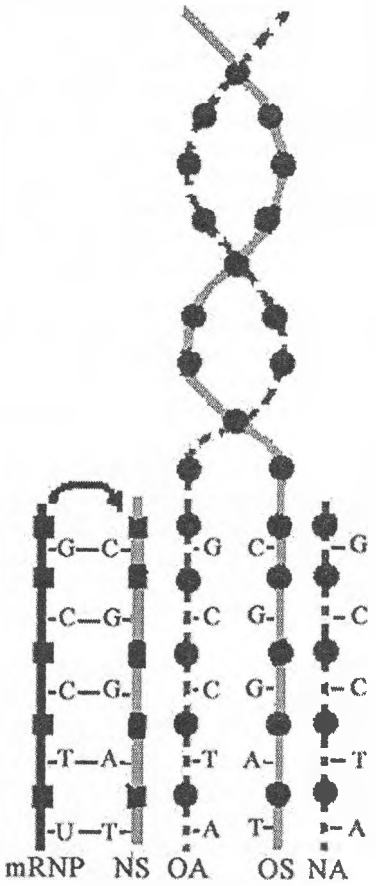

Fig. 1. A model for deblockage of a gene by maternal mRNP
Sense DNA strands — grey; antisense DNA strands — dashline; OA and OS — the old antisense and sense strands; NS and NA —the newly synthesized DNA strands; mRNP — maternal messenger ribonucleoprotein; Black dots — nucleosomes; black squares-mRNA+ deblocking Hox protein complex; a structural gene (NS) is present in the newly synthesized sense strand only; the complementary mRNA recognizes it and the Hox proteins are selectively attached to the gene (NS), which is now permanently deblocked

during development. The attachment of special proteins by mRNA to complementary DNA resulting in gene deblockage indicates that in the addition of the well known process DNA-RNA-protein, a feedback mechanism, namely protein –RNA–DNA exists and is pivotal in the processes of epigenesis. What a wonderful resolution of the theoretical quest against the dogma [21, 22].

Many additional details accompanying the action of the maternal mRNPs need to be elucidated. However, their fundamentally vital role described herein is obvious (albeit not recognized till now), and it explains many previously unanswered fundamental questions regarding the processes of epigenesis.

Given this new conceptual framework, novel avenues of inquiry are possible. Of immediate concern would be the characterization of the specific non-histone proteins in meiotic nuclei that pack the maternal mRNAs and prevent their translation. Once their composition is known, in vitro transcription of given genes in the presence of these proteins will create mRNPs, capable of unlocking the desired genes of cells during replication. With this mechanism in hand, selective transdifferentiation of cells in vitro for use in cell therapy would provide powerful new medical tools.

References

1. Alberts, B., D. Bray, J. Lewis, M. Raff, K. Roberts, J. Watson. Molecular Biology of the Cell, 2nd ed. New York & London, Garland Publ. Inc., 1998.
2. Anastassova-Kristeva, M., A. I. Hadjioloff, A. Bradinska, L. Kancheva. Morphological and histochemical studies of the meiotic prophase in chicken oocytes. – Proc. Inst. Morphol. Bulgarian Acad Sci., **14**, 1970, 45-67.
3. Anastassova-Kristeva, M. The nucleolar cycle in man. – J. Cell Sci., **25**, 1977, 103-110.
4. Anastassova-Kristeva, M. The origin and development of the immune system with a view to stem cell therapy. – J. of Hematotherapy and Stem Cell Research **12**, 2003, 137-154.
5. Bhattacharia, S. Human gene on/off switches to be mapped. New Scientist.com. news service, 2003, October 07.
6. Blumberg, B., Ch. Wright, E. De Robertis, K. Cho. Organizer-Specific Homeobox Genes in Xenopus laevis Embryos. – Science, **253**, 1991,194-196.
7. Britten, R., E. Davidson. Gene regulation for higher cells: a theory. – Science, **165**, 1969, 349-357.
8. Cho, K., E. Morita, Ch. Wright, E. De Robertis. Overexpression of a Homeodomain Protein Confers Axis-Forming Activity to Uncommitted Xenopus Embryonic cells. – Cell, **65**, 1991, 55-64.
9. Dalton, S., E. Stead, J. White, R. Faast, D. Rivett, M. Bettess, S. Goldstone, P. Cartwrite. Control of Cell Division in pluripotent cells: understanding cell proliferation during embryogenesis and during stem cell differentiation. – In: 32nd Annual Conference of the Society of Reproductive Biology, Goldcoast, 9-12 Sept. 2001.
10. Davidson, E., R. Britten. Organization, transcription and regulation in the animal genome. – Quart. Rev.Biol., **48**, 1973, 565-613.
11. Davidson, E., B. Hough-Evans, R. Britten. Molecular Biology of the Sea Urchin Embryo. – Science, **217**, 1982, 17-26.
12. Dykxhoorn, D. M., C. D. Novina, P. A. Sharp. Killing the Messenger: Short RNA's that Silence Gene Expression. – Nature Rev. Molecular Cell Biol., **4**, 2003, 457-467.
13. Eisenberg, J. C., S. C. R. Elgin. Antagonising the neighbours. – Nature, **438**, 2005, 1090-1091.
14. Franke, W. W., U. Scheer, M. Trendellenburg, H. Zentgraf, H. Spring. Morphology of Transcriptionally Active Chromatin. – In: Cold Spring Harbor Symposia on Quantitative Biology. Vol. XLII. 1978, 755-772.
15. Gall, J. G., H. G. Callan. 3H-uridine incorporation in lampbrush chromosomes. – Proc. Natl. Acad. Sci. U.S., **48**, 1962, 562-570.
16. Garcia-Fernandez, J. The genesis and evolution of homeobox gene clusters. – Nature Reviews Genetics, **6**, 2005, 881-892.
17. Hopper, A., N. Hart. Foundations of Animal Development. New York, Oxford, Oxford University Press, 1985, 1-590.
18. Jenkins N. A., J. F. Kaumeyer, E. M. Young, A. R. Raff. A Test for Masked Message: The Template Activity of Messenger Ribonucleoprotein Particles Isolated from Sea Urchin Eggs. – Developmental Biology, **63**, 1978, 279-298.
19. Kaumeyer, J. F., N. A. Jenkins, R. A. Raff. Messenger Ribonuclein Particles in Unfertilized Sea Urchin Eggs. – Developmental Biology, **63**, 1978, 266-278.
20. Marmorstein, R. Protein Modules that Manipulate Histone Tails for Chromatin Regulation. – Nature Reviews Molecular Cell Biology, **2**, 2001, 422-432.
21. Mattick, J. S. Chalenging the dogma: the hidden layer of non-protein-coding RNAs in complex organisms. – Bio Assays, **25**, 2003, 930-939.
22. Mattick, J. S. Program of complex organisms. – Scientific American. October 2004, 61-67.
23. Miller, O. L., B. R. Beatty. Visualization of nucleolar genes. – Science, **164**, 1969, 955-957.
24. Moon, R. T., K. D. Moe, M. B. Hille. Polypeptides of Nonpolyribosomal Messenger Ribonuclein Complexes of Sea Urchin Eggs. – Biochemistry, **19**, 1980, 2723-2730.

25. M o r g a n, T. Experimental Embryology. New York, Columbia University Press, 1927, 1-468.
26. P e a r s o n, J. C., D. L e m o n s, W. Mc G i n n i s. Modulating Hox gene functions during animal body patterning. – Nature Reviews Genetics, **6**, 2005, 893-904.
27. S k i p p e r, M. Interfering with Development. – Nature Reviews Genetics, **4**, 2003, 852.
28. S t e i n, G., J. S t e i n, L. K l e i n s m i t h. Chromosomal proteins and gene regulation. – Sci. Am., **232**, 1975, 47-57.
29. V o g t, W. Gestaltungsanalyse am Amphibiankernen mit ortlichen Vitalfarbung. – W. Roux' Arch. Entwicklungsmech. Org., **120**, 1929, 385-706.
30. Y o u n g, E. M., R. A. R a f f. Messenger Ribonuclein Particles in Developing Sea Urchin Embryos. – Developmental Biology, **72**, 1979, 24-40.
31. Y o u n g, E. Packaging proteins may be second genetic code. New Scientist.com. August 09, 2001.

Institute of Experimental Morphology and Anthropology with Museum
Bulgarian Anatomical Society

Acta morphologica et anthropologica, 12
Sofia • 2007

In Memoriam

Spassimir D. Nikolov (1939-2006)

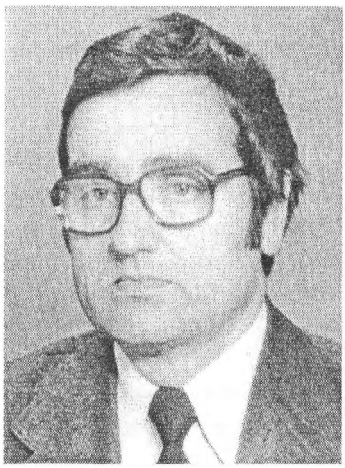

Spassimir Dimitrov Nikolov was born in Bulgaria on July 23, 1939. He graduated from the Medical University in Sofia and was awarded the university doctor's degree in 1963 (MD). Since 1964 he occupied the position of an assistant professor in the Chair of Anatomy at the Medical University in the city of Varna. Dr. S. Nikolov specialized in human anatomy under the guidance of Professor G. Schumacher in the Chair of Anatomy at the University of Rostock, Professor Schibler in the Chair of Anatomy at the University of Würzburg and in the Chair of Anatomy at the University of Leipzig. He attained the academic rank Associate professor in 1974 and Professor in 1989.

Dr S. Nikolov got his CSc (PhD) degree by the thesis "On the microvascularization of the main saliva glands" in 1970 and was awarded the DSc (DMSc) degree ("Ultramorphological characteristics of the vascular endothelial cells in view of their major functional trends") in 1987.

From 1992 through 2000 Professor S. Nikolov was Head of the Chair of Anatomy, Histology and Embryology at the Medical University of Varna and serving also as Deputy-Rector of the Medical University (Varna) for the period 1990-1994.

Professor S. Nikolov was author of over 120 scientific publications, co-author of 3 textbooks of "Human Anatomy" (1995), "Topographic Anatomy of Man" (1998) and "Handbook on Exercises in Dissection in Anatomy"(1997). Save for his tutorship of many students in anatomy he has been the scientific supervisor of PhD students.

Professor Spassimir Nikolov was member of the German Anatomical Society, an Honorary Member of the Romanian Society of Anatomists, member of the European Association of Chemical Anatomy, member of Executive Board of the Anatomists' Society of the Balkan countries and the Black Sea region. He was a long year member of the Executive Board of the Bulgarian Anatomical Society and organized a great number of successful national congresses and symposia with international participation. Due to his initiative in the city of Varna have been organized the "International Symposia on Clinical Anatomy" — the first one in 1994 and the oncoming 8th symposium will be held in 2006.

These scientific meetings are known and well-established in the European and international morphological community and are linked to his name.

Professor S. Nikolov has been visiting (invited) professor in 8 renowned European Universities and a participant in a large number of international and national scientific venues.

Professor S. Nikolov independently of his outstanding and long-lasting university teacher career was an active participant in many social events. As a municipal counselor in the city of Varna he was Head of Commission on Education and Science for the period 1991-1999.

On February 8, 2006, Professor Spassimir Nikolov passed away in the city of Varna at the age of 66 after a painful and long illness.

We, all the near and far friends and colleagues of his, will dearly miss him, but we will do the best we can to continue what he had begun.

Yordan Alexiev Yordanov
Editor-in-Chief

INSTRUCTION TO AUTHORS

SUBMISSION: Original papers and review articles written in English are considered and should be sent to the Editor-in-Chief.

Address:

Bulgarian Academy of Sciences
Institute of Experimental Morphology and Anthropology with Museum
Acad. G. Bonchev Str., Bl. 25,
1113 Sofia
Bulgaria
Our e-mail address is: <iemabas@bas.bg>

Manuscripts should not exceed 10 standard pages including abstract, captions, references and figures (3 copies — two copies in English and one copy in Bulgarian, and a disc using WINWORD 7.0, Times New Roman 12 pt).

CONDITIONS: In submitting a paper, the author should state in the covering letter that the article has not been published elsewhere and has not been submitted for publication elsewhere. All manuscripts are subject to editorial review.

ARRANGEMENT:

Title page. The first page of each paper should indicate the title, the authors' names and institute where the work was conducted, followed by abstract and key words.

Abstract. It should contain no more than 150 words.

Key words. For indexing purposes, a list of up to 5 key words in English is essential.

Tables and illustrations. Tables and captions to the illustrations should be submitted on separate sheets. The proper place of each figure in the text should be indicated in the left margin of the corresponding page. All illustrations (photos, graphs and diagrams) should be referred to as "figures" and given in abbreviation "Fig.". The author's name, the number of the figure with indication of its proper orientation (top, bottom) should be slightly marked on the back of each figure. All illustrations should be submitted in duplicate too.

References. They should be indicated in the text by giving the corresponding numbers in parentheses. The "References" should be typed on a separate sheet. The names of authors should be arranged alphabetically according to family names, first the articles in Roman alphabet, followed by the articles in Cyrillic alphabet. Articles should include the name(s) of author(s), followed by the full title of the article or book cited, the standard abbreviation of the journal (according to British Union Catalogue), the volume number, the year of publication and the pages cited. For books – the city of publication and publisher. In case of more than one author, the initials for the second, third, etc. authors precede their family names. Example:

Tuohy, V. K., Z. Lu, R. A. Sobel, R. A. Laursen, M. B. Lees. A synthetic peptide from myelin proteolipid protein induces experimental allergic encephalomyelitis. — J. Immunol., **141**, 1988, 1126-1130.

Norton, W. T., W. Cammer. Isolation and characterization of myelin. — In: Myelin (Ed. P. Morell). New York, Plenum Press, 1984, 147-180.

Further details. Use only standard symbols and abbreviations in the text and illustrations. Manuscripts, figures and diagrams should not be folded.

Full address. The exact postal address completed with postal code of the senior author must be given. If correspondence is handled by someone else, indicate this accordingly.

ISSN 0861-0509

AIMS AND SCOPE

Acta morphologica et anthropologica publishes original and review articles in the following sections:

Section A – Morphology: 1. Neurobiology;
2. Structure and Metabolism of the Cells;
3. Cell Differentiation and Kinetics; 4. Cellular Immunology;
5. Experimental Cytology; 6. New Methods.

Section B – Anthropology: 1. Physical Development;
2. Somatotype and Body Composition;
3. Population Genetics and Medical Anthropology;
4. Paleoanthropology and Paleopathology; 5. Anatomy.